RESEARCH & DEVELOPMENT

Surface Layer Bond Stresses and Strength

Y. Richard Kim, Ph.D., P.E., F. ASCE
Akhtar A. Tayebali, Ph.D., P.E.
Murthy N. Guddati, Ph.D.
Afshin Karshenas, Ph.D.
Seong-Hwan Cho, Ph.D.
Dept. of Civil, Construction, & Environmental Engineering
North Carolina State University

NCDOT Project 2013-04
FHWA/NC/2013-04
December 2015

Surface Layer Bond Stresses and Strength

FINAL REPORT

Submitted to:
North Carolina Department of Transportation
Office of Research
(Research Projection No. HWY-2013-04)

Submitted by

Y. Richard Kim, Ph.D., P.E., F.ASCE
Jimmy D. Clark Distinguished University Professor
Campus Box 7908
Department of Civil, Construction & Environmental Engineering
North Carolina State University
Raleigh, NC 27695-7908
Tel: 919-515-7758, Fax: 919-515-7908
kim@ncsu.edu

Akhtar A. Tayebali, Ph.D., P.E.
Professor

Murthy N. Guddati, Ph.D.
Professor

Afshin Karshenas, Ph.D.
Former Graduate Research Assistant

Seong-Hwan Cho, Ph.D.
Former Graduate Research Assistant

Department of Civil, Construction & Environmental Engineering
North Carolina State University
Raleigh, NC

December 2015

Technical Report Documentation Page

1. Report No. FHWA/NC/2013-04	2. Government Accession No.	3. Recipient's Catalog No.
4. Title and Subtitle Surface Layer Bond Stresses and Strength		5. Report Date December 2015
		6. Performing Organization Code
7. Author(s) Y. Richard Kim, Akhtar A. Tayebali, Murthy N. Guddati, Afshin Karshenas, and Seong-Hwan Cho		8. Performing Organization Report No.
9. Performing Organization Name and Address Campus Box 7908, Dept. of Civil, Construction, & Environmental Engrg. NCSU, Raleigh, NC 27695-7908		10. Work Unit No. (TRAIS)
		11. Contract or Grant No.
12. Sponsoring Agency Name and Address NC Department of Transportation Research and Analysis Group 1 South Wilmington Street Raleigh, NC 27601		13. Type of Report and Period Covered Final Report
		14. Sponsoring Agency Code 2013-04
15. Supplementary Notes		

16. Abstract

The primary objective of this research is to develop a comprehensive guideline to minimize the debonding distress in asphalt pavements. A particular focus of the study is the distribution and dissipation of shear stresses under traffic loading and ways that such stress affects the interlayer bonding. The systematic and mechanistic framework developed in this study includes a computational analysis methodology that is used to determine the critical stress and strain states in layered asphalt pavements under moving vehicle loads using a computational analysis program. Moreover, the comprehensive framework includes the following: a direct shear test protocol that can be used in the laboratory to evaluate the shear bond strength between the asphalt layers, a shear strength database for different tack coat materials at various confining pressures, temperatures, and loading rates, a mechanistic prediction model for shear strength, and descriptions of the effects of various pavement and environmental factors on the debonding distress. A particular focus of this study is to evaluate the distribution of stresses and strains under traffic loading using a computational pavement analysis program in order to investigate the ways that such stresses and strains affect interlayer debonding. Then, these states of stress and strain determined from the computational analysis of the asphalt pavement section are reflected in a test protocol that can be used to evaluate the interface shear bond strength in the laboratory, especially in terms of the selection of the appropriate level of normal confining stress for the shear strength test.

The time-temperature superposition (t-TS) principle is verified for the interface shear bond strength and interlayer shear stiffness that have been evaluated using the developed test protocol. Once the t-TS principle for interface shear bond strength is proven to be completely valid for specimens with different tack coat materials at the layer interface, shear strength mastercurves are constructed. Also, a procedure for the development of an interface shear strength model equation from the shear strength data sets obtained at different temperatures, loading rates, and normal confining stresses through the interface shear bond strength tests is described.

This research presents the concept of maximum shear ratio (MSR) as a means of determining the debonding potential of asphalt pavement. The MSR was defined as the maximum value of the shear ratio, i.e., the shear ratio at a given location at the layer interface, which is the ratio between the shear stress at that location and the shear bond strength determined for the shear strain rate and normal confining stress at that location. In this study, the MSR concept is coupled with the shear bond strength predictive model in order to propose a mechanistic framework to determine the debonding potential of asphalt pavement.

17. Key Words Bond strength, shear, layer interface,	18. Distribution Statement		
19. Security Classif. (of this report)	20. Security Classif. (of this page)	21. No. of Pages 286	22. Price

Form DOT F 1700.7 (8-72) **Reproduction of completed page authorized**

DISCLAIMER

The contents of this report reflect the views of the authors and are not necessarily the views of North Carolina State University. The authors are responsible for the facts and the accuracy of the data presented herein. The contents do not necessarily reflect the official views or policies of the North Carolina Department of Transportation at the time of publication. This report does not constitute a standard, specification, or regulation.

ACKNOWLEDGEMENTS

This research was sponsored by the North Carolina Department of Transportation. The Steering and Implementation Committee was comprised of Clark Morrison, Ph.D., P.E. (Chair), Mustan Kadibhai, P.E. (PM), Judith Corley-Lay, Ph.D., P.E., Josh Holland, P.E., Brian J. Hunter, P.E., Wendi O. Johnson, P.E., James B. Phillips, P.E., Nilesh Surti, P.E., Todd W. Whittington, P.E., Mrinmay Biswas, Ph.D., P.E. (Friend), Ron Hancock, P.E. (Friend), and Christopher A. Peoples (Friend). These advisors have given invaluable direction and support to the research team throughout the project.

EXECUTIVE SUMMARY

The importance of proper bonding at the asphalt concrete (AC) layer interface cannot be overemphasized when discussing the performance of AC pavements. Several pavements in North Carolina have experienced premature cracking, and forensic investigations have revealed that the debonding of the top surface layer is the primary reason for these failures. A strong bond between the layers is critical to dissipate shear stresses into the entire pavement structure. In contrast, insufficient bonding may cause slippage and activate distress mechanisms that will rapidly lead to total failure of the pavement.

The primary objective of this research is to develop a comprehensive guideline to minimize the debonding distress in asphalt pavements. This guideline will include an analysis framework to determine the critical stresses in layered asphalt pavement, a test method that can be used preferably in the field to measure the interface bond strength between the asphalt layers, recommendations for tack coat materials and rates for various existing pavement surface conditions, and assessment of the effects of various pavement and environmental factors on the interface bond strength. A particular focus of the study is the distribution and dissipation of shear stresses under traffic loading and ways that such stress affects the interlayer bonding.

The systematic and mechanistic framework developed in this study includes a computational analysis methodology that is used to determine the critical stress and strain states in layered asphalt pavements under moving vehicle loads using a computational analysis program. Moreover, the comprehensive framework includes the following: a direct shear test protocol that can be used in the laboratory to evaluate the shear bond strength between the asphalt layers, a shear strength database for different tack coat materials at various confining pressures, temperatures, and loading rates, a mechanistic prediction model for shear strength, and descriptions of the effects of various pavement and environmental factors on the debonding distress. A particular focus of this study is to evaluate the distribution of stresses and strains under traffic loading using a computational pavement analysis program in order to investigate the ways that such stresses and strains affect interlayer debonding. Then, these states of stress and strain determined from the computational analysis of the asphalt pavement section are reflected in a test protocol that can be used to evaluate the interface shear bond strength in the laboratory, especially in terms of the selection of the appropriate level of normal confining stress for the shear strength test.

The time-temperature superposition (t-TS) principle is verified for the interface shear bond strength and interlayer shear stiffness that have been evaluated using the developed test protocol. Once the t-TS principle for interface shear bond strength is proven to be completely valid for specimens with different tack coat materials at the layer interface, shear strength mastercurves are constructed. In addition, the validation of the t-TS principle is extended to include the shear strength of GlasGrid-reinforced asphalt concrete specimens with two different types of tack coat, PG 64-22 binder and SS-1 emulsion, between the layers. Then, the effects of geosynthetic interlayer materials on shear bond strength are discussed. Also, a procedure for the development of an interface shear strength model equation from the shear strength data sets

obtained at different temperatures, loading rates, and normal confining stresses through the interface shear bond strength tests is described.

This research presents the concept of maximum shear ratio (MSR) as a means of determining the debonding potential of asphalt pavement. The MSR was defined as the maximum value of the shear ratio, i.e., the shear ratio at a given location at the layer interface, which is the ratio between the shear stress at that location and the shear bond strength determined for the shear strain rate and normal confining stress at that location. In this study, the MSR concept is coupled with the shear bond strength predictive model in order to propose a mechanistic framework to determine the debonding potential of asphalt pavement.

The research products from this study will be used to provide pavement design elements and construction procedures or guidelines to reduce the likelihood of debonding of the top surface layer in an asphalt pavement. The results of this study will enable pavement designers to select appropriate tack materials for specific applications to reduce the likelihood of debonding of the surface layer, thereby leading to savings in pavement maintenance and rehabilitation costs.

TABLE OF CONTENTS

LIST OF FIGURES

LIST OF TABLES

Chapter 1 Introduction

1.1 Research Needs and Significance

Asphalt pavements constitute over 90 percent of pavements in the United States. Most asphalt pavement structures are composed of more than one asphalt concrete layers, which are bonded together using a tack coat. Therefore, the life and performance of the pavement depend not only on the properties of each layer, such as stiffness, modulus, and fracture energy, but also on the quality of the bond between the adjacent layers. The importance of proper bonding between the structural layers cannot be overemphasized when discussing the performance of asphalt concrete pavements. A strong interlayer bond between the layers is critical in order to dissipate the stress throughout the entire pavement structure. In contrast, a poor interface bond may lead to several types of premature distress, such as slippage cracking, top-down cracking, premature fatigue cracking, and delamination. Delamination or debonding problems are particularly more severe for asphalt pavements that are subjected to heavy vehicle loads, especially horizontal forces that are due to braking and turning of vehicles. The undetected delamination that is due to inadequate bonding at the layer interface can eventually result in localized slippage failure at the surface layer. Furthermore, poor bonding may activate distress mechanisms that can rapidly lead to the total failure of the pavement because the debonded layers can no longer act as a monolithic pavement section and therefore cannot provide the intended load-bearing capacity of those layers. Thus, the interface bond between pavement layers is a key factor that affects the performance of any pavement structure.

The forensic investigations of several highway projects in North Carolina (Park 2013 and Tayebali et al. 2004) clearly indicate that pavement failure often occurs at the layer interface due to the poor bond between adjacent asphalt concrete layers. Consequently, the debonding of adjacent layers, especially within the top surface layers of an asphalt pavement, is a contributing factor to the premature cracking of the pavement. In these studies, although it is not clear whether cracking or debonding occurred first, the debonding nonetheless contributed to the distress and eventual failure of the pavement.

Figure 1-1 schematically illustrates the shear and tension distress modes that can occur at a pavement surface interface. The failure of the pavement interface under traffic loading can be attributed to either or both of the shear and tension distress modes. Debonding occurs when the shear or tensile stress exceeds the shear or tensile strength of the material at the interface of two asphalt layers. Therefore, the prevention of debonding requires a good understanding of the distribution of these stresses along the bonded interface.

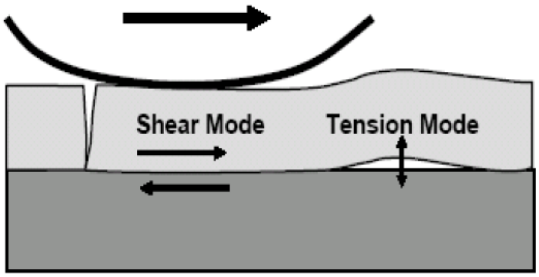

Figure 1-1 Distress modes at pavement interface under service conditions (Mohammad et al. 2012 and Raab et al. 2004).

Although much attention has been paid to characterizing and modeling the behavior of asphalt concrete experimentally, relatively little attention has been paid to characterizing and modeling interlayer bonding. To prevent the distresses associated with the debonding of pavement layers, a tack coat should be selected based on the type and level of the critical stress at the interface between the pavement layers. However, current pavement design methods lack a systematic and mechanistic approach to the design of pavement layer interfaces. Therefore, the selection of a tack coat as a bonding material currently is based on empirical methods and manufacturers' recommendations (Karshenas et al. 2014).

To develop an acceptable design method, a reliable analysis procedure and associated test methods are necessary to determine the shear bond strength between the pavement layers. The need for a standard test method to evaluate the interface shear bond strength has led to extensive research over the last decade throughout the world. Several researchers have shown that parameters such as normal stress, temperature, loading rate, tack coat type and application rate, aggregate gradation and compaction of asphalt layers, binder type, and surface roughness, to name a few, affect the interface bond strength (Canestrari et al. 2013, Mohammad et al. 2012, and Raab et al. 2009). Among these parameters, the effects of temperature, tack coat type and application rate, and surface roughness on interface bond strength are well known, but the extent of the effect of normal stress is still under debate. Therefore, several types of direct shear tests with and without normal confinement currently are used to evaluate interface bond strength.

1.2 Research Objectives

The primary objective of this research is to develop a comprehensive guideline to minimize the debonding distress in asphalt pavements. This guideline will include an analysis framework to determine the critical stresses in layered asphalt pavement, a test method that can be used preferably in the field to measure the interfacial bond strength between the asphalt layers, recommendations for tack coat materials and rates for various existing pavement surface conditions, and descriptions of the effects of various pavement and environmental factors on the

interface bond strength. A particular focus of this study is the distribution and dissipation of shear stresses under traffic loading and ways that these stresses affect interlayer bonding.

Chapter 2 Computational Analysis

2.1 Mechanistic Approach to Predict Shear Failure at the Tack-Coated Interface in a Layered Asphalt Structure

In order to evaluate the effect of the tack coat on the quality of the interface bond, it is necessary to understand and quantify the distribution of the stress levels at the layer interface under realistic loading conditions. Therefore, the stress levels under moving loads were evaluated to determine the critical stresses at the layer interface using the Layered ViscoElastic pavement analysis for Critical Distresses (LVECD) computer program developed at North Carolina State University (NCSU). Typical material properties and three typical pavement structures commonly constructed in North Carolina were used in the simulations; these typical structures include thin, intermediate, and thick pavements. The analysis was conducted at four temperatures (5°C, 20°C, 40°C, and 60°C), three speeds (8 km/hour (5 mph), 40 km/hour (25 mph), and 88 km/hour (55 mph)), and three axle loads (53.4 kN (12 kips), 80 kN (18 kips), and 106.8 kN (24 kips)). Two types of tire rolling conditions, i.e., free rolling and braking, also were considered in this computational analysis. The stress and strain levels computed from the pavement responses using the LVECD program were used to better understand the critical stresses that are involved in debonding and ways that such stresses are affected by pavement design parameters and environmental conditions. Detailed information about these computational simulations can be found in Appendix B.

2.1.1 LVECD Program Simulation Results

The critical conditions in terms of shear stress levels were determined from the results obtained from the evaluation of temperature, speed, load level, structure, and rolling resistance coefficients. Figure 2-1 shows the curves for shear stress versus depth under the braking state. The rolling resistance coefficient of 0.55 was used for the braking condition, as it is the most critical for each coefficient under consideration. The conditions specified in Figure 2-1, i.e., thin pavement, 106.8 kN (24 kips), 5°C, 88 km/hour (55 mph), and rolling resistance coefficient of 0.55 for the braking condition, are the critical conditions for the LVECD program simulations in terms of shear stress levels. The analysis results show that the shear stress initially increases with depth until it reaches a depth of 5.08 cm (2.0 in.), or 3.81 cm (1.5 in.) around the interface depth, except for at 60°C under the center of the tire, and finally shows a tendency to decrease until it reaches the bottom of the asphalt layer at 10.16 cm (4 in.) deep at all temperatures. The analysis results show that the location of the maximum shear stress is at a depth of 5.08 cm (2.0 in.) below the surface course, and that the shear stress around the layer interface is a significant factor that can induce pavement distress and interface debonding. That is, the interface could experience large amounts of repeated shear stress that in turn could lead to interface debonding in an asphalt pavement structure.

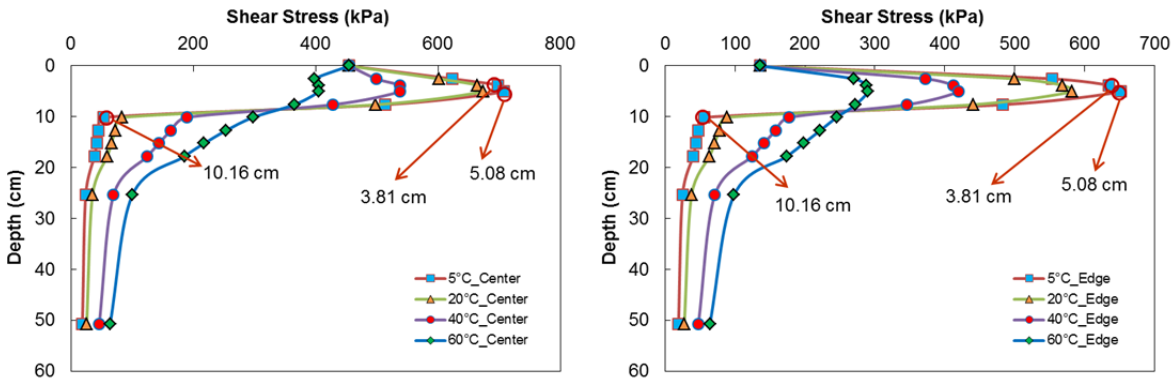

(a) (b)

Figure 2-1 Shear stress distribution as a function of depth at different temperatures: (a) at center of tire and (b) at edge of tire for thin pavement, 106.8 kN (24 kips), 88 km/hour (55 mph), rolling resistance coefficient of 0.55.

2.1.2 Maximum Shear Ratio and Interface Shear Failure Criterion

In order to design a pavement layer interface correctly, the stress states at the pavement interface and in the asphalt layers should be predicted accurately. Therefore, the relationships among shear strength, shear strain rate, and normal stress at the interface of a layered pavement structure should be properly understood and included effectively in the design of the interface. When the shear bond strength of a tack material is to be determined in a shear test, it is important to use the normal confining pressure that is calculated at the interface of interest in a given pavement section using pavement analysis that can represent the *in situ* environmental and traffic loading conditions as realistically as possible.

This section presents a mechanistic procedure that can predict shear failure at the asphalt layer interface by using the shear strength relationships developed by Canestrari et al. (2013). For the purpose of this study, the states of the stress and strain at the layer interface were analyzed for the various conditions cited in Section 2.1. The axle load was applied in a single tire configuration with 827.4 kPa (120 psi) tire-pavement contact pressure. The wheel was assumed to be in the braking state with the coefficient of friction between the tire and pavement surface assumed to be 0.55 (NHTSA 2009) and in the free rolling state. Figure 2-2 and Figure 2-3 present the stress distributions at the layer interface under braking and free rolling conditions, respectively, as determined from the LVECD program.

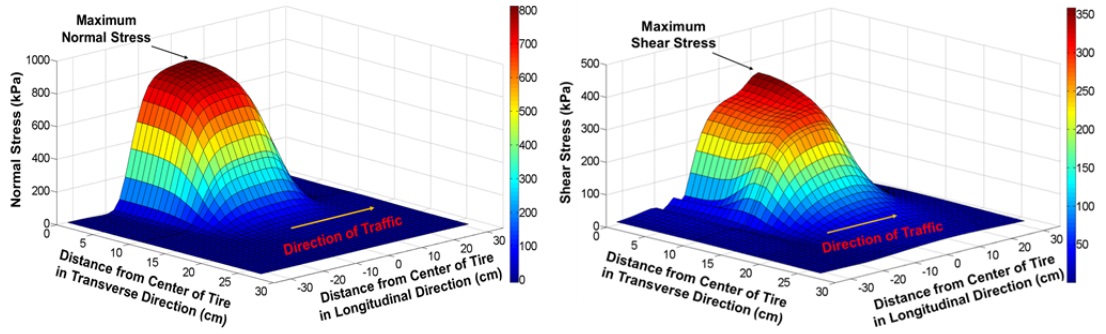

(a) (b)

Figure 2-2 Single tire stress distribution at the layer interface: (a) normal stress and (b) shear stress for intermediate pavement, 80 kN (18 kips), 8 km/hour (5 mph), 60°C, at 3.81 cm (1.5 in.) depth under braking condition. Note: Half of the tire imprint is shown due to symmetry.

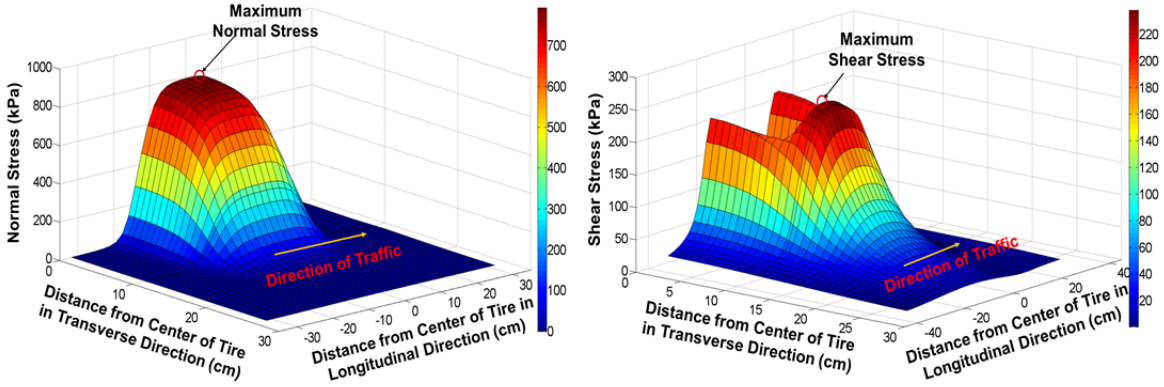

(a) (b)

Figure 2-3 Single tire stress distribution at the layer interface: (a) normal stress and (b) shear stress for intermediate pavement, 80 kN (18 kips), 8 km/hour (5 mph), 60°C, at 3.81 cm (1.5 in.) depth under free rolling condition. Note: Half of the tire imprint is shown due to symmetry.

In order to determine the integrity of the interface bond under wheel loading, the asphalt concrete layers in the pavement structures were assumed to be tacked using the same material (cationic tack) as was used in the study by Canestrari et al. (2013). The shear bond strength (τ_s) for each point under consideration at the layer interface was computed using the strain rate and the corresponding normal stress (normal confining stress). As is evident from the literature, researchers typically compare the induced shear stress at the interface layer due to wheel loading (in most cases at the edge of the tire) directly to the shear bond strength obtained from laboratory or field testing. If, at any location on the interface, the induced shear stress level is higher than the shear bond strength level, then this occurrence would simply imply imminent shear failure in the asphalt concrete layers. However, it is important to note the contribution of normal stress in the failure criterion.

A profile of the shear stress ratio (τ_{max} / τ_s) under the tire at the asphalt concrete layer interface was developed to determine the maximum ratio, which is termed the maximum shear ratio (MSR) and is defined in this study as a failure criterion. The shear ratio is given by Equation (1). If the maximum shear ratio (MSR) is higher than 1.0, then shear failure would occur at the asphalt concrete layer interface. In addition, the MSR that is close to 1.0 indicates a high potential of shear failure between the asphalt concrete layers due to repeated braking.

$$\text{Shear ratio (SR)} = \frac{\tau_{max}}{\tau_s} \qquad (1)$$

where

$$\tau_{max} = \sqrt{(\tau_{xz})^2 + (\tau_{yz})^2}$$

τ_{xz} = shear stress in the transverse direction at the interface calculated by the LVECD program,

τ_{yz} = shear stress in the longitudinal direction at the interface calculated by the LVECD program, and

τ_s = shear bond strength (function of normal stress) obtained from the Canestrari et al. (2013) equations.

Figure 2-4 shows the profiles of the shear ratios under the tire at the layer interface for different conditions that were randomly chosen from various conditions, even though all the conditions under consideration are not presented in this report. Based on all of the conditions under consideration in this study, the location of the MSR under the braking condition was found to be on the central longitudinal axis all the time, although the distance from the center of the tire imprint along the central longitudinal axis may vary slightly. On the other hand, the location of the MSR under the free rolling condition was found to be around the edge of the tire on the central transverse axis all the time. The MSRs at the asphalt concrete layer interface under the braking condition present more critical values than under the free rolling condition. Figure 2-5 provides guidance for the selection of the appropriate level of normal confining stress on the central longitudinal axis of the tire at the layer interface that corresponds to the location of the MSR.

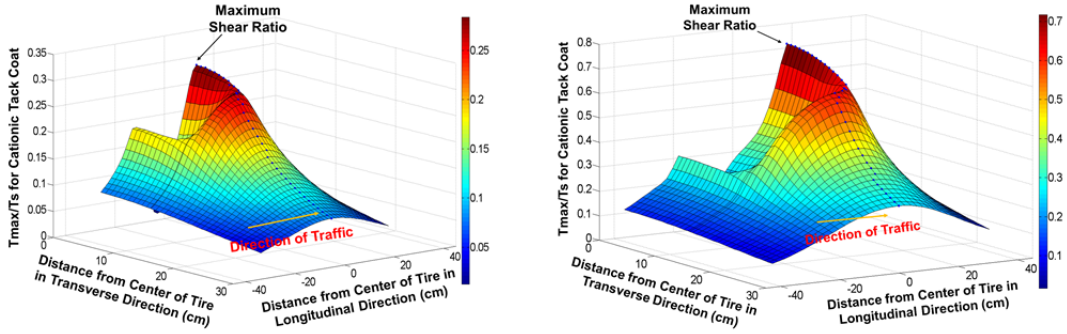

(a) (b)

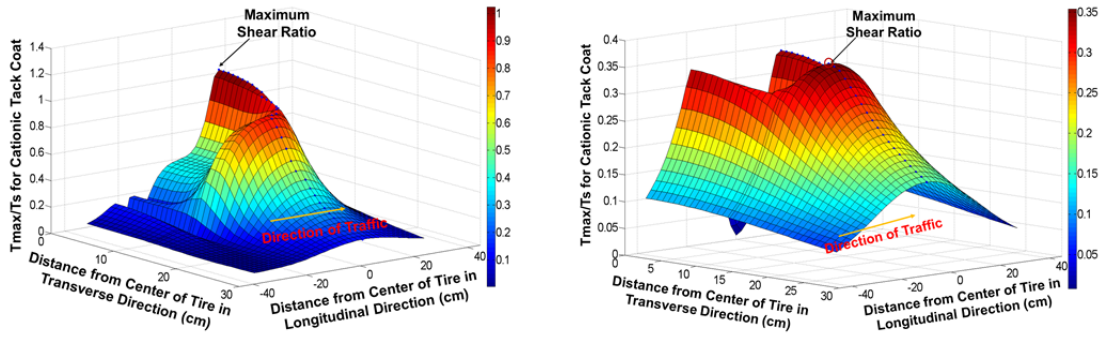

(c) (d)

Figure 2-4 Shear ratio profiles under the tire at the layer interface: (a) thin pavement, 53.4-kN (12 kips) axle load, 88 km/hour (55 mph), 5°C, braking condition; (b) intermediate pavement, 106.8-kN (24 kips) axle load, 8 km/hour (5 mph), 20°C, braking condition; (c) thick pavement, 80-kN (18 kips) axle load, 40 km/hour (25 mph), 60°C, braking condition; and (d) thin pavement, 106.8-kN (24 kips) axle load, 88 km/hour (55 mph), 5°C, free rolling condition. Note: The rolling resistance coefficient of 0.55 is used under braking condition.

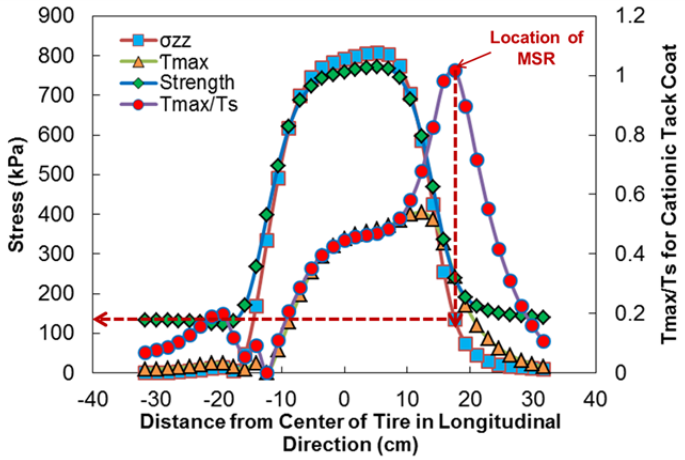

Figure 2-5 Shear ratio, shear strength, and shear and normal stress levels in the longitudinal direction under the central axis of the tire at the layer interface for intermediate pavement, 80 kN (18 kips), 8 km/hour (5 mph), 60°C, at 3.81 cm (1.5 in.) depth, braking condition.

2.2 Mechanistic Approach to Predict Tensile Cracking

To predict tensile cracking in the surface layer of a multilayered pavement structure, the material response (tensile strength) of the asphalt layer and the structural response or state of stress in the structure (tensile stress) should be defined. The material responses should be predicted using proper test methods to measure the tensile strength of the pavement layer material. In addition, the structural responses should be computed using suitable analysis software that can accommodate the required material models.

2.2.1 Tensile Stress Analysis in the Surface Layer of a Pavement Section

The stress distribution in the pavement layers were predicted based on a wheel in the braking state with the standard axle load of 80 kN (18 kips) and tire pressure of 827.4 kPa (120 psi) moving at the speed of 8 km/hour (5 mph) and with the pavement temperature of 60°C (140°F). Different friction coefficients of 0.35, 0.45, and 0.55 were assumed between the tire and the pavement surface. The stress levels at the surface of the pavement with the friction coefficient of 0.55 are shown in Figure 2-6.

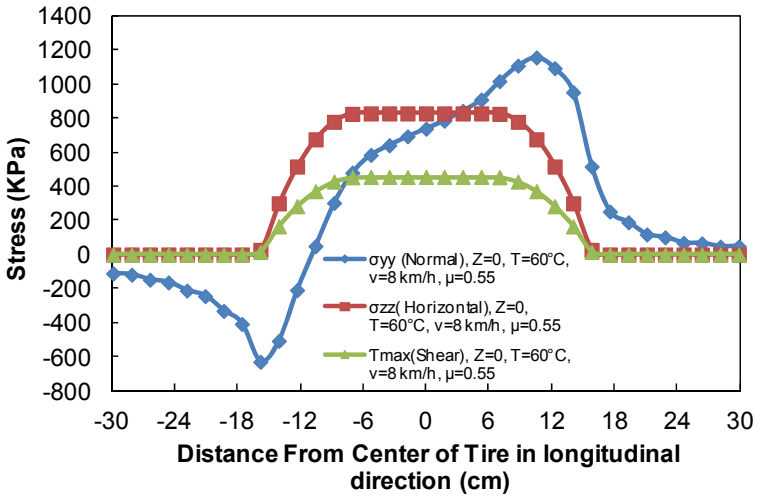

Figure 2-6 Stresses at the surface of pavement due to a braking wheel: v = 8 km/hr (5 mph), 0.55 friction coefficient, and 60°C (140°F). Note: Tensile stress is negative.

The maximum horizontal tensile stress on the surface of the pavement behind the tire with the assumed analysis conditions (T = 60°C, v = 8 km/hr, and μ = 0.55) was predicted to be 647 kPa (93.8 psi). The tensile strength of the asphalt layer should be estimated and compared to the tensile stress at the surface of the pavement to forecast the tensile failure (vertical crack) behind the tire imprint. Based on the stress distribution shown in Figure 2-6, the schematic failure modes at the interface and in the surface layer of the pavement structure are illustrated in Figure 2-7.

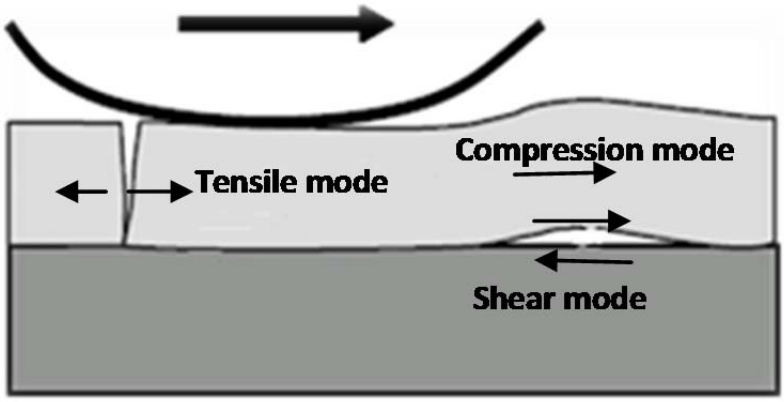

Figure 2-7 Schematic failure modes at the interface and in the surface layer.

2.2.2 Tensile Failure Prediction Due to a Braking Wheel

The tensile stress in the surface layer of the asphalt pavement that is due to a braking wheel should be compared to the predicted tensile strength of the asphalt layer to forecast the tensile failure behind the tire. The ratio of the computed tensile stress (σ_{max}) to the tensile strength (f_t) is used as the tensile failure criterion. The maximum tensile stress ratio is termed the *critical tensile ratio* (CTR). The tensile strength of the asphalt concrete mixture was predicted using a model equation proposed by Li et al. (2012). This model is a function of the tensile strain rate and temperature.

Pavement temperature, vehicle speed, and the friction coefficient between the tire and the asphalt surface together affect the structural responses and tensile strength of the pavement structure. The effects of each of these factors were evaluated in this study. Detailed information can be found in Appendix B.

Figure 2-8 shows the location of the maximum horizontal tensile stress on the surface of the pavement. The maximum horizontal tensile stress occurs at 15.7 cm (6.18 in.) from the center of the tire in the opposite direction to the applied braking shear force, i.e., just behind the tire. The maximum compression stress occurs at 10.57 cm (4.16 in.) from the center of the tire in the direction of traffic.

The contours for the principal horizontal stress on the surface of the pavement structure are presented in Figure 2-9. The pavement structure was analyzed at 60°C (140°F) with a wheel moving at the speed of 8 km/hr (5 mph) in the braking state. The friction coefficient between the wheel and the pavement surface is 0.55.

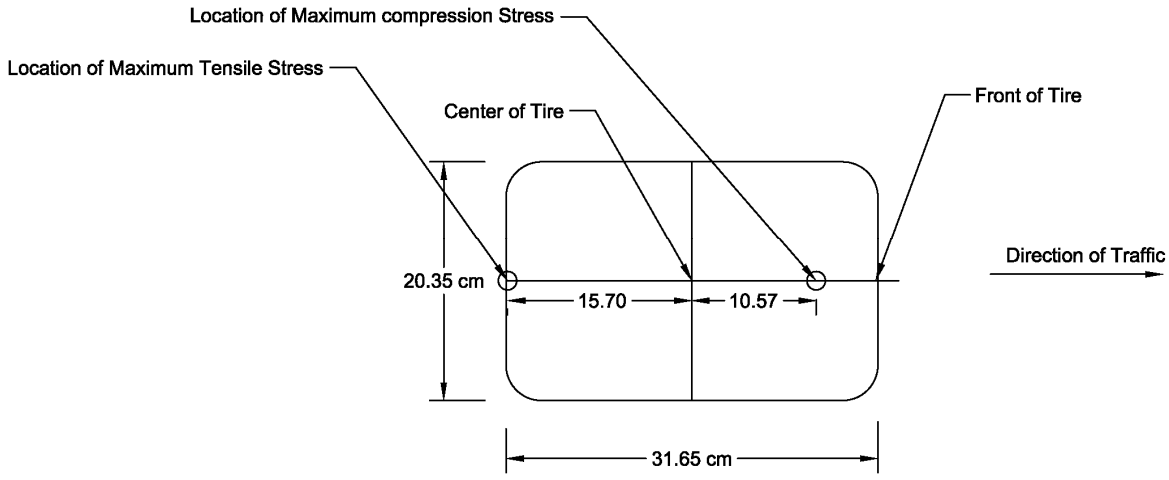

Figure 2-8 Location of the maximum tensile stress and maximum compression stress at the surface of the pavement in the central longitudinal axis of the tire imprint.

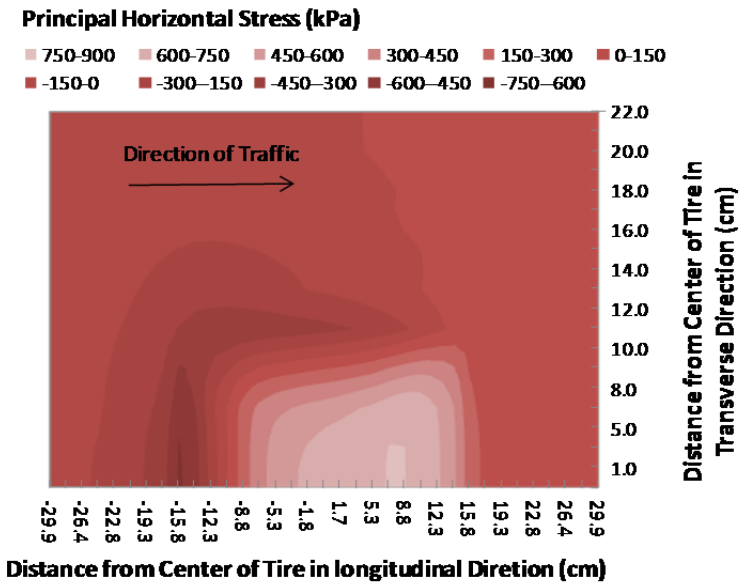

Figure 2-9 Principal horizontal stress on the surface of the pavement with a bonded interface due to a braking wheel at 60°C (140°F), 8 km/hr (5 mph), and friction coefficient of 0.55. Note: Half of the tire imprint is shown due to symmetry.

2.2.3 Debonded Pavement Analysis

To study the behavior of the debonded surface layer in a multilayered pavement structure, a model was developed for the LVECD computer program in which the debonded interface is represented as a thin layer with a very low modulus of elasticity value between the asphalt layers. A 1-mm thick elastic layer with a modulus of elasticity of 1 kPa and Poisson's ratio of 0.499 was modeled between the S9.5B asphalt surface layer and the I19B layer. The pavement was analyzed for two load cases of a rolling wheel and a braking wheel with the coefficient of friction of 0.55 between the tire and the pavement surface. The load was an 80-kN (18-kip) standard axle moving at the speed of 8 km/hour (5 mph). The tire load was applied using a single tire configuration with 827.4 kPa (120 psi) tire pressure at 60°C (140°F).

Stress Distribution in the Debonded Pavement Due to a Rolling Wheel

Figure 2-10 shows the stress distribution on the surface of the debonded pavement due to a rolling wheel moving at the speed of 8 km/hour (5 mph).

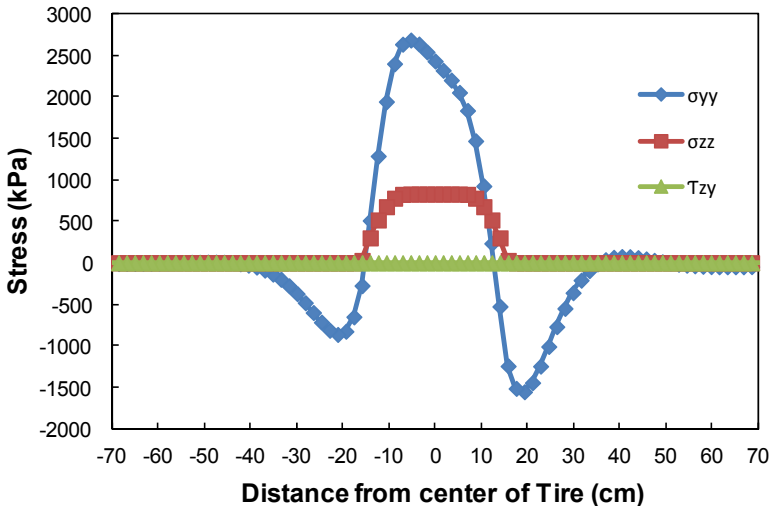

Figure 2-10 Stress distribution on the surface of the debonded pavement in the central longitudinal axis of the wheel imprint due to the rolling wheel, 8 km/hr (5 mph), and 60°C (140°F).

The coefficient of friction between the tire and the pavement was assumed to be zero in this analysis case. As shown in Figure 2-10, the shear stress on the surface of the pavement is zero ($\tau_{zy} = 0$), which is due to the rolling state of the wheel. The maximum normal stress (σ_{zz}) on the surface of the pavement is 827.4 kPa (120 psi), which is equal to the assumed tire pressure. The maximum horizontal tensile stress of 1,550 kPa (225 psi) occurs at 19.3 cm (7.6 in.) from the center of the wheel imprint in front of the wheel. The tensile stress behind the wheel is 825 kPa (119.6 psi) at 19.3 cm from the center of the wheel in the opposite direction of the traffic.

Using a model equation proposed by Li et al. (2012), the tensile strength of the hot-mix asphalt (HMA) pavement at 60°C (140°F) with a vehicle moving at the speed of 8 km/hr (5 mph) was predicted to be 430 kPa (62.3 psi). Comparing the tensile stress on the surface of the debonded pavement and the tensile strength shows that the tensile stress levels are much higher than the tensile strength levels. Therefore, the debonded pavement will crack in front of the tire and behind the tire due to a rolling wheel at the speed of 8 km/hr (5 mph) and at the temperature of 60°C (140°F).

The contours of the principal horizontal stress on the surface of the pavement with the debonded interface between the pavement layers are shown in Figure 2-11. As shown in Figure 2-11, a rolling wheel moving over a debonded surface asphalt layer will cause a circular pattern of tensile stress around the wheel and can result in the delamination of the debonded pavement.

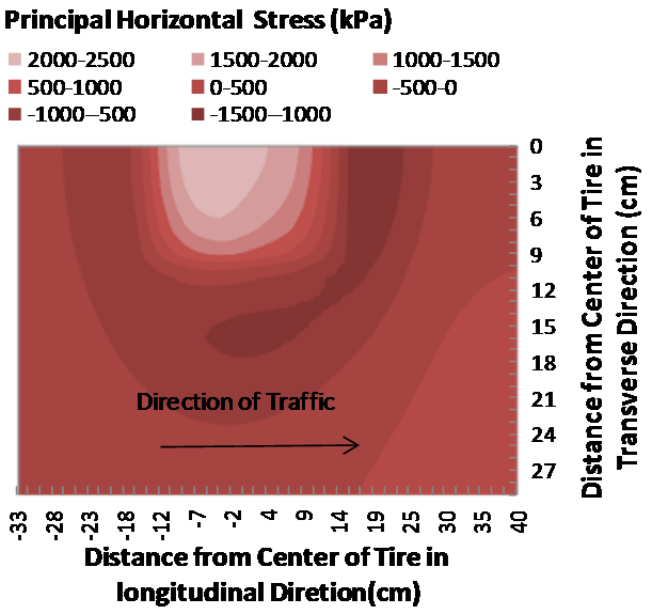

Figure 2-11 Principal horizontal stress on the surface of the pavement with the debonded interface due to a rolling wheel at 8 km/hr (5 mph) and at 60°C (140°F). Note: Half of the tire imprint is shown due to symmetry.

The stress at the interface between the two debonded asphalt layers (i.e., the stress at the bottom of the top layer) that is due to the rolling wheel is presented in Figure 2-12. The maximum normal stress (σ_{zz}) at the interface is 736 kPa (106 psi) and the shear stress between the asphalt layers at the interface is zero, which indicates no shear transfer between the surface layer and the underlying layer. The maximum horizontal tensile stress at the bottom of the surface layer occurs at 5.2 cm from the center of the tire in the opposite direction of the traffic, as shown in Figure 2-12. The horizontal tensile stress at the bottom of the surface layer is 2,328 kPa (337.6 psi), which is much higher than the tensile strength of the HMA, and causes a vertical crack at the bottom of the pavement that is located 5.2 cm (2.05 in.) from the center of the tire.

Figure 2-13 shows the horizontal stress on the surface of the pavement and at the bottom of the top layer that is at the debonded interface due to a rolling wheel. The compressive horizontal stress (σ_{yy}) on the surface of the pavement at the center of the tire imprint and the tensile horizontal stress at the interface between the debonded asphalt layers at the center of the tire imprint indicate the bending of the surface asphalt layer separately, as a beam. The bending of the surface layer introduces high horizontal tensile stress levels in front of the tire imprint and behind the tire imprint due to the negative moment at the surface asphalt layer.

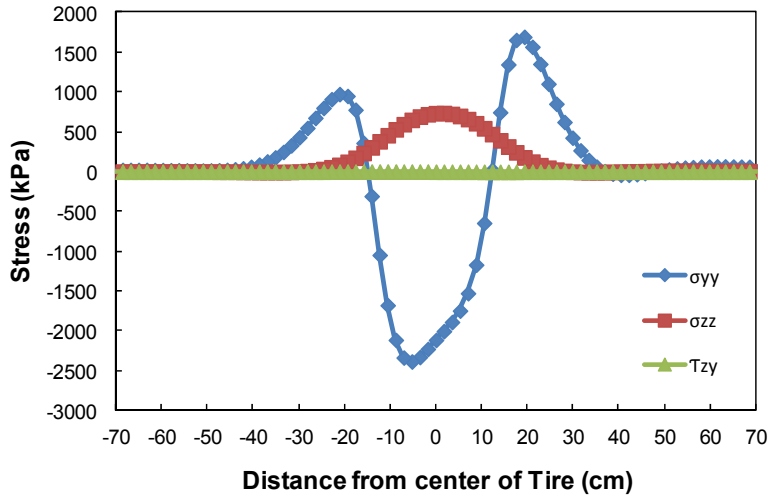

Figure 2-12 Stress distribution at the interface of debonded pavement layers due to a rolling wheel in the central longitudinal axis of tire: 8 km/hr (5 mph) and 60°C (140°F).

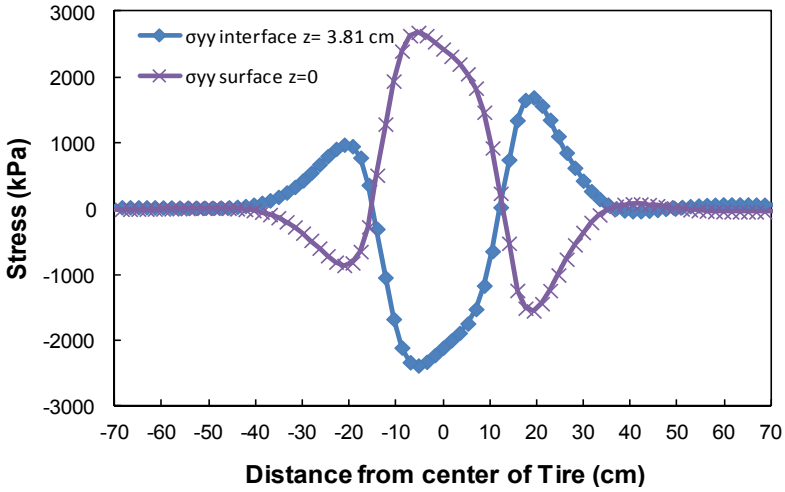

Figure 2-13 Horizontal stress (σ_{yy}) at the top (surface) and bottom (interface) of the debonded surface asphalt layer at the central longitudinal axis of the wheel Note: Tensile stress is negative.

Figure 2-14 shows the approximate locations of the tensile cracks due to a rolling wheel in a schematic debonded pavement section.

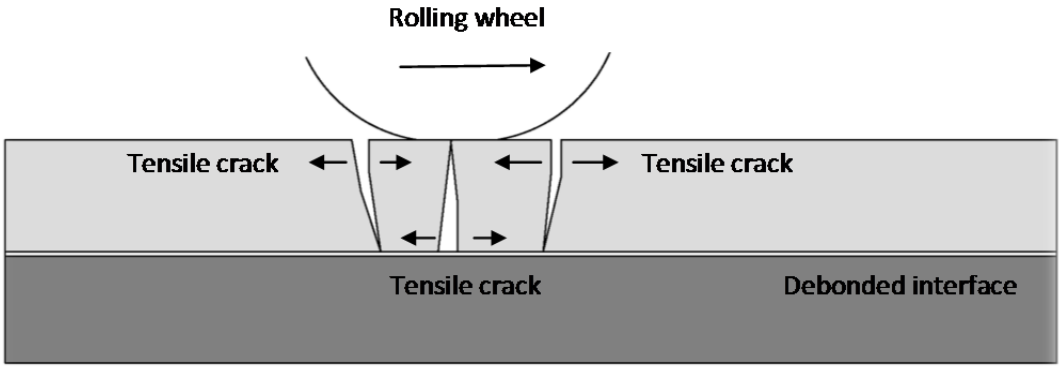

Figure 2-14 Schematic tensile cracks in the debonded surface layer due to a rolling wheel.

The stress on the surface of the bonded pavement section (i.e., without the thin debonded layer) that is due to a rolling wheel moving with the speed of 8 km/hr (5 mph) at 60°C (140°F) is illustrated in Figure 2-15. As shown in Figure 2-15, the shear stress at the surface of the pavement is zero (a rolling wheel condition) and the horizontal tensile stress in front of the tire is about 64 kPa (9.2 psi), which is lower than the tensile strength of the asphalt concrete. The horizontal compressive stress at the surface of the pavement is 720 kPa (104.4 psi) and is located 7 cm (2.75 in.) from the center of the tire in the opposite direction of the traffic.

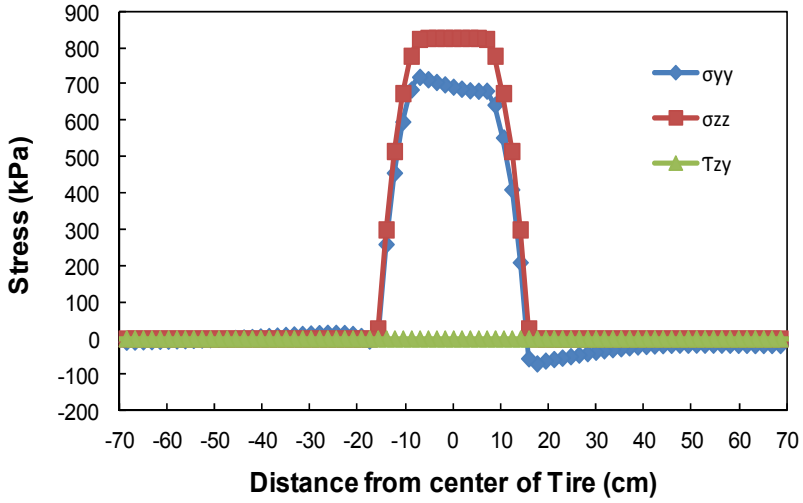

Figure 2-15 Stress at the surface of the pavement due to a rolling wheel on the bonded pavement at the central longitudinal axis of the wheel: 8 km/hr (5 mph) and 60°C (140°F).

The stress at the interface between the surface layer and the underlying asphalt layer of the bonded pavement due to a rolling wheel is shown in Figure 2-16. At the interface, only horizontal compression stress develops, and there is no horizontal tensile stress, which indicates the complete interaction between the asphalt layers as a composite structure. The shear stress at the interface is introduced due to the bending of the bonded pavement layers.

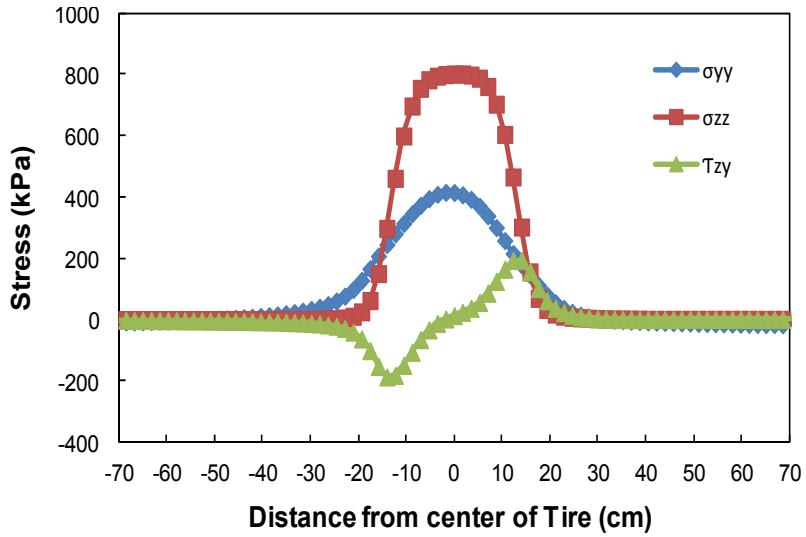

Figure 2-16 Stress at interface due to a rolling wheel on bonded pavement at the central longitudinal axis of the tire imprint: 8 km/hr (5 mph) and 60°C (140°F).

Stress in the Debonded Pavement with a Wheel in the Braking State

Figure 2-17 shows the stress at the surface of the pavement due to a wheel in the braking state moving at the speed of 8 km/hr (5 mph) with the coefficient of friction of 0.55 between the tire and pavement at 60°C (140°F). The maximum shear stress (τ_{zy}) at the surface of the pavement is 455 kPa (66 psi) and the maximum vertical stress (σ_{yy}) is 827 kPa (120 psi), which is equal to the tire pressure. As illustrated in Figure 2-17, the maximum horizontal tensile stress (σ_{yy}) on the surface of the pavement behind the tire is 1,676 kPa (243 psi) and in front of the tire is 811 kPa (117.6 psi), which are higher values than the tensile strength of 446 kPa (64.7 psi) of the pavement. Therefore, a braking wheel moving over a debonded pavement may cause vertical tensile cracking on the surface of the pavement in front of the tire and behind the tire.

Figure 2-18 shows the principal horizontal stress on the surface of the debonded pavement due to the braking wheel moving at the speed of 8 km/hr (5 mph) with the coefficient of friction of 0.55 between the tire and pavement at 60°C (140°F). As is shown, the braking wheel causes tensile cracks around the wheel on the surface of the pavement.

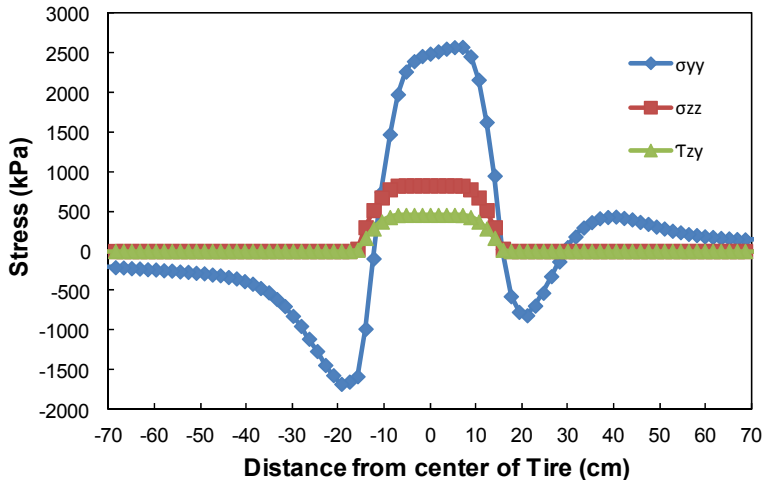

Figure 2-17 Stress on the surface of the debonded pavement due to a braking wheel at the central longitudinal axis of the tire: 60°C (140°F), 8 km/hr (5 mph), and 0.55 friction coefficient.

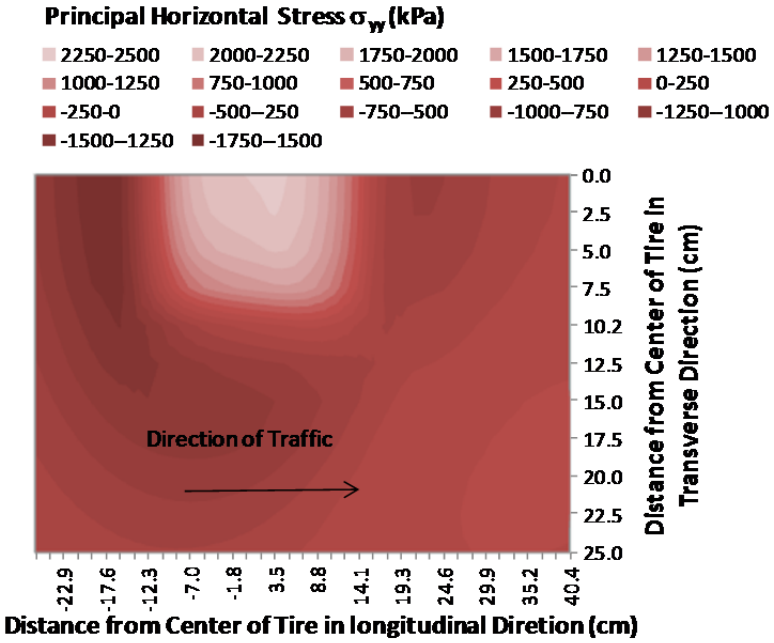

Figure 2-18 Principal horizontal stress on the surface of the pavement with the debonded interface due to a braking wheel at 60°C (140°F), 8 km/hr (5 mph), and friction coefficient of 0.55. Note: Half of the tire imprint is shown due to symmetry.

At the bottom of the surface layer, the maximum horizontal tensile stress occurs 3.5 cm from the center of the tire in the opposite direction of the traffic, as shown in Figure 2-19. This horizontal tensile stress can cause vertical cracking at the bottom of the surface layer (i.e., top-down cracking).

According to a study by Chen (2010), crescent-shaped surface cracks that occur soon after the construction of HMA pavement, as shown in Figure 2-20, are possibly due to the debonded interface, which can be the result of an improper tack coat application. Comparing the photographs shown in Figure 2-20 with the principal horizontal stress shown in Figure 2-18 indicates the similarity of the crack pattern around the braking wheel to that of the maximum tensile principal horizontal stress. As a result, it can be concluded that a braking wheel moving on a debonded surface layer will cause slippage cracking behind the contact point of the tire and crescent-shaped surface cracking around the tire.

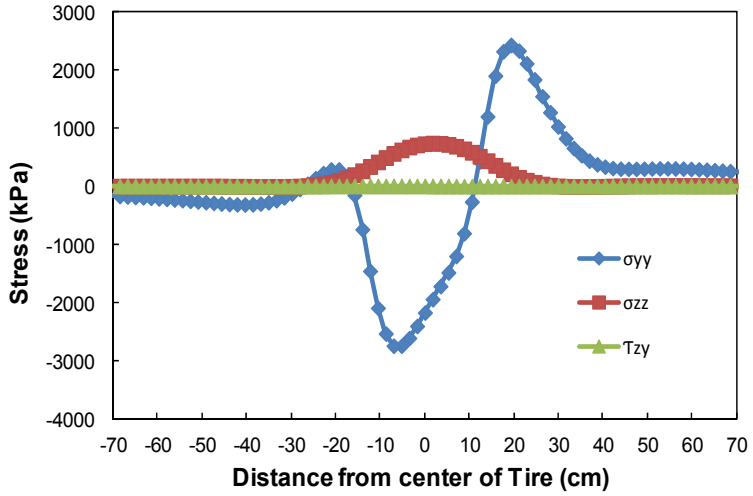

Figure 2-19 Stresses at the interface of the debonded pavement due to a braking wheel at the central longitudinal axis of the wheel: 60°C (140°F), 8 km/hr (5 mph), and 0.55 friction coefficient.

Figure 2-20 Premature slippage failure with crescent-shaped cracks after one day of traffic (Chen 2010).

Chapter 3 Experimental Program

3.1 Materials

The RS9.5B mixture, which is a mixture type commonly used in North Carolina, was used for this study. This mixture was mixed at a production plant and sampled during construction. It was reheated and compacted following a separation process developed at NCSU in order to reduce the specimen-to-specimen variability. Four types of tack coat material, i.e., CRS-2, CRS-1h, NTCRS-1hM (trackless tack coat), and no tack coat emulsions, were used in this study. Tack coat residual rates that typically are used in laboratory applications differ from the tack coat application rates used in the field. The tack coat residual rate is the amount of actual asphalt binder that remains after the water that is retained in the asphalt emulsion has evaporated, whereas the tack coat application rate is the amount of liquefied asphalt that is sprayed by the distributor (California Department of Transportation 2009). However, if an asphalt binder (i.e., PG 64-22) is utilized as a tack coat material, the tack coat residual rate applied to the pavement surface is equivalent to the applied application rate. It is noted that the application rate of 0.181 L/m^2 (0.04 gal/yd^2) used in this study is not the tack coat residual rate but the tack coat application rate commonly used in the field in North Carolina. A non-milled surface condition was used for this study.

3.2 Dynamic Modulus (|E*|) Testing

Dynamic modulus (|E*|) tests were conducted for the RS9.5B mixture in the lab in order to obtain the basic viscoelastic properties, i.e., the dynamic modulus values and time-temperature (t-T) shift factors. These tests were performed in stress-controlled mode at frequencies of 25, 10, 5, 1, 0.5, and 0.1 Hz and temperatures of -10°C, 5°C, 20°C, 40°C, and 54°C. The load level was adjusted for each condition to produce total strain amplitudes of about 50 to 75 micro-strains, which are within the linear viscoelastic range. Table 3.1 presents the averaged t-T shift factor function coefficients for the RS9.5B mixture. These coefficients were used later for the horizontal shifting of the interface shear bond strength data obtained by the Modified Advanced Shear Tester (MAST) at several temperatures and constant displacement control rates. Figure 3-1 presents the mastercurve for the RS9.5B mixture.

Table 3.1 Averaged fitting coefficients of time-temperature shift factor function.

Parameters	RS9.5B
α_1	0.0005055
α_2	-0.1544783
α_3	0.7597547

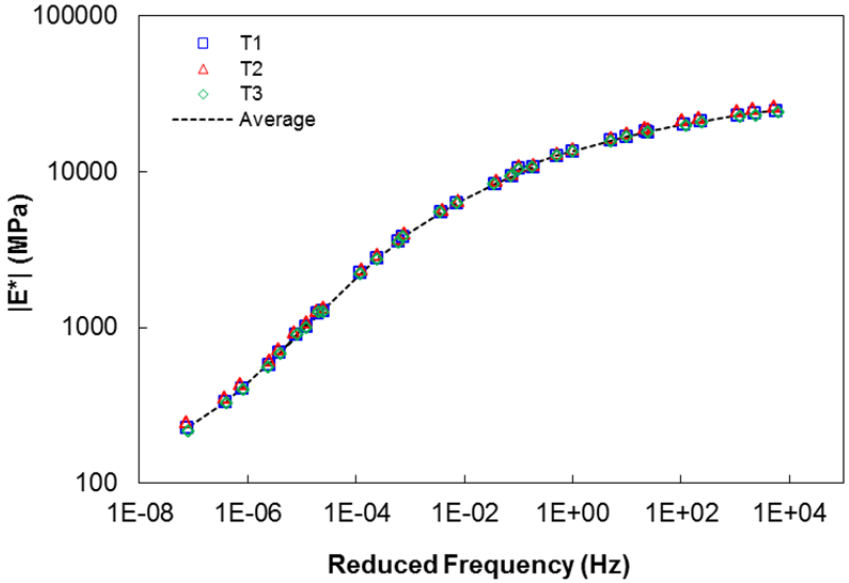

Figure 3-1 Dynamic modulus mastercurve for RS9.5B mixture.

3.3 Modified Advanced Shear Tester (MAST)

The MAST was designed to investigate the shear properties of uniform asphalt mixtures as well as interlayer interfaces and to resolve the problems inherent of many of the current devices used for shear testing. Figure 3-2 presents illustrations of the MAST, which is a direct shear apparatus that is capable of testing 152.4-mm (6 in.) and 101.6-mm (4 in.) square-shaped specimens as well as 101.6-mm (4 in.) diameter cylindrical specimens for direct shear. This device can perform not only a simple shear bond strength test but can also test for shear fatigue resistance under different environmental conditions (i.e., load- or displacement-controlled mode at various temperatures). One of the distinctive features of the MAST is that the initial normal confining stress that is applied to a specimen can be controlled by tightening a set of bolts while monitoring the load level during testing using an in-line load cell. This application method for normal confining stresses was inspired by Adam Zofka's shearing device (Zofka et al. 2015), the Advanced Shear Tester. For this study, the comprehensive shear bond strength study performed using the MAST for laboratory-fabricated samples and a computational analysis study were used later to determine the critical conditions for the debonding distress.

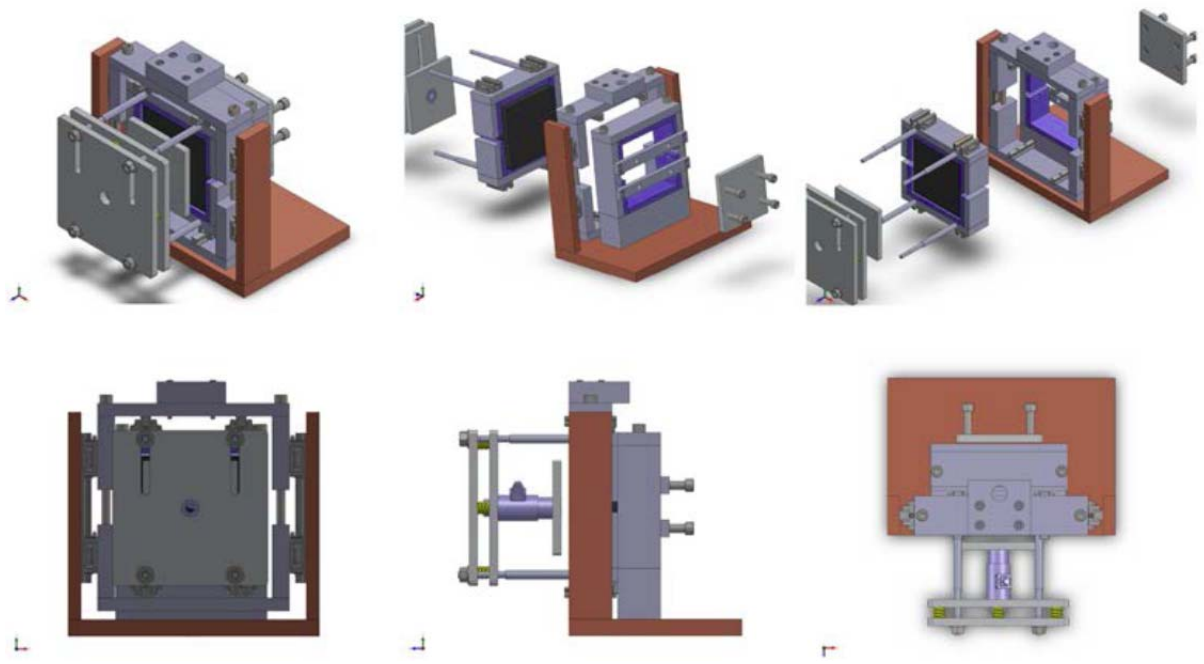

Figure 3-2 Illustrations of the Modified Advanced Shear Tester (MAST).

3.4 Laboratory Specimen Fabrication

The MAST, as originally designed, uses a specimen composed of two symmetrical asphalt layers obtained from slabs compacted by a steel wheel compactor to examine the interface shear bond strength. However, for this study, gyratory-compacted shear test specimens with a double layer were fabricated using the gyratory compactor. To produce the desired test specimens, the first stage of fabrication was to create a one-layered cylindrical specimen 150 mm (6 in.) in diameter and 50.8 mm (2 in.) in height using the Servopac Superpave gyratory compactor, manufactured by IPC Global of Australia. The remainder of the fabrication process used for this study is as follows.

Once HMA has been poured into the gyratory compactor mold, the compactor compacts the mixture to a height of 50.8 mm (2 in.). After cooling, a tack coat is applied uniformly to achieve a consistent thickness on the top of the bottom layer. This process involves using a paint brush to apply the tack coat with an application rate of 0.181 L/m^2 (0.04 gal/yd^2) after placing the specimen on a sensitive balance. The specimen is then cured for various curing periods as determined by the evaporation test (curing time test) for each emulsion type. During the curing period, the water evaporates, leaving only residual asphalt on the surface.

After curing, the same compaction process used for the bottom layer is repeated on top of the bottom layer to produce the upper asphalt concrete layer to 50.8 mm (2 in.) in height. At this time, the bottom layer, where the tack coat has been applied and has already cured, is placed into the gyratory compactor mold again.

After compacting the upper layer, the specimens are sealed in bags and placed in an unlit cabinet to reduce the aging effects. Then, in order to maintain consistent air void distribution, thereby obtaining specimens of uniform quality for testing, the specimens are cored and cut to a height of 76.2 mm (3 in.) and a diameter of 101.6 mm (4 in.) before testing.

3.5 Simulation of Debonding Distress Mechanisms

3.5.1 Loading Rate

Based on the literature review for loading rates used in shear strength tests (Bernier et al. 2012), the base loading rate of 50.8 mm/min (2 in./min) was selected for this study. This rate is commonly used in monotonic shear testing, i.e., controlled crosshead (CX) strain tests. Two additional loading rates, 0.508 mm/min (0.02 in./min) and 5.08 mm/min (0.2 in./min), which are hundred times and ten times slower, respectively, than the base loading rate, were selected as well.

3.5.2 Temperature

The selection of proper test temperatures is an important decision because asphalt material is very sensitive to temperature/time. The temperatures chosen for laboratory testing, especially the high temperatures, should represent the field conditions because debonding problems usually occur at high temperatures. To identify the temperature test conditions for this study, the highest pavement temperature data at a depth of 3.81 cm (1.5 in.) below the surface course, as provided by the Enhanced Integrated Climatic Model (EICM) for the Raleigh, North Carolina area, were utilized. The highest pavement temperature at a depth of 3.81 cm (1.5 in.) in the Raleigh area was 52.78°C (127°F). In order to encompass this highest temperature, 53°C (127.4°F) was chosen as the high temperature for the lab tests in this study. The low temperature for lab testing was selected as 5°C, which is the temperature used in LVECD program simulations.

In order to satisfy the t-TS principle, it is important to observe the overlaps of reduced strain rates from adjacent temperatures. The number of temperatures and the temperatures that should be used depend on the t-T shift factor. The test temperatures can be determined according to the following scheme. For example, the lowest reduced strain rate at 5°C was used initially in this study. Then, this rate was divided by the highest strain rate at an unknown temperature. After that, the shift factor function was employed to solve for the unknown temperature. By repeating this process, two more temperatures, 19°C and 35°C, were chosen as intermediate temperatures to satisfy the t-TS principle. In other words, intermediate temperatures were determined to ensure sufficient overlap of the reduced strain rates between adjacent temperatures. The validity of the t-TS principle can be checked by comparing the shear strength values determined from two adjacent temperatures but at the same reduced strain rates.

3.5.3 Normal Confining Stress

The spectrum of normal confining stresses that typically is used to evaluate shear bond strength using shear test devices encompasses zero to full passive confinement. Recent studies conducted by several researchers (Mohammad et al. 2012, West et al. 2005, and Canestrari and Santagata 2005) indicate that the interface bond strength increases with the application of a normal confining stress in conjunction with other test parameters, such as rate of loading and temperature.

In this study, the shear strength levels for different normal stress magnitudes and temperatures were computed with a displacement rate of 2.5 mm/min using Canestrari et al.'s (2013) equations for cationic emulsion, as shown in Figure 3-3. According to Figure 3-3, a normal confining stress has a significant effect on the interface bond strength.

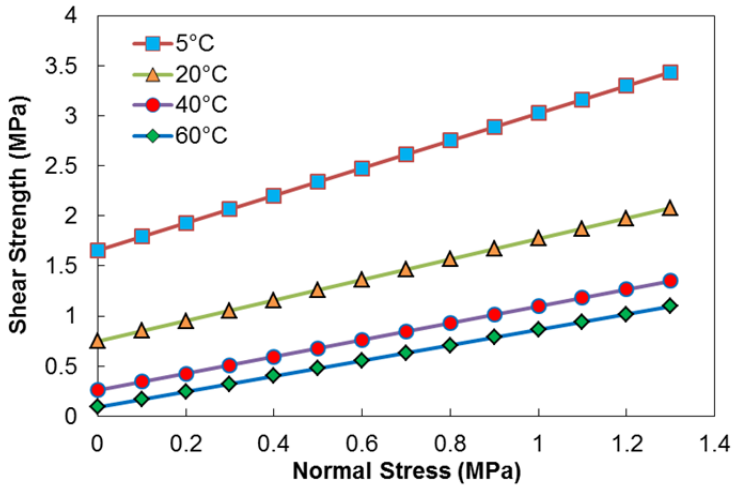

Figure 3-3 Shear strength versus normal stress for 100-mm (4 in.) samples, 2.5 mm/min rate of loading, and cationic emulsion, based on equations by Canestrari et al. (2013).

However, the question remains as to the level of normal confining stress that should be used in direct shear testing to evaluate the interface bond strength. A mechanistic methodology is necessary to provide guidance for the selection of the appropriate level of normal confining stress. In order to determine the appropriate confining stress level for evaluating the shear bond strength of an asphalt concrete interface, it is necessary to understand and quantify the pavement responses computed using the LVECD program for the various conditions of the three different pavement structures. The state of the stress and strain in the pavement section should be reflected in the selection of the appropriate level of the normal confining stress.

The method presented in Figure 2-5 was used in this study to find the magnitude of the normal stress level that corresponds to the location of the MSR. Using this method, the range of normal stress that corresponds to the location of the MSR for each rolling resistance coefficient for the conditions under consideration in this study was determined. It was found that the normal

confining stress (normal stress) ranges from 162.63 kPa (23.59 psi) to 278.28 kPa (40.36 psi). In order to encompass the range of normal confining stresses, three normal confining stress levels of 68.95 kPa (10 psi), 275.79 kPa (40 psi), and 482.63 kPa (70 psi) were chosen for the experimental program in this study.

3.6 Interface Shear Bond Strength Test

In this study, interface shear bond strength tests were conducted using two-layered asphalt concrete specimens with various interlayer conditions. The MAST and a digital image correlation (DIC) system in constant displacement-control mode were used to measure the maximum shear load and its corresponding shear displacement in order to evaluate the interface shear bond strength. The tests were performed at the three loading rates, four temperatures, and three normal confining stresses in tension mode until failure occurred in the specimen. Prior to testing, samples were conditioned in an environmental chamber to maintain the test temperature for three hours, and a normal confining stress level was confirmed if the desired confining stress level was achieved. The load application program for shear tests consists of a five-second rest period followed by three different loading rates with ramp shapes.

3.7 Pneumatic Adhesion Tensile Testing Instrument (PATTI) Test

Due to the observed difficulty in attempting to develop the proper bond strength between the contact surfaces of the previously mentioned test instruments and the existing tack-coated asphalt surface, the research team proposed placing an aluminum plate on the existing asphalt surface before the application of the tack coat in the field, and then performed the bond strength test in the lab using the sample collected on the aluminum plate.

The Pneumatic Adhesion Tensile Testing Instrument (PATTI) was selected to measure the tensile bond strength of a tack coat applied on the aluminum plate *in situ*. PATTI is an ASTM D4145 Type IV adhesion tester. The ASTM D4145 standard covers the procedures to measure the pull-off strength of a coating system from metal substrates (ASTM D4541). The major advantage of the PATTI test is that it is a standard procedure. In addition, PATTI tests can be performed in a controlled environment (i.e., temperature- and humidity-controlled) in a climate chamber and also can be performed in the field. The ASTM D4145 adhesion tester type IV is a self-aligning automated PATTI that has a control module, detaching assemblies or pistons, and a pressurized air source, as shown in Figure 3-4. The PATTI test pullout stub used in this study has a diameter of 12.5 mm (0.5 in.). The pistons are available in several different sizes and load ranges.

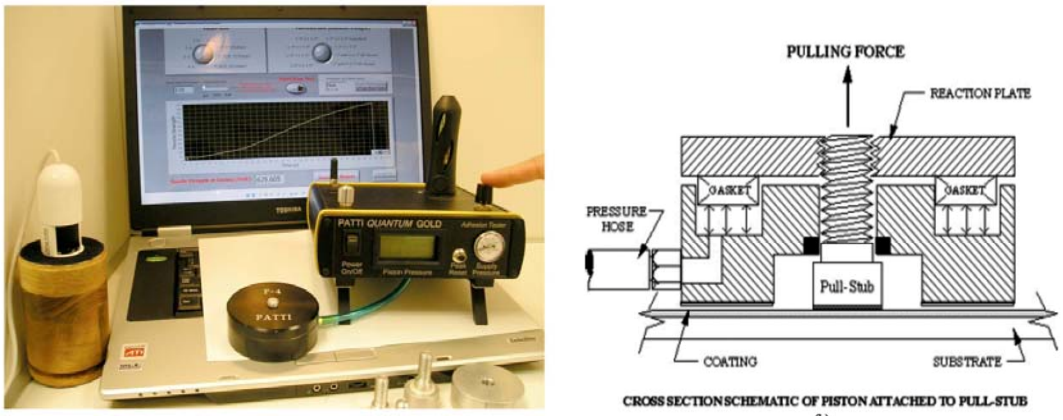

(a) (b)

Figure 3-4 (a) PATTI (type IV self-alignment adhesion tester) and (b) schematic of PATTI piston (ASTM D4145 2009).

Chapter 4 Test Results and Discussion

4.1 Interface Shear Bond Strength Results

Figure 4-1 presents the interface shear bond strength test results for the specimens with CRS-2 emulsion at the layer interface at the loading rate of 5.08 mm/min (0.2 in./min), normal confining stress of 482.63 kPa (70 psi), and at 35°C. Figure 4-1 (a) and (b) show the typical crosshead linear variable differential transducer (LVDT) displacement measurements and the stress responses in a monotonic tension test, respectively.

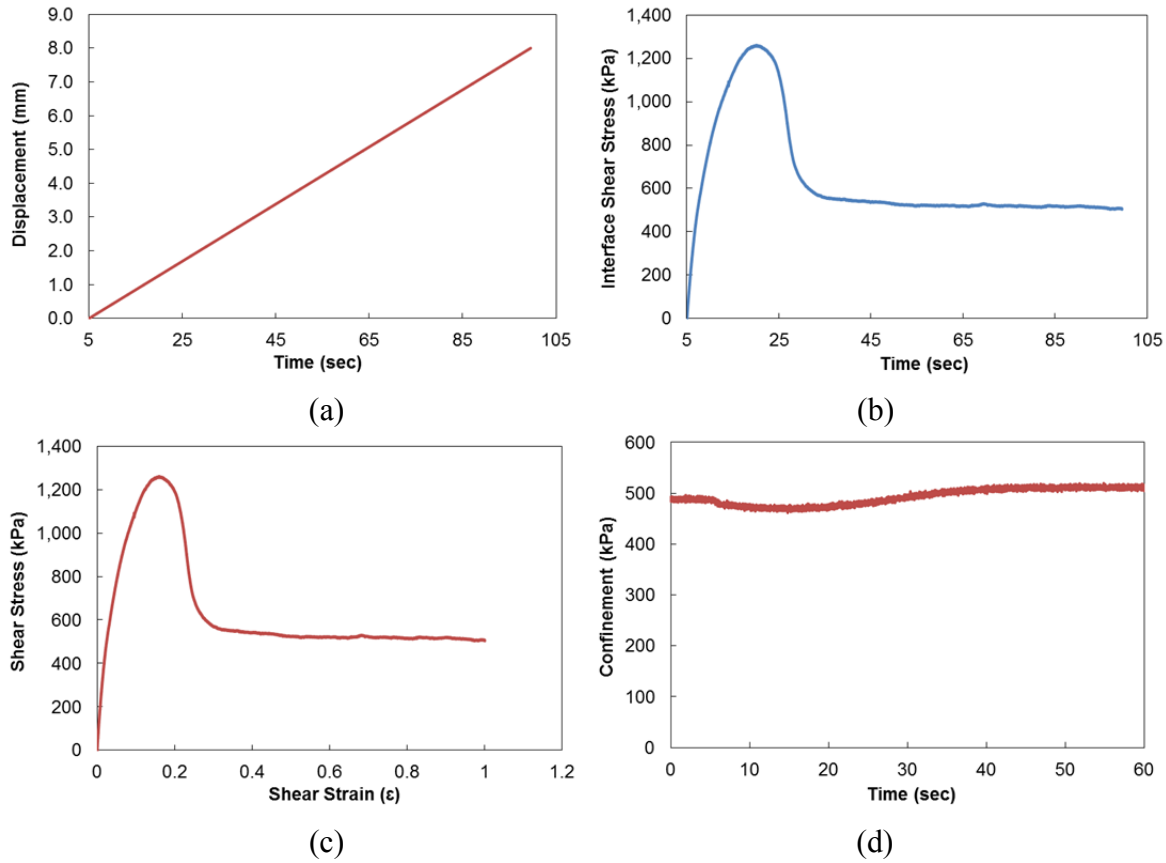

Figure 4-1 Interface shear bond strength results: (a) displacement versus time, (b) interface shear stress versus time, (c) shear stress versus shear strain, and (d) normal confining stress (confinement) versus time: CRS-2 emulsion, 5.08 mm/min (0.2 in./min) loading rate, 482.63 kPa (70 psi) normal confining stress, and at 35°C (95°F).

As shown in Figure 4-1 (d), the normal confining stress initially is maintained at a desired level, but it gradually decreases as the specimen approaches the failure point. After failure occurs, the normal confining stress level slightly increases. This phenomenon results from the fact that

the possible friction that could occur among the components involved in applying the normal confining stress was eliminated in the design stage of the MAST, and consequently, a set of four springs allows for dilation of the sample.

In the interface shear bond strength tests, failure occurred exactly at the layer interface of all the samples, as shown in Figure 4-2.

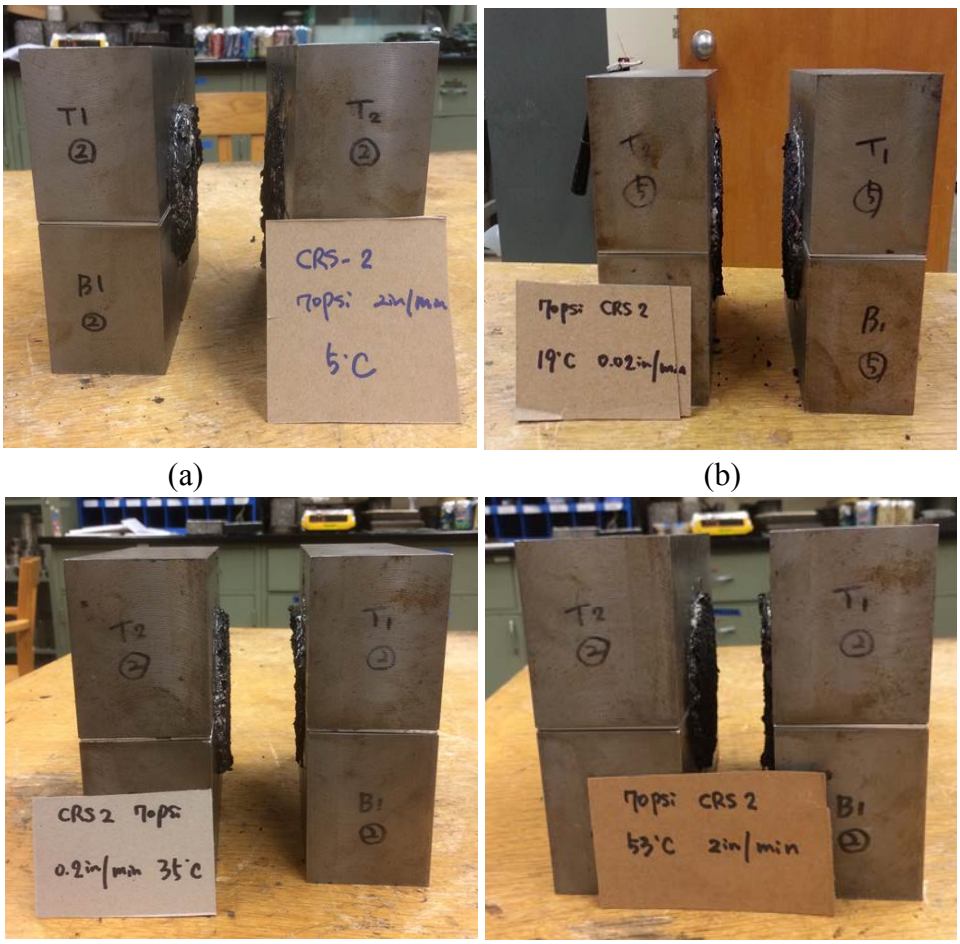

(a) (b)

(c) (d)

Figure 4-2 Failure mode of the interface shear bond strength test samples for different test conditions: (a) 50.8 mm/min (2 in./min) at 5°C, (b) 0.508 mm/min (0.02 in./min) at 19°C, (c) 5.08 mm/min (0.2 in./min) at 35°C, and (d) 50.8 mm/min (2 in./min) at 53°C: CRS-2 emulsion and 482.63 kPa (70 psi) normal confining stress.

4.2 Validation of Time-Temperature Superposition Principle for Interlayer System with Tack Coat

Asphalt concrete is well known as thermorheologically simple (TRS) material if it is constrained within the linear viscoelastic range. The time-temperature superposition (t-TS)

principle is a well-known characteristic of TRS materials. This study investigated whether asphalt concrete material with a tack coat as an interlayer system is also TRS material in shear failure mode. Shear tests were conducted at different loading rates and temperatures using the Modified Advanced Shear Tester (MAST).

4.2.1 Phase 1: Verification of Time-Temperature Superposition Principle for Shear Strength

The applicability of the t-TS principle for shear strength was shown to be valid using samples fabricated with each study emulsion at the layer interface and specific normal confining stresses, as presented in Table 4.1.

Table 4.1 Shear strength test combination for each phase.

Tack Coat	Normal Confining Stress		
	68.95 kPa (10 psi)	275.79 kPa (40 psi)	482.63 kPa (70 psi)
CRS-2	Phase 2	Phase 2	Phase 1
CRS-1h	Phase 2	Phase 2	Phase 1
NTCRS-1hM (Trackless)	Phase 2	Phase 1	Phase 2
No Tack Coat	Phase 1	Phase 2	Phase 2

Shear strength data at various temperatures can be shifted horizontally onto an arbitrarily selected reference temperature to form a single curve, which is called the mastercurve, assuming that the t-TS principle is valid even in shear failure mode. For this study, 5°C was chosen as the reference temperature. Figure 4-3 shows the interface shear strength with respect to the reduced DIC strain rate for the samples, with each study emulsion at the layer interface under the specific normal confining stress. The validity of the t-TS principle was confirmed by comparing the shear strength values determined from two adjacent temperatures but at the same reduced DIC strain rate. One representative curve, termed the *shear strength mastercurve*, is presented in Figure 4-3 for each study emulsion. The figure also shows that the shear strength mastercurve follows a power form and is a function of both shear strain rate and temperature, thereby demonstrating that the t-TS principle is valid for shear strength using the dynamic modulus shift factors. It is worth noting that the t-T shift factors that were determined from the dynamic modulus tests were used successfully to develop the shear strength mastercurves presented in Figure 4-3.

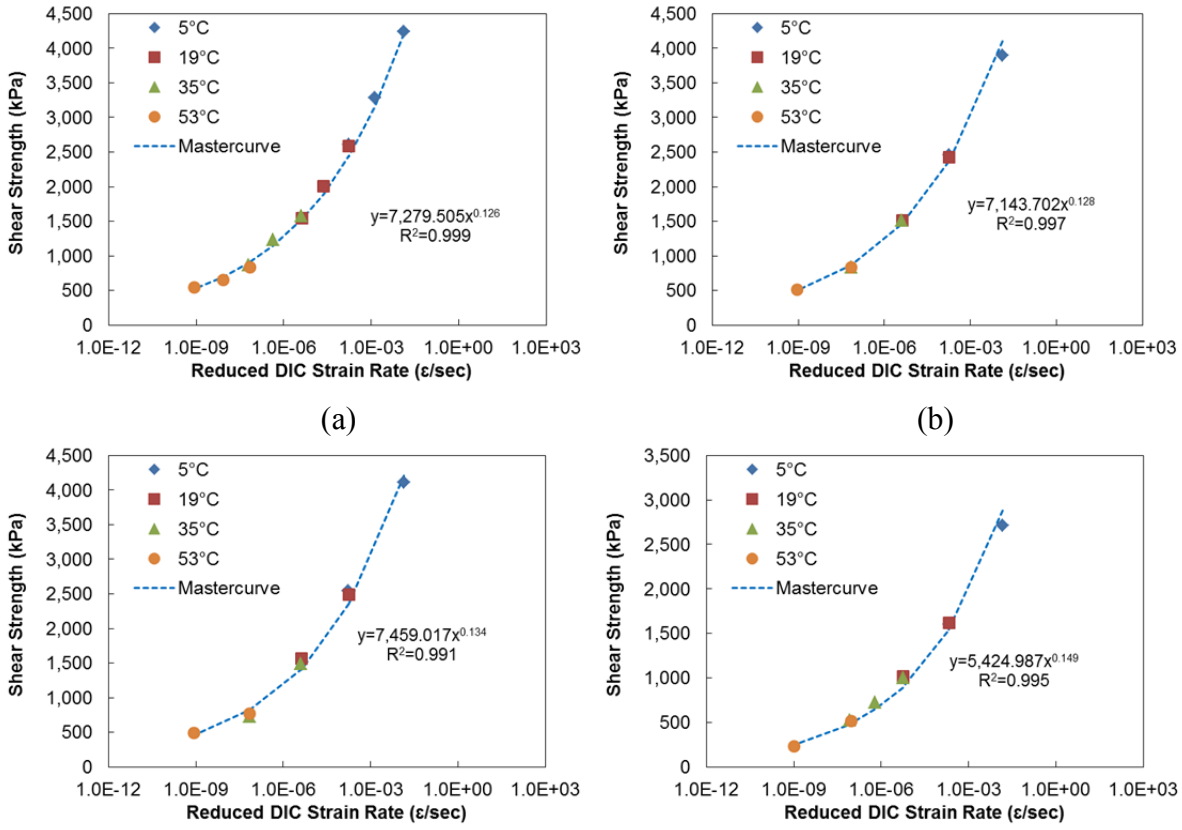

Figure 4-3 Verification of t-TS principle for shear strength and mastercurves: (a) CRS-2 emulsion and 482.63 kPa (70 psi) normal confining stress, (b) CRS-1h emulsion and 482.63 kPa (70 psi) normal confining stress, (c) NTCRS-1hM (trackless) emulsion and 275.79 kPa (40 psi) normal confining stress, and (d) no tack coat and 68.95 kPa (10 psi) normal confining stress.

4.2.2 Phase 1: Verification of Time-Temperature Superposition Principle for the Interlayer Shear Stiffness

In this section, the t-TS principle is verified for the interlayer shear stiffness, which is assumed to be a characteristic value that can be used to measure the level of interlayer bonding. In this study, a new calculation method to determine the interlayer shear stiffness is proposed based on the idea that data that deviates from a pure power law cannot be utilized to apply the t-TS principle in a state of growing damage (Chehab et al. 2002). Thus, DIC displacement following a pure power law until failure of the specimen and the corresponding shear stress amplitude in an interface shear stress-displacement curve were used to calculate the interlayer shear stiffness value. Detailed information regarding this calculation method can be found in Appendix D.

Consequently, if the DIC displacement following a pure power law until failure of the specimen and the corresponding shear stress amplitude are used for the interlayer shear stiffness

calculation, then the applicability of the t-TS principle is verified for the interlayer shear stiffness, as shown in Figure 4-4.

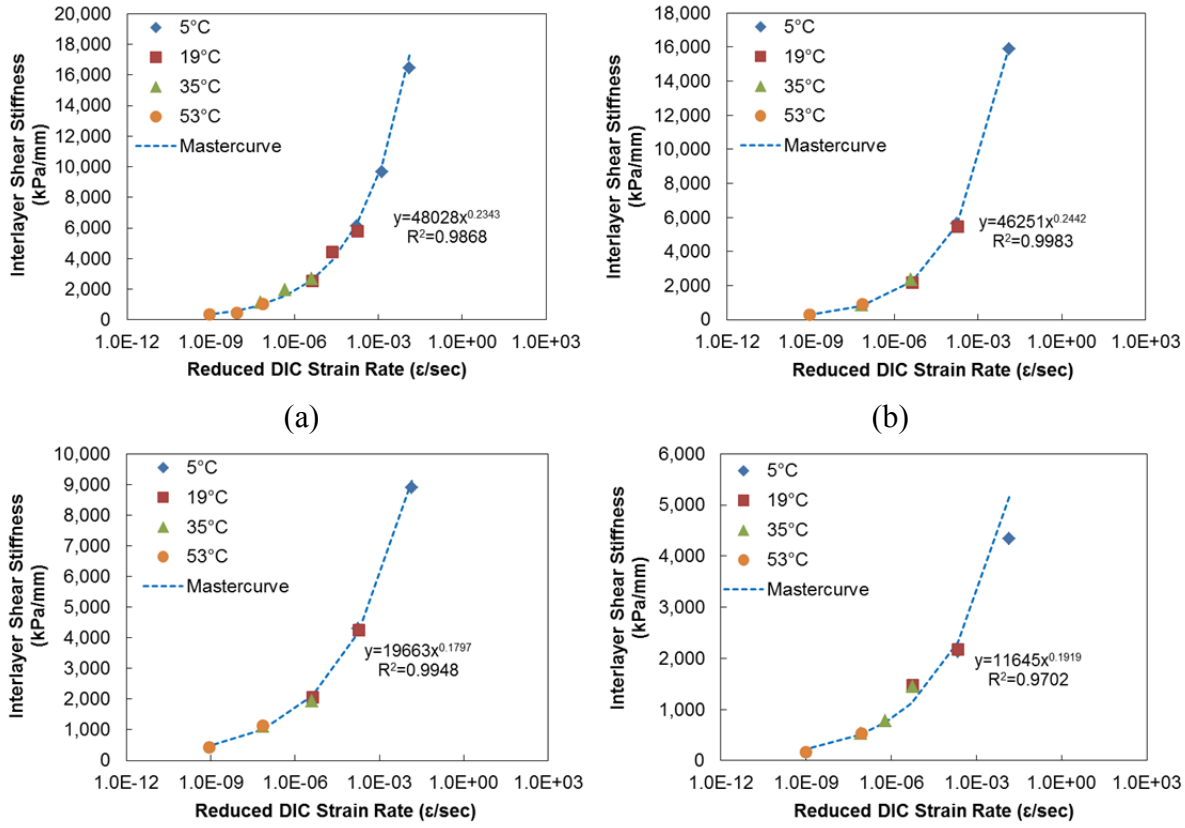

Figure 4-4 Verification of t-TS principle for interlayer shear stiffness using DIC displacement following a pure power law: (a) CRS-2 emulsion and 482.63 kPa (70 psi) normal confining stress, (b) CRS-1h emulsion and 482.63 kPa (70 psi) normal confining stress, (c) NTCRS-1hM (trackless) emulsion and 275.79 kPa (40 psi) normal confining stress, and (d) no tack coat and 68.95 kPa (10 psi) normal confining stress.

4.2.3 Phase 2: Development of Shear Strength Mastercurve

The main purpose of the application of the t-TS principle is the development of a shear strength mastercurve that reflects the function of the reduced strain rate at a desired reference temperature. Developing such a mastercurve enables the determination of the strength of a material at any strain rate and temperature combination. In this study, the t-TS principle for shear strength was proven to be completely valid for specimens with different tack coat materials at the layer interface in Phase 1. In this section, shear strength mastercurves are developed for the remaining test combinations, as presented in Table 4.1, using four reduced strain rates.

Effects of Loading Rate and Temperature

Figure 4-5 presents the shear strength mastercurves developed at various confining stresses using samples with the four different study emulsions at the layer interface. It is well known that shear strength increases at a high reduced strain rate (low temperature/high strain rate combinations). As shown in Figure 4-5, the strength mastercurves indicate the increase in shear strength as the reduced strain rate increases.

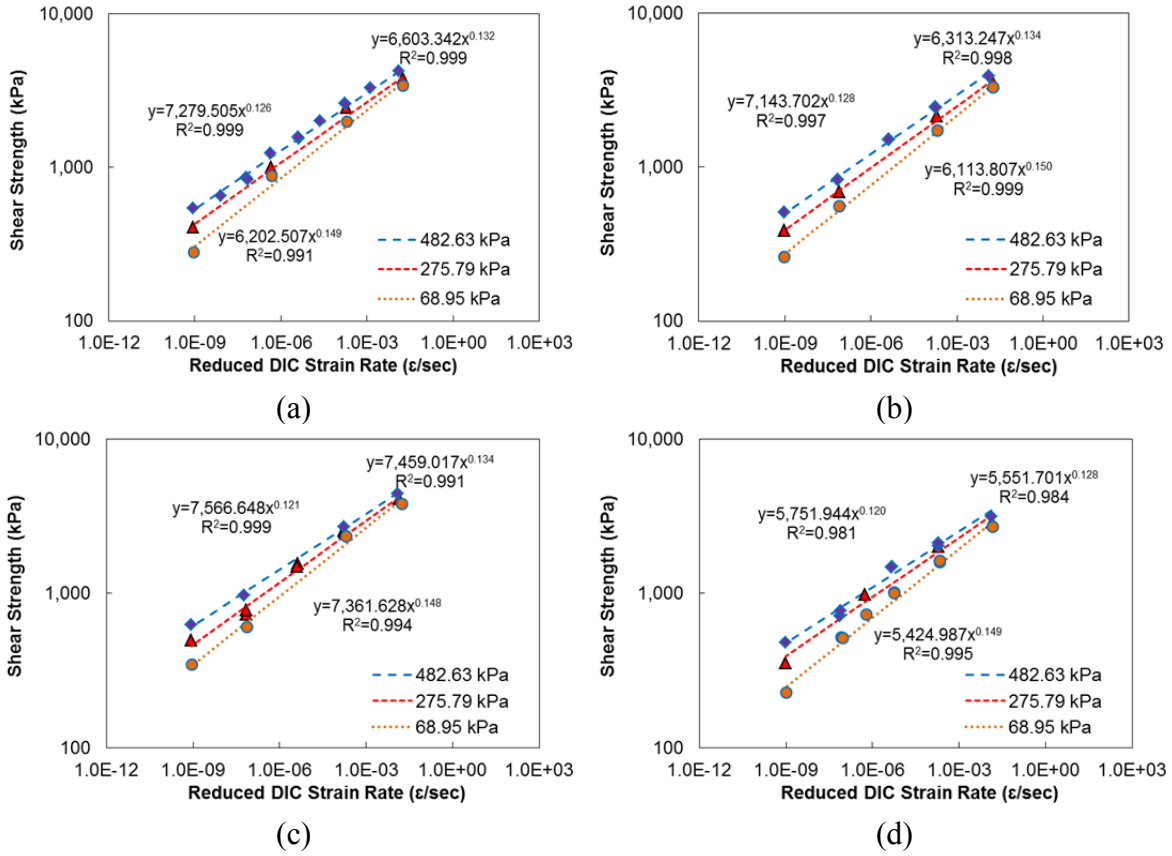

Figure 4-5 Shear strength mastercurves developed at various confining stresses: (a) CRS-2 emulsion, (b) CRS-1h emulsion, (c) NTCRS-1hM (trackless) emulsion, and (d) no tack coat. Note: The numbers in the legends represent the normal confining stresses used in this study.

Effect of Normal Confining Stress

Figure 4-5 also indicates that the shear strength obviously increases with the application of a normal confining stress at a low reduced strain rate (i.e., high temperature/low strain rate combinations). That is, the shear strength clearly is affected by the normal confining stress, whereas the effect of a normal confining stress is less for a high reduced strain rate, i.e., when the temperature is low and/or the strain rate is fast. Generally, a greater normal confining stress causes higher shear strength levels, which is observed more obviously at a low reduced strain rate (i.e., high temperature/low strain rate).

Effect of Tack Coat Type

Four types of tack coat material were tested in this research: CRS-2, CRS-1h, NTCRS-1hM (trackless tack coat), and no tack coat. Figure 4-6 shows the effects of the different tack coats on the shear strength values determined at three different normal confining stresses. Among the emulsified tack coats, NTCRS-1hM (trackless tack) exhibits the highest interface shear strength, followed by CRS-2, CRS-1h, and no tack coat, as shown in Figure 4-6. Also, it is noted that the CRS-2 emulsion has slightly higher strength values than the CRS-1h emulsion, as the CRS-2 samples contain a larger quantity of asphalt residue at the layer interface than the CRS-1h samples.

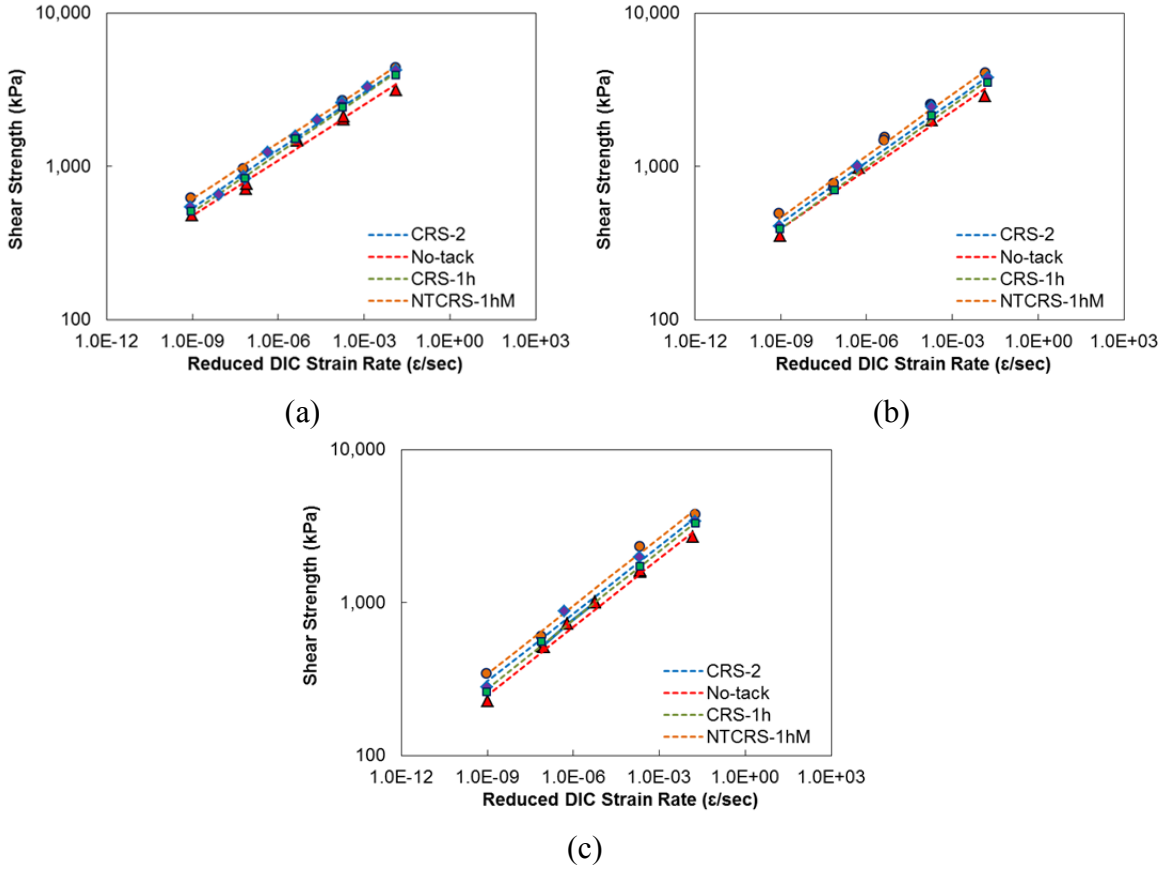

Figure 4-6 Effects of different tack coat materials on shear strength: (a) 482.63 kPa (70 psi) confining stress, (b) 275.79 kPa (40 psi) confining stress, and (c) 68.95 kPa (10 psi) confining stress.

4.3 PATTI Test Results

In this section, the results of the PATTI tests for two emulsions (CRS-2 and CRS-1h) at four temperatures (5°C, 19°C, 35°C, and 53°C) are presented. Paper was placed around the pullout stub to prevent the emulsion from adhering to the bottom of the PATTI pressure ring. All

tests were performed in an environmental chamber after one hour of conditioning at each test temperature.

As shown in Figure 4-7, failure occurred in the binder (i.e., cohesion failure of the emulsion); this failure occurred for all of the tested samples.

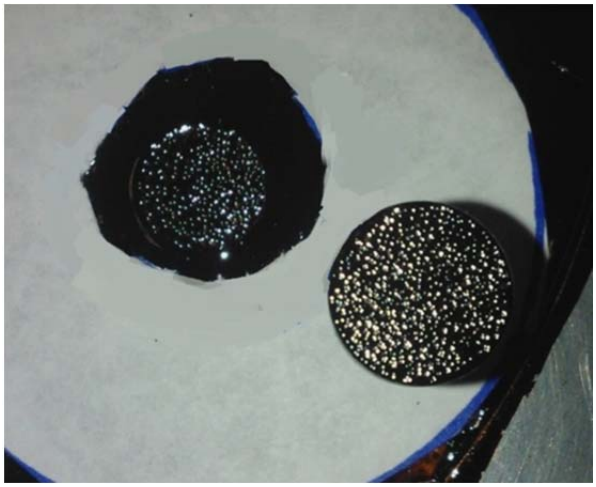

Figure 4-7 Failure mode of the PATTI test samples (i.e., cohesion failure of the emulsion).

According to the results of the PATTI pullout tests for the CRS-1h and CRS-2 emulsions on an aluminum plate, the CRS-1h emulsion showed higher tensile strength than the CRS-2 emulsion. The loading rate for the PATTI test was maintained at around 689.47 kPa/s (100 psi/s). The PATTI bond strength test results for the CRS-1 and CRS-2 emulsions can be found in Appendix D.

Figure 4-8 presents the semi-log plots of stress versus temperature for the CRS-2 and CRS-1h asphalt emulsions. The prediction functions shown in Figure 4-8 were used to predict the tensile bond strength of the tack coats applied to the aluminum plate. Knowing the temperature, the bond strength of the tested emulsions could be predicted by the functions shown in Figure 4-8 for the CRS-1h and CRS-2 emulsions.

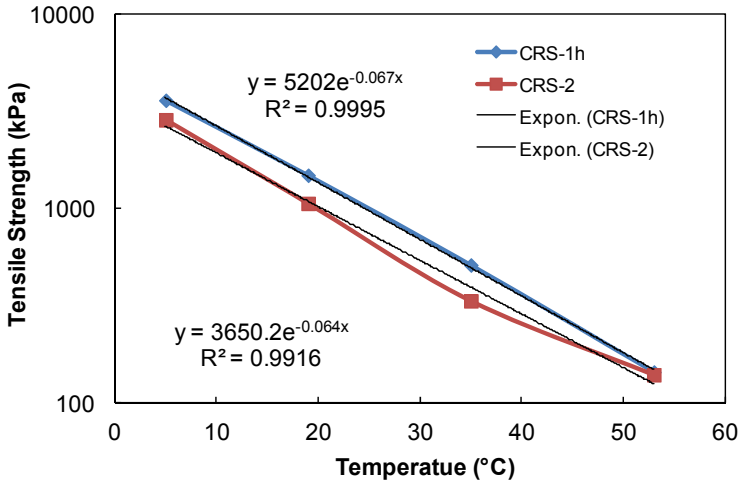

Figure 4-8 PATTI test prediction equations.

Chapter 5 Analysis Framework

5.1 Development of Model Equation for the Prediction of Interface Shear Strength

In this section, a universal model equation is presented that can determine the shear strength at the interface of asphalt concrete layers with different tack coat materials, based on the shear strength data sets tested at various temperatures, loading rates, and normal confining stresses. Specifically, this model equation enables the prediction of the shear strength of asphalt concrete pavements that have tack coat materials between the layers at any strain rate and temperature combination as well as at any normal confining stress. In order to develop the prediction model equation for interface shear strength, correlation analysis was conducted for the shear strength data measured at various temperatures, loading rates, and normal confining stresses. Figure 4-5 (in the previous section) shows that shear strength as a function of reduced strain rate indicates a strong power function with a high regression coefficient. Figure 5-1 shows that shear strength is linearly dependent on the normal confining stress.

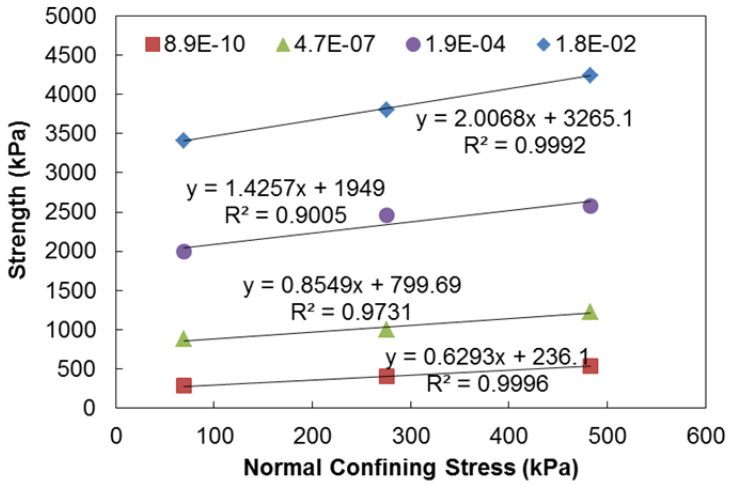

Figure 5-1 Correlation between shear strength and normal confining stress (layer interface condition: CRS-2 emulsion). Note: The numbers in the legends represent different reduced strain levels.

The comprehensive correlation analysis of the shear strength data sets led to the following Equation (2) to predict the shear strength at the layer interface in terms of the effects of normal confining stress.

$$\tau_f = (a \times \dot{\gamma}_R^{\ b}) \times \sigma_c + c \times \dot{\gamma}_R^{\ d} + e \times \sigma_c = (a \times \dot{\gamma}_R^{\ b} + e) \times \sigma_c + c \times \dot{\gamma}_R^{\ d} \qquad (2)$$

where

τ_f = shear strength at the layer interface, kPa,

$\dot{\gamma}_R$ = reduced shear strain rate, and

σ_c = normal confining stress, kPa.

The corresponding coefficients *a*, *b, c, d,* and *e* in Equation (2) are shown in Table 5.1 for four different asphalt layer interface conditions, i.e., for the four different tack coat materials.

Table 5.1 Coefficients for different asphalt layer interface conditions.

Layer Interface Condition	a	b	c	d	e	R^2
No Tack Coat	1.2058	0.0329	5229.5	0.1612	0.15	0.988
CRS-2	2.6116	0.0685	6140.4	0.1564	0.18	0.997
CRS-1h	1.8174	0.0564	6075.3	0.1566	0.16	0.994
NTCRS-1hM (Trackless)	1.9341	0.0496	6956.0	0.1528	0.20	0.990

Figure 5-2 presents comparisons between the shear strength mastercurves predicted by the universal model equation and the shear strength mastercurves determined from actual tested

shear strength data. This figure indicates that the developed model can accurately predict the interface shear strength for each tack coat at any strain rate and temperature combination as well as at any normal confining stress. The ultimate goal of this model is to predict the interface shear strength for a given tack coat condition based on the shear strain rate and normal stress state determined from the LVECD program for any given pavement structure. Further, the model can contribute to the development of a mechanistic framework that can prevent shear bond failure between the asphalt layers by comparing the shear stress calculated from the pavement analysis program for a critical condition to the shear strength determined from the prediction model developed in this study.

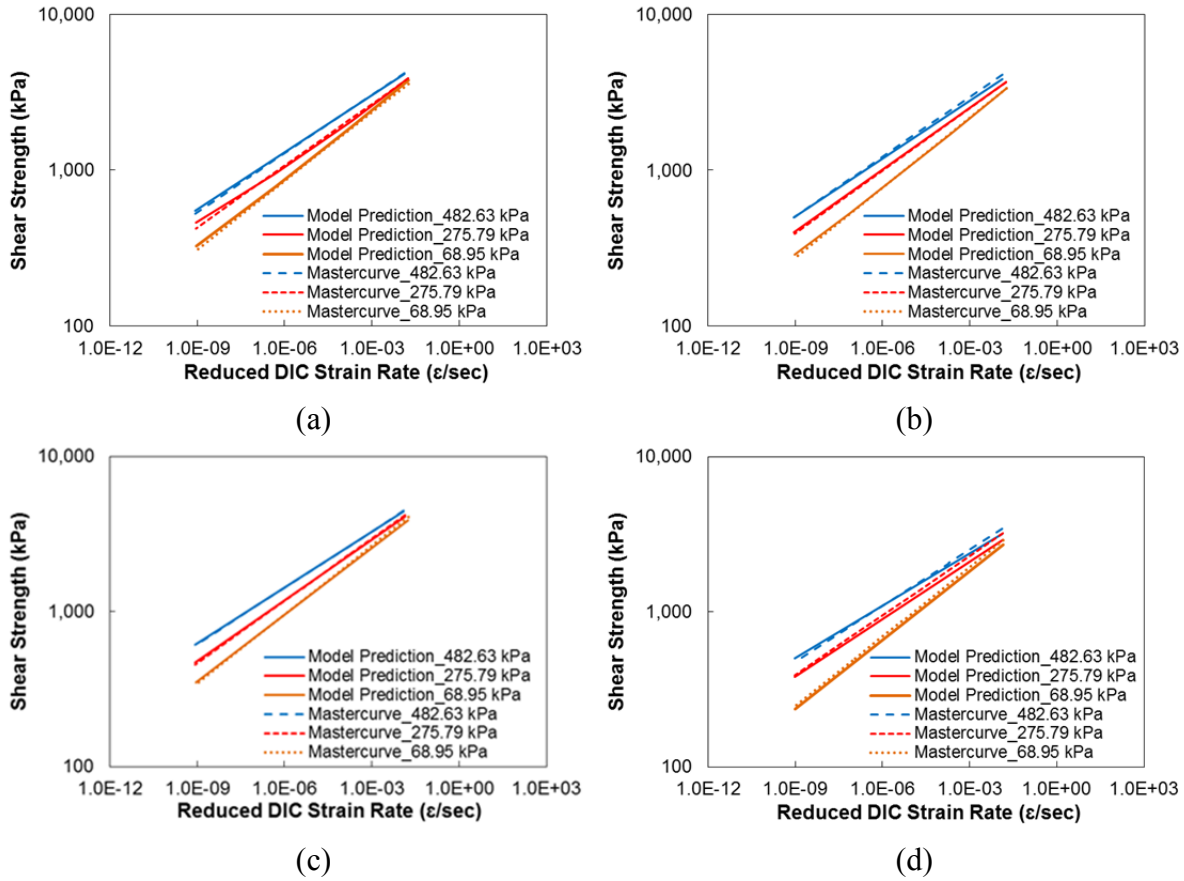

Figure 5-2. Comparisons between shear strength mastercurves predicted by Equation (2) and shear strength mastercurves determined from actual shear strength data sets: (a) CRS-2, (b) CRS-1h, (c) NTCRS-1hM (trackless), and (d) no tack coat.

5.2 Development of Analysis Framework for Determination of Interface Debonding Potential

This section provides an analysis framework to evaluate the debonding potential at the asphalt concrete layer interface. This analysis framework includes procedures for the prediction of the interface shear strength using Equation (2), the calculation of the shear stresses for the given conditions using the LVECD program, and determination of the MSR as a shear failure criterion.

The states of the stress and strain at the layer interface were analyzed for the various conditions cited in Section 2.1 using the LVECD program. It is noted that the computational simulation conditions and parameters used in the LVECD program are identical to those used in the previous simulations described in Chapter 2, except that the material properties of the typical surface layer are substituted by the specific material properties used in the experimental tests of

this study. From the LVECD simulations, shear stresses, normal stresses, and shear strain rates at various locations of the layer interface of interest are determined under moving wheel loads. Then, the calculated shear strain rates and normal stresses and predicted temperature at the interface are used in Equation (2) to determine the shear bond strength levels (τ_s) at various locations of the layer interface for the given tack coat material. Lastly, a profile of the shear stress ratio, i.e., the ratio of the computed shear stress (τ_{max}) to the shear bond strength (τ_s), under the tire at the asphalt concrete layer interface, was generated to determine the MSR, which then could be used to determine the integrity of the interface bond.

The MSRs for asphalt concrete layers with different tack coat materials between the layers at different temperatures, speed levels, axle loads, and pavement structures under the 'only rolling' resistance coefficient of 0.55 for the braking condition are tabulated in Table D.12 through Table D.15 in Appendix D. The rolling resistance coefficient of 0.55 was used because it provides the most critical shear stress values compared to the other coefficients under consideration (i.e., 0.35 and 0.45).

One noteworthy point that can be observed from Table D.12 through Table D.15 in Appendix D is that all the MSRs are less than 1.0, which indicates no shear failure at the asphalt concrete layer interface. However, this result does not fully represent the critical states under realistic loading conditions in service because the computational simulations performed in this research consider only one single braking action. The debonding distress in the field might occur under repeated braking conditions or at a single braking action, depending on the speed and weight of the vehicle. Therefore, a MSR close to 1.0 implies a much higher potential for the interface debonding distress between the asphalt concrete layers due to repeated braking. Consequently, an asphalt concrete layer with no tack coat at the layer interface has a much higher potential for the interface debonding distress because it has higher MSR values than the other conditions in Table D.12 through Table D.15 in Appendix D.

According to the MSR results, a slower speed clearly corresponds to a higher shear ratio. That is, although both the shear stress and shear strength values increase as the vehicle speed increases, the shear ratio could be higher at a slower speed than at a faster speed because the rate of reduction in shear strength as the speed decreases is much greater than that of shear stress. Also, the MSR increases with an increase in temperature. Moreover, as the axle load increases, the MSR increases as well. It should be noted that the results in Table D.12 through Table D.15 indicate that the higher temperature, lower speed, and heavier axle load are critical conditions with respect to the debonding distress at the asphalt concrete layer interface.

The NTCRS-1hM (trackless tack coat) emulsion has the highest shear strength of all the emulsions, thereby obtaining a better bond at the layer interface than the other emulsions. Consequently, all the pavement structures with the NTCRS-1hM emulsion as a tack coat material at the asphalt concrete layer interface indicated better resistance against the debonding distress with lower MSRs than the pavements with the other tack coat conditions, as expected. Therefore, these tables indicate that a better quality of tack coat could reduce the possibility of the

debonding distress as well as confirm the need for a tack coat between the asphalt structural layers.

5.3 Prediction of the Interface Shear Strength between Asphalt Layers

The PATTI test results were compared to the interface shear strength test results obtained for the laboratory gyratory-compacted specimens. The interface shear strength was measured by the MAST in displacement mode. Conversely, PATTI was used to perform the tensile bond strength tests in load-controlled mode. Therefore, to compare the results obtained from the two test devices (i.e., the MAST and PATTI), the stress rates of the shear strength tests needed to be predicted using a proper approximation method.

The chord method was used in this study to approximate the stress rates of the test results obtained using the MAST. In the chord method, the slope of the chord between points within 2.5 percent and 45 percent of the shear strength on the shear stress versus time graph was assumed as the stress rate of the shear strength test. In the region below 45 percent of the shear strength, the development of cracks was assumed to be at a minimum, and the material was assumed to be in the elastic range and the deformation assumed to be linear. The calculated stress rates for the CRS-2 and CRS-1h emulsions at the temperatures of 5°C, 19°C, 35°C, and 53°C with the different strain rates are presented in Appendix D.

The relationship between the strain rate and stress rate for each temperature was developed by plotting the stress rates versus the strain rates. Using the averaged stress rate for each temperature, the shear strain rate at each temperature was calculated using the developed equation for each emulsion. The strain rate that corresponded to each temperature for the PATTI tests was divided by the shift factor for that temperature (asphalt mixture shift factor) to calculate the reduced strain rate. The interface shear strength for each emulsion was calculated using Equation (2). A correlation equation between the tensile bond strength measured by PATTI and the interface shear bond strength measured by the direct shear test of the interface with normal confining pressure was developed to predict the interface shear bond strength for each emulsion. The calculated interface shear strength values versus the tensile bond strength values for the CRS-2 and CRS-1h emulsions at the confining pressures of 482.6 kPa (70 psi), 275.8 kPa (40 psi), and 69 kPa (10 psi) are shown in Figure 5-3 for the CRS-2 and CRS-1h emulsions, respectively. Detailed information can be found in Appendix D.

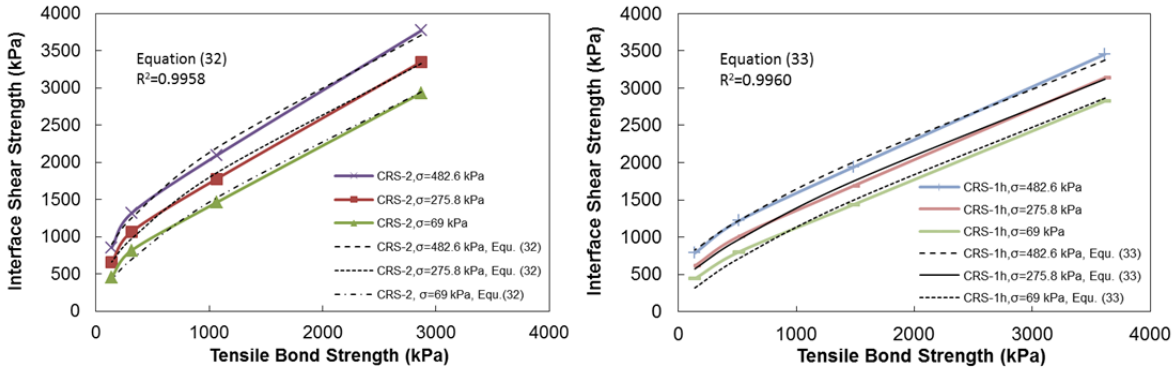

(a) (b)

Figure 5-3 Interface shear strength versus tensile bond strength for each emulsion: (a) CRS-2 and (b) CRS-1h.

Chapter 6 Conclusions and Recommendations

6.1 Conclusions

This research presents an analytical and experimental framework to evaluate the potential for debonding at the layer interface of asphalt concrete pavements, which is critical to the design and performance of highway asphalt pavements. In this study, computational analysis was conducted to determine the critical stress and strain states in layered asphalt pavements under moving vehicle loads using the LVECD computer program. This computational analysis led to a greater understanding of the critical stresses that are involved in debonding and the ways that such stresses are affected by pavement design parameters and environmental conditions. Moreover, a direct shear test protocol that can be used in the laboratory to evaluate the shear bond strength between asphalt layers was developed. Then, interface shear bond strength tests were conducted using two-layered asphalt concrete specimens with various interlayer conditions using the MAST and DIC system in constant displacement-control mode. The applicability of the t-TS principle was verified for both interface shear bond strength and the interlayer shear stiffness values measured from the two-layered specimens with various interlayer conditions. Then, a shear strength mastercurve was constructed to determine the shear strength of a material at any strain rate and temperature combination. In addition, a prediction model was developed that can determine the shear bond strength at the interface of asphalt concrete layers with different tack coat materials at various temperatures, loading rates, and normal confining stresses. Further, a mechanistic methodology was introduced for the evaluation of the debonding potential at the layer interface of asphalt concrete pavements using the model equation (Equation (2)) to predict interface shear strength, shear stress levels determined from computational analysis, and the MSR concept as a shear failure criterion. The systematic and mechanistic framework developed in this study employs the MSR concept as a shear failure criterion and provides a tool to evaluate the effects of various loading, environmental, and pavement factors on the debonding potential of asphalt pavements. The overall advantages of the mechanistic framework and approach using the LVECD analysis tool will help lead to better understanding of the debonding mechanism, proper selection of the tack coats, and economic benefit in highway pavement maintenance and rehabilitation costs.

The effect of the debonding of the surface layer on the overall behavior of the pavement structure was demonstrated. In a pavement with a debonded surface layer, a rolling wheel passing over the pavement creates tensile vertical cracking around the wheel and creates the delamination distress.

Despite the importance of the tack coat application on the bond strength of the asphalt interface and the long-term behavior of the pavement structure, no standard quality control method is currently available to ensure the proper application of tack coats *in situ*. During the last decade, several instruments have been developed by various researchers to evaluate the bond

strength of tack coats in the field immediately after the application of the tack coat on the existing asphalt layer and before the construction of the subsequent asphalt layer. Two instruments for testing tack coat performance in the field, i.e., ATacker™ and TACKY, were evaluated as part of this study. Based on the tests results, these instruments are not recommended for field tack coat material quality control at the current performance level of the instruments.

The following conclusions have been drawn based on the computational analysis and experimental work conducted in this research:

6.1.1 Computational Analysis Work

- The LVECD program analysis results show that the location of the maximum shear stress is at a depth of 5.08 cm (2.0 in.) below the surface course and that the shear stress around the layer interface is a significant factor that can induce pavement distress and interface debonding.
- The effects of temperature, speed, load level, structural type, and rolling resistance coefficient in terms of stress were evaluated using LVECD program simulations. Based on the evaluation of these parameters, the critical conditions for the LVECD program simulations in terms of shear stress levels were determined as the following: thin pavement, 106.8 kN (24 kips), 5°C, 88 km/hour (55 mph), and a rolling resistance coefficient of 0.55 for the braking condition.
- The LVECD program simulations were performed to evaluate the shear bond failure at the asphalt concrete layer interface under wheel loading using the MSR concept as a shear failure criterion. The states of the stress and strain were then analyzed to predict the shear strength and to determine the critical location for shear failure.
- Both maximum normal stress and shear stress at the layer interface were located on the central longitudinal axis of the tire under the braking condition. Maximum normal stress occurred at the center of the tire on the central longitudinal axis, whereas maximum shear stress occurred around the edge of the tire on the central transverse axis under the free rolling condition.
- The shear ratio, defined as the maximum shear stress at the layer interface under a moving load over the interface shear bond strength determined from the shear strain rate and normal stress at a specific location under the tire, was used to determine the critical location for shear failure. Based on all of the conditions under consideration in this study, the location of the MSR under the braking condition was found to be on the central longitudinal axis all the time, although the distance from the center of the tire imprint along the central longitudinal axis might vary slightly. On the other hand, the location of the MSR under the free rolling condition was found to be around the edge of the tire on the central transverse axis all the time.
- In this research, a MSR that is close to 1.0 implies a high potential for interface debonding between the asphalt concrete layers due to the repeated braking conditions. An asphalt concrete layer with no tack coat at the layer interface showed a much higher

potential for the interface debonding with higher MSR values than the asphalt concrete layers with tack coats. In contrast, all the pavement structures with the NTCRS-1hM emulsion as the tack coat material at the asphalt concrete layer interface showed the best resistance to the debonding distress. Therefore, this outcome suggests that a better quality of tack coat could reduce the possibility of the debonding distress and confirms the overall need of a tack coat between the asphalt layers.

- Although the largest shear stresses were obtained from thin pavement, 106.8 kN (24 kips), 5°C, 88 km/hour (55 mph), and a rolling resistance coefficient of 0.55 for the braking condition using the LVECD simulations, the analysis of the MSR indicates that a high temperature, low speed, and heavy axle load are critical conditions that are conducive for the debonding distress at the asphalt concrete layer interface. A thin pavement structure is more vulnerable to the debonding distress at the asphalt concrete layer interface than other structures.
- The design of the interface between HMA layers should be included in the overall design of an asphalt pavement structure. In the interface design methodology presented in this study, the relationships among shear strength, shear strain rate, and normal stress at the interface of a layered pavement structure are included in the design of the interface in a layered pavement structure. The direct shear test with normal confining pressure should be used to predict the shear bond strength of the interface with a specific tack coat material.
- The horizontal tensile stress in the surface layer of the pavement structure that is behind the point of contact of the tire on the surface can cause crescent-shaped tensile cracks behind the tire on the surface layer. Therefore, the pavement surface layer should be designed for tensile failure at the critical conditions, i.e., high friction coefficient, high temperature, and low speed of the design vehicle. The tensile ratio, which is defined as the horizontal principal stress on the surface of the pavement over the tensile strength that corresponds to the tensile strain rate and temperature, is considered as the tensile failure criterion for the surface layer.
- Analysis of a pavement structure with a debonded surface layer in this study showed that debonding of the interface leads to the development of the delamination distress that is due to a rolling wheel and to the slippage distress in the pavement that is due to a braking wheel. A poor tack coat application in the field can cause debonding of the interface and overall failure of the pavement structure. Despite the importance of a proper tack coat application on the bond strength between the asphalt layers, currently no standard construction quality control procedure is available that ensures an appropriate tack coat application prior to the construction of the overlay.

6.1.2 Experimental Work

- In this study, a Superpave gyratory-based direct shear test protocol was developed that can be used in the laboratory to evaluate the shear bond strength between asphalt layers.

- A new direct shear device, MAST, which is capable of applying a normal confining stress to a specimen under constant normal stiffness (CNS) conditions in which normal stress is changeable during the shear loading process, was used successfully to evaluate the interface shear bond strength of cylindrical laboratory-fabricated specimens with various interlayer conditions between the asphalt layers.
- Debonding distress mechanisms were considered for the selection of the laboratory test conditions. In particular, the importance of normal confinement for shear bond strength evaluation was emphasized. Furthermore, the appropriate level of normal confining stress that represents the *in situ* environmental and traffic loading conditions was chosen for laboratory testing using a mechanistic methodology.
- In this study, a DIC system was applied successfully with an interface shear bond strength test to capture the failure behavior at the layer interface, instead of using conventional LVDTs that entail limitations due to the contact nature of the mounting method.
- The applicability of the t-TS principle was verified for both the interface shear bond strength and the interlayer shear stiffness measured from two-layered specimens with different tack coats at the layer interface using t-T shift factors determined from axial dynamic modulus tests. Also, a shear strength mastercurve that follows a power form was constructed to determine the shear strength of a material at any strain rate and temperature combination. This methodology helps to demonstrate that t-T shift factors determined from the dynamic modulus tests can be used successfully to develop shear strength mastercurves.
- Among the four emulsified tack coats tested in this study, the NTCRS-1hM (trackless tack) emulsion exhibited the highest interface shear strength followed by the CRS-2 and CRS-1h emulsions, and no tack coat.
- The verification of the t-TS principle was extended to include GlasGrid-reinforced asphalt concrete specimens with two different types of tack coat, PG 64-22 binder and SS-1 emulsion, between the layers. However, the application of t-T shift factors obtained from dynamic modulus tests of the mixture did not satisfy the t-TS principle for shear strength due to the presence of the GlasGrid embedded between the two layers. Hence, a new approach was attempted for studying the validity of the t-TS principle using the t-T shift factors of the PG binder and residue of the SS-1 emulsion. The results indicated that the t-T shift factor function determined for each tack coat is the appropriate function that can be used to shift the shear strength values of the GlasGrid-reinforced asphalt concrete interfaces and construct a unique shear strength mastercurve. A single mastercurve was constructed successfully for both the interface shear bond strength and the interlayer shear stiffness of the GlasGrid-reinforced asphalt concrete specimens, thereby clarifying that the t-TS principle is valid for GlasGrid-reinforced asphalt concrete specimens with PG 64-22 binder or SS-1 emulsion between the layers.

- A prediction model equation that can determine the shear strength for asphalt concrete layers with different tack coat materials between the layers was proposed based on the shear strength data sets tested at various temperatures, loading rates, and normal confining stresses. Comparisons between the shear strength mastercurves predicted by the proposed model equation and the shear strength mastercurves determined from actual tested shear strength data confirmed that the proposed model can provide an accurate prediction of the interface shear strength for each tack coat at any strain rate and temperature combination as well as at any normal confining stress.
- A prediction model allows the shear strength between the asphalt layers to be determined based on the states of the stress and strain calculated from a mechanistic pavement analysis program. Further, the model should be able to contribute to a mechanistic design that can prevent shear bond failure between the asphalt layers by comparing the shear stress calculated from the pavement analysis program for a critical condition to the shear strength determined from the prediction model developed in this study.
- For the quality control of tack coat materials in the field, PATTI can be used to evaluate the tensile bond strength of collected tack coat samples on an aluminum plate placed on the existing asphalt surface before the application of the tack coat by a distribution truck. The interface shear bond strength can be predicted using a correlation equation between the tensile bond strength measured by PATTI and the interface shear bond strength measured by direct shear tests of the interface with normal confining pressure.
- In this study, an *in situ* quality control methodology for tack coat materials is proposed to ensure the appropriate bonding quality of tack coat emulsions as well as to provide acceptable field performance. This methodology uses the PATTI test to evaluate the BBS of the tack coat material that is deposited onto aluminum plates from distribution trucks in the field. Quality control can be achieved by comparing the measured *in situ* BBS value at 12°C with the minimum required BBS value.

6.2 Recommendations for Further Research

The following recommendations for future research are based on the results of this study.

- Future research efforts are necessary to evaluate the accuracy and ruggedness of a new device that can ensure repeatability and reproducibility in order to develop AASHTO specification on this test method.
- Aggregate gradations, types of existing surface layer, and milling conditions can have a significant effect on interface bond strength; thus, these factors should be investigated using the same test protocol that was developed in this research.
- The MAST was designed to evaluate the shear properties of asphalt concrete specimens in both monotonic and cyclic modes. In this research, interface shear bond strength was evaluated only in monotonic mode. Therefore, shear tests of asphalt concrete with

interfaces should also be performed in cyclic mode to simulate the repetitive load of moving vehicles in order to measure the number of shear load cycles that is required to cause failure at the interface. Consequently, the bonding fatigue performance between two asphalt concrete layers should be evaluated in order to derive an interface shear fatigue law.

- More research efforts are required to develop advanced mechanistic approaches to evaluate the debonding potential under the repeated braking condition in order to simulate more realistic scenarios for highway asphalt pavements, rather than only under a single braking condition.
- Further research is required to establish specifications for a minimum limit of the shear bond strength to provide acceptable field performance by conducting more shear tests using both field cores and laboratory-fabricated specimens composed of various types of interlayer systems.
- The effects of the vertical tensile cracks behind the tire that are due to the wheel in the braking state on the interface bond strength and overall behavior of the pavement need to be determined.
- In this study, the tensile responses of asphalt pavements with debonded surface layers due to both the rolling and braking wheel conditions were investigated. The tensile responses of an asphalt pavement with a partially debonded interface between the asphalt layers also should be studied.
- Future research efforts are required to verify the t-TS principle for the BBS values measured from the PATTI tests.
- More research efforts are required to refine and validate the proposed *in situ* quality control methodology for various tack coats in the field as well as to perform curing time and temperature tests for different tack coat emulsions (CRS, CMS, SS, etc.).

REFERENCES

1. American Association of State and Highway Transportation Officials (AASHTO) (2013). *AASHTO TP 91-11: Standard Method of Test for Determining Asphalt Binder Bond Strength by Means of the Asphalt Bond Strength (ABS) Test.* AASHTO, Washington, D.C.
2. AASHTO (American Association of State Highway and Transportation Officials) (2011). *AASHTO TP-91: Standard Method of Test for Determining Asphalt Binder Bond Strength by Means of the Binder Bond Strength (BBS) Test*. AASHTO, Washington, D.C.
3. Alan, J. (2006). *Overview of Asphalt Emulsions*. Transportation Research Circular E-C102, Asphalt Emulsion Technology, ISSN 0097-8515, August.
4. Al Hakim, B. A. (2002). The Importance of Good Bond between Bituminous Layers. *Proceedings of the 9th International Conference on Asphalt Pavements*, Copenhagen.
5. Al-Qadi, I. L., S. H. Carpenter, Z. Leng, H. Ozer, and J. S. Trepanier (2008). *Tack Coat Optimization for HMA Overlays: Laboratory Testing.* Final Report No. FHWA-ICT-08-023, Illinois Department of Transportation, Illinois Center of Transportation, ICT-R55, September.
6. American Society for Testing and Materials (ASTM) (2011). *ASTM D2041: Standard Test Method for Theoretical Maximum Specific Gravity and Density of Bituminous Paving Mixtures*. ASTM International, West Conshohocken, PA.
7. American Society for Testing and Materials (ASTM) (2009). *ASTM D7497: Standard Practice for Recovering Residue from Emulsified Asphalt Using Low Temperature Evaporative Technique*. Annual Book of ASTM Standards.
8. American Society for Testing and Materials (ASTM) (2009). *ASTM D4541: Standard Test Method for Pull-Off Strength of Coatings Using Portable Adhesion Testers*. ASTM International, West Conshohocken, PA.
9. American Society for Testing and Materials (ASTM) (2008). *ASTM D6934: Standard Test Method for Residue by Evaporation of Emulsified Asphalt*. Annual Book of ASTM Standards.
10. American Society for Testing and Materials (ASTM) (2008). *ASTM D6937: Standard Test Method for Determining Density of Emulsified Asphalt*. Annual Book of ASTM Standards.
11. Asphalt Institute (2007). *The Asphalt Handbook MS-4*. Asphalt Institute, Lexington, KY.
12. Asphalt Institute (1989). *The Asphalt Handbook MS-4*, Asphalt Institute, Lexington, KY.
13. Bae, A., L. N. Mohammad, M. A. Elseifi, J. Button, and N. Patel (2010). Effects of Temperature on Interface Shear Strength of Emulsified Tack Coats and its Relationship to Rheological Properties. *Transportation Research Record: Journal of the Transportation Research Board*, Vol. 2180, pp. 102-109.
14. Bernier, A. and A. Zofka (2012). *Development of the Connecticut Advanced Shear Tester (CAST)*. Presented at the 87th annual AAPT meeting, Austin, TX, April.

15. Braham, A. F. (2008). *Fracture Characteristics of Asphalt Concrete in Mode I, Mode II, and Mixed-Mode*. Ph.D. dissertation, University of Illinois at Urbana-Champaign, IL.
16. California Department of Transportation (Caltrans) (2009). *Tack Coat Guidelines*. Caltrans, Sacramento, CA, www.dot.ca.gov/hq/construc/publications/tackcoatguidelines.pdf, accessed November, 2011.
17. California Department of Transportation (2003). *Maintenance Technical Advisory Guide (TAG)*. Caltrans Division of Maintenance.
18. Canestrari, F., G. Ferrotti, X. Lu, A. Millien, M. N. Partl, C. Petit, A. Phelipot-Mardele´, H. Piber, and C. Raab (2013). Mechanical Testing of Interlayer Bonding in Asphalt Pavements. *Advances in Interlaboratory Testing and Evaluation of Bituminous Materials*, RILEM State-of-the-Art Reports, Vol. 9, pp. 303-360.
19. Canestrari, F., G. Ferrotti, M. N. Partl, and E. Santagata (2005). Advanced Testing and Characterization of Interlayer Shear Resistance. *Transportation Research Record: Journal of the Transportation Research Board*, No. 1929, Transportation Research Board of the National Academies, Washington, D.C., pp. 68-78.
20. Canestrari, F. and E. Santagate (2005). Temperature Effects on the Shear Behavior of Tack Coat Emulsions Used in Flexible Pavements. *International Journal of Pavement Engineering*, Vol. 6, No. 1, March, pp. 39-46.
21. Chaignon, F. and J-C. Roffe (2001). *Characterization Tests on Bond Coats: Worldwide Study, Impact, Tests, Recommendations*. Canadian Technical Asphalt Association, Toronto, Canada, November.
22. Chehab, G. R., Y. Seo, and Y. R. Kim (2007). Viscoelastoplastic Damage Characterization of Asphalt–Aggregate Mixtures Using Digital Image Correlation. *International Journal of Geomechanics*, ASCE, Volume 7, No. 2, March/April, pp. 111-118.
23. Chehab, G. R. (2002). *Characterization of Asphalt Concrete in Tension using a Viscoelastoplastic Model*. Ph.D. dissertation, North Carolina State University, Raleigh, NC.
24. Chehab, G., Y. R. Kim, R. A. Schapery, M. Witczack, R. Bonaquist (2002). Time-Temperature Superposition Principle for Asphalt Concrete Mixtures with Growing Damage in Tension State. *Journal of Association of Asphalt Paving Technologists*, Vol. 71, pp. 559-593.
25. Chen, D. (2010). Slippage Failure of a New Hot-Mix Asphalt Overlay. *Journal of Performance of Constructed Facilities*, Vol. 24, No. 3, June 1, pp. 258-264.
26. Chen, J. and C. Huang (2010). Effects of Surface Characteristics on Bonding Properties of Bituminous Tack Coat. *Transportation Research Record: Journal of the Transportation Research Board*, No. 2180, Transportation Research Board of the National Academies, Washington, D.C., pp. 142-149.
27. Collop, A. C., M. H. Sutanto, G. D. Airey, and R. C. Elliott (2009). Shear Bond Strength between Asphalt Layers for Laboratory Prepared Samples and Field Cores. *Construction and Building Materials,* Vol. 23, Issue 6, June, pp. 2251-2258.

28. D'Andrea, A., C. Tozzo, A. Boschetto, and L. Bottini (2013). Interface Roughness Parameters and Shear Strength. *Modern Applied Science*, Vol. 7, No. 10.
29. DeBeer, M., C. Fisher, and L. Kannemeyer (2004). Towards the Application of Stress-In-Motion (SIM) Results in Pavement Design and Infrastructure Protection. *Proceedings of the 8th International Symposium on Heavy Vehicles, Weights and Dimensions*, Muldersdrift, Gauteng, South Africa.
30. DeBondt, A. and A. Scarpas (1994). *Theoretical Analysis of Shear Interface Setups*. Report No. 7-93-203-9, Road and Railway Research Laboratory, Delft University of Technology, Delft, The Netherlands.
31. Donovan, E. P., I. L. Al-Qadi, and A. Loulizi (2000). Optimization of Tack Coat Application Rate for Geocomposite Membrane on Bridge Decks. *Transportation Research Record: Journal of the Transportation Research Board*, Vol. 1740, pp. 143-150.
32. Eslaminia, M., S. Thirunavukkarasu, M. N. Guddati, and Y. R. Kim (2012). Accelerated Pavement Performance Modeling Using Layered Viscoelastic Analysis. *Proceedings of the 7th International RILEM Conference on Cracking in Pavements*, Delft, The Netherlands.
33. Flexible Pavements of Ohio (2012). *Proper Tack Coat Application*. Technical bulletin, Columbus, Ohio.
34. Florida Department of Transportation (2012). *Florida Method of Test for Field Evaluation of Structural Coating*. Florida Department of Transportation, FM 5-591.
35. Hachiya, Y. and K. Sato (1997). Effect of Tack Coat on Bonding Characteristics at Interface between Asphalt Concrete Layers. *Proceedings of the 8th International Conference on Asphalt Pavements*, pp. 349-362.
36. Hasiba, K. (2012). *Development of a Testing Approach for Tack Coat Application Rate at Pavement Layer Interfaces*. M.S. thesis, University of Illinois at Urbana-Champaign, IL.
37. Im, J. H. (2013). *Performance Evaluation of Chip Seals for High Volume Roads Using Polymer-Modified Emulsions and Optimized Construction Procedures*. Ph.D. dissertation, North Carolina State University, Raleigh, NC.
38. James, A. (2006). *Overview of Asphalt Emulsions*. Transportation Research Circular E-C102, Asphalt Emulsion Technology, Transportation Research Board of the National Academies, ISSN 0097-8515, August.
39. Karshenas, A. (2015). *Tack Coat Bond Strength Evaluation Methods and Mechanistic Design of the Interface for Multilayer Asphalt Pavement*. Ph.D. dissertation, North Carolina State University, Raleigh, NC.
40. Karshenas, A., S. H. Cho, A. A. Tayebali, M. N. Guddati, and Y. R. Kim (2014). Importance of Normal Confinement to Shear Bond Failure of Interface in Multilayer Asphalt Pavements. *Transportation Research Record: Journal of the Transportation Research Board*, No. 2456, pp. 170-177.
41. Kruntcheva, M. R., A. C. Collop, and N. H. Thom (2006). Properties of Asphalt Concrete Layer Interfaces. Technical Note, *Journal of Materials in Civil Engineering*, Vol. 18, No. 3, June, pp. 467-471.

42. Leng, Z., H. Ozer, I. L. Al-Qadi, and S. H. Carpenter (2008). Interface Bonding between Hot-Mix Asphalt and Various Portland Cement Surfaces: Laboratory Assessment. *Transportation Research Record: Journal of the Transportation Research Board*, No. 2057, pp. 46-53.
43. Li, N. and A. A. A. Molenaar (2012). Prediction of Tensile Strength of Asphalt Concrete. *Sustainable Construction Materials*, pp. 276-288.
44. Medani, T. O. (2006). *Design Principles of Surfacing on Orthotropic Steel Bridge Decks*. Ph.D. dissertation, Delft University of Technology, Delft, The Netherlands.
45. Michelin (2012). *Michelin Americas Truck Tires X One® Fuel Savings Page*, Retrieved from http://www.michelintruck.com/michelintruck_en_us/tires-retreads/xone/xOne-fuel-savings.jsp.
46. Mohammad, L. N., M. A. Elseifi, A. Bae, N. Patel, J. Button, and J. A. Scherocman (2012). *Optimization of Tack Coat for HMA Placement*. Publication NCHRP Report 712, Transportation Research Board of the National Academies, Washington, D.C.
47. Mohammad, L. N, A. Bae, M. A. Elseifi, J. Button, and J. A. Scherocman (2009). Evaluation of Bond Strength of Tack Coat Materials in the Field. *Transportation Research Record: Journal of the Transportation Research Board*, Vol. 2126, pp. 1-11.
48. Mohammad, L. N., M. A. Raqib, and B. Huang (2002). Influence of Asphalt Tack Coat Materials on Interface Shear Strength. *Transportation Research Record: Journal of the Transportation Research Board*, No. 1789, Transportation Research Board of the National Academies, Washington, D.C., pp. 56-65.
49. Mukhtar, M. T. and B. J. Dempsey (1996). *Interlayer Stress Absorbing Composite (ISAC) for Mitigating Reflection Cracking in Asphalt Concrete Overlays*. Final Report Project IHR-533, Illinois Cooperative Highway Research Program.
50. National Association of Australia State Road Authorities (NAASRA) (1987). *A Guide to the Visual Assessment of Pavement Condition.* Milsons Point, N.S.W, Australia.
51. National Highway Traffic Safety Administration (NHTSA) (2009). *Federal Motor Vehicle Safety Standards; Air Brake Systems*. 49 CFR Part 571, Docket No. NHTSA–2009-0083.
52. NCDOT (North Carolina Department of Transportation) (2012). *Standard Specifications for Roads and Structures*. NCDOT, Raleigh, NC.
53. Novak, M., B. Birgisson, and R. Roque (2003). Near-Surface Stress States in Flexible Pavements Using Measured Radial Tire Contact Stresses and ADINA. *Computers and Structures*, Vol. 81, pp. 859-870.
54. Park, H. J. (2013). *Investigation of Primary Causes of Load-Related Cracking in Asphalt Concrete Pavement in North Carolina*. Ph.D. dissertation, North Carolina State University, Raleigh, NC.
55. Partl, M. N. and C. Raab (1999). Shear Adhesion between Top Layers of Fresh Asphalt Pavements in Switzerland. *Proceedings of the 7th CAPSA Conference on Asphalt Pavements for Southern Africa*, Victory Falls, Zimbabwe.

56. Paul, H. R. and J. A. Scherocman (1998). Friction Testing of Tack Coat Surfaces. *Transportation Research Record: Journal of the Transportation Research Board*, No. 98-1092, pp. 6-12.
57. Prapaitrakul, N., R. Han, X. Jin, A. E. Martin, and C. J. Glover (2010). Comparative Study on Recovered Binder Properties Using Three Asphalt Emulsion Recovery Methods. *Journal of Testing and Evaluation*, pp. 1-7.
58. Raab, C. and M. Partl. (2004). *Interlayer Shear Performance: Experience with Different Pavement Structures*. Third Eurasphalt and Eurobitume Congress, Vienna, 2004.
59. Raab, C., M. N. Partl, and A. O. Abd El Halim (2009). Evaluation of Interlayer Shear Bond Devices for Asphalt Pavements. *The Baltic Journal of Road and Bridge Engineering*, No. 4, Vol. IV, pp. 186-195.
60. Romanoschi, A. S. and J. B. Metcalf (2001). Characterization of Asphalt Concrete Layer Interfaces. *Transportation Research Record: Journal of the Transportation Research Board*, No. 1778, Transportation Research Board of the National Academies, Washington, D.C., pp. 132-139.
61. Safavizadeh, A. and Y. R. Kim (2014). Mode II Fatigue and Reflective Cracking Performance of GlasGrid-Reinforced Asphalt Concrete under Repeated Loading. *Proceedings of the 12th ISAP Conference on Asphalt Pavements*, Raleigh, North Carolina, pp. 1893-1902.
62. Seo, Y., Y. R. Kim, M. W. Witczak, and R. Bonaquist (2002). Application of Digital Image Correlation Method to Mechanical Testing of Asphalt–Aggregate Mixtures. *Transportation Research Record: Journal of the Transportation Research Board*, No. 1789, Washington, D.C., pp. 162-172.
63. Sholar, G. A., G. C. Page, J. A. Musselman, P. B. Upshaw, and H. L. Moseley (2002). *Preliminary Investigation of a Test Method to Evaluate Bond Strength of Bituminous Tack Coat*. Research Report FL/DOT/SMO/02-459, Florida Department of Transportation, Gainesville, FL.
64. Siddharthan, R. V., N. Krishnamenon, M. El-Mously, and P. E. Sebaaly (2002). Investigation of Tire Contact Stress Distributions on Pavement Response. *Journal of Transportation Engineering*, ASCE, Vol. 128, No. 2, March/April, pp. 136-144.
65. Su, K., L. Sun, Y. Hachiya, and R. Maekawa (2008). *Analysis of Shear Stress in Asphalt Pavements under Actual Measured Tire-Pavement Contact Pressure*. 6th ICPT, Sapporo, Japan, July.
66. Takamura, K. (2000). Comparison of Emulsion Residues Recovered by Forced Airflow and RTFO Drying. *ISSA/AEMA Proceedings*, March 12-15, pp. 1-17.
67. Tandon V. and S. R. Eedula (2006). *Tack Coat Field Acceptance Criterion*. FHWA / TX - 06/0-5216-1, Center for Transportation Infrastructure Systems, University of Texas at El Paso.
68. Tashman L., K. Nam, T. Papagiannakis, K. Willoughby, L. Pierce, and T. Baker (2008). Evaluation of Construction Practices That Influence the Bond Strength at the Interface

between Pavement Layers. *Journal of Performance of Constructed Facilities*, Vol. 22, No. 3, pp. 154-161.
69. Tashman, L., K. Nam, and T. Papagiannakis (2006). *Evaluation of the Influence of Tack Coat Construction Factors on the Bond Strength between Pavement Layers*. Washington Center for Asphalt Technology, Pullman, WA.
70. Tayebali, A. A., M. S. Rahman, M. B. Kullkarni, and Q. Xu (2004). *A Mechanistic Approach to Evaluate Contribution of Prime and Tack Coat In Composite Asphalt Pavements*. Final Report, FHWA/NC/2004-05, North Carolina Department of Transportation, Department of Civil Engineering, North Carolina State University, June.
71. Tran, N. H., R. Willis, and G. Julian (2012). *Refinement of the Bond Strength Procedure and Investigation of a Specification*. NCAT Report No. 12-04, June.
72. Uzan, J., M. Livneh, and Y. Eshed (1978). Investigation of Adhesion Properties between Asphaltic Concrete Layers. *Asphalt Paving Technology*, Vol. 47, February, pp. 495-521.
73. Wang, H. (2011). *Analysis of Tire-Pavement Interaction and Pavement Responses using a Decoupled Modeling Approach*. Ph.D. dissertation, University of Illinois at Urbana-Champaign, Urbana, IL.
74. Wargo, A. (2015). *Laboratory and Field Investigation of Reflective Crack Mitigation in Layered Asphalt Concrete Pavements*. Ph.D. dissertation, North Carolina State University, Raleigh, NC.
75. West, R. C, J. Zhang, and J. Moore (2005). *Evaluation of Bond Strength between Pavement Layers*. NCAT Report No. 05-08, National Center for Asphalt Technology, December.
76. Wheat, M. (2007). *Evaluation of Bond Strength at Asphalt Interfaces*. M.S. thesis, Kansas State University, KS.
77. Willis, J. and D. Timm (2007). Forensic Investigation of Debonding in Rich-bottom Pavement. *Transportation Research Record: Journal of the Transportation Research Board*, No. 2040, Transportation Research Board of the National Academies, Washington, D.C., pp. 107-114.
78. Wood, T. J., D. W. Janisch, and F. S. Gaillard (2006). *Minnesota Seal Coat Handbook*. Minnesota Department of Transportation, Office of Minnesota Road Research.
79. Yoo, P. J., I. L. Al-Qadi, M. A. Elseifi, and I. Janajreh (2006). Flexible Pavement Responses to Different Loading Amplitudes Considering Layer Interface Condition and Lateral Shear Forces. *International Journal of Pavement Engineering*, Vol. 7, No. 1, March, pp. 73-86.
80. Yun, T., B. Underwood, and Y. R. Kim (2010). Time-Temperature Superposition for HMA with Growing Damage and Permanent Strain in Confined Tension and Compression. *Journal of Materials in Civil Engineering*, Vol. 22, No. 5, pp. 415-422.
81. Zou, X., H. Gong, B. Tang, D. X. Xiao, and D. Zhao (2012). Effects of Shear Stress on Pavement Cracking and Interface Disconnecting: A Case Study in Arkansas. Paper Prepared for Publication and Presentation at the 2013 Annual Meeting of the Transportation Research Board, July.

82. Zofka, A., M. Maliszewski, A. Bernier, R. Josen, A. Vaitkus, and R. Kleizienė (2015). Advanced Shear Tester for Evaluation of Asphalt Concrete under Constant Normal Stiffness Conditions. *Road Materials and Pavement Design*, DOI: 10.1080/14680629.2015.1029690.

APPENDIX A: Literature Review

This literature review presents an overview of studies that are relevant to bond strength and stress state at the layer interface.

1. Debonding Problem

Zou et al. (2012) extracted several cores from a pavement site that exhibited distress in order to investigate the causes of the distress. Figure A.1 shows two such distressed cores from the Zou et al. study. These researchers found that none of the cores had an intact interface between the top (first) layer and the bottom layers. They concluded that the first and most predominant cause of the observed distress and debonding was poor construction, as determined by the quantity and quality of the tack coat that is intended to protect the interface before the upper layers are paved. Another reason for the distress was shear stress, which is known to be a significant factor for interface debonding and pavement cracking. Based on the test results for shear stress, Zou et al. found the location of the maximum shear stress to be consistently between 4 cm and 6 cm below the surface course, where debonding frequently occurred, regardless of the thickness of the wearing course.

Figure A.1 Two cores extracted from the field (Zou et al. 2012).

Park (2013) also observed debonding in cores extracted from cracked areas, as presented in Figure A.2, in his study of the primary causes of cracking in asphalt pavement. He concluded that regions without debonding have relatively high alligator cracking index values, as shown in Figure A.3. The alligator cracking index was developed to assess the condition of existing pavements. Regions with debonding problems exhibit poorer pavement conditions than regions without a history of debonding.

Figure A.2 Debonding (layer interface separation) in core-extracted hole (NC-24) (Park 2013).

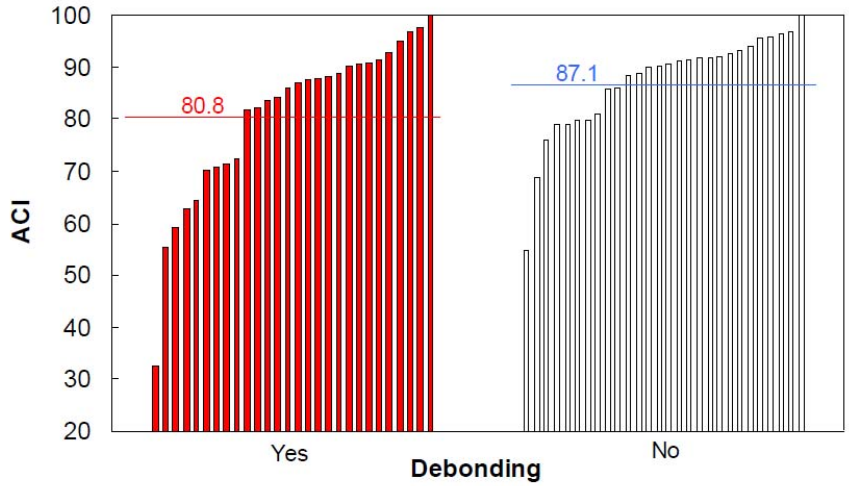

Figure A.3 Alligator cracking index values from the condition regions with and without debonding (Park 2013).

The causes of debonding in a multilayered pavement have been studied in many research projects, but are not yet completely known or understood. Some of the factors that appear to play a decisive role in debonding are as follows (Canestrari et al. 2013):

- Type of base course material
- Insufficient compaction of the base course or sub-base course or subgrade
- Segregation in the base course due to aggregate particles of large nominal size (40 mm) and lack of bitumen
- Type of bitumen used in the wearing course
- Climate temperature when the pavement is constructed
- Contamination of the surface of the lower layer

- The water flow between the layers or the water flow in the pavement due to surface cracking
- Poor or excessive tack coat application

Obviously, this list is not comprehensive and many more factors and their interactions may contribute to poor bonding between pavement layers. Furthermore, this list does not include the type of loading that is also likely to contribute to debonding and slippage failure.

2. Slippage Crack and Delamination Distress

Figure A.4 presents a schematic illustration of slippage cracking. Slippage cracks are crescent-shaped vertical cracks behind the tire in the surface course of the pavement layer. Generally, slippage cracks occur in the opposite direction of the braking force (Tayebali et al. 2004). According to Chen (2010), slippage cracks are possibly due to an improper tack coat application. Figure A.5 shows a slippage crack in a pavement section. To predict slippage failure in the surface layer for a multilayered pavement structure, the calculation of the stress distribution due to a braking wheel on the pavement surface and along the interface is critical.

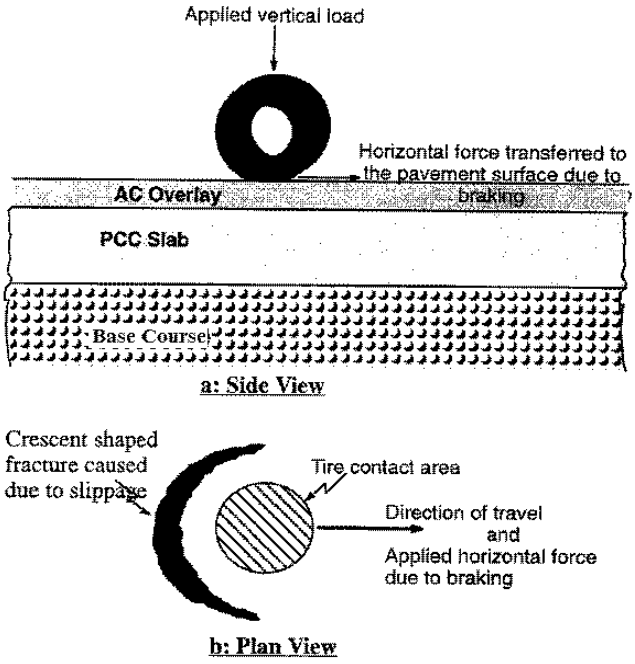

Figure A.4 Typical slippage failure (Tayebali et al. 2004 and Mukhtar et al. 1996).

Figure A.5 Crescent-shaped slippage crack (National Association of Australian State Road Authorities 1987).

Figure A.6 shows delamination distresses in an asphalt concrete pavement section. According to the National Association of Australian State Road Authorities (1987), delamination is the loss of a discrete area of the surface layer of an asphalt pavement and shows clear delineation of the surface layer from the layer below. Generally, delamination occurs in the wheel path, as shown in Figure A.6.

Figure A.6 Delamination distress in an asphalt pavement (National Association of Australian State Road Authorities 1987).

3. Asphalt Emulsions

Asphalt emulsions usually contain from 40 percent to 75 percent asphalt, 0.1 percent to 2.5 percent emulsifier agent, 25 percent to 60 percent water, and some other minor components (Alan 2006). Asphalt emulsions are in the form of liquid at ambient temperatures; therefore, their main application is to reduce the apparent viscosity of the asphalt so that it can be workable at low temperatures (California Department of Transportation 2003). Asphalt emulsion is the combination of two immiscible liquids and is produced by dispersing small droplets of one liquid

into the other. The particle size and particle distribution of the droplets in the emulsion depend on the mechanics and operating conditions of the manufacturing plant. Also, the particle size and distribution significantly affect the physical properties of the emulsion, such as viscosity and storage stability. For standard asphalt emulsions, asphalt droplets are dispersed in a continuous phase of water. In order to prevent early breaking of the emulsion, water is added to the emulsion instead of adding emulsion to the water. Warm water is preferred. The emulsifier provides an electric charge to the surface of the asphalt droplets so that they can repel each other. However, when the asphalt droplets achieve enough energy to overcome the emulsifier's effect, they start to adhere to each other and drain the water out.

Emulsions are classified according to the charge of the droplets and the curing time. The charge of the droplets in the emulsions is important for compatibility with aggregate particles. Cationic emulsions have droplets with a positive charge. Conversely, anionic emulsions have droplets with a negative charge. Emulsion names that begin with a 'C' indicate a cationic emulsion, and no 'C' is normally an anionic emulsion.

Emulsions also are classified according to the setting (curing) time, also known as flocculation and/or coalescence. The setting time is designated by the second set of letters in the designation. There are four terms: RS (rapid setting), MS (medium setting), SS (slow setting), and QS (quick setting). Rapid-setting emulsions cure quickly when they come in contact with aggregate particles that have a low surface area. Rapid-setting emulsions are very reactive and are used with unreactive aggregate. Their breaking time is faster than slow setting emulsions and, thus, their use allows faster traffic opening. Medium-setting emulsions also are used with aggregate particles that have low surfaces. Their curing time is slower than that of rapid-setting emulsions. Slow-setting emulsions are unreactive and are used with reactive aggregate particles that have high surface areas. Quick-setting emulsions are defined as emulsions that are intermediate in terms of reactivity between the medium-setting and slow-setting emulsions (James 2006).

Another designation that may be placed before the letters that designate the setting time is HF (high float) (e.g., CHFRS-2P), which indicates a high float emulsion that passes the float test. After high float emulsions are cured, a gel-type structure is formed in the asphalt residue that improves the performance of the emulsion for a wider temperature range and allows these emulsions to be applied to dusty aggregate.

Furthermore, '1' or '2' next to the letter designation for the setting time indicates the emulsion's viscosity. '1' is low viscosity and '2' indicates high viscosity. Some emulsions may have the letter 'h' at the end of the name, indicating hard base asphalt (Wood et al. 2006). In order to indicate the use of polymer modification in an emulsion, 'P' or 'L' is included in the last part of the name, indicating polymer or latex modification, respectively (Im 2013).

3.1. Application of Emulsions

Asphalt emulsions have many applications in the construction and maintenance of paved surfaces. The most common applications are explained below.

Surface treatments

Surface treatments are applied to existing pavement surfaces to protect the pavement and decrease the rate of deterioration of the pavement. The most commonly used surface treatments are seal coats. Emulsified asphalts are involved in all seal coats; therefore, a clear understanding of the advantages and limitations of asphalt emulsions is crucial for attaining the best results. For

surface treatments, asphalt emulsions can be used with damp aggregate and can be used at low temperatures, which helps to mitigate fire hazards that other products often present. Moreover, asphalt emulsions can be applied in most situations and to all available aggregates types. With the appropriate selection of emulsion type, grade, and application rate, asphalt emulsions can provide a fluid application that can be sprayed onto the surface, can be cured, and can quickly develop adhesion to the aggregate particles and to the surface. A properly designed asphalt emulsion also holds the aggregate particles tightly together to prevent the loss of aggregate during the service life of the pavement.

Asphalt pavement recycling and soil stabilization

Emulsified asphalts also can be used for various pavement recycling methods, such as hot in-place recycling, cold recycling, and full-depth reclamation. For full-depth reclamation, asphalt emulsions are used to produce a stabilized based course. In the case of high traffic pavements, polymer-modified emulsified asphalt is used.

Repair of pot-holes

When using asphalt emulsions to repair pot-holes, the methods typically employed are throw and roll, semi-permanent, and full-depth removal and replacement. These methods involve placing cold mix in the pot-hole with a shovel and then compacting the mix. Another method for repairing pot-holes is spray-injection that consists of blowing asphalt emulsion and coarse crushed aggregate particles together into the pot-hole. CRS-2, RS-2, and HFRS-2 emulsions are preferred for temperatures above 10°C. CMS-2, MS-2, and HFMS-2 emulsions perform better for temperatures below 10°C.

3.2. Tack Coat Materials

A tack coat is a very light application of diluted asphalt emulsion that is applied to bond a new overlay to the relatively non-absorptive top surface of an existing pavement layer prior to paving. According to the Asphalt Institute (2007), tack coat material provides a bond between the existing pavement surface and a new overlay in order to provide bond strength to the pavement structure and to prevent premature distress, such as slippage cracking. In order to attain the best performance of an asphalt pavement, the top surface of the existing pavement not only should be dried and cleaned completely, but the tack coat should be thin and uniform and should ‘break’ just before the new asphalt concrete layer is paved.

The process of breaking emulsion is characterized by the separation of liquid asphalt and water into two separate phases. After the water evaporates, the residual asphalt develops a bond with the underlying surface, displaying a color change from brown to black, as shown in Figure A.7. For the pavement to be structurally and functionally sound, proper bonding between the structural layers is essential.

(a) (b)

Figure A.7 Example of emulsion break: (a) unbroken emulsion and (b) after breaking.

Leng et al. (2008) found three factors that ensure good pavement performance: appropriate curing of the tack coat, careful selection of the type of tack coat material, and an optimal residual application rate and consistency of application onto the pavement surface. Figure A.8 presents proper and inadequate examples of tack coat application.

(a) (b)

Figure A.8 Uniformity of tack coat application: (a) proper application and (b) non-uniform application.

4. Factors that Affect Interface Bond Strength

Numerous factors affect the interface bond strength between asphalt concrete layers. To quantify this bond strength, each of these factors as well as their interactions should be examined. The complexity of the interactions between the factors is one of the reasons that interface bond strength is so difficult to quantify. Some of the most important parameters that affect bond strength are shown in Figure A.9 (Raab et al. 2009).

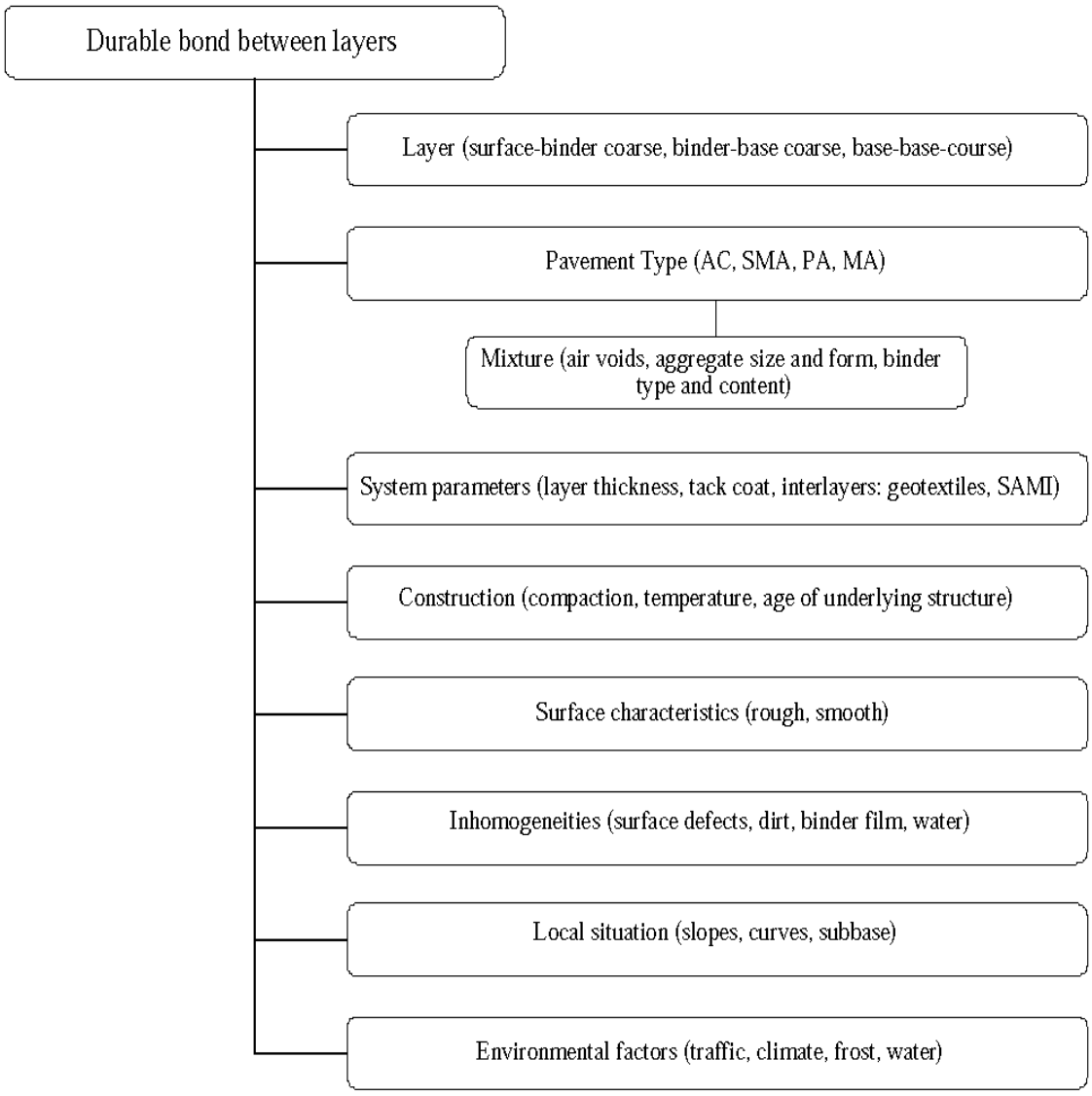

Figure A.9 Factors that affect a durable bond between pavement layers (Raab et al. 2009).

Moreover, the lack of a definitive standard for test methods to measure interface bond strength may be attributable partly to the different test methods that have been adopted by different researchers, which makes it difficult to compare test results. Based on past research into interface bond strength, the dependency of the interface bond strength on temperature and the deformation rate is not debated among researchers; however, many divergent results regarding the effects of normal confining stress, tack coat type and application rate, surface roughness, and so forth have been reported in different studies (Raab et al. 2009).

4.1. Types of Tack Coat Materials

Various types of materials, including asphalt emulsion, cutback asphalt, and trackless tack, have been used as the interface layer materials between asphalt concrete layers and between asphalt concrete (AC) layers and Portland cement concrete (PCC) layers. Based on a survey by

Paul and Scherocman (1998), the most commonly used emulsions are SS-1, SS-1h, CSS-1, and CSS-1h, and only one state (Georgia) uses hot asphalt (AC-20 and AC-30) for tack coats. According to a survey by Tayebali et al. (2004), the materials used for tack coats are: AC, AE-60, CMS-1, C-70, C-250, C-800, CMS-2, CRS-1, CRS-2, CRS-2h, CSS-1, CSS-1h, HFE-60, HFE-90, HFMS-1, HFMS-2, HFMS-2h, HFMS-2s, MC-250, MC-800, MS-1, MS-2, MS-2h, PG 58-22, PG 64-22, PG 67-22, RC-70, RC-T, RS-1, RS-2, SS-1, and SS-1h. The authors found that CMS-2 emulsion performs better than PG 64-22 when it is used as the interface material between PCC and asphalt concrete layers. They explain that this phenomenon is caused by slippage that occurs between the PCC and asphalt concrete layers due to the imperviousness of the PCC layer.

The National Cooperative Highway Research Program (NCHRP) Project 9-40 (Mohammad et al. 2012) included a comprehensive survey of tack coat practices worldwide. According to the results of the survey, the most commonly used tack coats on new, existing, and milled hot mix asphalt (HMA) surfaces are CSS-1h (32%-34%), SS-1 (30%-32%), SS-1h (29%-32%), and CSS-1 (21%-27%) asphalt emulsions. PG 64-22 is reported as the most often used asphalt cement at an average of 11 percent, and RC-70 as the most commonly used cutback (or liquid) asphalt at 5 percent to 7 percent. Regarding the performance of the different tack coat materials, Mohammad et al. (2002) observed that the CRS-2P emulsion performs better than the PG 64-22, PG 76-22M, SS-1, SS-1H, and CSS-1h emulsions with an optimal application rate of 0.02 gal/yd^2. West et al. (2005) found that PG 64-22 exhibits a higher bond strength than the other two study emulsions (CRS-2 and CSS-1), especially for fine-graded mixtures tested at a high temperature.

In the NCHRP Project 9-40 (Mohammad et al. 2012), four tack coat materials (trackless, CRS-1, SS-1h, and PG 64-22) were tested in the field and laboratory. Based on laboratory direct shear tests of cored samples taken from the field, the results show that the trackless tack coat exhibited the highest interface shear strength, and the CRS-1 emulsion exhibited the lowest interface shear strength. These results relate directly to the viscosity of the residual binders at the test temperature (25°C). In contrast to these results, field tensile strength tests of tack coats showed that the PG 64-22 binder provided the highest tensile strength.

4.2. Modified Emulsion versus Ordinary Emulsion

Based on the shear bond strength test results presented by Canestrari et al. (2005), as shown in Figure A.10, the modified emulsions provided higher interlayer shear resistance than a conventional tack coat at 20°C (68°F).

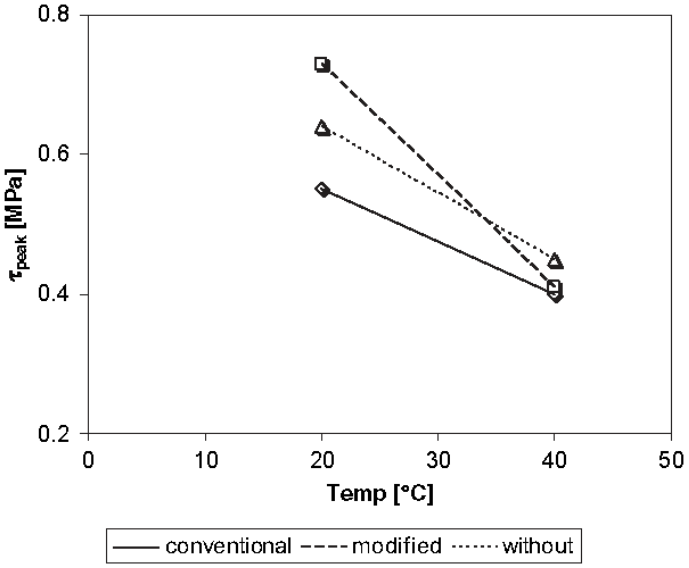

Figure A.10 Peak shear strength versus temperature for laboratory samples, short curing time, and 0.4 MPa confining normal force (Canestrari et al. 2005).

4.3. Tack Coat Application Rate

An optimal tack coat application rate is necessary to provide a good interface bond at low cost. Pavement surfaces of different ages may require different application rates to provide a proper bond between the existing asphalt concrete layer and subsequent asphalt layer.

Mohammad et al. (2002) evaluated shear strength using the Superpave Shear Tester. The study tack coats included two performance grade (PG) asphalt binders (PG 64-22 and PG 76-22M), and four emulsified asphalts (CRS-2P, CSS-1, SS-1, and SS-1h). Five application rates 0.0 (0.0), 0.09 (0.02), 0.23 (0.05), 0.45 (0.1), 0.90 (0.2) L/m^2 (gal/yd^2) were evaluated at two test temperatures, 25°C and 55°C (77°F and 131°F). The results indicate that CRS-2P emulsion is the best tack coat type and that an optimal residual application rate for CRS 2P emulsion is 0.02 gal/yd^2 (0.09 L/m^2). Mohammad et al. (2002) concluded that increasing the application rate at low temperatures generally results in decreased shear strength. In addition, they found that shear strength is not affected by the application rate at high temperatures.

Mohammed et al. (2009) also investigated three tack coat materials (CRS-1, SS-1h, and trackless) and an asphalt cement (PG 64-22) at an optimal residual rate of 0.053 gal/yd^2 (0.23 L/m^2). These tests were conducted to evaluate the interface bond strength of tack coats in the field at temperatures ranging from 30°C to 80°C (86°F to 176°F) using the Louisiana Tack Coat Quality Tester (LTCQT). The authors found that an increase in the viscosity of the tack coat material results in an increase in tensile strength.

In the NCHRP Project 9-40, *Optimization of Tack Coat for HMA Placement* (2012), the research team found that all tack coat materials show the highest interface shear strength at an application rate of 0.155 gal/yd^2 with respect to the interface shear strength in the field. Within the tested application rate range, it was difficult to determine the optimal residual application rate. This problem may have been due to the highly-oxidized HMA surface at the Louisiana Transportation Research Center's Pavement Research Facility site, which required greater

optimal tack coat rates than expected. This difficulty may also indicate that, under actual field conditions, optimal application rates are higher than those commonly predicted from laboratory-based experiments. The results of the interface shear bond strength tests for different existing surface conditions based on NCHRP Project 9-40 are shown in Figure A.11, Figure A.12, and Figure A.13.

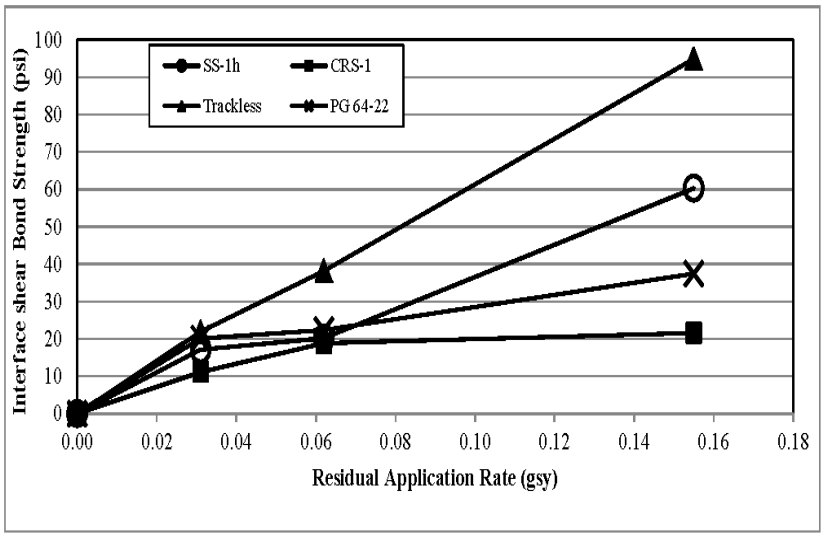

Figure A.11 Effects of residual application rates and tack coat types on interface shear strength for old HMA surface (Mohammad et al. 2012).

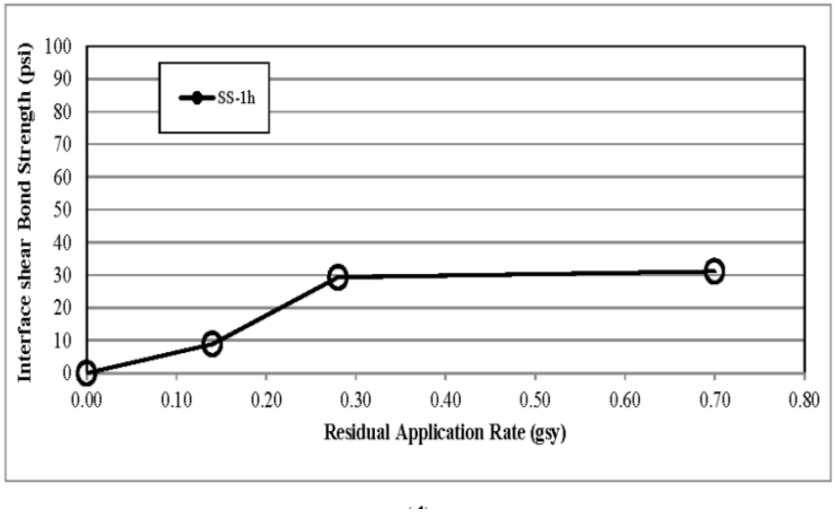

Figure A.12 Effects of residual application rates and tack coat types on interface shear strength for new HMA surface (Mohammad et al. 2012).

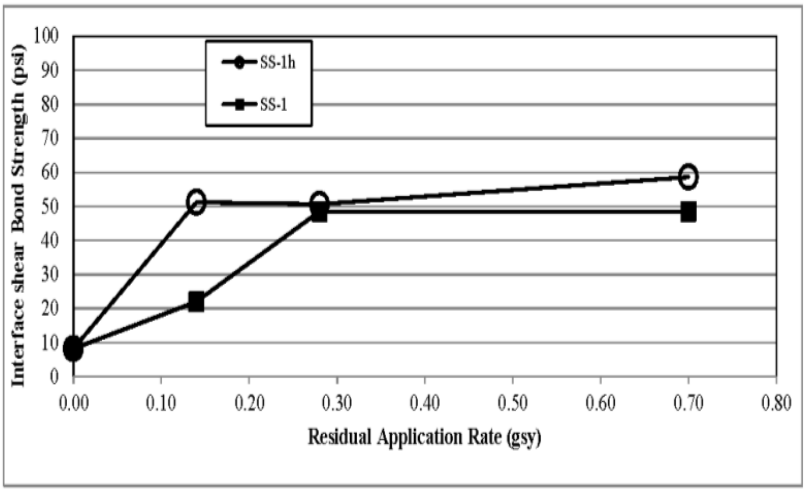

Figure A.13 Effects of residual application rates and tack coat types on interface shear strength for milled HMA surface (Mohammad et al. 2012).

Table A.1 presents the recommended tack coat residual application rates for different surface types according to NCHRP Project 9-40 (Mohammad et al. 2012).

Table A.1 Recommended tack coat application rates (Mohammad et al. 2012).

Surface Type	**Residual** Application Rate (gal/yd^2)
New Asphalt Mixture	0.035
Old Asphalt Mixture	0.055
Milled Asphalt Mixture	0.055
Portland Cement Concrete	0.045

In a study by Hachiya and Sato (1997), three cationic asphalt emulsions and three rubber-modified asphalt emulsions were investigated. These researchers concluded that, at the low temperature (0°C), rubber-modified asphalt emulsion (PK-HR2) provides the highest shear strength among the seven emulsions evaluated. At the high temperature (40°C), the rubber-modified asphalt emulsions (PK-R80, PK-HR1 and PKHR2) are almost equally effective. The optimal application rate for this study was 0.04 gal/yd^2.

Hasiba (2012) found that the optimal tack coat residual rate for SS-1vh emulsion is 0.04 gal/yd^2 for unmilled surfaces, whereas the optimal residual rate for milled HMA is 0.06 gal/yd^2. Chen and Huang (2010) found the optimal residual application rate for CRS emulsion to be close to 0.027 gal/yd^2.

According to North Carolina Department of Transportation (DOT) specifications (2012), the required tack coat application rate is 0.04 to 0.08 gal/yd^2. *The Asphalt Handbook* (MS-4) (1989) specifies application rates ranging from 0.05 to 0.15 gal/yd^2 for an emulsion diluted with one part water to one part emulsion, which is equivalent to residual application rates between 0.02 and 0.05 gal/yd^2. The lower application rates are recommended for new or subsequent layers, whereas the intermediate application rates are for normal surface conditions of an existing,

relatively smooth pavement. The upper application rate limit is for old oxidized, cracked, pocked, or milled asphalt pavements and PCC pavements.

Tashman et al. (2006) found that the absence of a tack coat does not significantly affect the bond strength at the interface for milled sections, whereas it severely decreases the strength at the interface for non-milled sections.

Analysis of experimental results by Kruntcheva et al. (2006) indicates that a dry and clean interface with no tack coat has similar properties to the same interface with a standard quantity of tack coat. The authors found that the interface properties depend on the type of materials in contact rather than on the amount of the applied tack coat and/or the interface conditions. They concluded that "under these circumstances there is no need for tack coat."

Some international recommendations and suggestions about optimal tack coats are as follows (Canestrari et al. 2013):

- In India, the amount of the tack coat is chosen as a function of the existing pavement surface conditions in terms of bitumen content.
- The Federal Aviation Administration confirmed that the amount of a tack coat must be chosen carefully, taking into account the condition of the existing pavement surface, both for airport pavements and road construction.
- British Standards states that the amount of tack coat (emulsion with modified bitumen) is a function of the bitumen content of the asphalt layers for new construction and of the existing pavement conditions for maintenance intervention.

Table A.2 shows tack coat application rates based on the manual, *Flexible Pavements of Ohio* (Flexible Pavements of Ohio 2012).

Table A.2 Tack coat application rates (Flexible Pavements of Ohio 2012).

Existing Pavement Condition	Residual L/m^2 (gal/yd^2)	Undiluted L/m^2 (gal/yd^2)	Diluted (1:1) L/m^2 (gal/yd^2)
New Asphalt	0.135 to 0.18 (0.03 to 0.04)	0.225 to 0.27 (0.05 to 0.06)	0.45 to 0.54 (0.10 to 0.12)
Oxidized Asphalt	0.225 to 0.27 (0.05 to 0.06)	0.36 to 0.405 (0.08 to 0.09)	0.675 to 0.81 (0.15 to 0.18)
Milled Surface (Asphalt)	0.225 to 0.27 (0.05 to 0.06)	0.36 to 0.405 (0.08 to 0.09)	0.675 to 0.81 (0.15 to 0.18)
Milled Surface (PCC)	0.18 to 0.225 (0.04 to 0.05)	0.27 to 0.36 (0.06 to 0.08)	0.54 to 0.675 (0.12 to 0.15)
Portland Cement Concrete	0.18 to 0.225 (0.04 to 0.05)	0.27 to 0.36 (0.06 to 0.08)	0.54 to 0.675 (0.12 to 0.15)

4.4. Curing Time

Studies in the literature generally lack complete agreement on how long a tack coat should remain uncovered before the subsequent asphalt layer is placed. According to Chaignon and Roffe (2001), inadequate emulsion curing can be the difference between effective and

ineffective tack coat applications, and curing times range from 20 minutes for a broken emulsion to several hours for a dry emulsion. Paul and Scherocman (1998) found that many state DOTs specify a minimum time between the tack coat application and placement of HMA to provide an adequate curing time for the emulsion to break and set. Three state DOTs set a maximum time that a tack coat can be left before placing the asphalt concrete. The Alaska DOT specifies a maximum setting period of two hours for CSS-1 emulsion. The Arkansas DOT specifies a maximum setting period of 72 hours for SS-1 emulsion, and the Texas DOT specifies a maximum setting period of 45 minutes for the SS-1 and MS-2 emulsions. Four states indicate that paving is required the same day the tack coat is applied.

Hachiya and Sato (1997) reported that higher interface shear strength values are achieved with longer curing times for tack coats prior to testing, based on simple shear tests and simple tension tests. Sholar et al. (2004) concluded that shear strength increases with curing time. Chen and Huang (2010) found a slight increase in shear strength by increasing the curing time to 45 minutes. Hasiba (2012) found that the optimal curing time for SS-1hp, HFE, and SS-1vh emulsions is two hours. However, the study conducted by Tashman et al. (2006) concluded that curing time has little effect on the interface shear strength.

4.5. Temperature

NCDOT specifications (2012) require that tack coats be applied only when the surface to be treated is dry and when the atmospheric temperature in the shade away from artificial heat is 35°F or above. West et al. (2005) found that, on average, bond strength values are 2.3 times higher at 50°F than at 77°F, and bond strength values at 140°F are about one-sixth of the bond strength values at 77°F. Uzan et al. (1978) concluded that shear resistance at the interface increases significantly with increasing vertical pressure and decreases with increasing temperature. The shear resistance peaks at an optimal tack coat application rate that is dependent on the test temperature. The stiffness decreases with an increase in the temperature and vice versa. Romanoschi and Metcalf (2001) found that temperature affects the maximum shear strength and interface reaction modulus (K) with and without a tack coat.

4.6. Normal Confining Stress

Canestrari and Santagata (2005) showed that as normal stress increases, dilatancy decreases, and an increase in the applied normal stress causes an increase in the peak shear stress. They concluded that, compared to samples without a tack coat, samples with a tack coat exhibited high peak shear stress at failure at all test temperatures and for each level of normal stress.

West et al. (2005) tested the effects of tack coats at three temperatures (10°C, 25°C, and 60°C) and three normal pressure levels (0, 10, and 20 psi). They concluded that at high temperatures, when normal pressure increases, the bond strength increases, whereas at intermediate and low temperatures, the bond strength is not sensitive to normal pressure. In the NCHRP Project 9-40 (2012), the tack coat interface shear strength was tested under 0 psi and 20 psi confining pressure. The ratio of the interface shear strength between these two test conditions increased as the residual application rate decreased. As the residual application rate decreased, an increase in the confining pressure resulted in a more pronounced contribution of the effect of roughness and aggregate resistance to sliding at the interface. However, at higher residual application rates (greater lubrication), the effect of aggregate roughness and resistance to sliding was less critical, because most of the interface shear strength was derived from the tack coat

material. The effect of confinement was found to be more pronounced under dusty and dry conditions.

4.7. Surface Condition: Milled versus Non-milled

According to the study by Tashman et al. (2006), milled sections have higher shear strength values than non-milled sections. Figure A.14 shows the effects of milling on shear bond strength with different tack coat application rates and curing times, which were measured using a Florida DOT (FDOT) testing instrument.

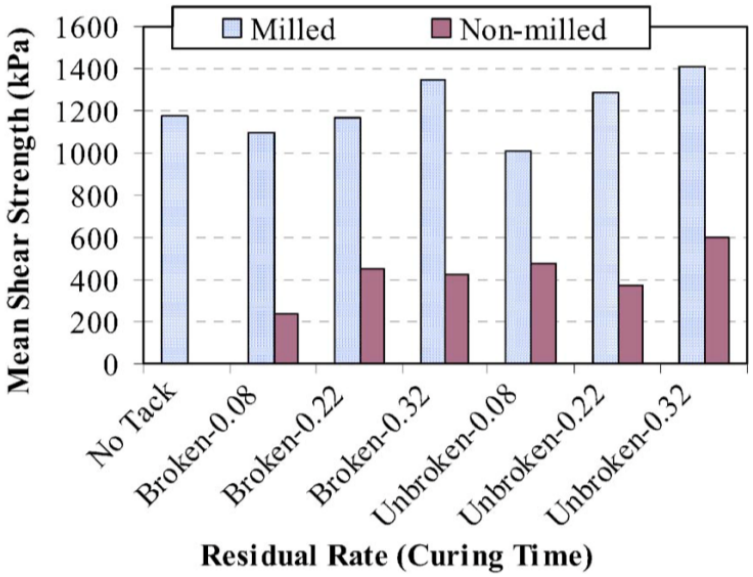

Figure A.14 Effect of residual rate (CSS-1, L/m^2) nested within curing time for milled and non-milled surfaces in FDOT shear strength test (Tashman et al. 2006).

4.8. Base and Subgrade Strength

According to a study conducted by Chen (2010) based on dynamic cone penetrometer (DCP) tests performed at the site of a pavement that was distressed due to slippage failure, slippage distress is not associated with the base or subgrade stiffness.

4.9. Surface Roughness

D'Andrea et al. (2013) studied the correlation between the interface surface roughness parameter measured by a laser scanner with the interface shear strength. They found that for higher texture peaks, stronger resistance parameters were achieved, probably due to a better interlock between the superposed layers. Examples of the laser-scanned surfaces of the interface are shown in Figure A.15.

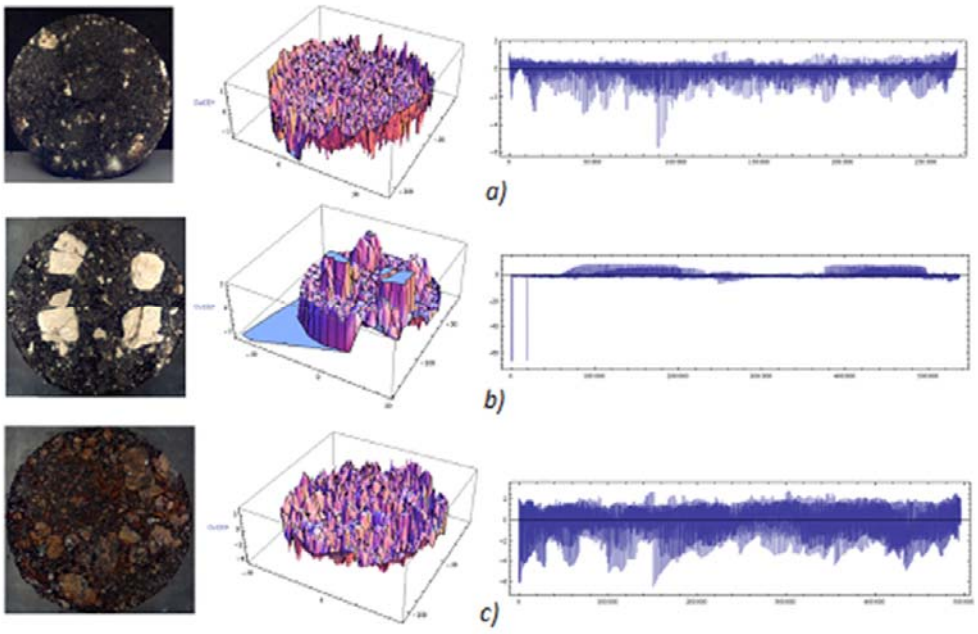

Figure A.15 Graphical results for different interface surface conditions: a) surface with no treatment, b) chipping 5/10, and c) 'debitumening' (D'Andrea et al. 2013).

5. *In Situ* Tack Coat Interface Bond Strength Test Methods

Due to the need for a proper quality control and tack coat material selection method, several *in situ* tack coat evaluation test methods and instruments have been proposed. In this section, some of the current field test methods for evaluating tack coat bond strength are presented.

5.1. Louisiana Tack Coat Quality Tester (LTCQT)

Mohammad et al. (2009) developed the LTCQT to evaluate the bond strength of tack coats in the field immediately after application. The LTCQT was developed based on several modifications to the ATacker™ device developed by InstroTek, Inc. Figure A.16 shows the ATacker™ test device. In the ATacker™ test procedure, a contact plate applies a constant normal pressure on the pavement surface after the application of the tack coat on the existing asphalt surface. The plate is then pulled off by rotating the torque shaft, and the tensile strength between the plate and tack coat surface is measured.

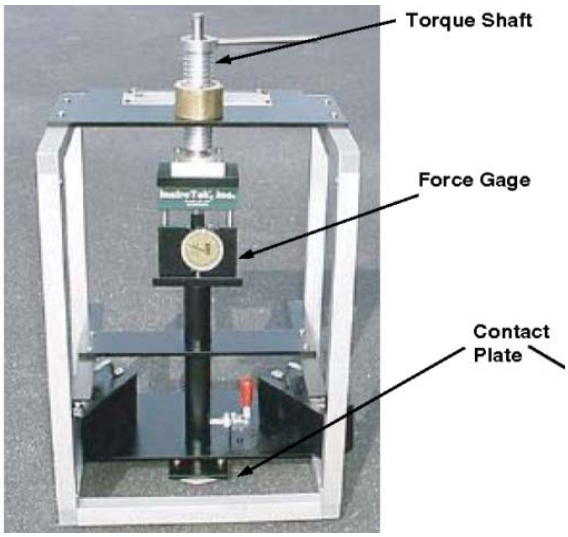

Figure A.16 ATacker™ test device (Mohammad et al. 2012).

The manual loading of the pull-off plate of the ATacker™ test instrument was observed to cause an inconsistent loading rate that can affect the tensile strength measurements. The main modification of the ATacker™ device for the development of the first generation of the LTCQT was to automate the load application by installing electronic sensors to measure load and deformation (Mohammad et al. 2009). In the second generation of the LTCQT, the sensitivity of the load cell, sensitivity of the actuator, and the bond strength between the plate and the tack coat were modified. Figure A.17 shows the second-generation LTCQT. During the LTCQT tack coat field evaluation tests, the metal plate showed poor adhesion to the tack-coated asphalt surface. Several materials were evaluated to attach to the metal plate to improve the bond between the instrument and the tack-coated surface. Polyethylene foam was found to provide good adhesion to the tacked surface (Mohammad et al. 2012).

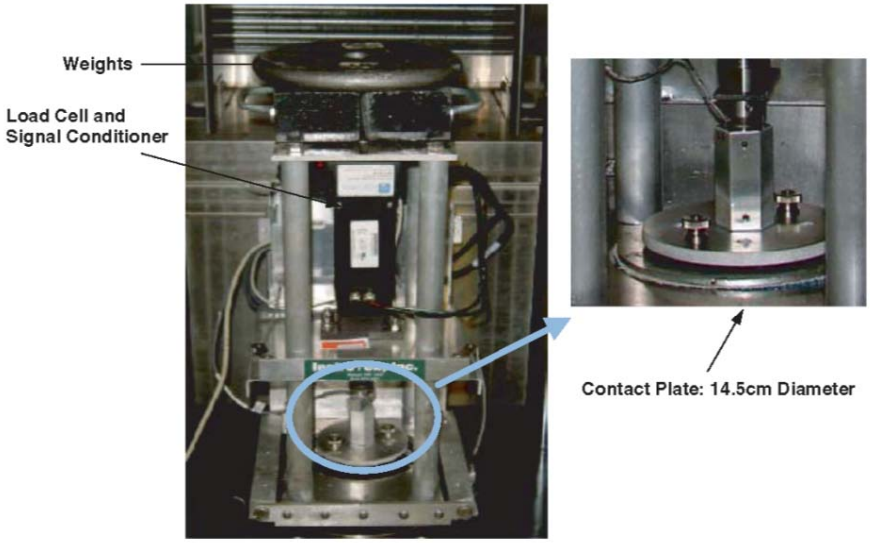

Figure A.17 Second-generation LTCQT device with 14.5-cm diameter contact plate (Mohammad et al. 2009).

The LTCQT has the following components and specifications.

- LTCQT: The device is equipped with a closed-loop servo-motor actuator for precision control of the rate of displacement during testing. It is capable of measuring loads up to 446 N (100 lb) with an accuracy of ±1 percent. The displacement of the actuator is measured using a position transducer that has a total travel distance of 100 mm.
- Computer and software: The software is designed such that it displays the time, normal load, and displacement of the actuator continuously during testing while graphically illustrating the relationship of the normal load and time. It allows the user to input the required compressive load, the time to hold the compressive load, and the displacement rate required. The actual holding time of the compressive load is displayed during testing as well as the actual displacement rate. In addition, the software allows the user to move the actuator manually.
- Heating source: The infrared reflective heating (IRH) lamp is equipped with a 250-watt, 120-volt bulb. It is designed such that it can be positioned six inches from the surface so that heating can be conducted without the device making contact with the tacked surface.
- Weights: The weights are equal to or greater than the expected maximum normal load. Note that the normal load applied by the machine cannot exceed 446 N (100 lb).
- Temperature control devices and thermometer: The temperature control device can adjust the surface temperature to the required test temperature. It is recommended that a fan be used to cool the tacked surface and a heat gun be used to heat the tacked surface. An infrared thermometer should be utilized for measuring the temperature of a tacked surface without directly contacting the test area.

The LTCQT tack coat bond strength test procedure is shown in Figure A.18. In the first step, an IRH lamp is used to accelerate the breaking and curing of the tack coat. The surface

temperature is allowed to cool down to the testing temperature, and the LTCQT is placed on the cured tacked surface. A compressive normal stress of 10.8 kPa (1.57 psi) is applied to the surface by the LTCQT loading plate for three minutes. Then, a tensile force is applied at a displacement rate of 0.2 mm/s (0.00787 in./s) until failure. The test results for a series of LTCQT tests for a temperature range from 30°C to 80°C (86°F to 176°F) and four tack coat materials at a residual application rate of 0.23 L/m^2 (0.05 gal/yd^2) are shown in Figure A.19. The temperatures presented in these graphs are the ones that were measured at the end of each test (Mohammad et al. 2009).

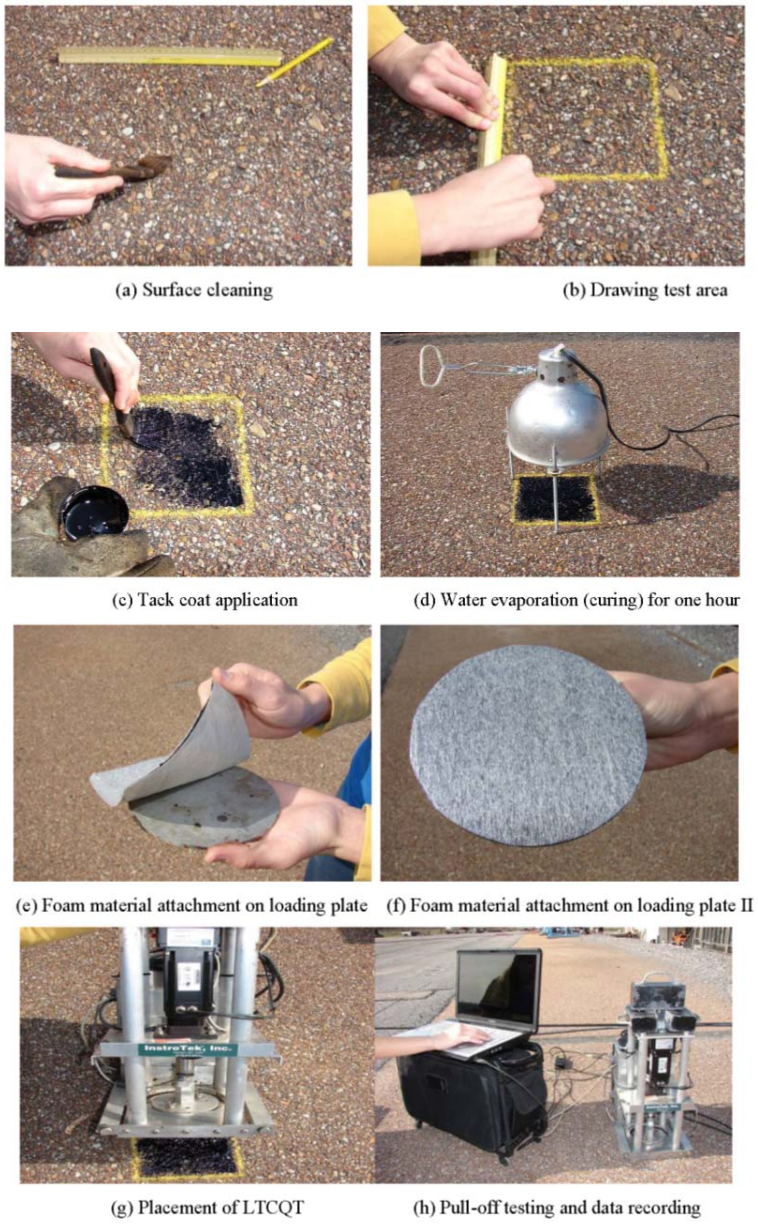

Figure A.18 LTCQT test procedure (Mohammad et al. 2009).

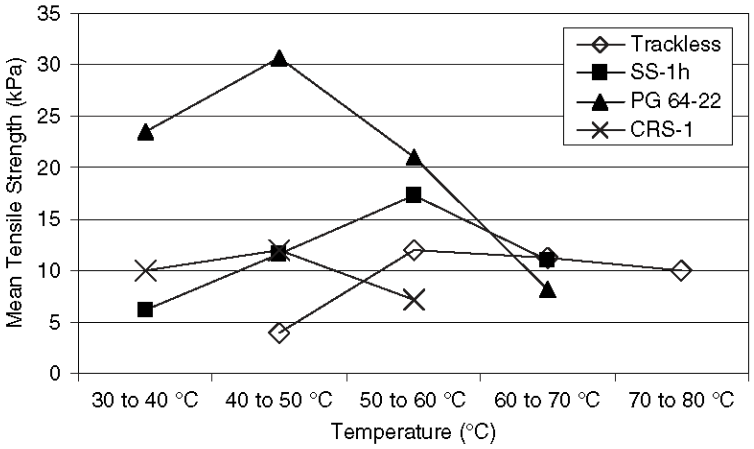

Figure A.19 Variation of mean tensile strength versus temperature for tack coats tested by LTCQT (Mohammad et al. 2009).

5.2. University of Texas at El Paso (UTEP) Pull-off Test

The pull-off test was developed at the University of Texas, El Paso (UTEP) (Tashman et al. 2006). It measures the tensile strength of the tack coat materials prior to the installation of a new overlay. After the tack coat is applied, curing time is allowed to set the tack coat material. Then, the pull-off test device is placed on the tack-coated surface. As is shown in Figure A.20, after placing the contact plate on the tacked surface by rotating the torque wrench clockwise, a 18.14-kg (40-lb) load is placed on the weight key at the top of the device for 10 minutes prior to testing in order to set the contact plate. Subsequently, the load is removed, and the torque wrench is rotated counter-clockwise to detach the contact plate from the tacked surface. Figure A.20 shows the UTEP pull-off test set-up (Tashman et al. 2006).

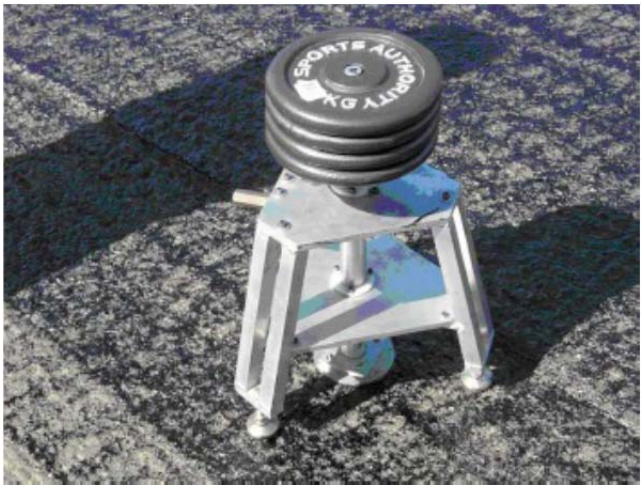

Figure A.20 UTEP pull-off test set-up (Tashman et al. 2008).

The test results for PG 64-22 are shown in Figure A.21. The tests were performed in the laboratory at three different set times and at three different temperatures.

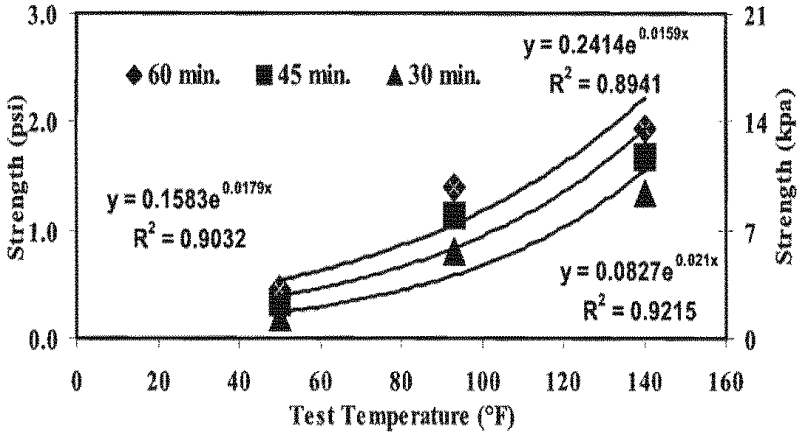

Figure A.21 UTEP laboratory test results for PG 64-22 asphalt binder (Tandon et al. 2006).

Tashman et al. (2006) reported that the UTEP pull-off contact plate did not adhere as well to the milled surface in their study as it did to the non-milled surface. Hence, the UTEP pull-off test results indicate that the non-milled sections had greater tensile strength than the milled sections, which is not the case and is mainly due to the lack of proper adhesion between the contact plate and the tack coat surface.

6. Laboratory Shear Test Methods

One of the major objectives of this study is to develop and implement appropriate test methods to characterize the parameters for interface bonding between two asphalt concrete layers in shear mode. The parameters obtained using the proposed test methods will provide the necessary inputs for the computational model.

The following sections present an extensive overview of existing shear test methods that are used to evaluate interface bond strength.

6.1. Florida DOT Shear Test

The FDOT test method is used to determine the interface bond strength between two layers of asphalt pavement in shear mode. The FDOT has adopted a procedure that does not include the application of normal confinement force; the resulting specification is designated as FM 5-599 (FDOT 2012). The test device accommodates 150-mm (6.0-in.) diameter samples and has a 9.5-mm (3/8-in.) diameter locking pin that is used to align the two platens.

In the FDOT shear test, the field core is placed between the shear plates so that the direction of traffic marked on the core is parallel to the shear direction, as shown in Figure A.22. The core is then deformed at a constant rate of 50 mm/min until failure occurs. Before performing the test, the field core is conditioned at a temperature of 25°C for two hours. The interface bond strength can be calculated by dividing the load by the cross-sectional area, as shown in the following equation.

$$IBS = \frac{P_{ult}}{\frac{\pi D^2}{4}}$$

where

IBS = interlayer bond strength (psi),
P_{ult} = ultimate load applied to specimen (lb), and
D = diameter of test specimen (in.).

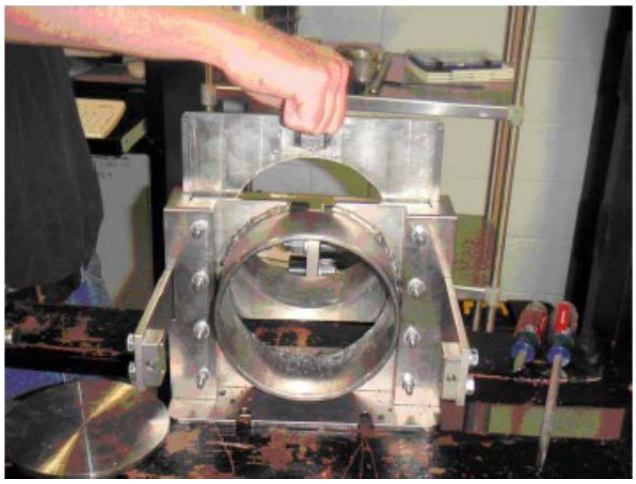

Figure A.22 Florida DOT shear test set-up (Tashman et al. 2006).

Figure A.23 shows the tests results for the milled and non-milled field cores tested using the FDOT shear strength test device.

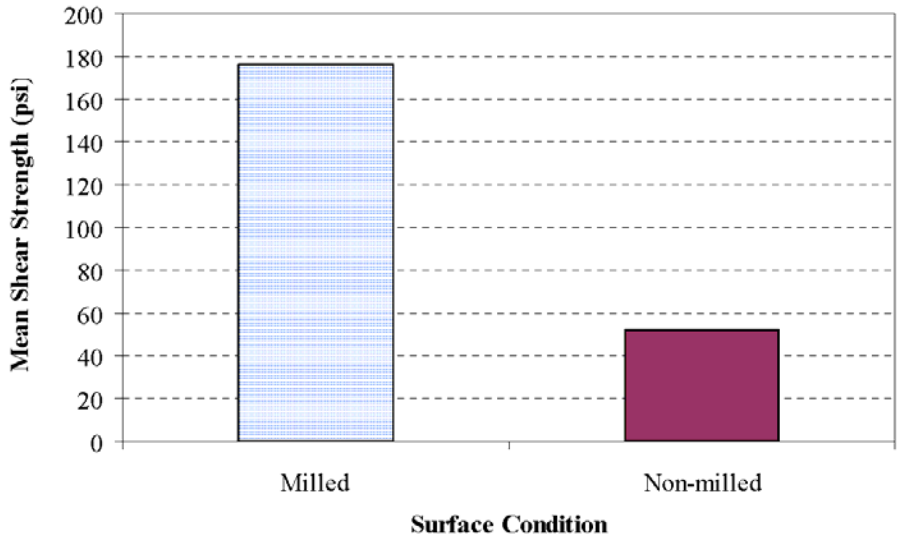

Figure A.23 Effect of surface condition on the shear bond strength measured by FDOT shear test device (Tashman et al. 2006).

6.2. Virginia Shear Fatigue Test

Donovan et al. (2000) conducted a laboratory study at Virginia Tech using the Virginia shear fatigue test to optimize the application rate of tack coats for geocomposite membranes and overlaid bridge decks. The test device is designed to allow the application of cyclic loads on an interlayer that is sandwiched between PCC and HMA. The Virginia shear fatigue test apparatus, shown in Figure A.24, measures the number of shear load cycles that is required to cause failure at the interface. The approach of using cyclic loading is believed to simulate the movement of vehicles on the pavement and, thus, can be used to determine the optimal application rate for the tack coat material. For this test, a cyclic shear load of 0.1 second half-sine wave with a deflection of 0.4 mm is applied, followed by a relaxation period of 0.9 second. The test utilizes composite cylindrical specimens (diameter of 93.7 mm) of HMA compacted on top of concrete cores. This test provides the maximum shear strength at each cycle as well as the maximum shear strength versus the number of cycles to failure. The authors recommend an application rate of 1.40 kg/m^2 (2.58 lbs/yd^2) when the geocomposite is in contact with an HMA base. They recommend an application rate of 1.50 kg/m^2 (2.77 lbs/yd^2) when the geocomposite is in contact with an HMA wearing surface, and 1.75 kg/m^2 (3.23 lbs/yd^2) when the tack coat is in contact with PCC.

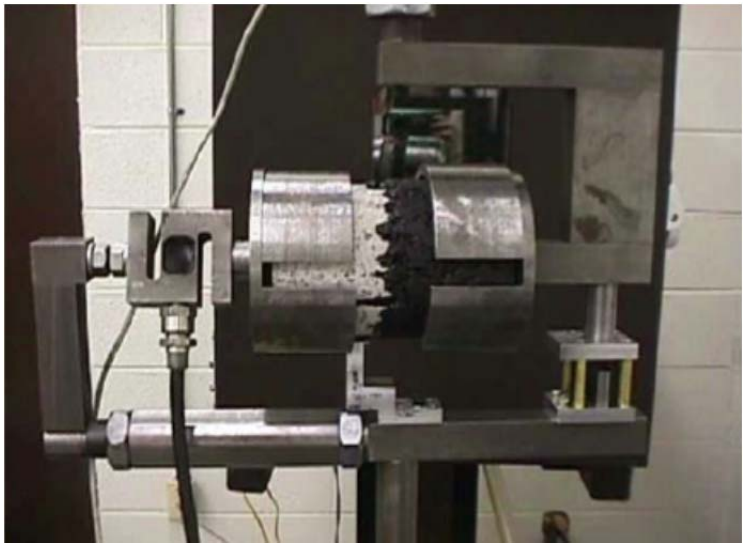

Figure A.24 Virginia shear fatigue test set-up (Donovan et al. 2000).

6.3. Direct Shear Apparatus Developed at the Illinois Center for Transportation

The direct shear test apparatus developed at the Illinois Center for Transportation is designed to apply shear force in the vertical direction and normal force in the horizontal direction. The effects of the bending moment induced by the eccentricity of the shear force are eliminated by the U-shaped loading arm, shown in Figure A.25. During testing, the vertical load is applied to the HMA while the PCC is held stationary. This device accommodates 100-mm (3.94-in.) diameter specimens and can run both monotonic and fatigue cyclic tests. The interface shear strength is evaluated using a monotonic mode of loading at a constant displacement rate of 12 mm/min (0.47 in./min). Two test modes also can be utilized to evaluate the performance of tack coats using this device: the cyclic mode, which evaluates performance based on the number of

cycles to failure, and the monotonic mode, which evaluates the tack coat strength based on the peak load before failure.

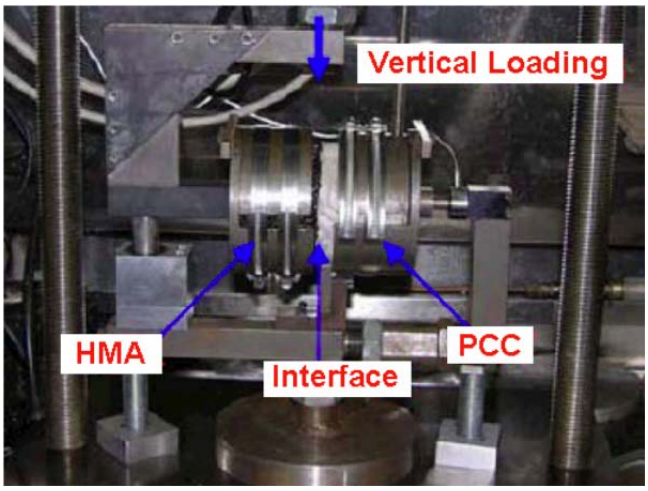

Figure A.25 Direct shear test apparatus developed at the Illinois Center for Transportation (Leng et al. 2008).

6.4. Louisiana Interlayer Shear Strength Tester (LISST)

A direct shear testing device, known as the Louisiana interlayer shear strength tester (LISST), was invented to characterize interface shear strength. As shown in Figure A.26, this device can accommodate specimens up to 101.6 mm (4 in.) in diameter. The test can be performed monotonically at a shear rate of 2.54 mm/sec (0.1 in./sec). Bae et al. (2010) investigated the effects of temperature on tack coats by studying the shear strength performance at various temperatures. The results show an increasing trend with application rate; accordingly, the best performance is seen at 0.706 L/m^2 (0.156 gal/yd^2). In addition, the interface shear strength decreases as the temperature increases.

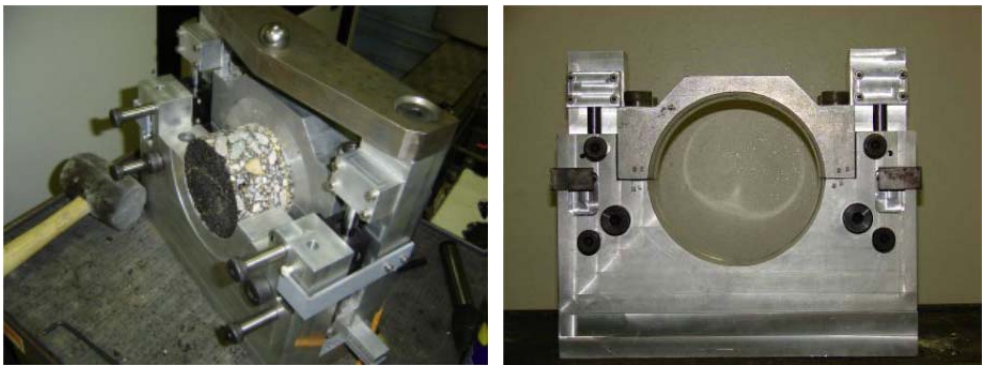

Figure A.26 Louisiana interlayer shear strength tester (Bae et al. 2010).

6.5. Direct Shear Device

A study conducted by Chen and Huang (2010) analyzed the effects of several surface properties in order to determine the behavior of tack coats. As shown in Figure A.27, the direct

shear device used in the study applies a vertical normal load and a horizontal shear load in order to analyze the behavior at the interface. Constant displacement of 2.5 mm/min (0.1 in./min) is applied in the horizontal plane. Both shear force and displacement measurements are recorded using a data acquisition system.

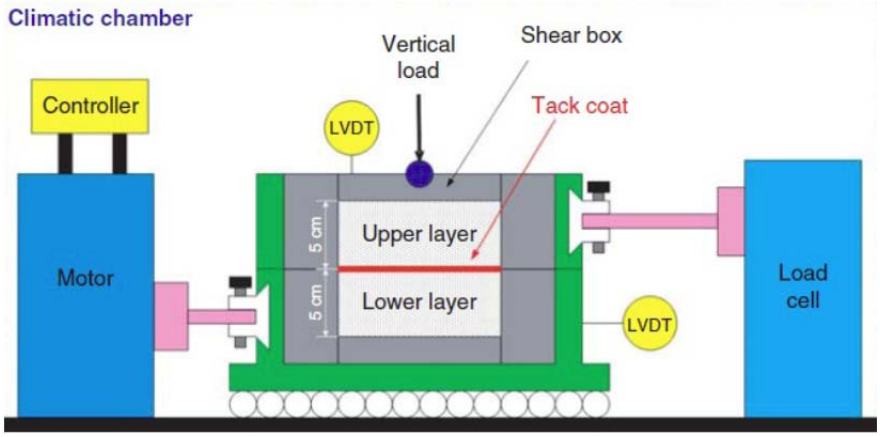

Figure A.27 Diagram of direct shear device (Chen and Huang 2010).

6.6. Tack Coat Shear Test Device

The tack coat shear test device shown in Figure A.28 is custom-designed to evaluate the bond strength between pavement layers. This device, developed by Al-Qadi et al. (2008), conducts shear load-related tests to evaluate the tack coat bonding performance between the asphalt concrete layers as well as between the asphalt concrete-PCC layers, and measures the changes in shear load, dilation, and shear displacement that occur during testing.

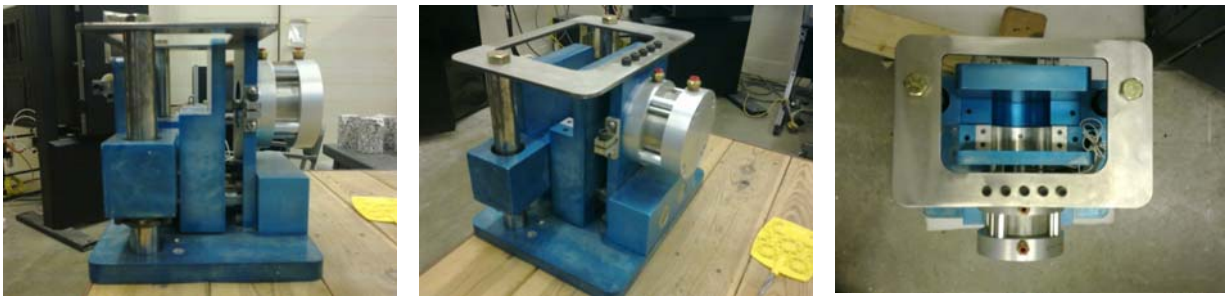

Figure A.28 Tack coat shear test device (Al-Qadi et al. 2008).

These tests can be conducted in monotonic loading mode to measure the maximum shear load and its corresponding shear displacement to evaluate the interface strength. In addition, the device can be used to perform fatigue shear tests that apply cyclic loads at different desired frequencies and, thus, can simulate field conditions. In the monotonic displacement-controlled testing mode with a shear rate of 0.127 mm/sec (0.005 in./sec), the shear load and displacement are measured in terms of testing time. The relationship between the shear strength and displacement can be plotted, ensuring that the displacement value starts from zero.

6.7. Four-Point Shear Test

The TU-Delft four-point shear test (Medani 2006) is used to study shear failure and sometimes creep properties in cement concrete, rocks, composite materials, and metals. The basic principle behind the four-point shear test is the creation of a vertical plane in the specimen that contains a highly concentrated shear force and a zero bending moment. Later, researchers at the University of Illinois at Urbana-Champaign (UIUC) developed the so-called Mode II Fracture Test, which is based on the TU Delft four-point shear test and captures mode II fracture work from the point of crack initiation (Braham 2008). The test samples used for the UIUC-modified four-point shear test are 100-mm tall, 75-mm thick, and 165-mm wide, with 12.5-mm notches cut into the top and bottom of each sample. However, with peak vertical loads of almost 25 kN, this set-up creates huge horizontal forces that cause the fixtures to deform during testing. Therefore, in order to reduce the horizontal forces on the equipment, the sample size was reduced at UIUC to 50-mm tall, 75-mm thick, and 165-mm wide with 8-mm notches cut into the top and bottom of each specimen. Figure A.29 shows a sample in the test fixture. The load-line displacement can be run with a constant head displacement of 5.0 mm/min. The crack tip sliding displacement can be run at a constant opening of 0.7 mm/min. These rates were chosen in order to match the rates used in the single-edge notched beam test.

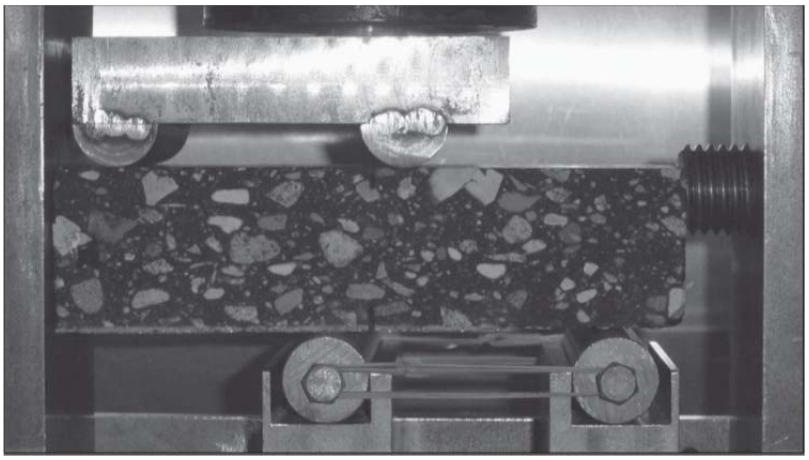

Figure A.29 Four-point shear test device modified by UIUC (Braham 2008).

6.8. Shear Fatigue Test

Romanoschi and Metcalf (2001) proposed a laboratory test configuration to perform shear fatigue tests on asphalt concrete with interfaces in order to simulate the repetitive load of moving vehicles. For this test, cylindrical asphalt specimens with diameters of 100 mm are placed into two metal cups spaced at 5 mm. The test device is designed such that adjustments can be made so that the asphalt interface is always between the two cups. The specimens are subjected separately to normal and shear loads. In order to include normal force, this device allows for the longitudinal axis of the test specimen to be at a 25.5° angle to the vertical axis. This angle was chosen because the shear stress at the interface is half the normal pressure at this angle. A vertical load is applied with a minimum of 10 percent of the maximum load and with a frequency of 5 Hz. So, the total time is 0.2 second and the length of the pulse is 0.05 second, simulating a vehicle pass at 50 km/hr. These fatigue tests were performed at 25°C on two types of interface (with and without a tack coat). Four normal stresses (0.50, 0.75, 1.00, and 1.25 MPa)

can be selected to be within the range of normal stress values encountered at the interfaces of actual road pavements. Figure A.30 presents a schematic of this test device.

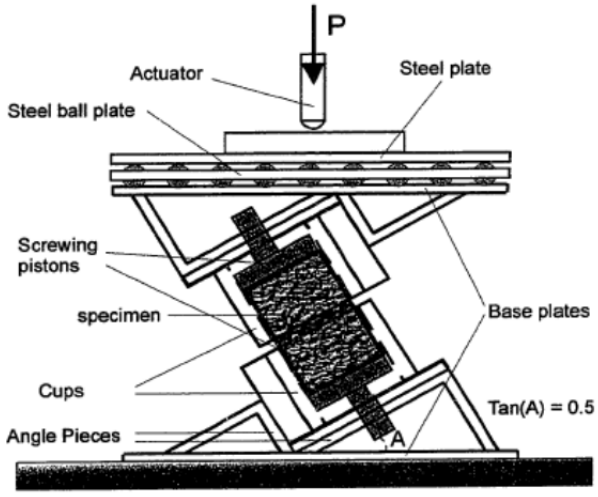

Figure A.30 Schematic of shear fatigue test (Romanoschi and Metcalf 2001).

Elastic and permanent displacements at the interface in both the normal and tangential directions are recorded for each cycle, and the cyclic tests are stopped when the permanent shear displacement (PSD) at the interface reaches 6 mm or when it is determined that the number of load cycles that corresponds to a PSD of 6 mm could be extrapolated. The authors remark that the PSD value increases at a constant rate with the number of load cycles, and the shear stress is uniformly distributed over the interface area. The PSD value increases up to the point when the interface fails; after that, the friction between the layers that are in contact at the interface will continue to resist the relative movement of the two layers. In order to characterize the evolution of the PSD with the number of load repetitions, the authors computed the parameter ND1, which represents the number of load cycles that leads to an increase in the PSD of 1 mm. The parameter ND1 gives information about the interface bond fatigue performance; the higher the ND1, the more durable the interface. From this results analysis, the authors found that the ND1 varies greatly even for the same normal stress, and only for the highest normal stress is the ND1 greater than the interface without a tack coat, which clearly indicates that an interface with a tack coat has a longer life than an interface without a tack coat. In addition, the asphalt interface may also fail in fatigue, and this fatigue test can be used for a comparative evaluation of the durability of different types of interface.

6.9. Kansas State University (KSU) Bond Strength Test

The test device known as the KSU bond strength tester was invented by Wheat (2007) to investigate the effects of different shear stress planes on the bond strength of tack coats. Figure A.31 shows a photograph of this test device. It includes two supports, one that holds the bottom part of the specimen and the other that holds the top layer of the specimen as well as changes the direction of the load force. The angle between the specimen axis and the actuator axis can be adjusted from 0° to 45°, which allows different planes of shear stress to act on the specimen. This device can accommodate specimens up to 101.6 mm (4 in.) in diameter. Two linear variable displacement transducers (LVDTs) are set up to measure normal displacement, and one LVDT is

set up to measure radial displacement. Two test modes can be utilized to evaluate the bond strength of tack coats using this device: the cyclic mode, which utilizes a maximum displacement of 10 mm and displacement rate of 0.05 mm/sec of the vertical actuator, and the monotonic mode, which is performed under sinusoidal loading at six different frequencies (25, 10, 5, 1, 0.5 and 0.1 Hz). Wheat (2007) concluded from his study that, because no effects of tack coat application rate or interface type on shear strength were observed, these strength tests should not be used to optimize the tack coat application.

Figure A.31 KSU bond strength test device (Wheat 2007).

6.10. Ancona Shear Testing Research and Analysis (ASTRA) Device

The ASTRA device, designed at the Universita Politecnica delle Marche in Ancona Italy, is a direct shear test box that can evaluate the strength of tack coat interfaces at various controlled temperatures. A schematic of this device can be seen in Figure A. 32. This device can apply a vertical normal load together with a horizontal shear load at the interface of a double-layered specimen. The interface is placed within a gap to ensure that the shear load is applied at the weakest plane where failure due to shear displacement occurs. The significant feature of this test device is that measurements of displacements in the normal direction as well as in the shear direction are possible. The standard temperature condition is 20°C. A cylindrical specimen 100 mm in diameter is placed in two independent half-boxes and mounted on a movable table. A constant vertical load, which corresponds to a normal stress of 0.2 MPa in the standard condition, is applied to the specimen. The lower movable table is moved at a constant displacement rate (2.5 mm/min in standard condition) and transfers the shear force at the interface. During the test, the shear force, the vertical displacement, and the horizontal displacement are continuously recorded, thereby obtaining the maximum interlayer shear stress. This stress value characterizes the interlayer shear resistance and is used as a parameter to determine repeatability.

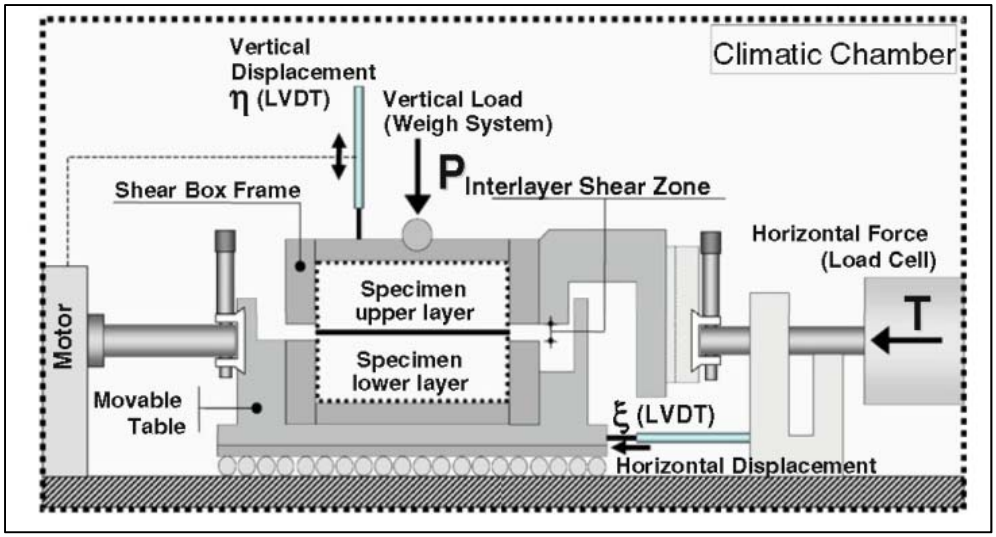

Figure A. 32 Schematic of ASTRA device (Tashman 2006).

6.11. Double Shear Tester (DST)

The North Carolina State University (NCSU) asphalt research team has studied interface bonding mechanisms using the double shear tester (DST), shown in Figure A.33. This device was developed recently by the NCSU research team (Safavizadeh and Kim 2014) to investigate the interfacial shear strength and fatigue performance of three-layered asphalt specimens. Specifically, the DST is an upright testing machine that is used to measure the shear properties at the interfaces of a three-layered specimen. The double shear test uses a symmetrical specimen that consists of three layers and two interfaces that are bonded two by two using the same interlayer characteristics. The two outside layers of the specimen are fixed, and the central layer is subjected to a cyclic load. The advantage of the double shear test over the single interlayer shear test is that the two interfaces symmetrically undergo a relatively pure shear stress, whereas in the single interlayer test normal forces are introduced to the interface at areas close to the loading plates, which can lead to bending problems in these tests. However, the NCSU research team recently found that it is not practically possible to induce symmetrical crack propagation at the both interfaces using the DST.

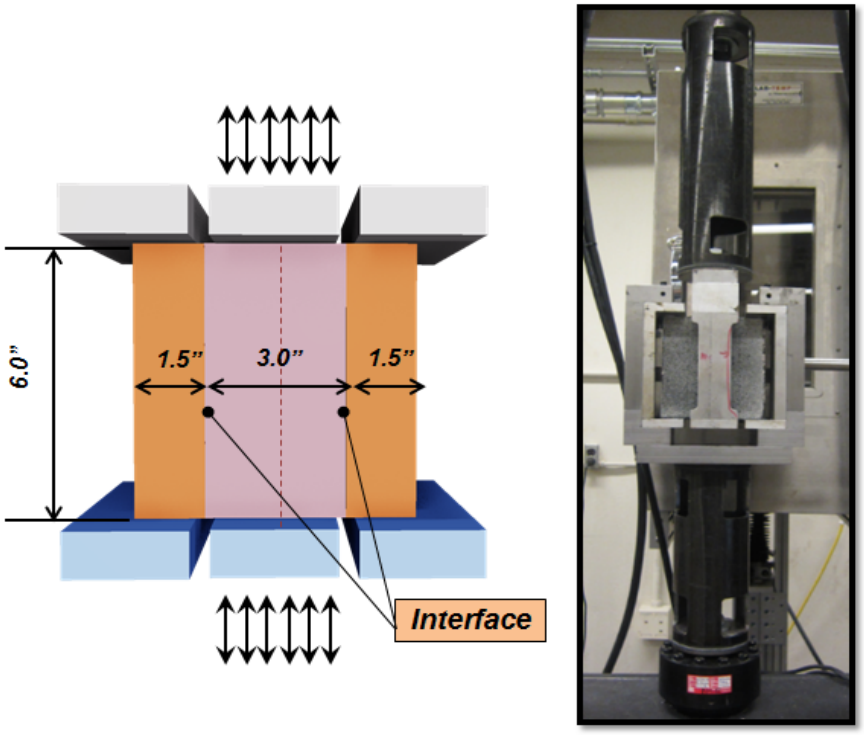

(a) (b)

Figure A.33 (a) Schematic of DST specimen and loading mechanism, and (b) DST installed in the MTS loading frame.

7. Interface Bonding Condition

In order to understand the effects of interface shear characteristics on pavement responses and also to predict interface failure, a constitutive model, or theoretical stress-strain relationship, for interfaces is necessary. In addition, to study the behavior of pavement under traffic loading and to predict the stress-strain distribution in multilayered pavement structures, knowledge of interface bonding conditions is essential. According to the RILEM *Interlaboratory Mechanical Testing of Interlayer Bonding in Asphalt Pavements* (Canestrari et al. 2013), the interlayer mechanical behavior can be modeled using elastic theory. The interlayer can be considered as thin material with a shear modulus *G* and thickness *h*. The interlayer shear stress (τ) causes a relative shear displacement ($\Delta\xi$) between the two layers. These relationships are expressed as:

$$\tau = G \cdot \frac{\Delta\xi}{h} = G \cdot \gamma$$

where γ represents the shear strain of the thin interface material in the equation. It is possible to obtain Goodman's constitutive law that describes the interface behavior in multilayered elastic systems as follows:

$$\tau = K \cdot \Delta\xi$$

In this equation, K (equal to G/h) represents the interlayer shear stiffness expressed in MPa/mm or kPa/mm, which is the slope of a shear stress-displacement curve. The parameter K can be assumed to be a characteristic value to measure the level of interlayer bonding.

In the case of a fully bonded interface, the following relationships are valid: $K = \infty$ and $\Delta\xi = 0$, whereas in the case of fully debonded layers, the interface conditions are represented in terms of $K = 0$ and $\tau = 0$.

The actual K value is essential to evaluate the pavement's bearing capacity for the rational design and maintenance of flexible pavements. For modeling purposes, Al Hakim (2002) identified two limiting values for K, where K below 10^{-2} MPa/mm represents the perfect slippage condition (complete debonding), and K above 10^{2} MPa/mm indicates perfect bonding (Canestrari et al. 2013). As shown in Figure A.34, when a full bond between all the pavement layers is ensured, the maximum tensile strain is located at the bottom of the pavement. In contrast, if one or more interfaces are not fully bonded, high tensile strains occur at the slipping interfaces.

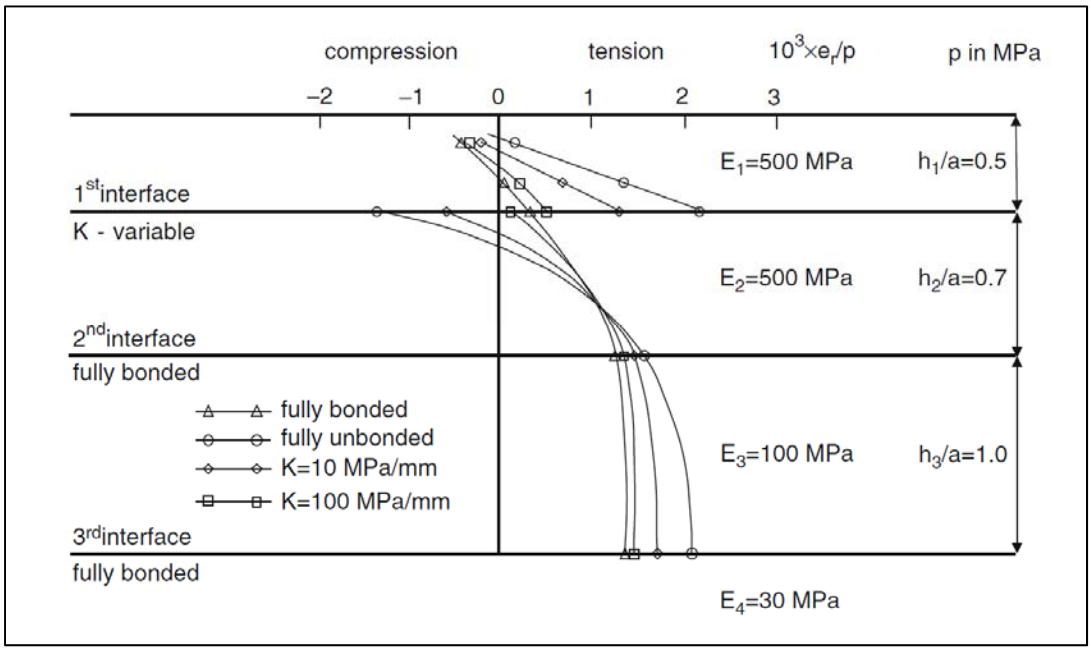

Figure A.34 Distribution of strain vs. depth (Canestrari et al. 2013).

8. Computational Analysis of Interface Stress Distributions

Several computational analysis methods have been employed to evaluate the bond strength and stress at an interface of pavement structures. According to the literature review, DeBondt and Scarpas analyzed shear stress to evaluate the conditions generated by a shear tester (DeBondt 1994). Romanoschi and Metcalf (2001) used a constitutive model to evaluate the conditions at the interface of extracted cores at different temperatures and normal stress levels. Kruntcheva et al. (2006) conducted a study using several finite element models to better understand the stress distribution at the interface.

By using the so-called *Waterways Engineering Station Layer Elastic Analysis* (WESLEA), Willis and Timm (2007) developed three strain profiles in a forensic investigation of debonded pavements obtained from the National Center for Asphalt Technology (NCAT) pavement test track. These specimens included a fully-bonded pavement, a pavement where the

stone matrix asphalt (SMA) debonded from the hot mix asphalt (HMA), and a pavement where both the SMA and the rich-bottom layers had debonded. Based on the results of their analysis, as shown in Figure A.35, Willis and Timm (2007) showed that the critical strain locations change depending on where the loss of the bond, i.e., debonding, occurs.

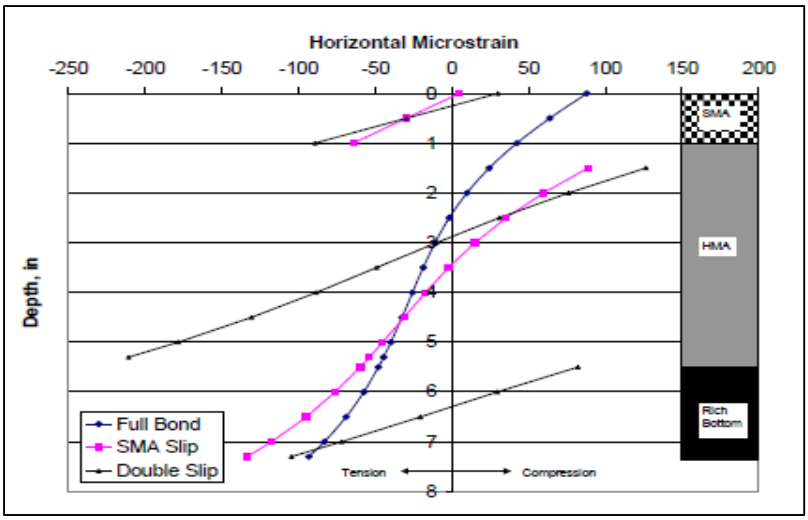

Figure A.35 Theoretical strain profile of debonded pavement (Willis and Timm 2007).

The authors (Tran et al. 2012) of NCAT Report No. 12-04 conducted structural pavement analysis using the BISAR pavement modeling program, which models static loads instead of moving loads seen in the field, to evaluate factors that affect interface stresses. They found that a minimum bond strength requirement for a pavement interface could be determined using the shear stress in the top two inches of the asphalt pavements generated by BISAR.

Based on the results of the structural pavement analysis shown in Figure A.36, the researchers for NCAT Report No. 12-04 suggest that a bond strength level of at least 92 psi (634.32 kPa) is necessary to maintain a good bond between the surface and binder layers when the thickness of the surface layer is 0.5 in. (1.27 cm). They also found that the interface shear stress level decreases for thicker surface layers, as evidenced by 40 psi (275.79 kPa) at a depth of two inches (5.08 cm).

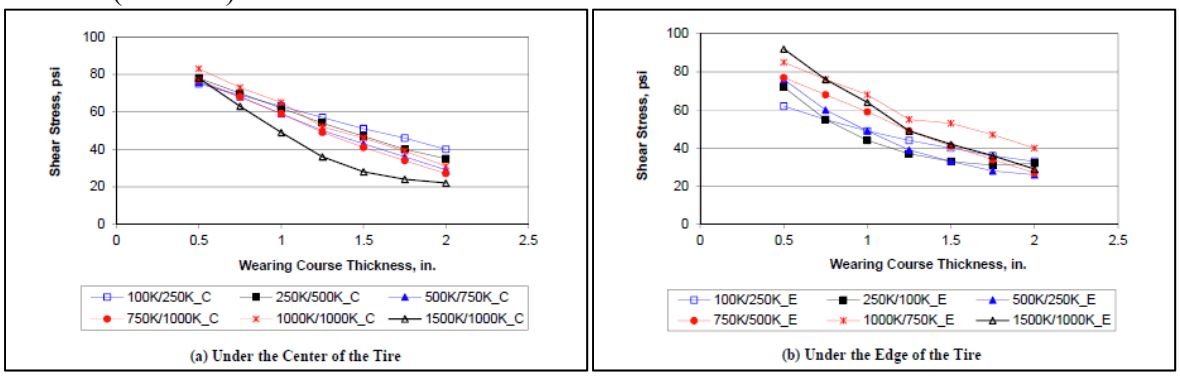

Figure A.36 Shear stress variation with seasonal asphalt concrete stiffness variation (Tran et al. 2012).

Su et al. (2008) conducted three-dimensional finite element analysis to evaluate the effects of tire pressure and stress components in terms of vertical and horizontal stresses on shear stress. They found that the maximum shear stress occurs directly under the edge of the tire, irrespective of loading conditions. As shown in Figure A.37, their analysis results show that the shear stress under the tire edge increases initially with depth in all cases, reaching the maximum value at an approximate depth of 60 mm, after which it decreases from the peak value.

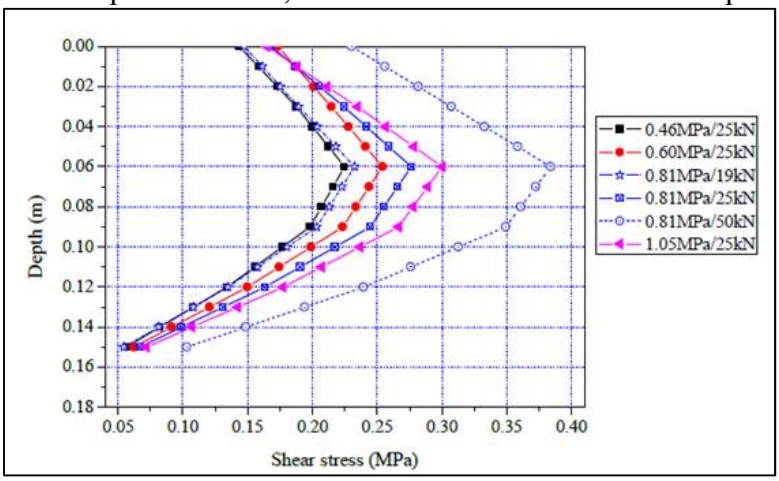

Figure A.37 Shear stress distribution as a function of depth (Su et al. 2008).

The research conducted by Novak et al. (2003) shows similar curves for depth versus shear stress, as shown in Figure A.38.

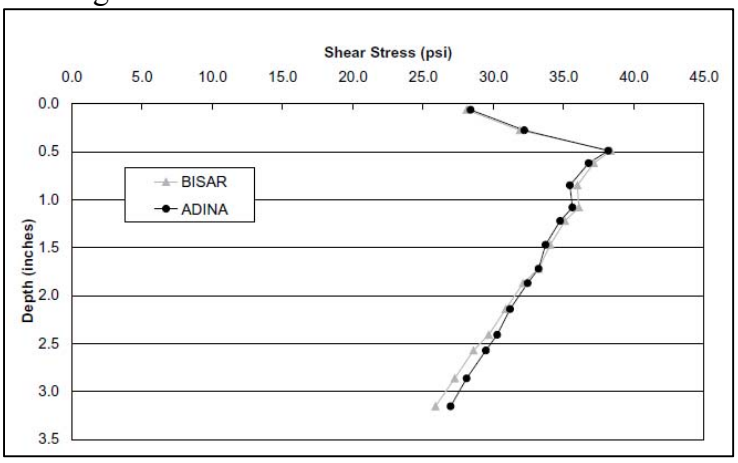

Figure A.38 Comparison of shear stress levels under the tire edge of a two-dimensional axisymmetric circular uniform vertical load as predicted using BISAR and ADINA (Novak et al. 2003).

Su et al. (2008) also investigated the effects of interface conditions on shear stress, focusing on cases of no bonding and full bonding between the asphalt layer and the base course. The condition of the interface between the layers is known to make an important contribution to pavement performance in a multilayered pavement system. Figure A.39 shows the shear stress contours on the vertical plane at the edge of the tire for the two cases. They found that both the range and magnitude of the shear stress for the no bonding condition were greater than for full

bonding. Poor bonding at the interface, which means a situation somewhere between no bonding and full bonding, resulted in higher shear stress levels than at full bonding (Su et al. 2008).

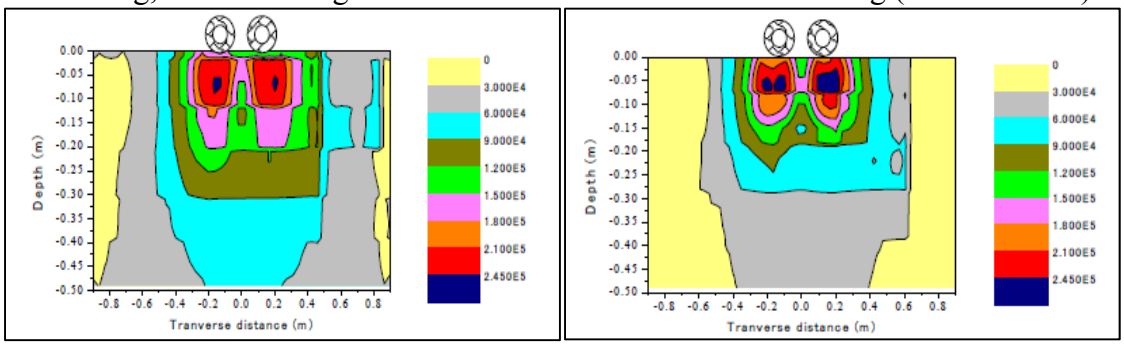

(a) Full bonding (b) No bonding

Figure A.39 Shear stress distribution through depth under different interface conditions (Su et al. 2008).

APPENDIX B: Computational Analysis

1. Analysis of Stress Distribution at Interface

In order to evaluate the effect of the tack coat on the quality of the interface debonding, it is necessary to understand and quantify the distribution of the stress levels at the layer interface under realistic loading conditions. Therefore, the stress levels under moving vehicle loads were evaluated to determine the critical stresses at the layer interface using the Layered ViscoElastic pavement analysis for Critical Distresses (LVECD) computer program developed at North Carolina State University (NCSU). Typical material properties and three typical pavement structures commonly constructed in North Carolina were used in the computational simulations; these three pavement structures are thin, intermediate, and thick pavements, as shown in Figure B.1. The analysis was conducted at four temperatures, 5°C, 20°C, 40°C, and 60°C, three different speeds, 8 km/hour (5 mph), 40 km/hour (25 mph), and 88 km/hour (55 mph), and three axle loads, 53.4 kN (12 kips), 80 kN (18 kips), and 106.8 kN (24 kips). Two types of tire rolling conditions, i.e., free rolling and braking, were considered in this computational analysis

The stress and strain levels computed from the pavement responses using the LVECD program were used to better understand the critical stress that is involved in debonding and the ways that such stress is affected by pavement design parameters and environmental conditions. The computational simulation conditions used in this study are summarized in Table B.1.

Table B.2 presents the layer thicknesses and typical material properties used in the computational simulations.

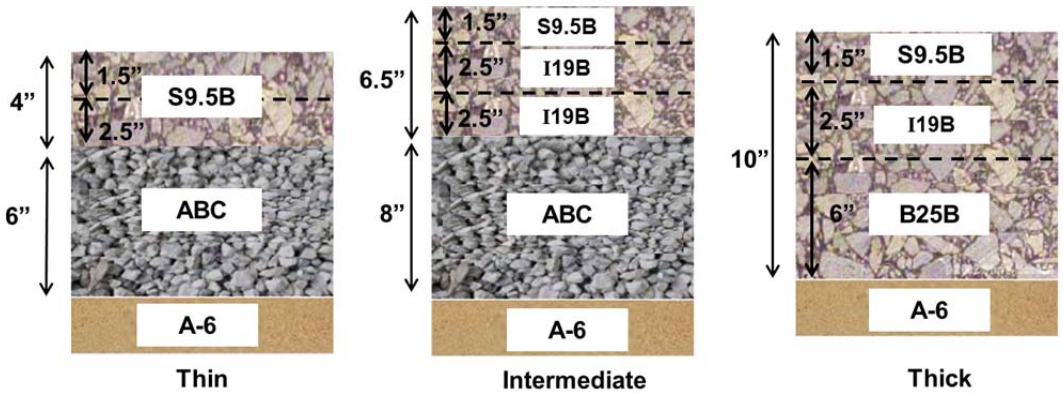

Figure B.1 Pavement structures used in computational simulations.

Table B.1 Summary of computational simulation conditions.

Simulation Conditions	
Pavement Structure	Thin, Intermediate, Thick
Axle Load	53.4 kN (12 kips), 80 kN (18 kips), and 106.8 kN (24 kips)
Speed	8 km/hour (5 mph), 40 km/hour (25 mph), 88 km/hour (55 mph)
Tire Rolling Condition	Free Rolling State, Braking State
Temperature	5°C, 20°C, 40°C, 60°C

Table B.2 Layer thicknesses and typical material properties.

Pavement Layer	**Material ID**	**Layer Thickness (cm)**	**Interface Location**	**Poisson's Ratio**
Thin Pavement Structure				
Asphalt Concrete	S9.5B*	10.16 (4 in.)	3.81 (1.5 in.)	0.35
Aggregate Base	ABC	15.24 (6 in.)		0.40
Subgrade	A6**	Infinite		0.45
Intermediate Pavement Structure				
Asphalt Concrete	S9.5B*	3.81 (1.5 in.)	3.81 (1.5 in.)	0.35
	I19B*	12.70 (5 in.)		
Aggregate Base	ABC	20.32 (8 in.)		0.40
Subgrade	A6**	Infinite		0.45
Thick Pavement Structure				
Asphalt Concrete	S9.5B*	3.81 (1.5 in.)	3.81 (1.5 in.)	0.35
	I19B*	6.35 (2.5 in.)		
	B25B*	15.24 (6 in.)		
Subgrade	A6**	Infinite		0.45

Note: *The first letter indicates the layer type, i.e., S for surface, I for intermediate, and B for base course. The number between the two letters is the nominal maximum aggregate size (NMAS). The last letter indicates the traffic

volume, which in turn determines the asphalt binder grade: B indicates less than 3 million equivalent single axle loads (ESALs) and PG 64-22 binder.

**AASHTO soil classification system

2. Overview of the LVECD Program

The NCSU research team developed the LVECD program to simulate both pavement performance and pavement responses using moving traffic loads and pavement temperature data. The LVECD program utilizes layered viscoelastic analysis and a time-scale separation scheme to improve the computing efficiency of the stress-strain calculations (i.e., the response analysis). This program combines the concepts of Fourier transform and finite element discretization in order to provide simulation times that are orders of magnitude shorter than those of conventional three-dimensional (3-D) finite element methods (Eslaminia et al. 2012). That is, the LVECD method can capture the effects of viscoelasticity and the moving nature of traffic loads with high efficiency.

The time-scale separation scheme was developed under the assumption of gradual changes in damage (over a few weeks) and pavement temperature (over a few hours). This scheme allows millions of cycles to be reduced to hundreds of cycles by integrating the analysis with an extrapolation technique. The entire procedure, from entering inputs to viewing outputs, is operated via a user-friendly graphic interface (as shown in Figure B.2) that is similar to that found in Pavement ME software. Structural information, such as layer thickness and viscoelastic continuum damage (VECD) properties, which can be obtained through the simplified VECD (S-VECD) test protocol, can be entered easily.

The LVECD program has been designed to use pavement temperature data provided by the Enhanced Integrated Climate Model (EICM) software for performing thermal analysis. The EICM program provides hourly temperatures of asphalt pavements in terms of pavement depth. The traffic data window allows users to enter various types of vehicle loading. For example, standard loading, such as equivalent single-axle load (ESAL) inputs, single wheel data, and user-defined vehicle configurations, can be simulated. Analysis results (i.e., damage evolution, stress, and strain) can be evaluated in terms of spatial distribution and time history distribution.

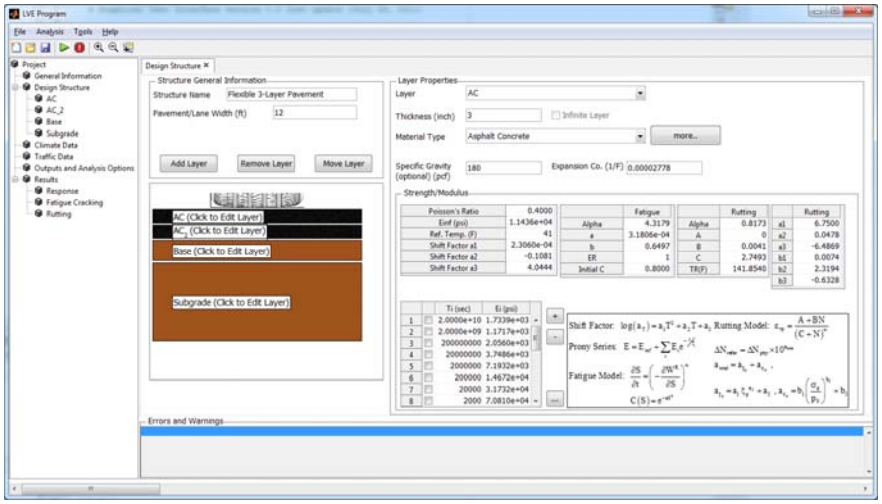

Figure B.2 LVECD program input window.

3. Parameters used in LVECD Program Simulations

3.1. Dynamic Modulus (|E*|) Values and Time-Temperature (t-T) Shift Factors

Dynamic modulus tests were performed for each study mixture to obtain basic viscoelastic properties, i.e., the dynamic modulus (|E*|) values and time-temperature (t-T) shift factors. Asphalt concrete in the linear viscoelastic range is known to be thermorheologically simple material and, as such, the effects of time and temperature can be combined into a joint parameter, i.e., reduced time/frequency, f_R, using the t-T shift factor (a_T), as shown in Equation (3) and Equation (4).

$$f_R = f \times a_T \tag{3}$$

where

f = frequency in Hz and

a_T = shift factor.

$$\log\left(a_T\right) = \alpha_1 T^2 + \alpha_2 T + \alpha_3 \tag{4}$$

where

$\alpha_1, \alpha_2, \alpha_3$ = regression coefficients and

T = temperature.

In this process, the data sets at various temperatures are shifted with respect to time until the curves merge into a single smooth function, which allows for the horizontal shifting of the data onto an arbitrarily selected reference temperature curve to form a single curve, the mastercurve. The mastercurve then is used to describe the constitutive behavior of the asphalt concrete over a wide range of temperatures and frequencies. Figure B.3 presents the results for each mixture at several different temperature/frequency combinations. Table B.3 presents the data for various temperatures and frequencies for each mixture. The t-T shift factor is the amount of horizontal shift in log scale that is required to create the continuous curve. The amount of shifting is dependent on the temperature chosen as the reference temperature and, therefore, varies according to temperature, as shown in Figure B.4. Table B.4 presents the fitting coefficients of the t-T shift factor function for each mixture. The data are generated by calculating the appropriate reduced frequency using the shift factor function equation, Equation (3), with the coefficients shown in Table B.4 and interpolating the data shown in Figure B.5 at the respective reduced frequency.

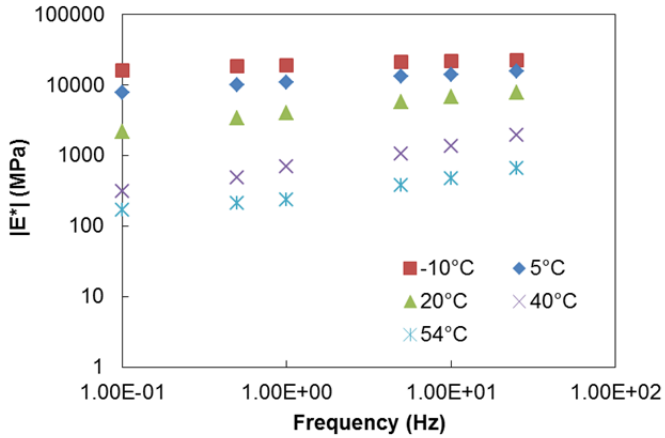

(a)

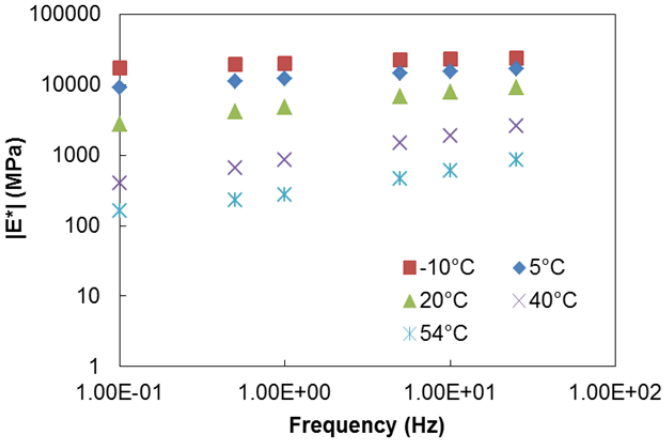

(b)

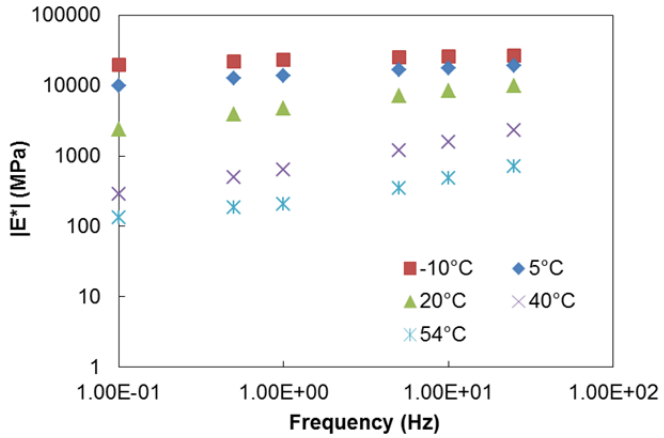

(c)

Figure B.3 Typical unshifted dynamic modulus values for each mixture: (a) S9.5B, (b) I19B, and (c) B25B.

Table B.3 Linear viscoelastic properties of the study mixtures at selected frequencies and temperatures.

Mixtures		S9.5B		I19B		B25B	
Temperature (°C)	Frequency (Hz)	|E*| (MPa)	Phase Angle (deg)	|E*| (MPa)	Phase Angle (deg)	|E*| (MPa)	Phase Angle (deg)
-10	25	22801	6.0	23712	5.6	26784	7.1
	10	22008	6.1	23085	5.3	25951	7.7
	5	21309	6.4	22372	5.4	25204	8.0
	1	19152	7.2	20149	6.1	22952	9.0
	0.5	18352	7.7	19343	6.3	22031	9.0
	0.1	16190	9.2	17266	6.9	19853	9.2
5	25	15709	10.1	16974	7.9	19001	10.8
	10	14189	11.2	15550	9.8	17586	11.9
	5	13230	11.3	14529	10.1	16456	12.5
	1	10871	12.6	12131	11.3	13643	14.3
	0.5	9980	13.4	11191	12.0	12522	15.3
	0.1	7864	16.2	9041	14.5	9986	18.8
20	25	7926	17.1	9118	16.7	9904	20.8
	10	6735	18.9	7859	17.8	8350	23.1
	5	5839	20.4	6899	19.3	7123	25.0
	1	4013	24.1	4862	22.9	4696	30.0
	0.5	3420	25.6	4160	24.4	3904	32.4
	0.1	2192	30.3	2719	29.2	2379	37.7
40	25	1938	33.7	2576	32.2	2301	40.8
	10	1377	36.0	1863	35.8	1590	42.7
	5	1064	36.5	1472	36.7	1205	42.7
	1	693	40.1	849	39.1	632	43.1
	0.5	483	37.4	659	38.0	502	41.6
	0.1	308	35.3	405	36.8	291	36.8
54	25	658	39.6	863	38.8	713	44.4
	10	473	38.9	601	38.4	479	42.9
	5	378	37.3	465	36.8	350	40.6
	1	234	32.6	272	32.8	207	33.5
	0.5	209	29.5	229	30.6	187	29.1
	0.1	171	26.0	161	26.7	134	23.5

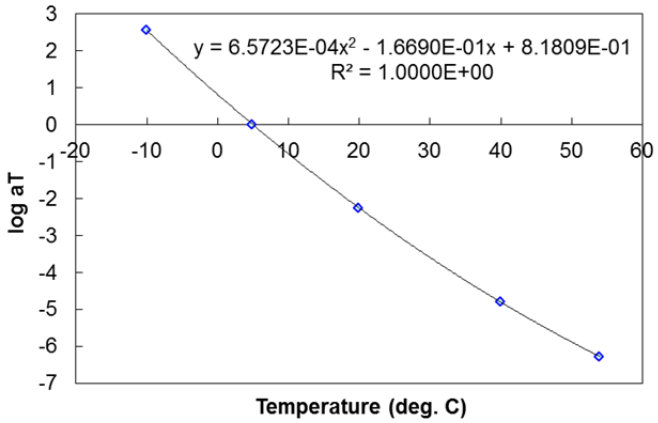

(a)

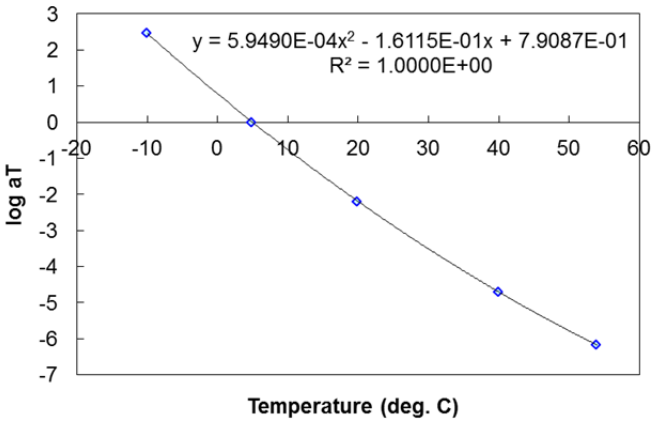

(b)

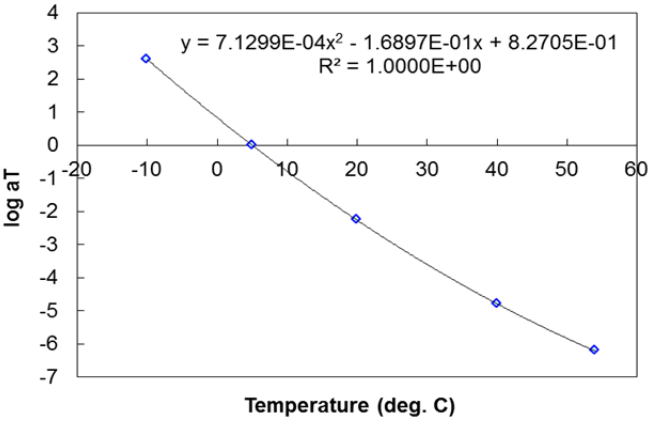

(c)

Figure B.4 Time-temperature shift factor function for each mixture: (a) S9.5B, (b) I19B, and (c) B25B.

Table B.4 Fitting coefficients of time-temperature shift factor function.

Parameters	S9.5B	I19B	B25B
α_1	0.000657	0.000595	0.000713
α_2	-0.166904	-0.161149	-0.168975
α_3	0.818090	0.790873	0.827049

A single mastercurve can be represented by a sigmoidal function, as shown in Equation (5) and Figure B.5.

$$\log|E^*| = a + \frac{b}{1+\frac{1}{e^{d+g*\log(f_R)}}} \tag{5}$$

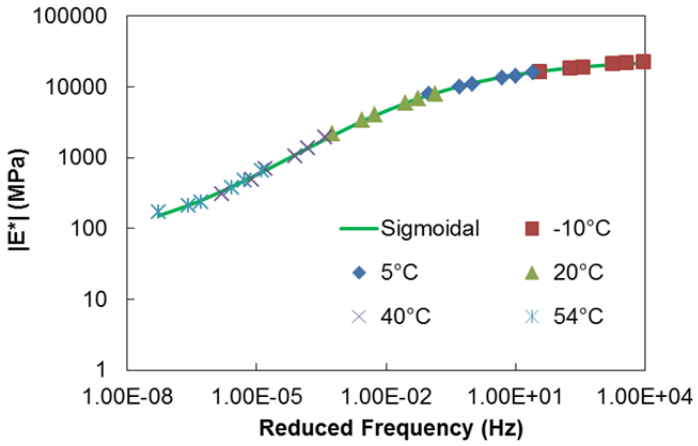

(a)

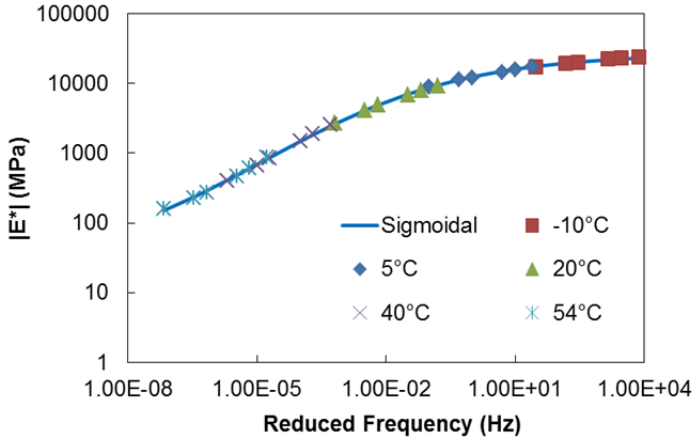

(b)

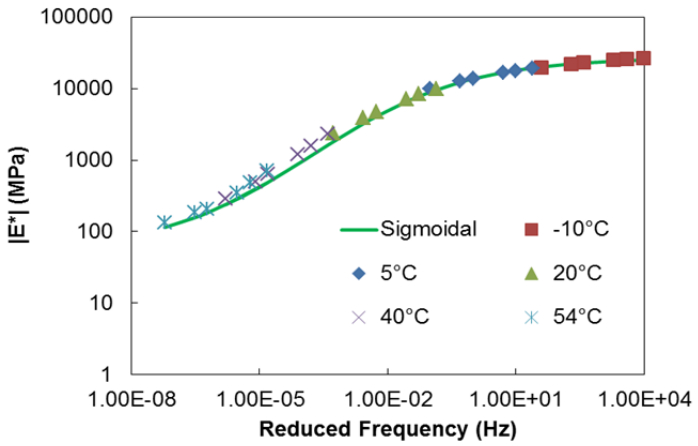

(c)

Figure B.5 Dynamic modulus mastercurve for each mixture: (a) S9.5B, (b) I19B, and (c) B25B.

Table B.5 Prony coefficients for relaxation modulus.

ρ_i (sec)	E_i (MPa)		
	S9.5B	I19B	B25B
2E+11	2.38	2.82	1.73
2E+10	4.13	4.84	3.10
2E+09	7.33	8.57	5.67
2E+08	13.42	15.86	10.71
2E+07	25.71	31.18	21.24
2E+06	52.45	65.98	45.30
2E+05	115.27	150.13	105.76
2E+04	270.18	356.33	268.88
2E+03	641.43	823.24	702.80
2E+02	1401.35	1685.67	1676.39
2E+01	2533.10	2821.99	3194.19
2E+00	3595.62	3759.34	4550.70
2E-01	3173.76	3476.25	4160.30
2E-02	3761.12	3756.60	4357.92
2E-03	3104.72	3081.01	3337.35
2E-04	2497.32	2440.15	2452.81
2E-05	1851.65	1802.00	1669.18
2E-06	1323.71	1286.44	1099.82
2E-07	917.49	893.45	705.84
2E-08	624.31	610.14	446.61
2E-09	419.32	411.78	279.86
2E-10	279.30	275.80	174.38
2E-11	185.00	183.77	108.26
E_∞	60.49	38.24	51.59

3.2. Material Properties for Each Pavement Layer

The aggregate base layer and the subgrade are assumed to be linear elastic materials in the LVECD program simulations. Table B.6 provides the modulus data used for each layer.

Table B.6 Material properties used in the LVECD program simulations.

Mixtures	Elastic Modulus (MPa)
S9.5B	Based on Mastercurve Developed using Table B.3 Data
I19B	Based on Mastercurve Developed using Table B.3 Data
B25B	Based on Mastercurve Developed using Table B.3 Data
Aggregate Base	275.79 (40,000 psi)
Subgrade	68.95 (10,000 psi)

3.3. Rolling Resistance Coefficients Due to Tire Rolling Condition

Because the tire-pavement contact stress is affected directly by the tire rolling conditions, two types of tire rolling conditions, i.e., free rolling and braking, were considered in this study. The rolling resistance coefficient used in this study can be also refered to as the friction of coefficient in physics. Based on the literature review, the rolling resistance coefficient for large truck tires ranges from 0.0045 to 0.008 (Michelin 2012). However, when a tire is under the free rolling condition, it is deemed reasonable to assume that the longitudinal contact stress (frictional force) is negligible because the tire has low rolling resistance under the free rolling condition. To confirm this assumption, two cases of the rolling resistance coefficients of 0 and 0.008 were compared. The LVECD program was used to determine the normal and shear stress distributions throughout the pavement depth for various temperatures, speed levels, axle loads, and pavement structures. Figure B.6 presents the example normal and shear stress distributions throughout the pavement depth for the intermediate pavement under a 80-kN wheel load moving at 88 km/hour at 5°C.

Figure B.6 shows no meaningful difference between the two cases; therefore, for the rest of this study, the rolling resistance coefficient was set to zero for the free rolling condition.

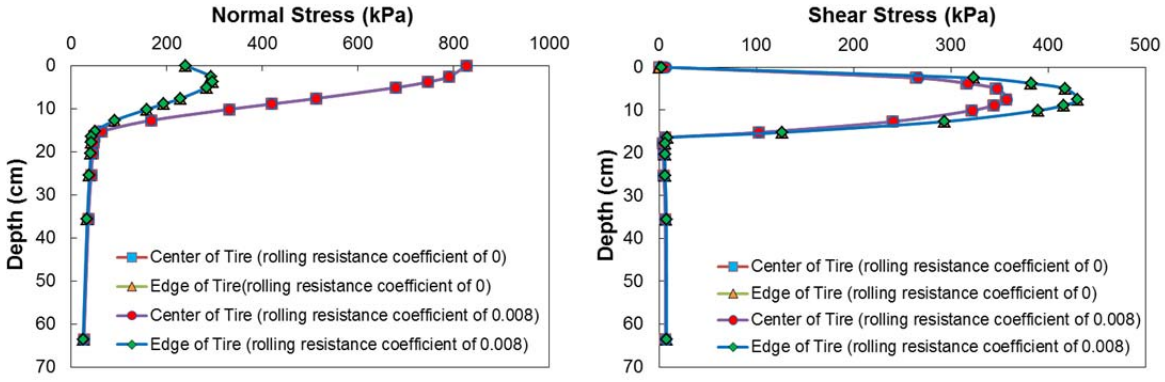

Figure B.6 Comparison of rolling resistance coefficients of 0 and 0.008. Conditions: intermediate pavement, 80-kN (18 kips), 88 km/hour (55 mph), and 5°C

For the braking condition, based on the results of a study of the stopping distances of truck tractors conducted by the National Highway Traffic Safety Administration (NHTSA), three rolling resistance coefficients, 0.35, 0.45, and 0.55, were determined to encompass the range of minimum and maximum coefficients, as presented in Table B.7, and were utilized for the braking state in the LVECD simulations.

Table B.7 Stopping distances and rolling resistance coefficients for braking state (NHTSA 2009).

Vehicle Speed (V) (mph)	Case (1)	Case (2)	Case (3)	Case (4)	Case (5)	Case (6)	Case (1)	Case (2)	Case (3)	Case (4)	Case (5)	Case (6)
	Stopping Distance (D) (feet)						Friction of Coefficient (f) ($f = V^2/(30D)$)					
20	32	35	30	35	38	28	0.42	0.38	0.44	0.38	0.35	0.48
25	49	54	45	54	59	43	0.43	0.39	0.46	0.39	0.35	0.48
30	70	78	65	78	84	61	0.43	0.38	0.46	0.38	0.36	0.49
35	96	106	89	106	114	84	0.43	0.39	0.46	0.39	0.36	0.49
40	125	138	114	138	149	108	0.43	0.39	0.47	0.39	0.36	0.49
45	158	175	144	175	189	136	0.43	0.39	0.47	0.39	0.36	0.50
50	195	216	176	216	233	166	0.43	0.39	0.47	0.39	0.36	0.50
55	236	261	212	261	281	199	0.43	0.39	0.48	0.39	0.36	0.51
60	280	310	250	310	335	235	0.43	0.39	0.48	0.39	0.36	0.51
Minimum							0.42	0.38	0.44	0.38	0.35	0.48
Maximum							0.43	0.39	0.48	0.39	0.36	0.51
Rolling Resistance Coefficient (Friction of Coefficient)							0.35, 0.45, 0.55					

(1) Loaded and unloaded buses
(2) Loaded single-unit trucks
(3) Loaded tractors with three axles and a gross vehicle weight rating (GVWR) of 70,000 lbs. or less, or with four of more axles and a GVWR of 85,000 lbs. or less; tested with an unbraked control trailer
(4) Loaded tractors with three axles and a GVWR greater than 70,000 lbs., or with four or more axles and a GVWR greater than 85,000 lbs; tested with an unbraked control trailer
(5) Unloaded single-unit trucks
(6) Unloaded tractors (bobtail)

3.4. Tire-Pavement Contact Pressure Distribution

Recent studies (Wang 2011, Su et al. 2008, Yoo et al. 2006, and Novak et al. 2003) have revealed that the tire-pavement contact pressure is non-uniform, and the effect of the non-uniform distribution of the contact pressure is important in accurate pavement response computations. In addition, the tire-pavement contact pressure distribution is affected significantly by tire inflation pressure, tire type, and tire load (Siddharthan et al. 2002).

The tire-pavement contact area in the LVECD program is assumed to be a rectangular shape with an aspect ratio of 11/7 (length/width). The rectangular shape of the tire-pavement contact area was determined by the NCSU research team based on the shape and magnitude data that De Beer et al. (2004) obtained from measurements taken under real trucks using the Stress-In-Motion (SIM) technology. The axle loads are applied in a single tire configuration with 827.4 kPa (120 psi) tire-pavement contact pressure. Constant pressure with smoothed sides for the distribution of the tire-pavement contact pressure was implemented in the LVECD program, as

shown in Figure B.7. The tire-pavement contact pressure distribution is based on fitting a quadratic function to the actual pressure in both the longitudinal and transverse directions.

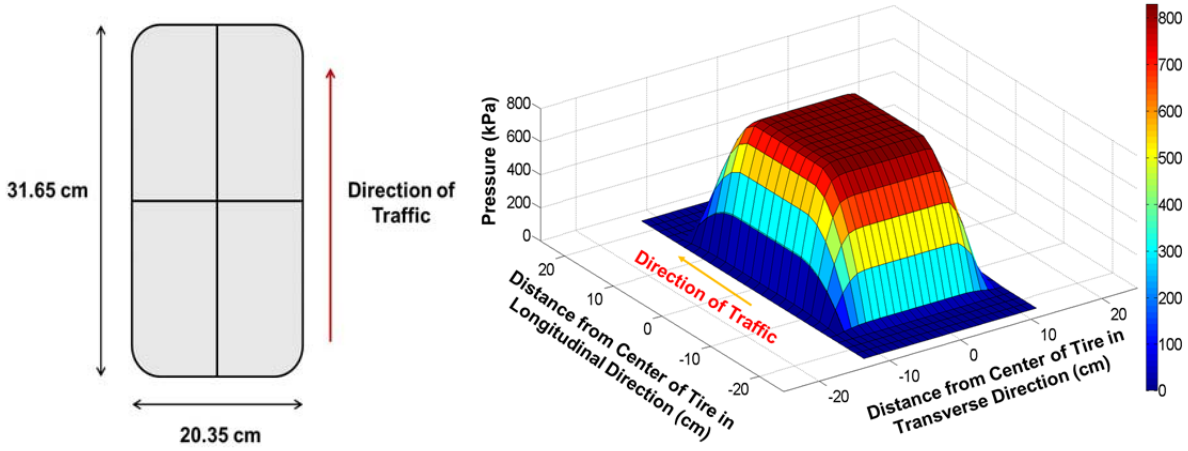

(a) (b)

Figure B.7 (a) Single tire footprint and (b) distribution of tire-pavement contact pressure for wheel load of 40 kN (9 kips).

3.5. Mesh Convergence Study

In finite element modeling, a fine mesh typically results in a more accurate solution than a coarse mesh. However, as a mesh is made finer, the computation time increases. Therefore, it is important to balance accuracy and computing resources. One way to achieve such balance is to perform a mesh convergence study. Figure B.8 presents the convergence analysis results for meshes of different sizes. The numbers in the legends represent the number of meshes within a pavement width of 3.66 m (12 ft) in the transverse direction. The number of meshes in the longitudinal traffic direction indicates the time step used in the finite element analysis. Two stress components, σ_{zz} and τ_{max}, are plotted in Figure B.8 at 3.81 cm (1.5 in.) pavement depth. σ_{zz} is the compressive stress in the vertical direction, and τ_{max} is the maximum shear stress on the horizontal plane at a certain pavement depth. The use of τ_{max} allows the most critical shear stress on the horizontal plane at a specific pavement depth, i.e., 3.81 cm (1.5 in.), to be found, as shown in Figure B.8. τ_{max} employed in this research is defined by the following equation:

$$\tau_{max} = \sqrt{(\tau_{yz})^2 + (\tau_{xz})^2} \quad (6)$$

where

τ_{xz} = shear stress in the transverse direction at the interface calculated by the LVECD program, and

τ_{yz} = shear stress in the longitudinal direction at the interface calculated by the LVECD program.

All the plots visually converge onto each other except for the mesh number of 100. Therefore, mesh number 200 was chosen as the optimal mesh size for this study. Thus, the number of horizontal divisions and the number of time steps were entered into the LVECD program using 200 as the mesh number.

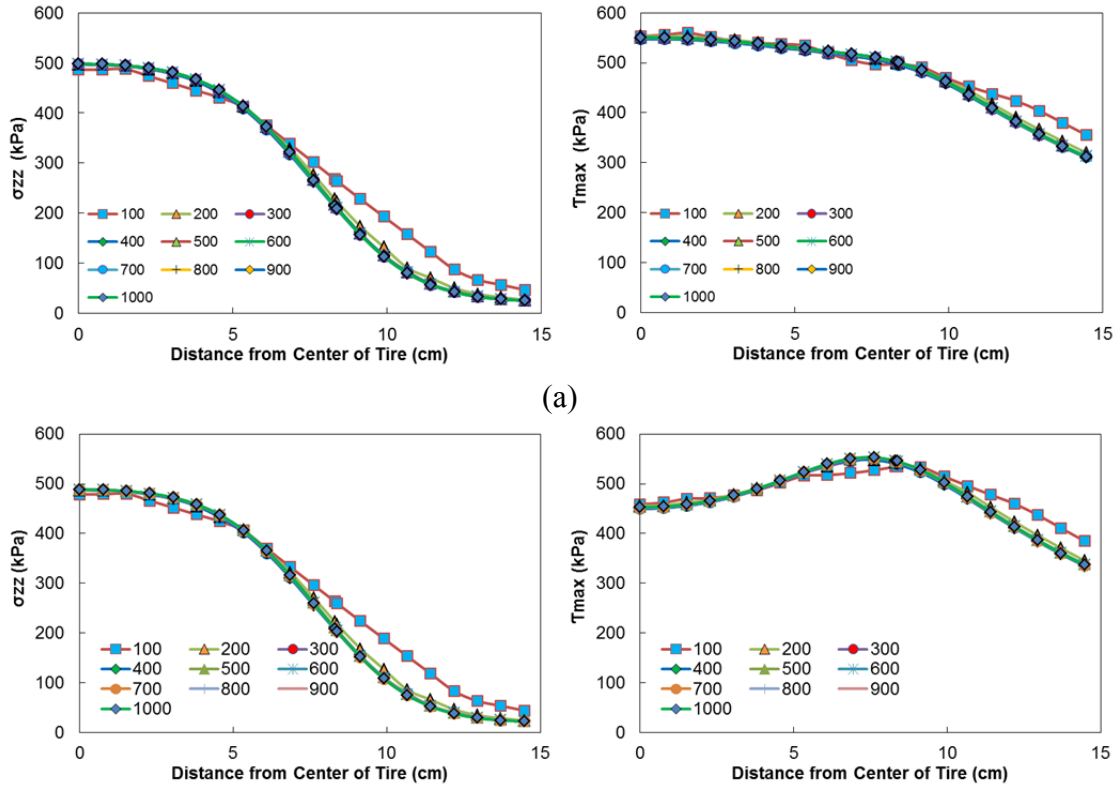

Figure B.8 Convergence analysis results in the transverse direction of the tire: (a) thin pavement, 53.4 kN (12 kips), 8 km/hour (5 mph), 5°C, braking condition at 3.81 cm (1.5 in.) depth; and (b) thin pavement, 53.4 kN (12 kips), 8 km/hour (5 mph), 5°C, free rolling condition at 3.81 cm (1.5 in.) depth. (The numbers in the legends represent the number of mesh elements within 3.66 m (12 ft) width of a pavement).

4. LVECD Program Simulation Results

In this section, the effects of temperature, speed, load level, structural type, and rolling resistance coefficient are evaluated in terms of stress.

4.1. Effect of Temperature

The magnitude of the stress in the thin pavement structure and intermediate pavement structure under braking conditions clearly is affected by different temperatures, as shown in Figure B.9, whereas the effect of temperature is less for the thick pavement structure with high load levels, i.e., 80 kN (18 kips) and 106.8 kN (24 kips), as the temperature increases. The normal stress is not affected by the different temperatures for the thick pavement. As for the magnitude of stress under free rolling conditions, even though it is less than the magnitude of the stress under braking conditions, the trend of the stress plots is similar to that under braking conditions in terms of the effect of temperature. It is noted that the shapes of the shear stress curves under the free rolling condition are different from those under the braking condition. That

is, the maximum shear stress occurs at the center of the tire under braking conditions, whereas it occurs around the edge of the tire under free rolling conditions, as shown in Figure B.9.

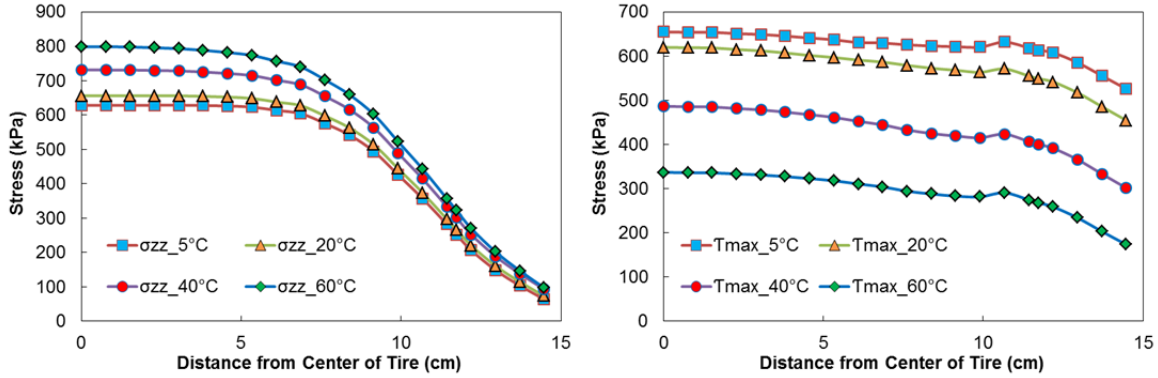

(a)

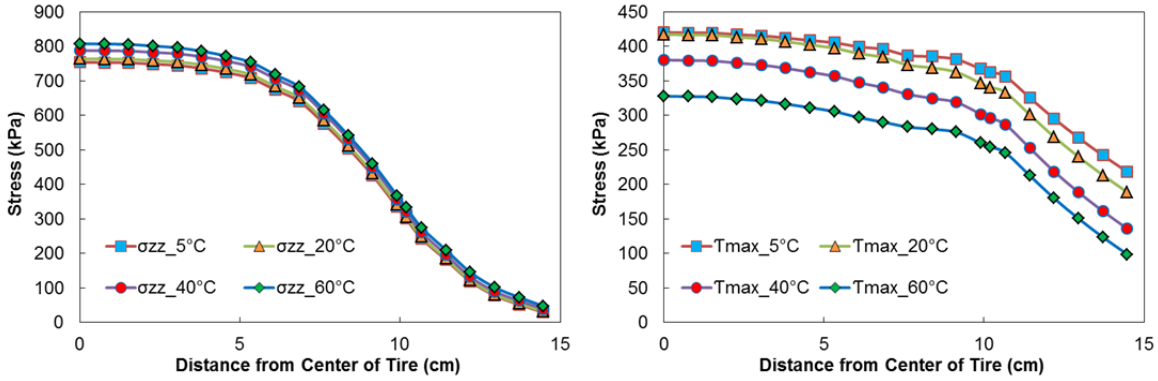

(b)

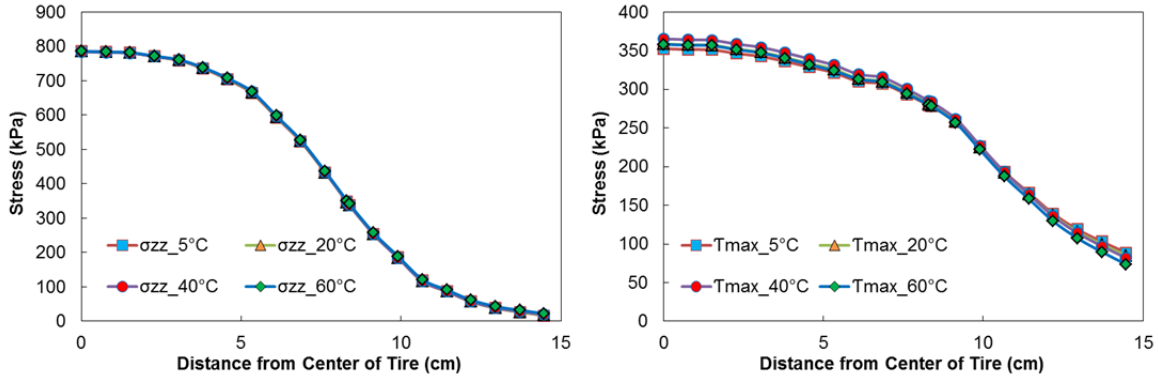

(c)

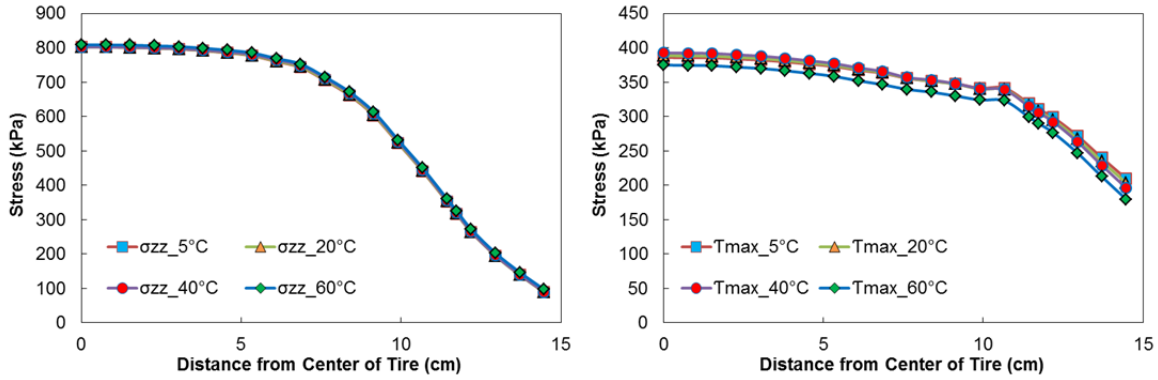

(d)

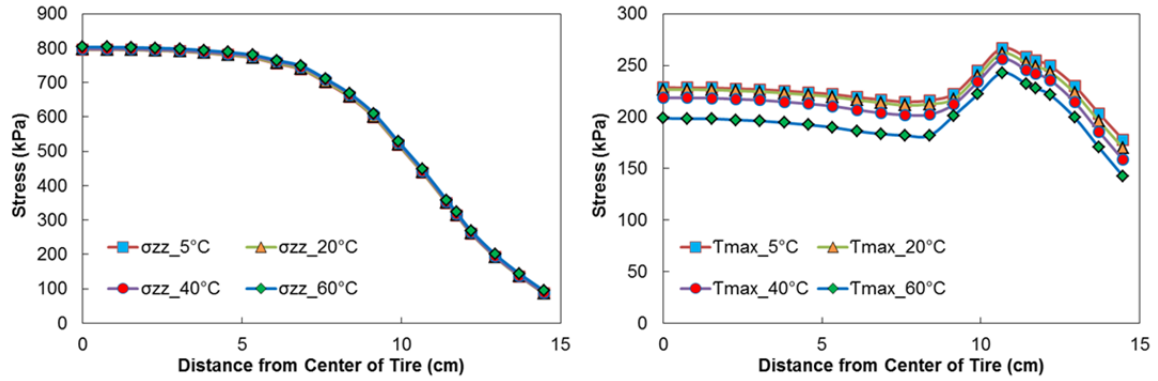

(e)

Figure B.9 Evaluation of temperature effect in the transverse direction of the tire: (a) thin pavement, 106.8 kN (24 kips), 88 km/hour (55 mph), at 3.81 cm (1.5 in.) depth, braking condition (rolling resistance coefficient of 0.35); (b) intermediate pavement, 80 kN (18 kips), 8 km/hour (5 mph), at 13.81 cm (1.5 in.), braking condition (rolling resistance coefficient of 0.45); (c) thick pavement, 53.4 kN (12 kips), 88 km/hour (55 mph), at 3.81 cm (1.5 in.), braking condition (rolling resistance coefficient of 0.55); (d) thick pavement, 106.8 kN (24 kips), 88 km/hour (55 mph), at 3.81 cm (1.5 in.) depth, braking condition (rolling resistance coefficient of 0.55); and (e) thick pavement, 106.8 kN (24 kips), 88 km/hour (55 mph), at 3.81 cm (1.5 in.) depth, free rolling condition.

4.2. Effect of Speed

The effect of speed on interface stresses is negligible at low temperatures, and it increases as temperature becomes higher for all three pavement structures under both braking and free rolling conditions, especially in terms of shear stress rather than normal stress, as shown in Figure B.10.

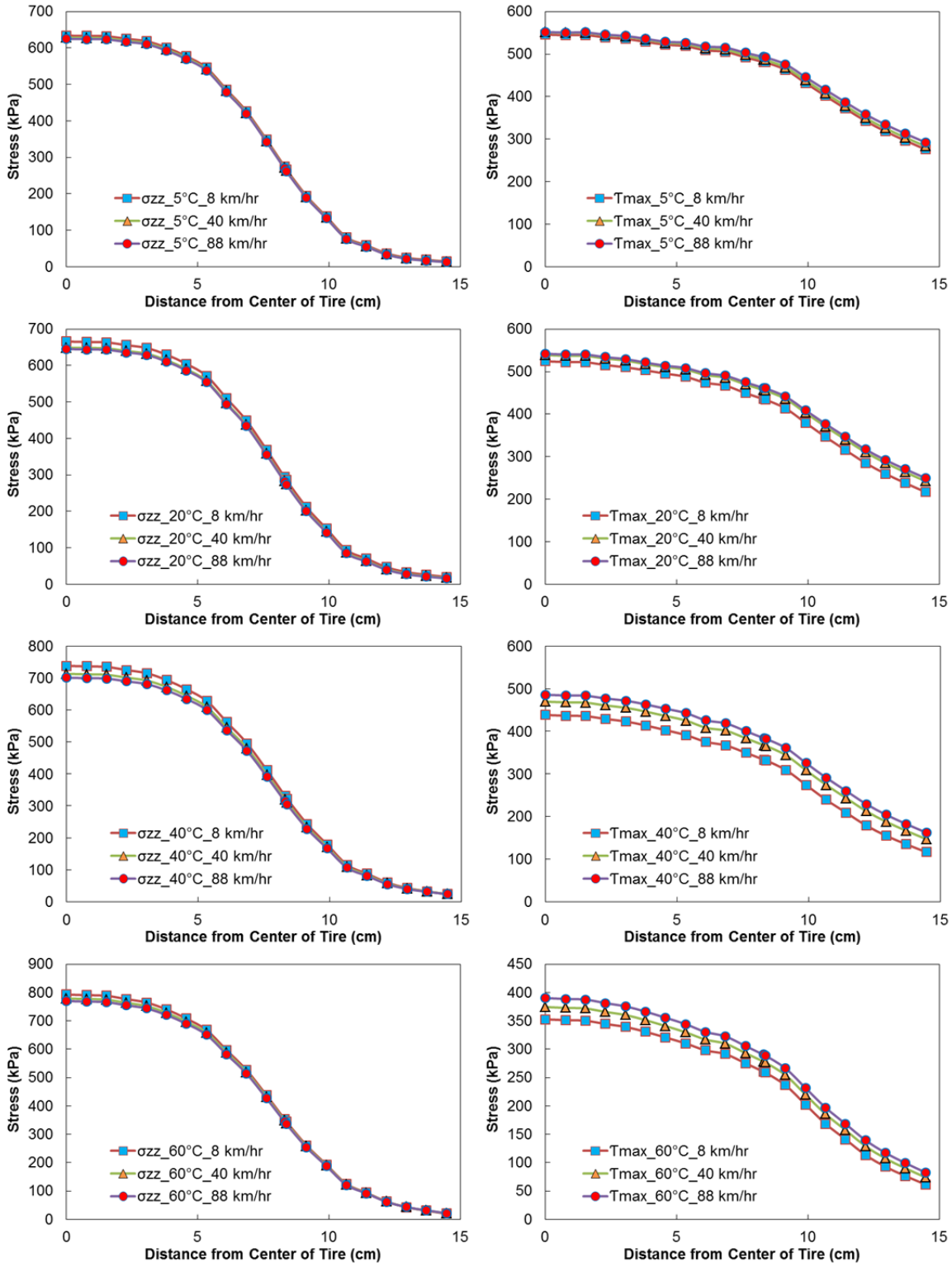

Figure B.10 Evaluation of speed effect in the transverse direction of the tire: thin pavement, 53.4 kN (12 kips), at 3.81 cm (1.5 in.) depth, braking condition (rolling resistance coefficient of 0.55).

4.3. Effect of Load Level

As shown in Figure B.11, the magnitudes of the normal stress and shear stress obviously are affected by the different load levels for all three pavement structures under both braking and free rolling conditions. However, the effect of the different load levels is less in the vicinity of the center of the tire at the higher temperatures (40°C and 60°C), especially in terms of shear stress. The thick pavement structure shows less effect from the different load levels in the vicinity of the center of the tire at the low temperature, 5°C, than the other pavement structures.

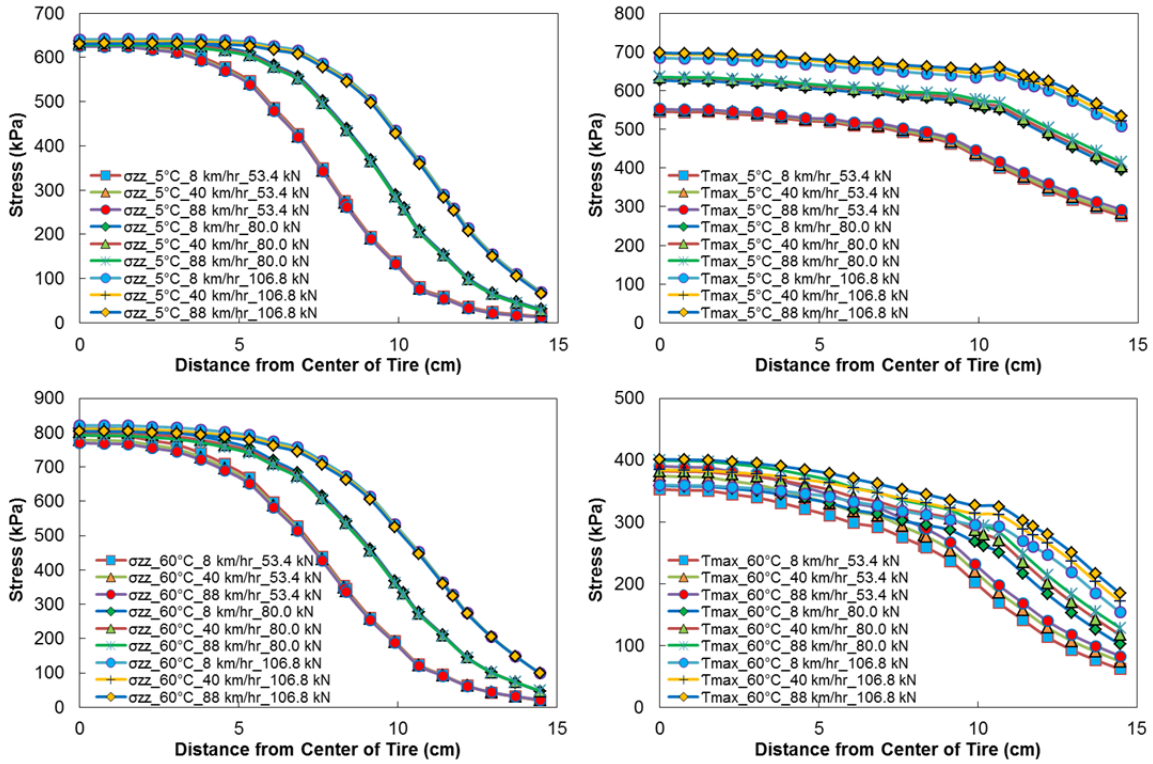

(a)

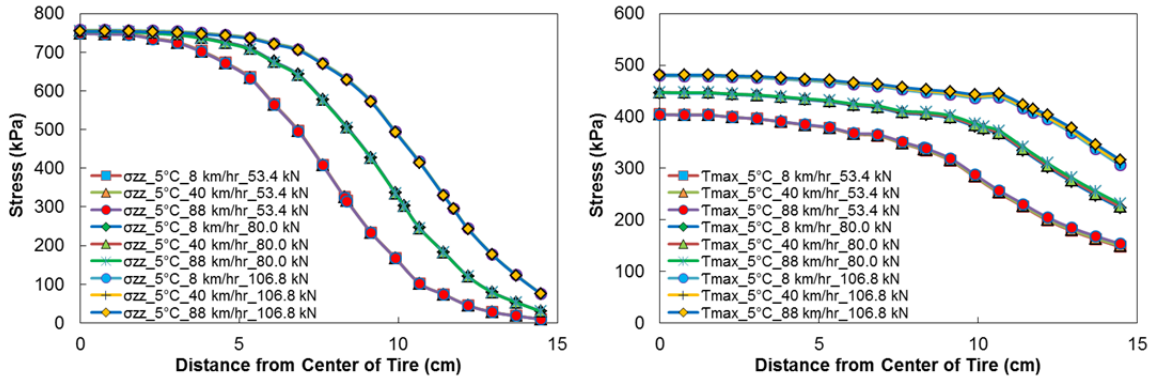

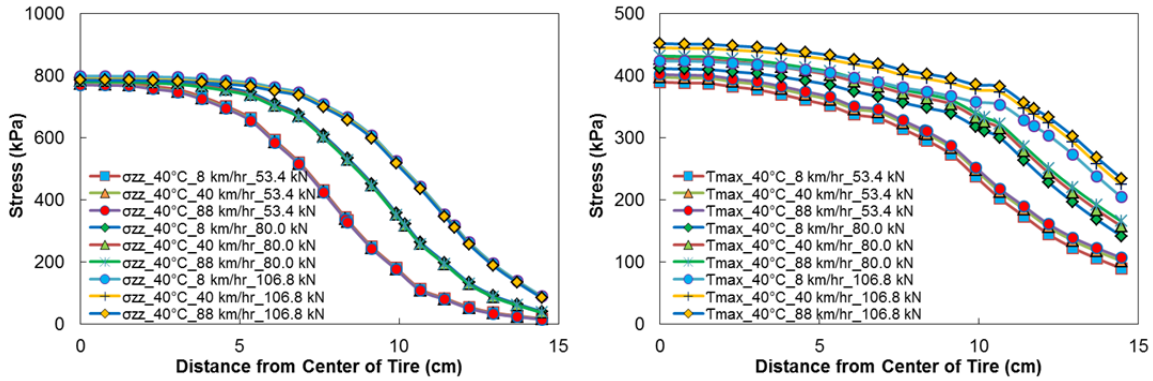

(b)

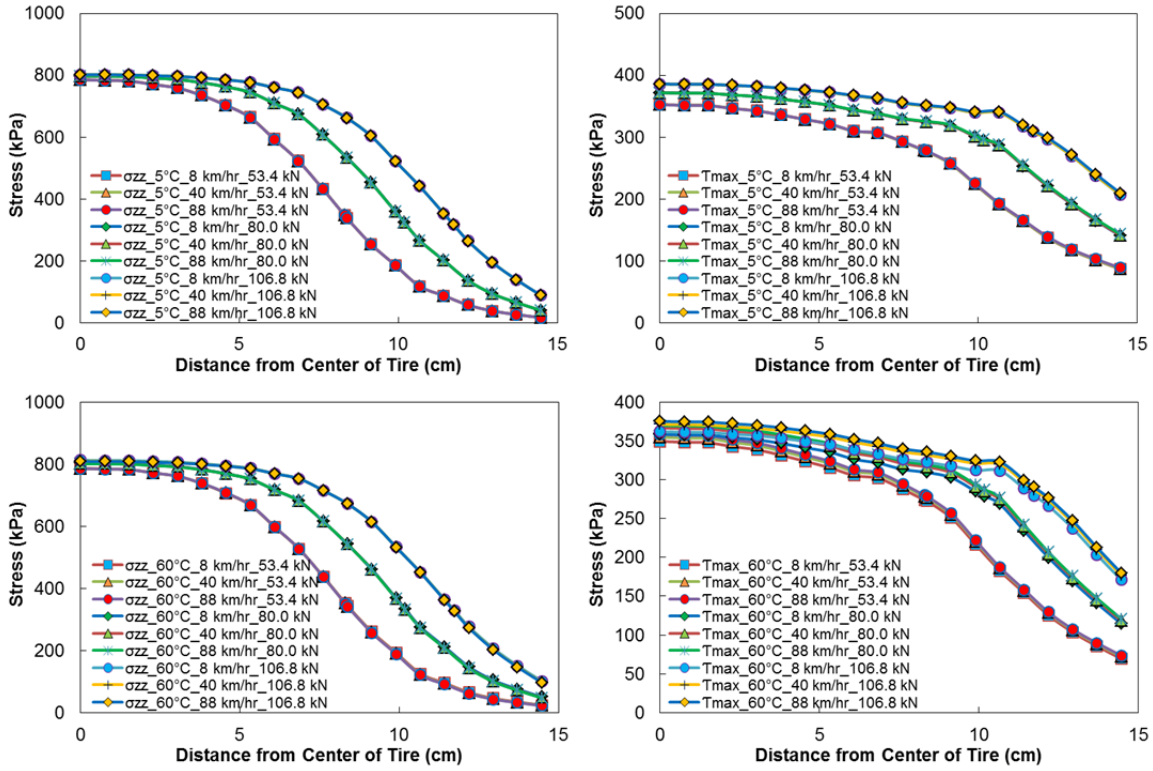

(c)

Figure B.11 Evaluation of load level effect in the transverse direction of the tire: (a) thin pavement at 3.81 cm (1.5 in.) depth; (b) intermediate pavement, at 3.81 cm (1.5 in.) depth; and (c) thick pavement, at 3.81 cm (1.5 in.) depth.

Note: The rolling resistance coefficient of 0.55 is used under the braking condition.

4.4. Effect of Structure Type

As shown in Figure B.12, the effect of the different structure types is clear, diminishing gradually with an increase in temperature. The magnitude of normal stress on the thick pavement structure is greater than on the thin pavement structure, whereas the magnitude of shear stress on the thick pavement structure is less than on the thin pavement structure at a depth of 3.81 cm (1.5 in.) below the surface course. As the temperature increases, the magnitude of normal stress increases, whereas the magnitude of shear stress decreases. In the legends of these figures, *TN*, *I*, and *TK* refer to thin, intermediate, and thick pavement structures, respectively.

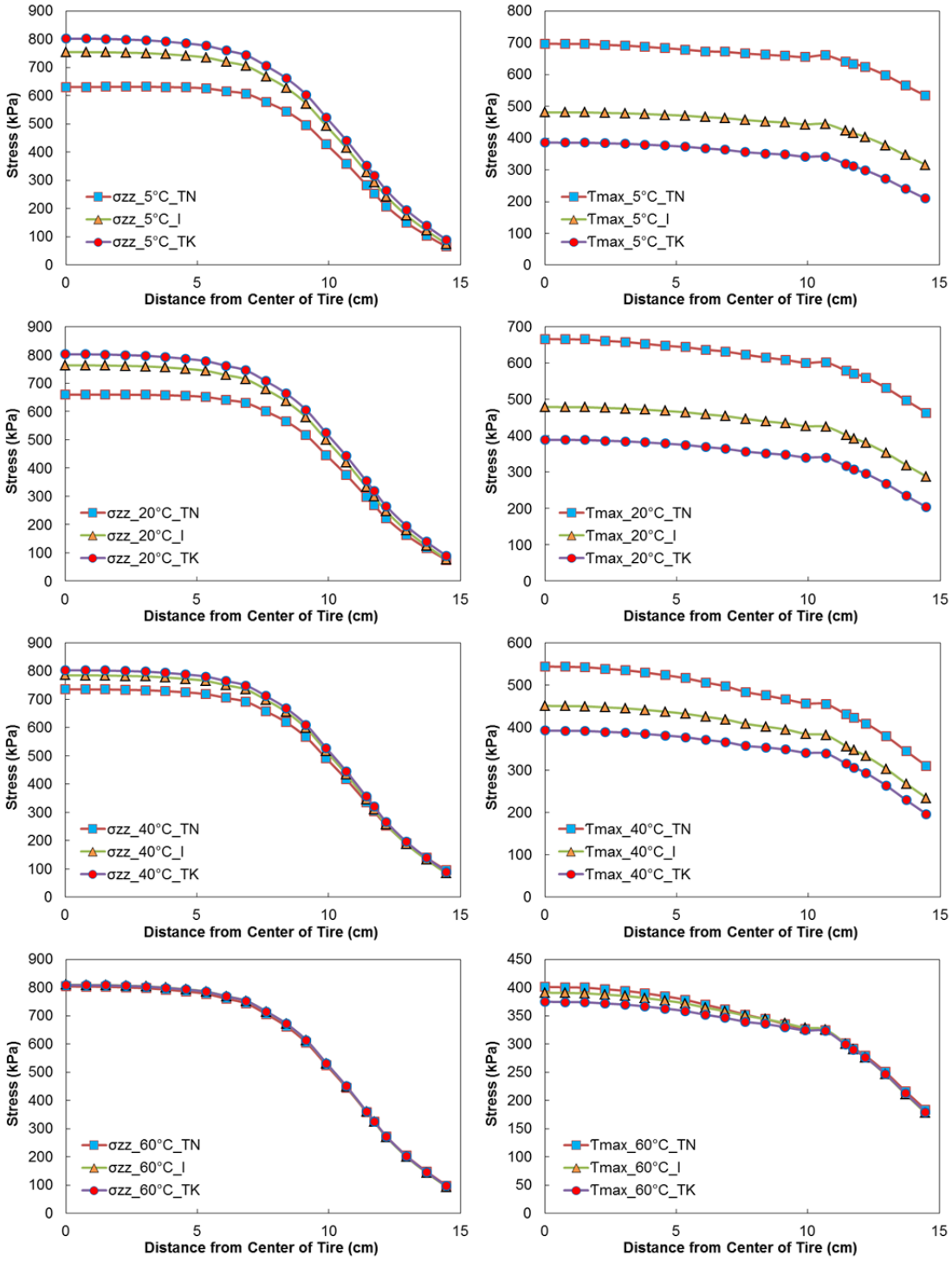

Figure B.12 Evaluation of structural effect in the transverse direction of the tire (106.8 kN (24 kips), 88 km/hour (55 mph), at 3.81 cm (1.5 in.) depth, braking condition (rolling resistance coefficient of 0.55).

4.5. Effect of Rolling Resistance Coefficient

The magnitude of the shear stress clearly is affected by the different rolling resistance coefficients for all the pavement structures, whereas the magnitude of the normal stress is not affected by them, as shown in Figure B.13. As the rolling resistance coefficient increases, the magnitude of the shear stress increases.

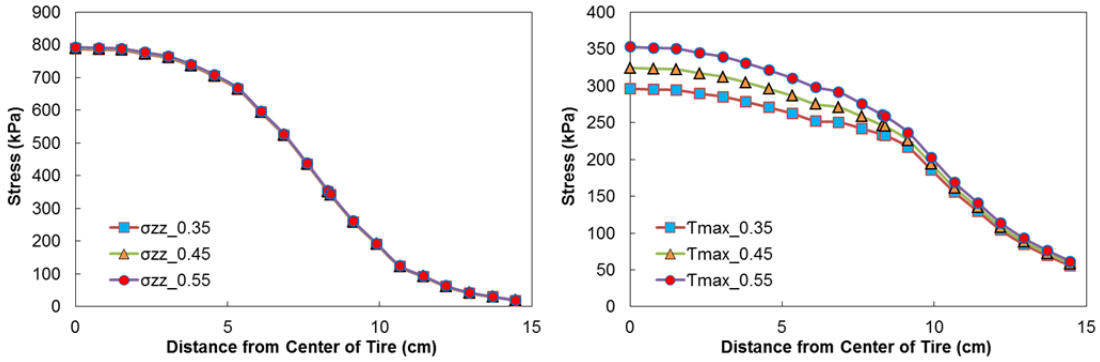

(a)

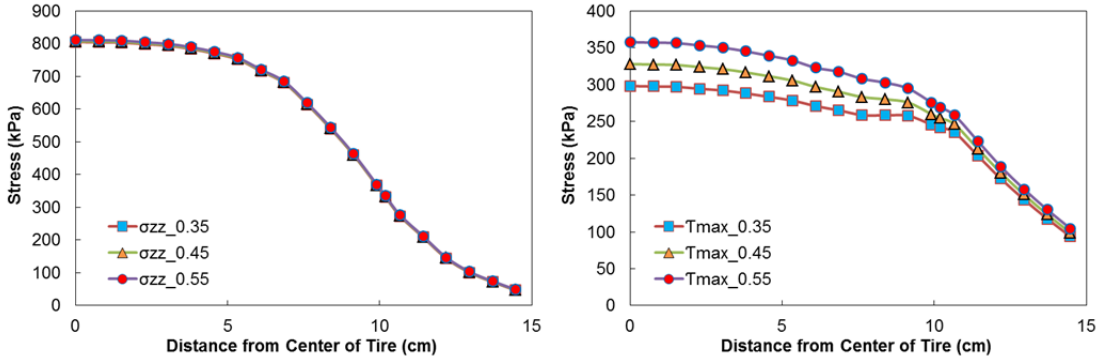

(b)

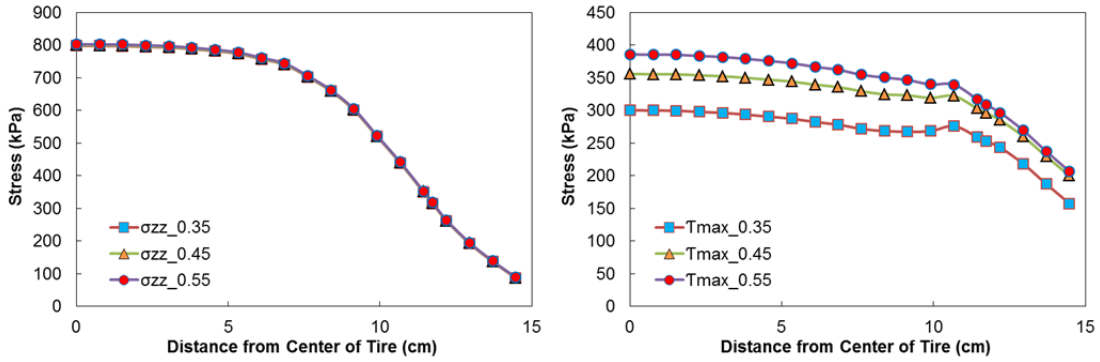

(c)

Figure B.13 Evaluation of rolling resistance coefficient effect in the transverse direction of the tire: (a) thin pavement, 53.4 kN (12 kips), 8 km/hour (5 mph), 60°C, at 3.81 cm (1.5 in.) depth; (b) intermediate pavement, 80 kN (18 kips), 8 km/hour (5 mph), 60°C, at 3.81 cm (1.5 in.) depth; and (c) thick pavement, 106.8 kN (24 kips), 8 km/hour (5 mph), 60°C, at 3.81 cm (1.5 in.) depth.

4.6. Determination of Critical Conditions

The critical conditions in terms of shear stress levels were determined based on the LVECD program simulation results for temperature, speed, load level, pavement structure, and rolling resistance coefficient. Figure B.14 shows the curves for shear stress versus depth under the braking condition. The rolling resistance coefficient of 0.55 was used for the braking condition as it is the most critical of the coefficients under consideration.

The conditions specified in Figure B.14 – i.e., thin pavement, 106.8 kN (24 kips), 5°C, 88 km/hour (55 mph), and rolling resistance coefficient of 0.55 for the braking condition – are the critical conditions for the LVECD program simulations. The analysis results show that the shear stress initially increases with depth until it reaches a depth of 5.08 cm (2.0 in.), or 3.81 cm (1.5 in.) around the interface depth, except at 60°C under the center of the tire, and finally shows a tendency to decrease until it reaches the bottom of the asphalt layer at 10.16 cm (4 in.) deep at all temperatures. The analysis results show that the location of the maximum shear stress is at a depth of 5.08 cm (2.0 in.) below the surface course and that the shear stress around the layer interface is a significant factor that can induce pavement distress and interface debonding. That is, the interface could experience large amounts of repeated shear stress that in turn could lead to interface debonding in an asphalt pavement structure.

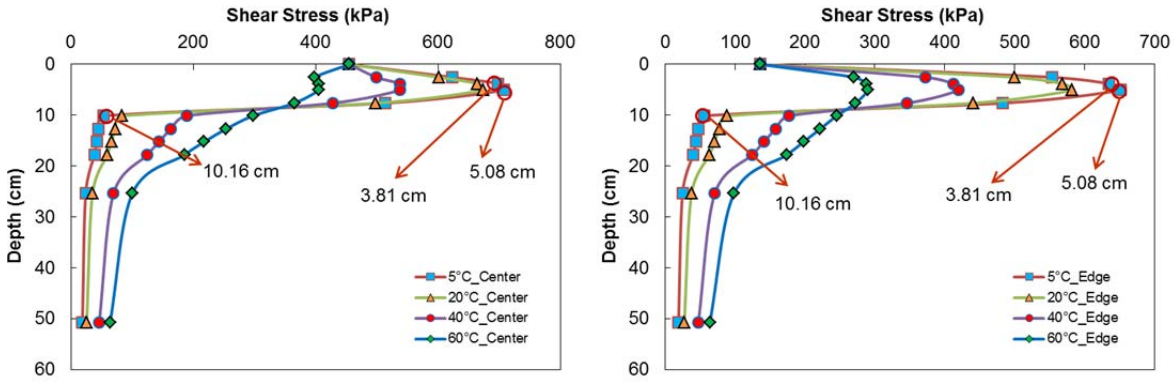

(b) (b)

Figure B.14 Shear stress distribution as a function of depth at different temperatures: (a) at center of tire and (b) at edge of tire: thin pavement, 106.8 kN (24 kips), 88 km/hour (55 mph), rolling resistance coefficient of 0.55.

Based on the simulation analysis results, in order to prevent debonding, a minimum bond strength requirement was determined for a pavement interface under the critical conditions, i.e., thin pavement, 106.8 kN (24 kips), 5°C, 88 km/hour (55 mph), and braking condition, using the shear stress level at the interface depth of 3.81 cm (1.5 in.); the interface shear stress level could be as high as 715 kPa (104 psi).

The study conducted by Zou et al. (2012) showed similar results. Zou et al. used the finite element analysis program ABAQUS to better understand the stress distribution at the interface by varying the thickness of the wearing course, the horizontal load level, the stiffness ratio, and the interface conditions between the wearing course and its underlying layer. Figure B.15 shows that the maximum shear stress does not occur at the surface but at around 4 cm below the surface course, regardless of the thickness of the wearing course.

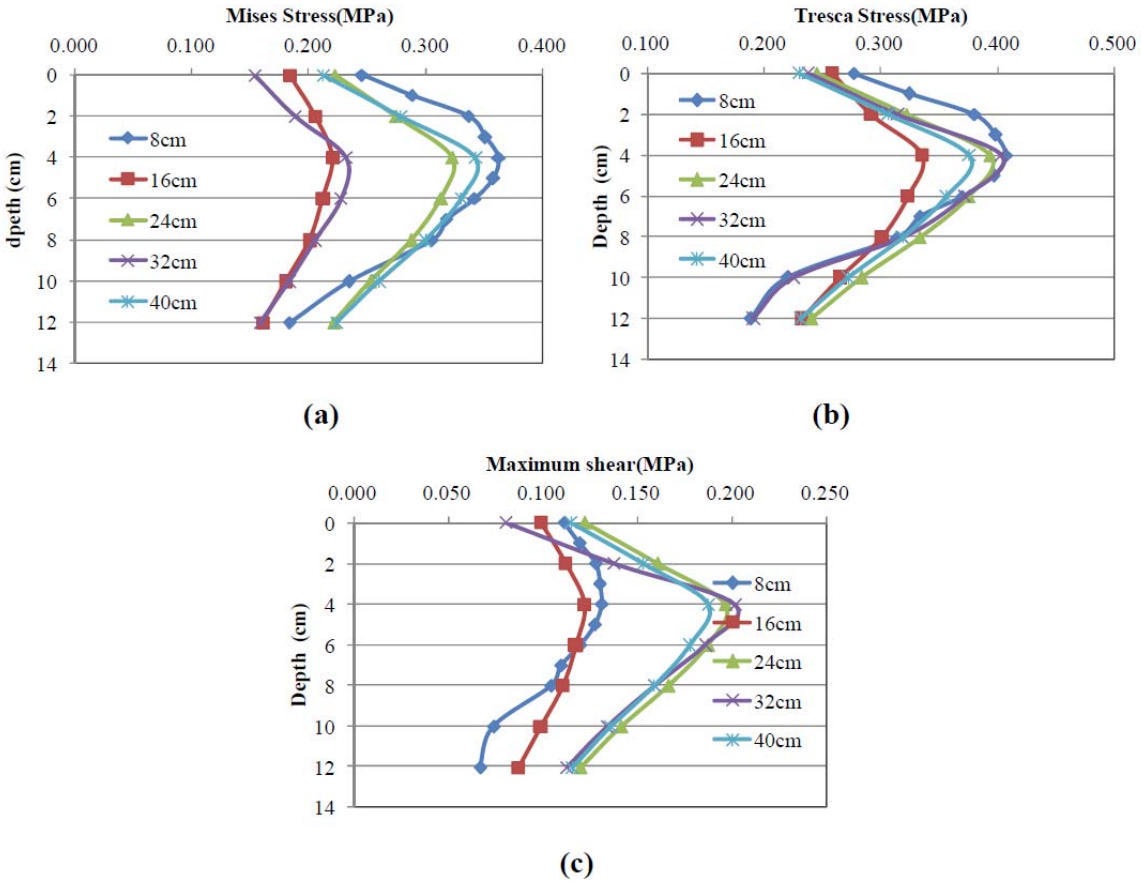

Figure B.15 Shear stress distribution as a function of depth at edge of tire for different thicknesses of the wearing course (Zou et al. 2012).

4.7. Analysis of Stress Distribution

Analysis of the stress distribution at the interface depth, i.e., 3.81 cm (1.5 in.), also was conducted in three-dimensional (3-D) space to confirm the two-dimensional (2-D) space analysis results for the critical conditions described above, as shown Figure B.16. The 3-D figures were derived from stress values computed from the pavement responses using the LVECD program, and a simple MATLAB code was necessary to present them. As shown in Figure B.16, the maximum normal and shear stress values of 634 kPa and 705 kPa, respectively, were verified at a depth of 3.81 cm, and they could be confirmed in the 2-D results for the different views as well.

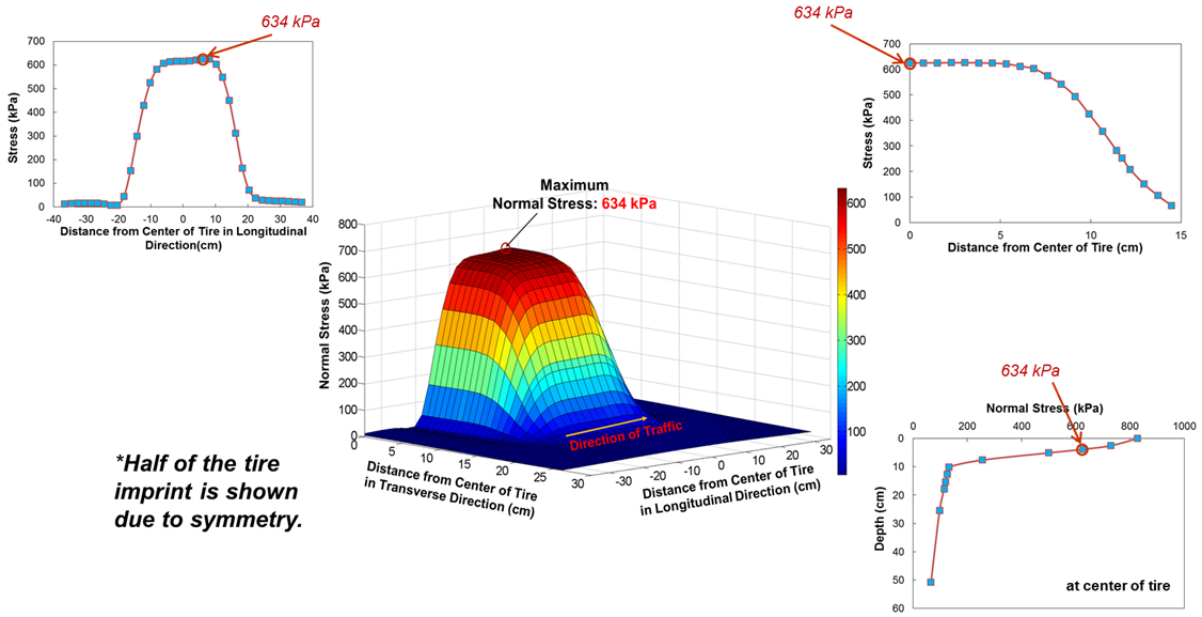

(a)

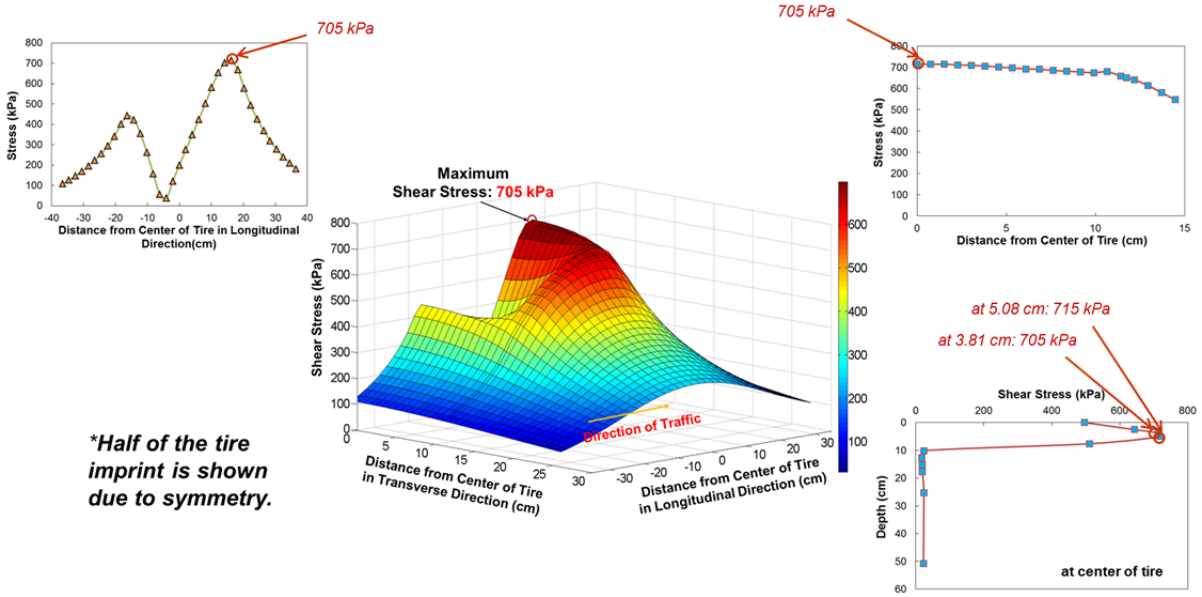

(b)

Figure B.16 Stress distribution in 3-D space: (a) normal stress and (b) shear stress: thin pavement, 106.8 kN (24 kips), 88 km/hour (55 mph), 5°C, braking condition (rolling resistance coefficient of 0.55), at 3.81 cm (1.5 in.) depth.

5. Mechanistic Approach to Predict Shear Failure at the Tack-Coated Interface in a Layered Asphalt Structure

5.1. RILEM Model for Interface Shear Strength

In RILEM inter-laboratory studies, Canestrari et al. (2013) measured the shear strength at the interface of samples that were cored from a newly-built *in situ* two-layer asphalt concrete pavement test section near Ancona, Italy, managed by the Universita` Politecnica delle Marche. The test section was 3.5-m wide and 20-m long with a 70-mm thick lower binder course and a 30-mm thick wearing course, as shown in Figure B.17. Three pavements with different interface conditions were used in the Canestrari et al. (2013) study:

- Pavement 1: without treatment (no tack coat)
- Pavement 2: pre-coated with a polymer-modified emulsion
- Pavement 3: pre-coated with a conventional cationic emulsion

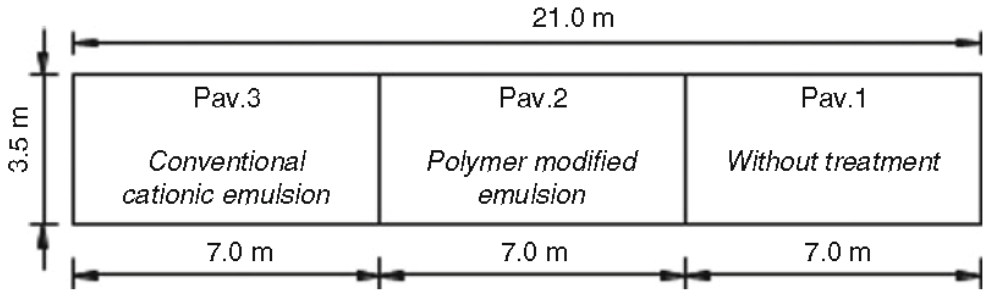

Figure B.17 RILEM trial pavement (Canestrari et al. 2013).

In the first step of the trial section construction, the unbound material was compacted to provide both a regular and flat base surface for placing the two uppermost courses. The same day, the binder course was laid and compacted, obtaining a layer thickness of about 70 mm (2.75 in.). Two weeks later, the polymer-modified emulsion and conventional cationic emulsion were applied manually with a brush on the binder course of Pavement 2 and Pavement 3, respectively. The application rate for the tack coat material was about 150 g/m^2 (0.034 gal/yd^2) of residual bitumen for both pavement sections. After six hours of curing for the emulsions, the wearing courses were laid and compacted. Figure B.18 shows the trial section construction. The RILEM test results for the original program are shown in Table B.8.

Figure B.18 RILEM trial section construction (Canestrari et al. 2013).

Table B.8 RILEM shear tests results (original program): Number of laboratories (p), mean shear stress (τ) and mean displacement (Δu) at maximum shear load (Canestrari et al. 2013).

			Pavement 1			Pavement 2			Pavement 3		
			p	τ	Δu	p	τ	Δu	p	τ	Δu
D	v	T	–	MPa	mm	–	MPa	mm	–	MPa	mm
mm	mm/min	°C	Shear test without normal stress								
150	50	10	3	1.07	1.50	3	2.04	2.56	3	2.22	2.35
		20	5	0.83	2.41	6	1.19	3.16	6	1.34	2.76
		25	2	0.61	2.55	2	0.88	4.30	2	1.02	4.31
		30	4	0.34	2.59	4	0.59	3.14	4	0.75	3.76
		40	1	0.19	2.26	1	0.34	3.47	1	0.36	3.58
100	50	10	3	1.09	1.19	3	2.34	1.54	3	2.43	1.63
		20	4	0.89	1.58	4	1.24	2.02	4	1.75	1.86
		30	3	0.51	2.16	3	0.74	2.51	3	0.95	2.55
100	2.5	10	4	0.61	1.56	4	1.15	2.31	4	1.24	2.28
		20	4	0.36	1.84	4	0.56	3.03	4	0.81	2.65
		30	4	0.23	2.63	4	0.34	2.76	4	0.44	2.98
150	2.5	30	1	0.28	4.11	–	–	–	–	–	–
150	1.27	30	1	0.26	4.51	–	–	–	–	–	–
150	25	30	–	–	–	–	–	–	1	0.67	4.66
150	12.7	30	–	–	–	–	–	–	1	0.56	5.78
			Shear test with normal stress of 0.049 MPa								
150	2.5	25	1	0.50	2.00	1	0.47	2.71	1	0.50	3.19
		30	1	0.42	1.86	1	0.36	2.76	1	0.45	3.21
		40	1	0.25	1.55	1	0.25	2.93	1	0.26	2.25
			Shear test with normal stress of 0.2 MPa								
100	2.5	10	1	0.65	2.14	1	0.95	3.11	1	1.35	4.66
		20	1	0.41	2.23	1	0.68	3.42	1	0.83	4.37
		30	1	0.32	2.86	1	0.37	2.96	1	0.50	3.97
			Shear test with normal stress of 0.483 MPa								
100	2.5	30	1	0.61	5.49	–	–	–	–	–	–
		40	1	0.62	6.28	–	–	–	–	–	–

In this section, a mechanistic procedure is presented that can predict the shear failure at the asphalt layer interface by using the shear strength relationships developed by Canestrari et al. (2013). Based on the shear strength test results for interfaces with specific tack coats, as mentioned above, Canestrari et al. (2013) proposed Equation (7) to calculate shear strength at different temperatures.

$$\tau_{T_x} = 10^{a \cdot T_x + b} \tag{7}$$

where

τ_{T_x} = shear strength at temperature T_x in MPa, and

T_x = temperature (°C).

Coefficients *a* and *b* in Equation (7) are shown in Table B.9 for the three pavement interface structures used in the Canestrari et al. (2013) study.

Table B.9 Coefficients *a* and *b* for three different asphalt layer interface conditions for shear test without normal stress (Canestrari et al. 2013).

D mm	v mm/min	Pavement 1 (No Tack)			Pavement 2 (Polymer-Modified Tack)			Pavement 3 (Cationic Tack)		
		a	b	R^2	a	b	R^2	a	b	R^2
100	2.5	-0.021	-0.013	1.00	-0.026	0.308	0.99	-0.023	0.334	0.99
100	50	-0.016	0.211	0.92	-0.025	0.612	1.00	-0.02	0.611	0.97
150	50	-0.026	0.369	0.94	-0.026	0.586	1.00	-0.026	0.638	0.99

Canestrari et al. (2013) proposed the following Equations (8) and (9) to consider the effects of loading rate and normal stress on shear strength, respectively.

$$\tau_{vx} = \tau_{v1} \cdot \left(\frac{v_x}{v_1}\right)^{0.22} \quad (8)$$

where

τ_{v1} = shear strength at displacement rate 1 (mm/min),

v_1 = test displacement rate 1,

τ_{vx} = shear strength at displacement rate x (mm/min), and

v_x = test displacement rate x.

$$\tau_{\sigma n} = (1 + 0.38 \cdot \sigma_n) \cdot \tau_{\sigma 0} + (0.74 \cdot \sigma_n) \quad (9)$$

where

$\tau_{\sigma n}$ = shear strength with normal stress σ_n (MPa),

$\tau_{\sigma 0}$ = shear strength without normal stress (MPa), and

σ_n = normal stress (MPa).

5.2. Pavement Analysis

In order to design pavement layer interfaces correctly, the stresses at the pavement interface and in the asphalt layers must be predicted accurately and the relationships among shear strength, shear strain rate, and the normal stress at the interface of a layered pavement structure should be understood and included in the design. When the shear bond strength of a tacking material is to be determined for a shear test, it is important to use the normal confining pressure that is calculated for the interface of interest in a given pavement section using pavement analysis that represents the *in situ* environmental and traffic loading conditions as realistically as possible.

For the purposes of this study, an intermediate pavement structure (shown in Figure B.19), one of the three pavement structures presented in Figure B.1, was analyzed under an 80-kN (18 kips) axle load moving at a speed of 8 km/hour (5 mph). The axle load was applied in a single tire configuration with 827.4 kPa (120 psi) tire-pavement contact pressure. The

temperature was fixed at 60°C in the shear strength prediction study. The wheel was assumed to be in the braking state with the coefficient of friction between the tire and pavement surface assumed to be 0.55 (NHTSA 2009).

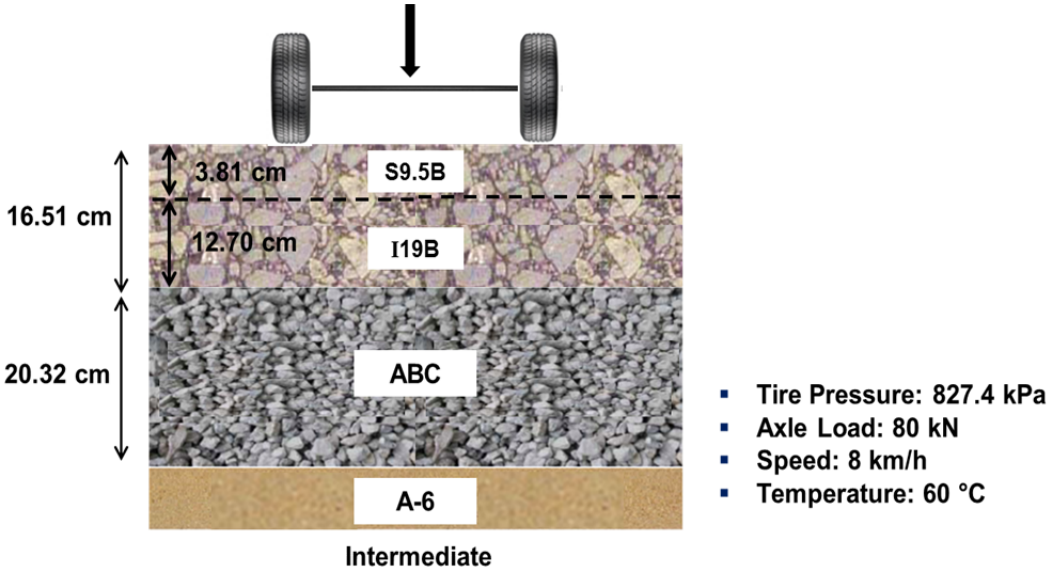

Figure B.19 Cross-section of intermediate pavement structure.

The intermediate pavement structure consists of an S9.5B asphalt concrete surface layer that is 3.81 cm (1.5 in.) thick over an I19B asphalt concrete layer that is 12.70 cm (5 in.) thick. The aggregate base course that is 20.32 cm (8 in.) thick and the subgrade layer (A6) are assumed to be composed of linearly elastic materials. The material properties used in this analysis are identical to those presented in Table B.2, Table B.3, and Table B.6. The states of the stress and strain were determined using the LVECD computer program in order to capture the effects of viscoelasticity and moving loads accurately. Figure B.20 presents the normal and shear stress distributions at the layer interface under braking conditions, respectively, as determined from the LVECD program analysis.

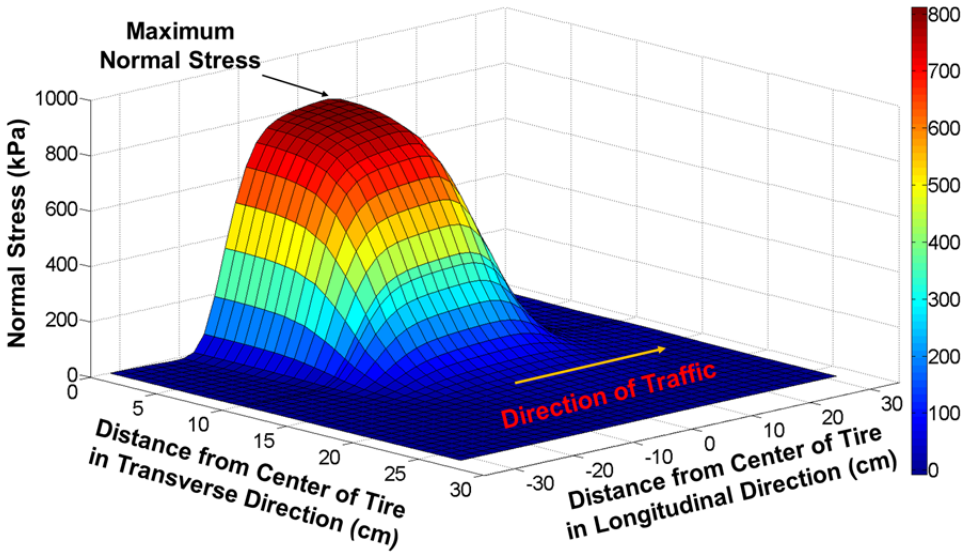

(a)

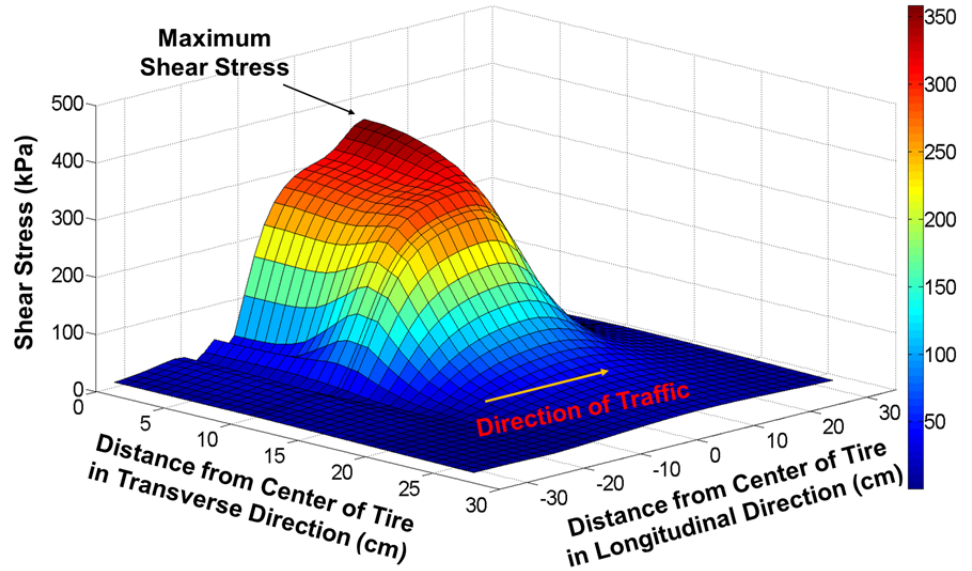

(b)

Figure B.20 Single tire stress distribution at the layer interface: (a) normal stress and (b) shear stress. Note: half of the tire imprint is shown due to symmetry.

The tire-pavement contact area in the LVECD program is rectangular as aforementioned in Appendix B 3.7. Figure B.21 shows the locations of the maximum shear stress and normal stress at the layer interface. The figure shows that the maximum shear stress at the layer interface occurs on the longitudinal axis at a distance of 12.30 cm (4.84 in.) from the center of the tire. The maximum normal stress at the layer interface is observed to be in the longitudinal direction at a distance of 5.30 cm (2.09 in.) from the center of the tire. It is noted that the shift in the location of the maximum normal stress off the center in the direction of traffic is attributed to the braking force.

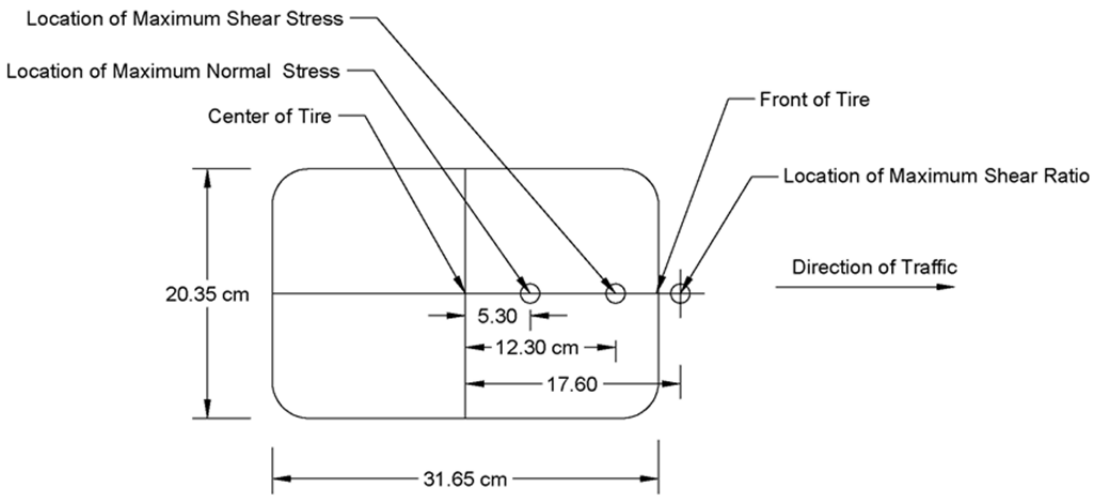

Figure B.21 Single tire footprint used in LVECD program and location of maximum shear stress, normal stress, and maximum shear ratio (Karshenas et al. 2014).

In order to compare the applied stress due to loading to the bond strength at the interface, it was necessary to determine the shear strain rate due to loading for use with the Canestrari et al. (2013) equations. Figure B.22 shows a typical shear strain history as a function of time for the central longitudinal axis of the tire at the layer interface. The shear strain at each point of interest was computed using Equation (10).

$$\gamma_{max} = \sqrt{(\gamma_{xz})^2 + (\gamma_{yz})^2} \tag{10}$$

where

γ_{xz} = shear strain in the transverse direction under the tire, and

γ_{yz} = shear strain in the longitudinal direction under the tire.

The shear strain levels for the parallel longitudinal axes in the transverse sections were determined from the LVECD program for the 8 km/hour (5 mph) speed under consideration. The shear strain history as a function of time was then used to compute the shear strain rates for each of the transverse sections using the bisectional method presented in Figure B.22.

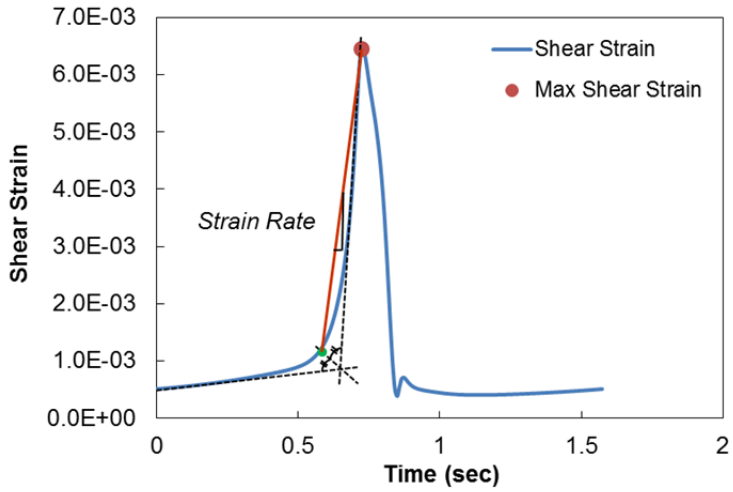

Figure B.22 Typical interface layer shear strain history.

5.3. Maximum Shear Ratio and Interface Shear Failure Criterion

In order to determine the integrity of the interface bond under wheel loading, it was assumed that the asphalt concrete layers in the pavement structure shown in Figure B.19 were tacked using the same material (cationic tack) as was used in the study by Canestrari et al. (2013). Using Equations (7), (8), and (9), the shear bond strength was computed for the 60°C condition using the normal stresses and shear strain rates determined from the LVECD program analysis. In order to use Equation (8), it was necessary to transform the rate of load application to a strain rate. This transformation was achieved by dividing the rate of loading used for the bond strength test shown in Table B.9 by the gap width between the two caps of the shear box used in the laboratory shear tests by Canestrari et al. (2013) in order to obtain the shear strain rate for the tests.

The shear bond strength (τ_s) for each point under consideration at the layer interface was computed using the strain rate and the corresponding normal stress (normal confining stress). As described in the literature, researchers typically compare the induced shear stress at the interface layer due to wheel loading (in most cases at the edge of the tire) directly to the shear bond strength obtained from laboratory or field testing. If, at any location on the interface, the induced shear stress level is higher than the shear bond strength level, then this occurrence would simply imply imminent shear failure in the asphalt concrete layers. However, it is important to note the contribution of normal stress in the failure criterion.

A profile of the shear stress ratio (τ_{max} / τ_s) under the tire at the asphalt concrete layer interface was developed to determine the maximum ratio, which is termed the maximum shear ratio (MSR) and is defined in this study as a failure criterion. The shear ratio is given by Equation (11). If the maximum shear ratio (MSR) is higher than 1.0, then shear failure would occur at the asphalt concrete layer interface. In addition, if the MSR is close to 1.0, it would mean a higher potential of shear failure between the asphalt concrete layers due to repeated braking.

Shear ratio (SR) = $\frac{\tau_{max}}{\tau_s}$ (11)

where

$\tau_{max} = \sqrt{(\tau_{xz})^2 + (\tau_{yz})^2}$

τ_{xz} = shear stress in the transverse direction at the interface calculated by the LVECD program,

τ_{yz} = shear stress in the longitudinal direction at the interface calculated by the LVECD program, and

τ_s = shear bond strength (function of normal stress) obtained from Equation (9).

Figure B.23 (a) and (b) show the distribution of the shear ratios at the layer interface; these illustrations assume the same cationic tack coat interface properties as those used by Canestrari et al. (2013). The MSR $(\tau_{max}/\tau_s)_{max}$ is observed to be around 0.88, accounting for the contribution of normal stress (normal confining stress) while determining the shear bond strength. The location of the MSR is 17.60 cm (6.93 in.) from the center of the tire imprint along the central longitudinal axis, which is just in front of the tire, as opposed to the locations of the maximum normal stress and shear stress that are within the tire imprint, as shown in Figure B.21. Figure B.24 provides guidance for the selection of the appropriate level of normal confining stress on the central longitudinal axis of the tire at the layer interface that corresponds to the location of the MSR. The magnitude of the normal stress that corresponds to the MSR is 0.13 MPa (18.85 psi), as shown in Figure B.24.

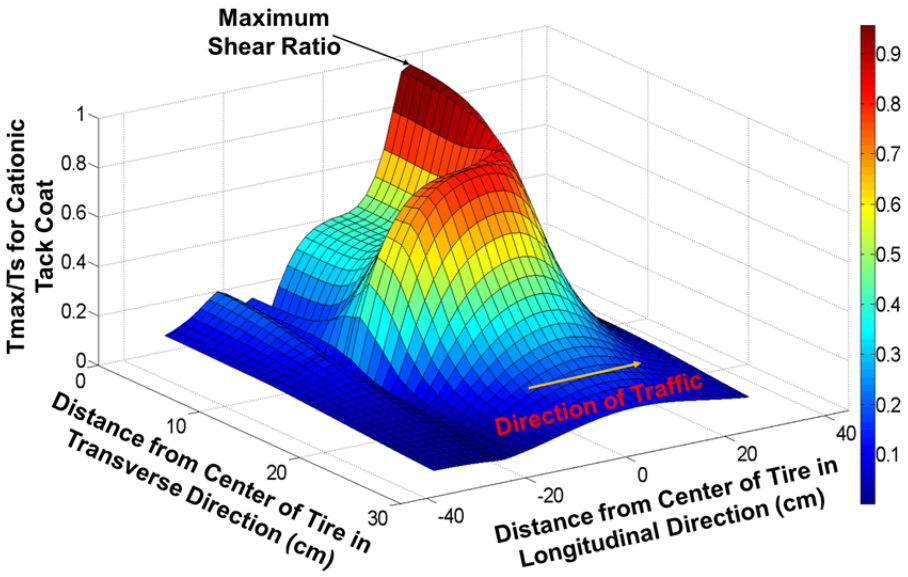

(a)

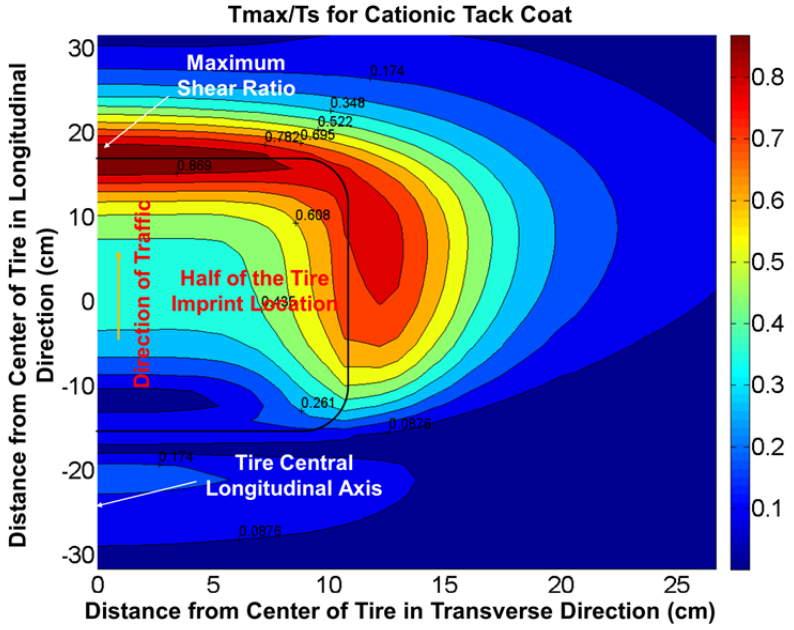

(b)

Figure B.23 (a) Shear ratio profile and (b) shear ratio contours under the tire at the layer interface. Note: half of the tire imprint is shown due to symmetry.

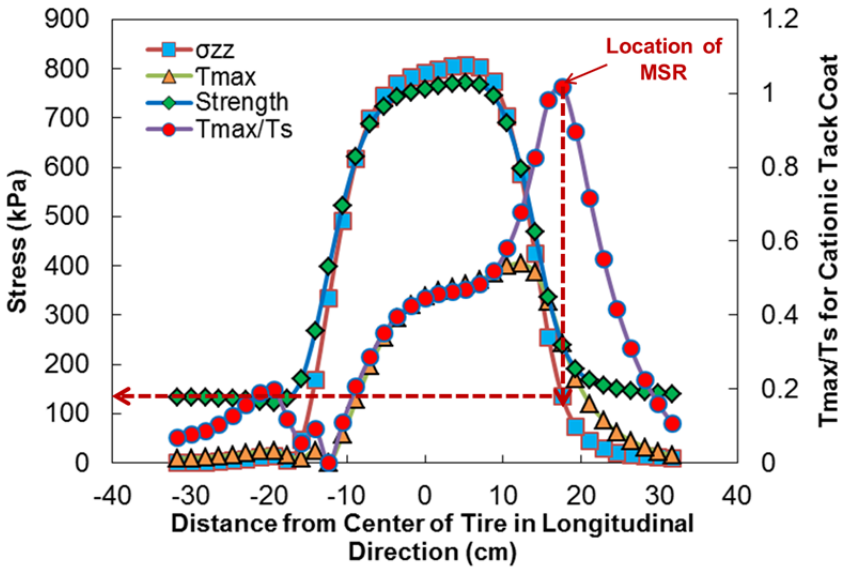

Figure B.24 Shear ratio, shear strength, and shear and normal stress levels in the longitudinal direction under the central axis of the tire at the layer interface: intermediate pavement, 80 kN (18 kips), 8 km/hour (5 mph), 60°C, at 3.81 cm (1.5 in.) depth, braking condition.

The analysis in this study suggests that the use of shear bond strength data without normal confinement for pavement design purposes would result in an overly conservative design on the one hand, and on the other hand, just the opposite with the use of bond strength data obtained under full passive confinement. Nevertheless, it is precisely because the unconfined shear bond strength data result in an overly conservative design and the test devices that do not apply normal confinement may be appropriate for tack coat material quality control/quality assurance (QC/QA) specifications, as the specifications will be on the conservative side. However, the use of unconfined shear bond strength may not be appropriate for design purposes because it could result in an overdesigned pavement section.

5.4. Location of Maximum Shear Ratio for Diverse Conditions

In addition to the conditions – i.e., intermediate pavement section, 80-kN (18 kips) axle load moving at a speed of 8 km/hour (5 mph), braking state (rolling resistance coefficient of 0.55), and temperature of 60°C – that are under consideration as described in Appendix B, Section B.5.2, the states of the stress and strain were analyzed also for the various conditions cited in Section B.1. Figure B.25 presents the normal and shear stress distributions at the layer interface under free rolling conditions, respectively.

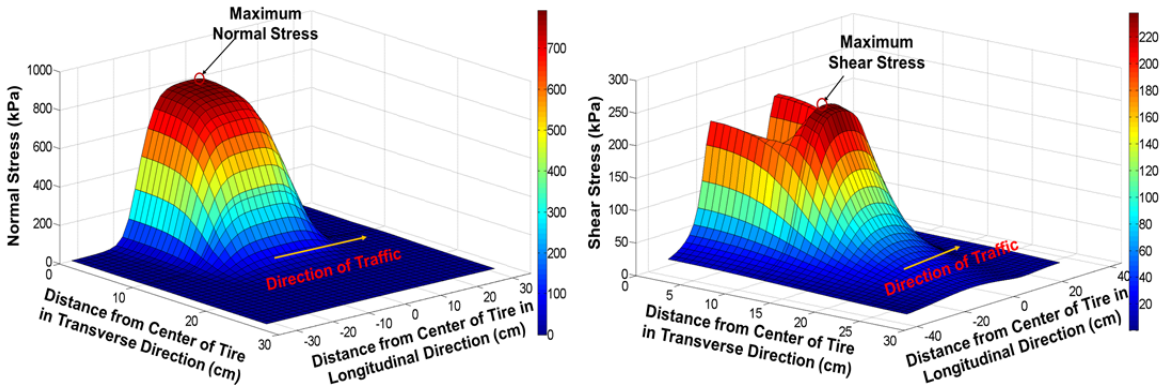

(a) (b)

Figure B.25 Single tire stress distribution at the layer interface: (a) normal stress and (b) shear stress: intermediate pavement, 80 kN (18 kips), 8 km/hour (5 mph), 60°C, at 3.81 cm (1.5 in.) depth under free rolling condition. Note: half of the tire imprint is shown due to symmetry.

It should be noted that under the free rolling condition, the maximum normal stress occurs at the center of the tire on the central longitudinal axis, whereas maximum shear stress occurs around the edge of the tire on the central transverse axis, as shown in Figure B.25. Thus, the shear bond strength levels (τ_s) were computed using the normal stresses and shear strain rates determined from the LVECD program analysis, as presented in Figure B.26.

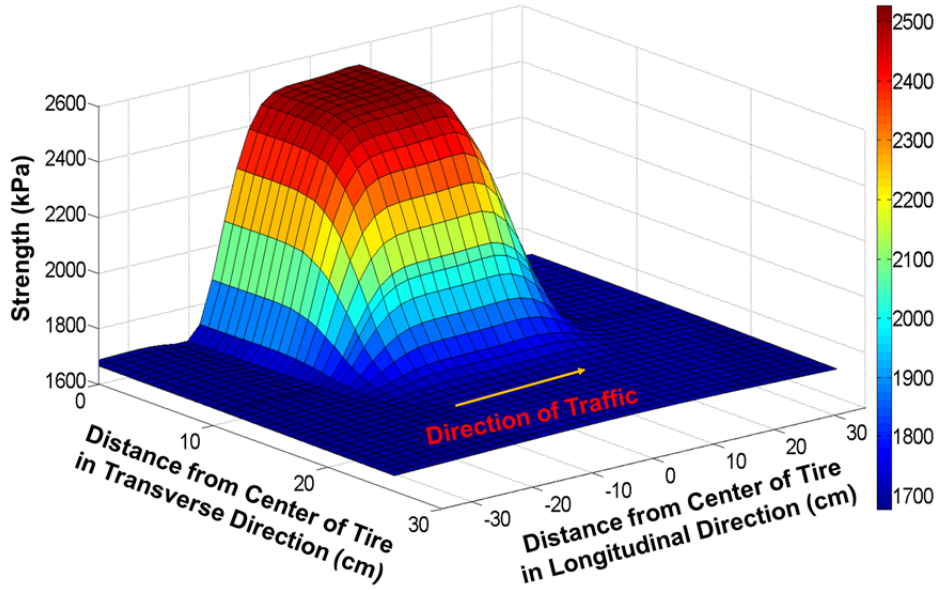

(a)

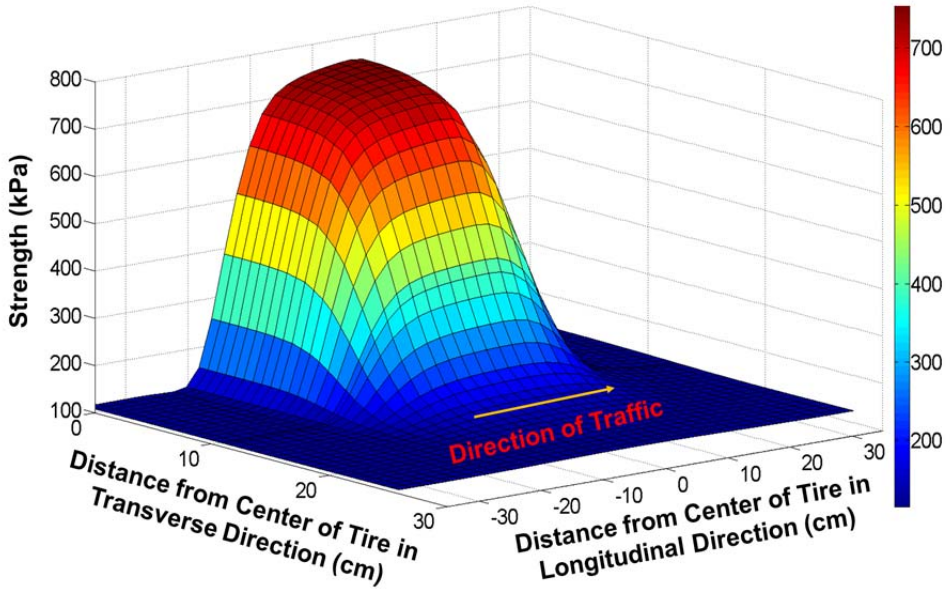

(b)

Figure B.26 Shear bond strength distribution at the layer interface under braking condition (rolling resistance coefficient of 0.55): (a) thin pavement, 106.8 kN (24 kips), 88 km/hour (55 mph), 5°C, at 3.81 cm (1.5 in.) depth and (b) thin pavement, 106.8 kN (24 kips), 8 km/hour (5 mph), 60°C, at 3.81 cm (1.5 in.) depth. Note: half of the tire imprint is shown due to symmetry

Finally, the computed shear stress (τ_{max}) and shear bond strength (τ_s) were used to determine the shear stress ratios, and then the location of the maximum shear stress ratio, or MSR, could be determined using the profile of the shear stress ratio (τ_{max} / τ_s) under the tire at the asphalt concrete layer interface. In other words, the analysis required to determine the integrity

of the interface layer bond using the cationic tack coat was conducted to encompass the following conditions: four temperatures, i.e., 5°C, 20°C, 40°C, and 60°C; three speeds, i.e., 8 km/hour (5 mph), 40 km/hour (25 mph), and 88 km/hour (55 mph); three axle loads, i.e., 53.4 kN (12 kips), 80 kN (18 kips), and 106.8 kN (24 kips); and three typical pavement structures, i.e., thin, intermediate, and thick pavements.

Figure B.27 presents example profiles of the shear ratios under the tire at the layer interface for different conditions that were randomly chosen from various conditions, even though all the conditions under consideration are not presented in this Appendix. For all the conditions considered in this study, the location of the MSR under the braking condition was found to be on the central longitudinal axis all the time, although the distance from the center of the tire imprint along the central longitudinal axis may vary slightly. On the other hand, the location of the MSR under the free rolling condition was found to be around the edge of the tire on the central transverse axis all the time. The MSRs at the asphalt concrete layer interface under the braking condition had more critical values than under the free rolling condition.

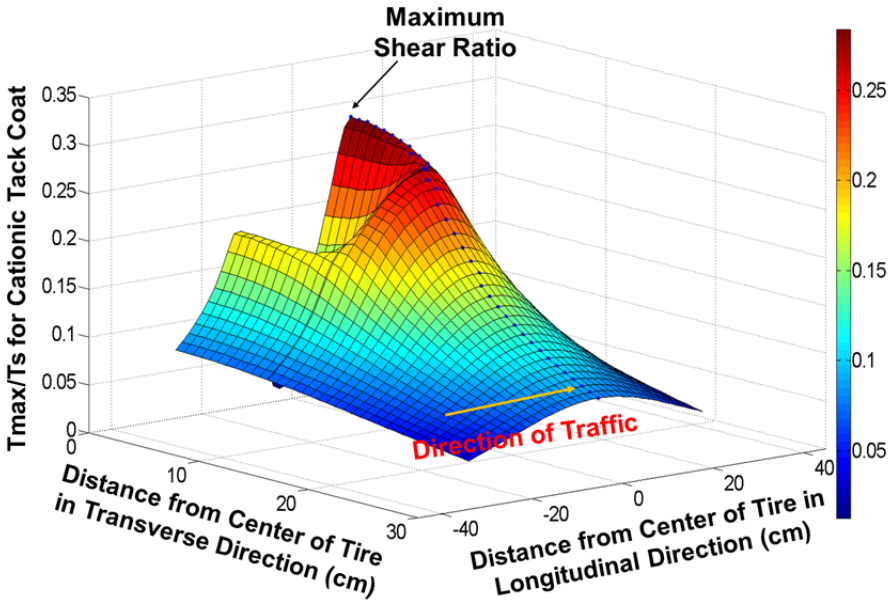

(a)

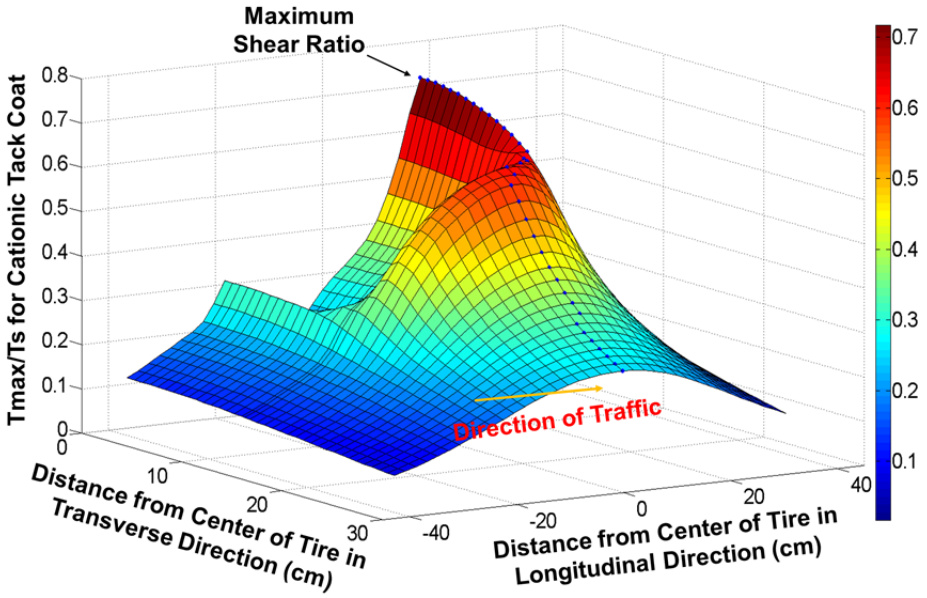
Maximum
Shear Ratio
Tmax/Ts for Cationic Tack Coat
0.8
0.7
0.6
0.5
0.4
0.3
0.2
0.1
0
0
10
20
30
Distance from Center of Tire in
Transverse Direction (cm)
-40
-20
0
20
40
Distance from Center of Tire in
Longitudinal Direction (cm)
Direction of Traffic
0.7
0.6
0.5
0.4
0.3
0.2
0.1

(b)

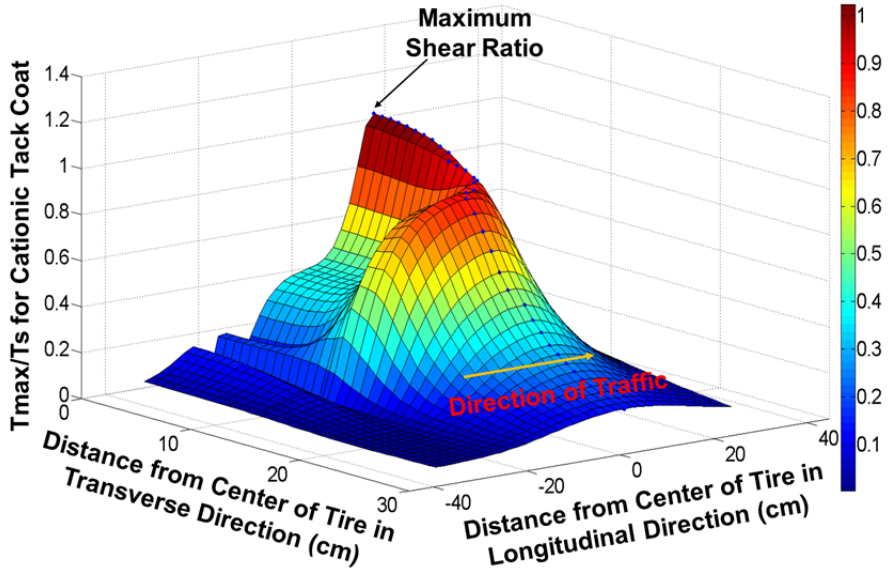
Maximum
Shear Ratio
Tmax/Ts for Cationic Tack Coat
1.4
1.2
1
0.8
0.6
0.4
0.2
0
0
10
20
30
Distance from Center of Tire in
Transverse Direction (cm)
-40
-20
0
20
40
Distance from Center of Tire in
Longitudinal Direction (cm)
Direction of Traffic
1
0.9
0.8
0.7
0.6
0.5
0.4
0.3
0.2
0.1

(c)

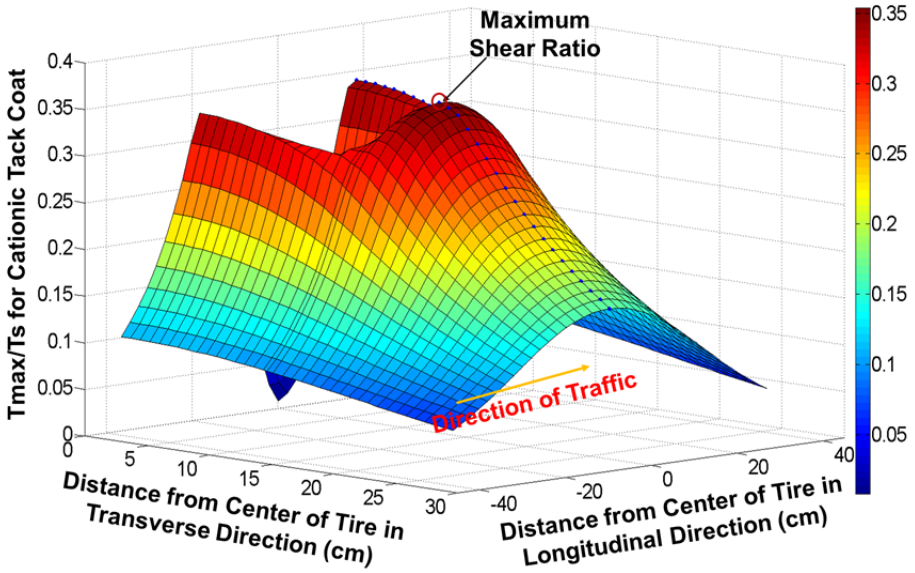

(d)

Figure B.27 Shear ratio profiles under the tire at the layer interface: (a) thin pavement, 53.4-kN (12 kips) axle load, 88 km/hour (55 mph), 5°C, braking condition; (b) intermediate pavement, 106.8-kN (24 kips) axle load, 8 km/hour (5 mph), 20°C, braking condition; (c) thick pavement, 80-kN (18 kips) axle load, 40 km/hour (25 mph), 60°C, braking condition; and (d) thin pavement, 106.8-kN (24 kips) axle load, 88 km/hour (55 mph), 5°C, free rolling condition. Note: the rolling resistance coefficient of 0.55 is used under braking conditions.

As aforementioned, the shear strain history as a function of time was used to compute the shear strain rate at each of the transverse sections using the bisectional method. The magnitude of the shear strain rate was used to calculate the shear strength, as proposed by Canestrari et al. (2013). Due to the viscoelastic nature of asphalt concrete and tack coat materials, the shear bond strength varies significantly as the shear strain rate changes. Therefore, the magnitude of the shear strain rate is an important parameter in the calculation of shear bond strength.

As for the magnitude of the shear strain rate on the central longitudinal axis that corresponds to the location of the MSR at the asphalt concrete layer interface under the braking state, as presented in Figure B.28, the shear strain rate increases as the temperature increases, whereas it decreases with an increase in axle load. In addition, as the speed increases, the strain rate also increases. The thin pavement has faster strain rates than the thick pavement.

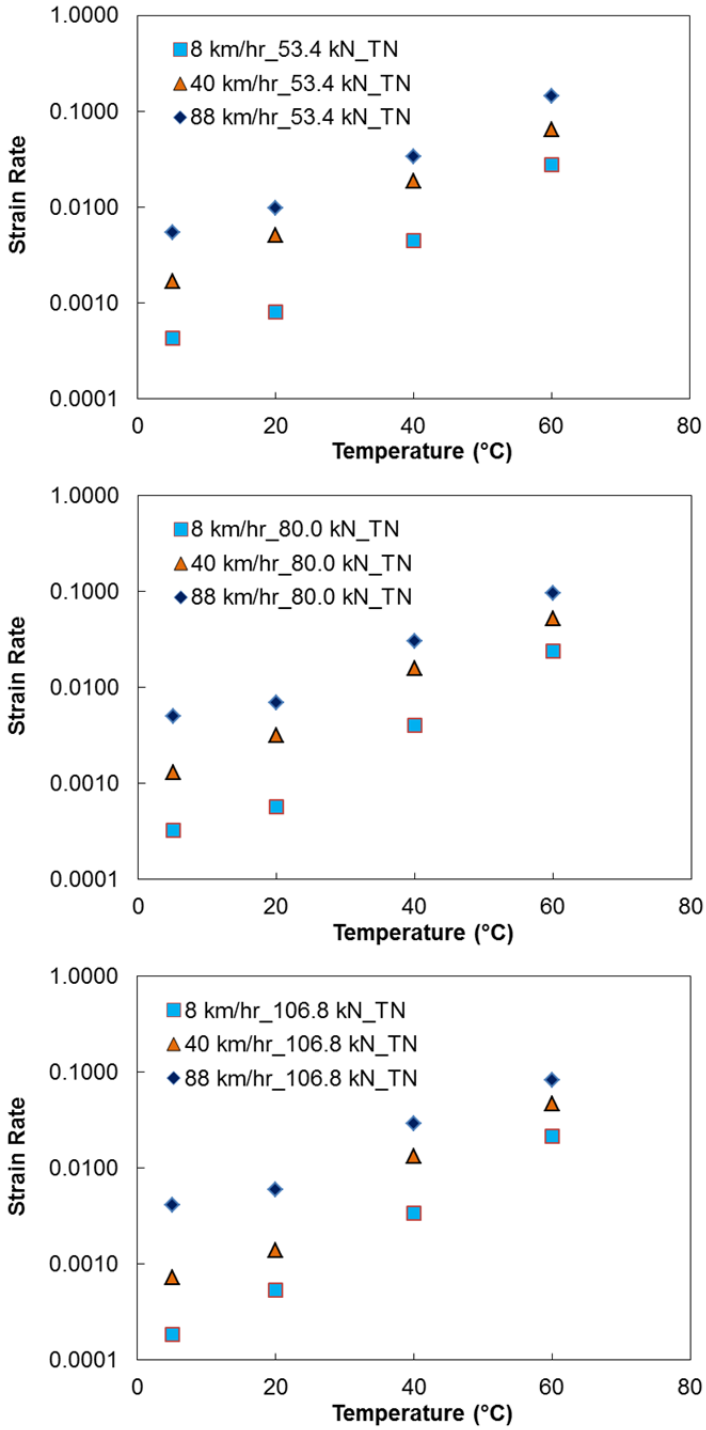
8 km/hr_53.4 kN_TN
40 km/hr_53.4 kN_TN
88 km/hr_53.4 kN_TN
Strain Rate
1.0000
0.1000
0.0100
0.0010
0.0001
0
20
40
60
80
Temperature (°C)
8 km/hr_80.0 kN_TN
40 km/hr_80.0 kN_TN
88 km/hr_80.0 kN_TN
Strain Rate
1.0000
0.1000
0.0100
0.0010
0.0001
0
20
40
60
80
Temperature (°C)
8 km/hr_106.8 kN_TN
40 km/hr_106.8 kN_TN
88 km/hr_106.8 kN_TN
Strain Rate
1.0000
0.1000
0.0100
0.0010
0.0001
0
20
40
60
80
Temperature (°C)

(a)

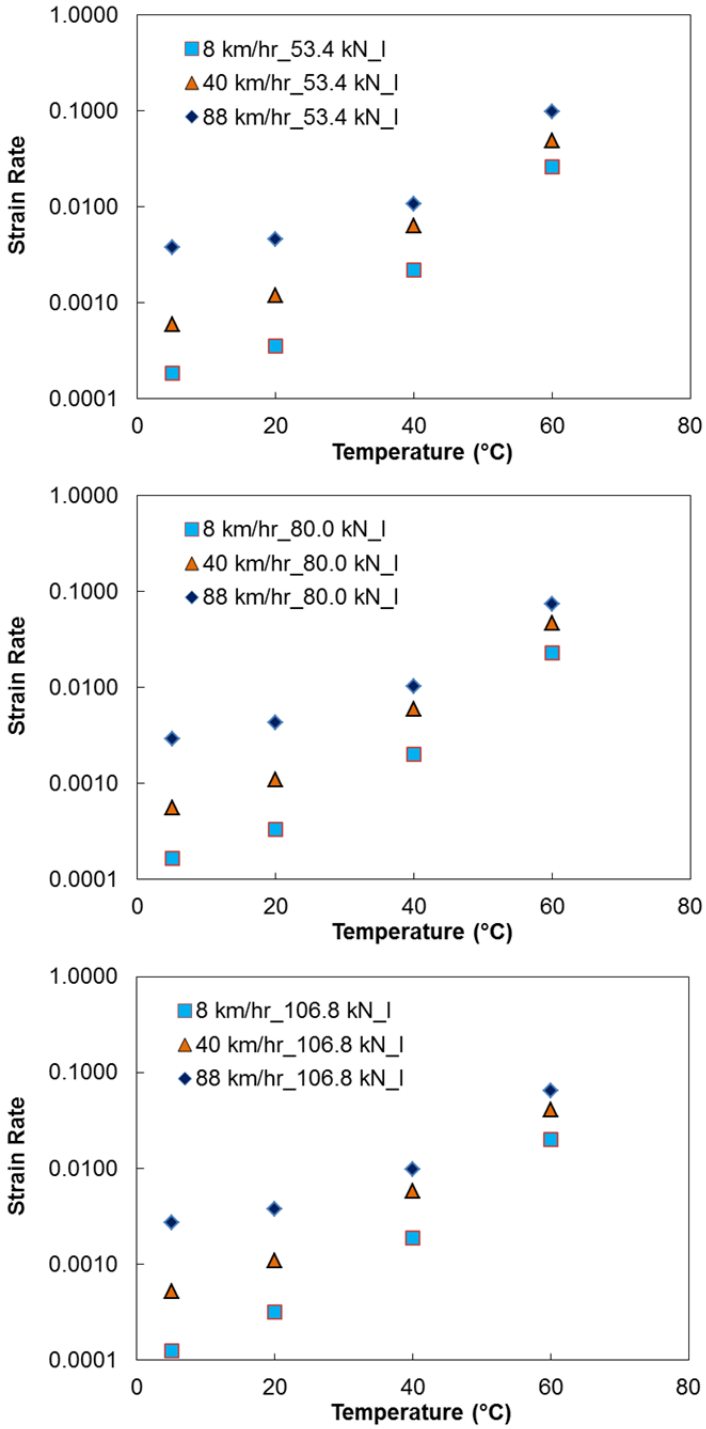
1.0000
0.1000
0.0100
0.0010
0.0001
Strain Rate
8 km/hr_53.4 kN_I
40 km/hr_53.4 kN_I
88 km/hr_53.4 kN_I
0
20
40
60
80
Temperature (°C)
1.0000
0.1000
0.0100
0.0010
0.0001
Strain Rate
8 km/hr_80.0 kN_I
40 km/hr_80.0 kN_I
88 km/hr_80.0 kN_I
0
20
40
60
80
Temperature (°C)
1.0000
0.1000
0.0100
0.0010
0.0001
Strain Rate
8 km/hr_106.8 kN_I
40 km/hr_106.8 kN_I
88 km/hr_106.8 kN_I
0
20
40
60
80
Temperature (°C)

(b)

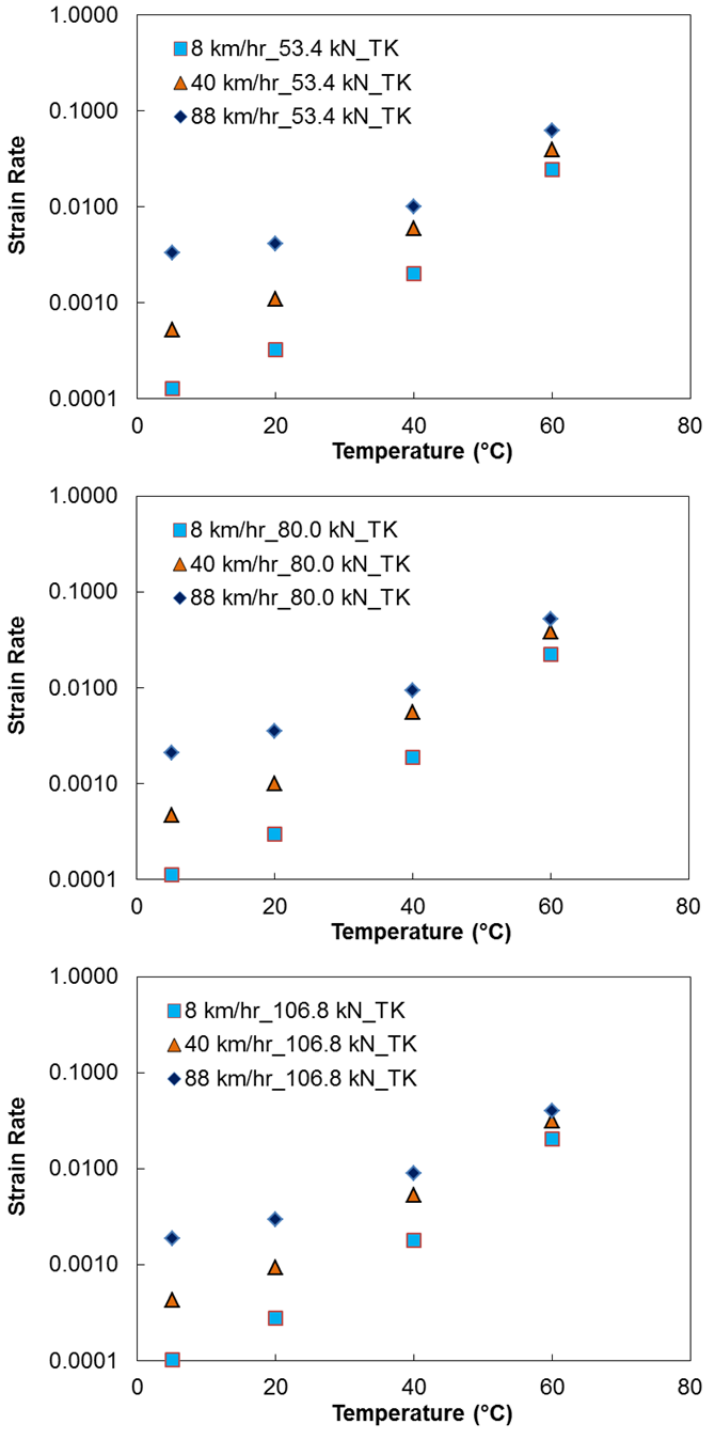

(c)

Figure B.28 Shear strain rates for the location of the MSR at the asphalt concrete layer interface under braking conditions (rolling resistance coefficient of 0.55): (a) thin pavement, (b) intermediate pavement, and (c) thick pavement.

6. Mechanistic Approach for Predicting Tensile Cracking

In order to predict tensile cracking in the surface layer of a multilayer pavement structure, the material responses (tensile strength) of the asphalt layer and the structural response or state of stress in the structure (tensile stress) should be defined. The material response should be predicted using proper tests methods to measure the tensile strength of the pavement layer material. Also, the structural responses should be computed using suitable analysis software, which should accommodate the required material models.

6.1. Tensile Stress Analysis in the Surface Layer of a Pavement Section

In this study, the stress distributions on the surface of the pavement structure and along the interface between the asphalt layers were calculated using the LVECD computer program. The pavement structure shown in Figure B.19 with the pavement layer material properties presented in Table B.3 and Table B.6 was used for analysis purposes and as the input data for the LVECD computer program.

The stress distributions in the pavement layers were predicted based on the assumption of a wheel in the braking state with the standard axle load of 80 kN (18 kips) and tire pressure of 827.4 kPa (120 psi) and moving at the speed of 8 km/hour (5 mph) with a pavement temperature of 60°C (140°F). Different friction coefficients, 0.35, 0.45, and 0.55, were assumed between the tire and the pavement surface. The stress values at the surface of the pavement with the friction coefficient of 0.55 are shown in Figure B.29.

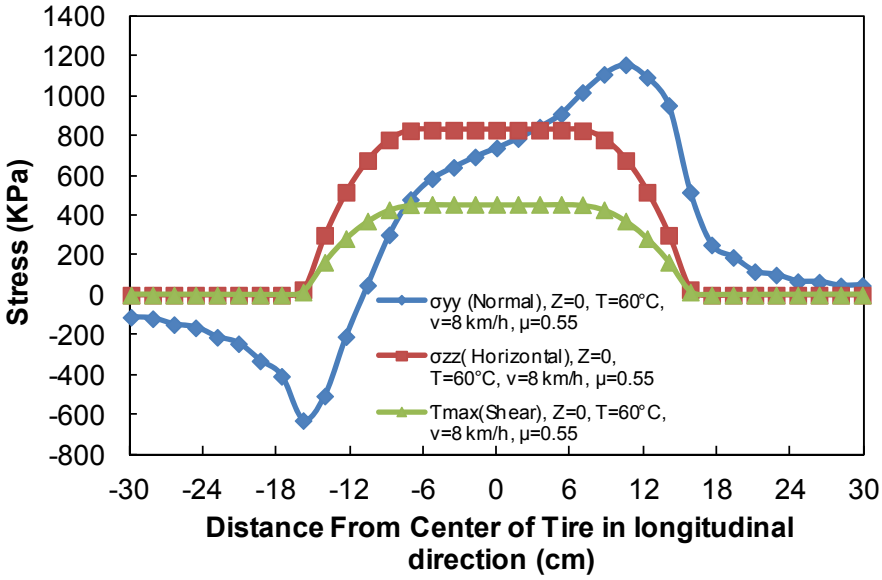

Figure B.29 Stress values at the surface of pavement due to a braking wheel, v = 8 km/hr (5 mph), friction coefficient of 0.55, and 60°C (140°F). Note: tensile stress is negative.

The maximum horizontal tensile stress behind the wheel on the surface of the pavement with the assumed analysis conditions (T = 60°C, v = 8 km/hr, and μ = 0.55) was predicted to be 647 kPa (93.8 psi). The tensile strength of the asphalt layer should be estimated and compared to the tensile stress at the surface of the pavement to forecast the tensile failure (vertical crack) behind the tire. Based on the stress distribution shown in Figure B.29, the schematic failure modes at the interface and in the surface layer of the pavement structure are illustrated in Figure

B.30. According to Karshenas et al. (2014), the location of the MSR is in front of the wheel, as shown in Figure B.30.

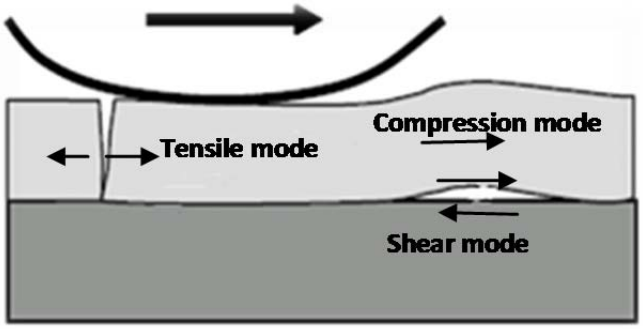

Figure B.30 Schematic failure modes at the interface and in the surface layer.

6.2. Predicting the Tensile Strength of an Asphalt Surface Layer

Due to the viscoelastic material characteristic of hot mix asphalt (HMA), the tensile strength of asphalt concrete is a function of the tensile strain rate and temperature. In a study by Li et al. (2012), a model was proposed for predicting the tensile strength of an asphalt concrete mixture. The model is based on uniaxial tensile strength tests of the asphalt concrete mixture and Dynamic Shear Rheometer (DSR) test results of the extracted binder (Li et al. 2012). Li et al. (2012) proposed Equation (12) for predicting the tensile strength of HMA. The model provides a realistic value for the tensile strength based on the asphalt mixture verification tests results. Figure B.31 presents the verification tensile test results and the prediction of the tensile strength by the model at different temperatures.

$$f_t = 6.05 - 5.636\,exp\left(-73.7\left[1+\left(\frac{0.0583}{\dot{\varepsilon}\cdot 10^{\frac{-18.4(T-20)}{122+(T-20)}}}\right)^{0.19}\right]^{4.33}\right) \quad (12)$$

where

f_t = tensile strength (MPa),

$\dot{\varepsilon}$ = tensile strain rate (s^{-1}), and

T = temperature (°C).

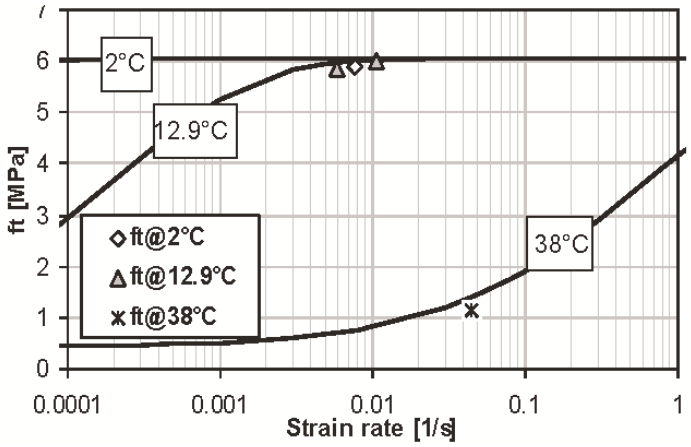

Figure B.31 Results of tensile strength verification tests and model tensile strength predictions (Li et al. 2012).

The small value of the mean percentage relative error (MPRE) shown in Table B.10 for the verification test results suggests that the model can predict the tensile strength of the asphalt mixture for a wide range of temperatures and strain rates with reasonable accuracy.

Table B.10 Results of verification test (Li et al. 2012).

Sample code	Temp. °C (°F)	Strain rate, $\dot{\varepsilon}$ [%/s]	f_t ,MPa (psi)	Predicted f_t, MPa (psi)	Error [%]
C-7-6	2 (35.6)	0.753	5.98 (867.3)	6.05 (877.47)	1.19
C-8-6	12.9 (55.22)	0.584	5.77 (836.8)	5.96 (864.42)	3.28
C-8-9	12.9 (55.22)	1.05	6.02 (873.1)	6.02 (873.1)	0.02
C-7-2	38 (100.4)	4.43	1.14 (165.3)	1.24 (179.8)	8.70
		MPRE		3.30	

Chehab (2002) constructed a mastercurve of the peak tensile stress with respect to reduced strain rate as shown in Figure B.32.

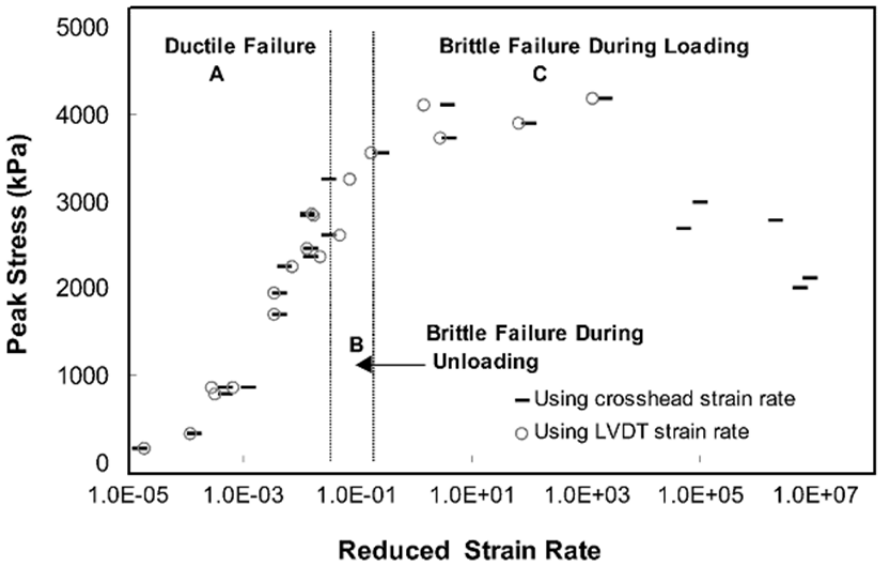

Figure B.32 Tensile strength mastercurve as a function of reduced strain rate (crosshead and LVDT) at 25°C (77°F) (Chehab 2002).

A comparison of the predicted tensile strength at 25°C (77°F) obtained by the Li et al. (2012) model, which is presented in Figure B.33, with the strength mastercurve constructed by Chehab (2002) shown in Figure B.32 indicates a very good correlation between the tensile strength measured by Chehab (2002) and the predicted tensile strength derived using Equation (12).

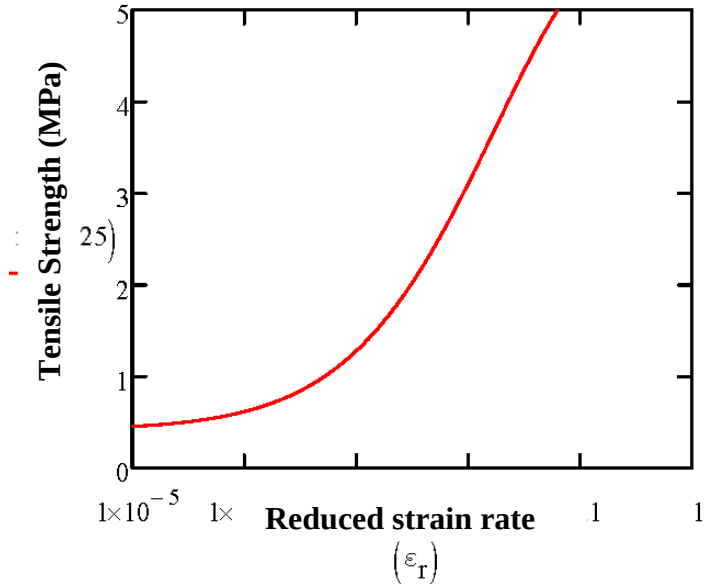

Figure B.33 Tensile strength of asphalt concrete mixture at 25°C (77°F) versus strain rate, based on Li et al. (2012) and calculated by Equation (12).

The tensile strain rates used in the tensile strength prediction model, Equation (12), were calculated using a bilinear method. Figure B.34 shows a typical tensile strain response calculated by the LVECD program at the surface of the pavement in the central longitudinal axis of the tire imprint. The procedure for the bilinear method calculation of the tensile strain rate is also shown in Figure B.34.

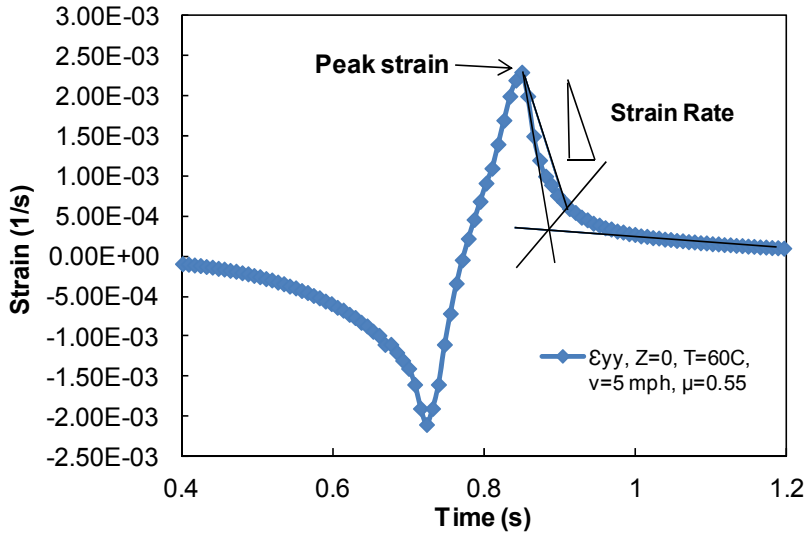

Figure B.34 Typical tensile strain history at the surface of the pavement in the central longitudinal axis of the tire imprint and bilinear calculation of strain rate.

6.3. Tensile Failure Prediction Due to Braking Wheel

The tensile stress in the surface layer of an asphalt pavement that is due to a braking wheel should be compared to the predicted tensile strength of the asphalt layer to forecast the tensile failure behind the tire. The ratio of the computed tensile stress (σ_{max}) to the tensile strength (f_t) is used as the tensile failure criterion. The maximum tensile stress ratio is termed the *critical tensile ratio* (CTR). The tensile stress ratio is given by Equation (13).

$$Tensile\,ratio(TR) = \frac{\sigma_{max}}{f_t} \tag{13}$$

where

$$\sigma_{\max} = \frac{1}{2}(\sigma_{xx} - \sigma_{yy}) \pm \sqrt{\frac{1}{2}(\sigma_{xx} - \sigma_{yy})^2 + \tau_{xy}^2}$$

σ_{xx} = horizontal tensile stress calculated in the pavement in the transverse direction by the LVECD program,

σ_{yy} = horizontal tensile stress calculated in the pavement in the longitudinal direction by the LVECD program,

τ_x =shear stress in the x-y plane calculated in the pavement by the LVECD program, and

f_t = tensile strength obtained from Equation (12).

Pavement temperature, vehicle speed, and the friction coefficient between the tire and the asphalt surface all affect the structural responses and tensile strength of a pavement structure. The effects of each of these factors are examined in the following sections.

6.3.1. Effect of vehicle speed on tensile failure

At a constant temperature and defined friction coefficient, the tensile stress at the surface of the pavement increases with a decrease in vehicle speed, as shown in Figure B.35 at two pavement temperatures of 60°C (140°F) and 20°C (68°F).

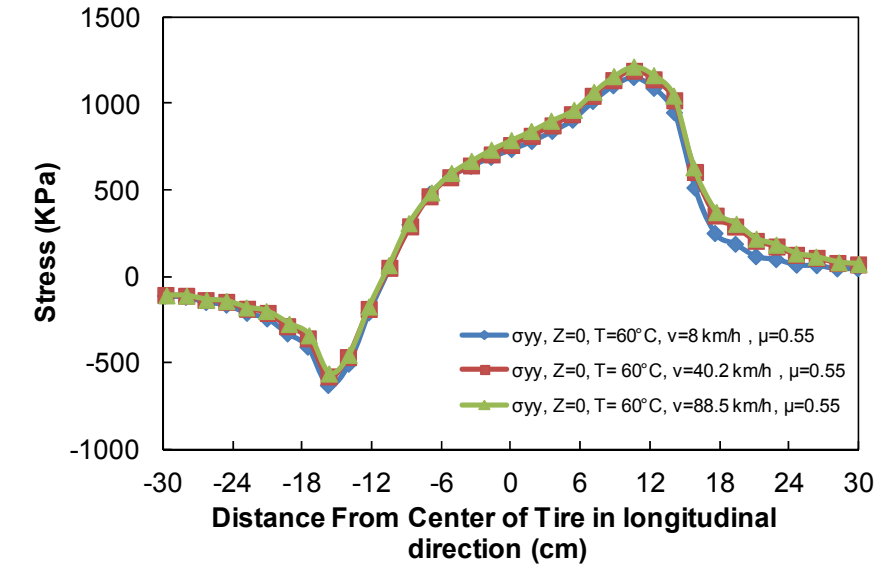

(a)

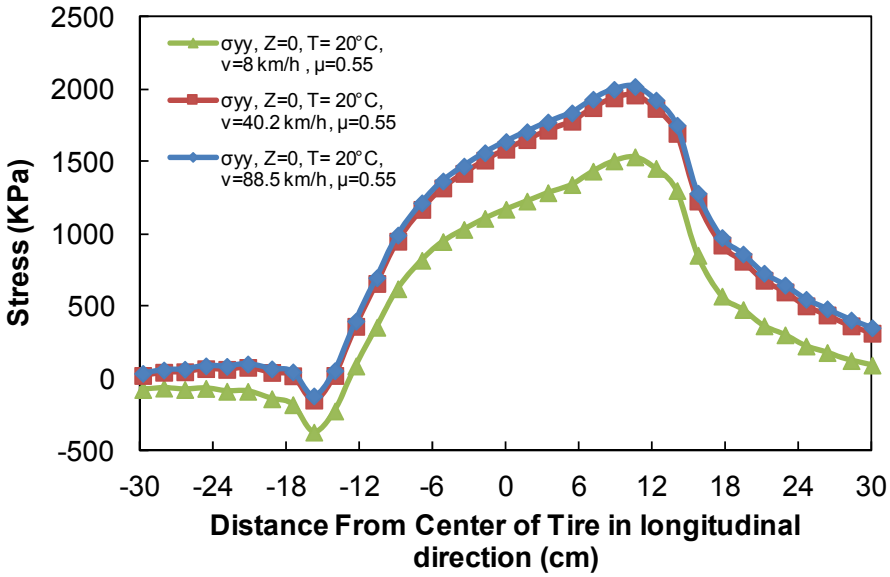

(b)

Figure B.35 Horizontal stress (σ_{yy}) on the surface of the pavement due to braking wheel: (a) 60°C (140°F) and (b) 20°C (68°F).

The tensile strength values of the asphalt pavement at 60°C (140°F) and 20°C (68°F) were calculated as the function of strain rates and temperatures using Equation (12). At 60°C (140°F) (high temperature), the tensile strength increases slightly at the higher speeds due to the higher strain rate, as shown in Figure B.36. However, at 20°C (68°F) (intermediate temperature), the tensile strength increases significantly due to the increasing vehicle speed (higher strain rate). The maximum tensile stress decreases slightly at the higher speeds for both temperatures, 20°C (68°F) and 60°C (140°F), as illustrated in Figure B.36.

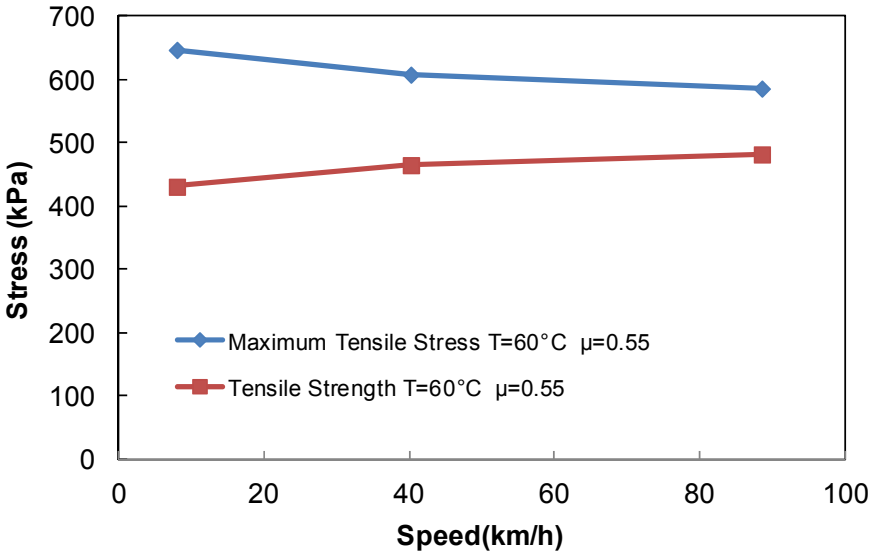

(a)

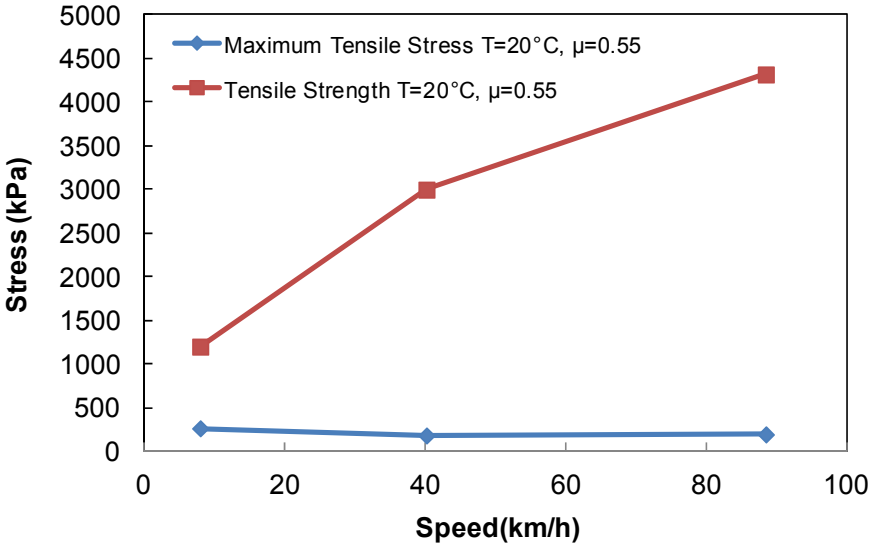

(b)

Figure B.36 Tensile strength and maximum tensile stress with respect to speed at (a) 60°C (140°F) and (b) 20°C (68°F).

Figure B.37 displays the location of the maximum horizontal tensile stresses on the surface of the pavement. The maximum horizontal tensile stress occurs at 15.7 cm (6.18 in.) from the center of the tire in the opposite direction to the applied braking shear force (behind the tire), and the maximum compression stress occurs at 10.57 cm (4.16 in.) from the center of the tire in the direction of traffic.

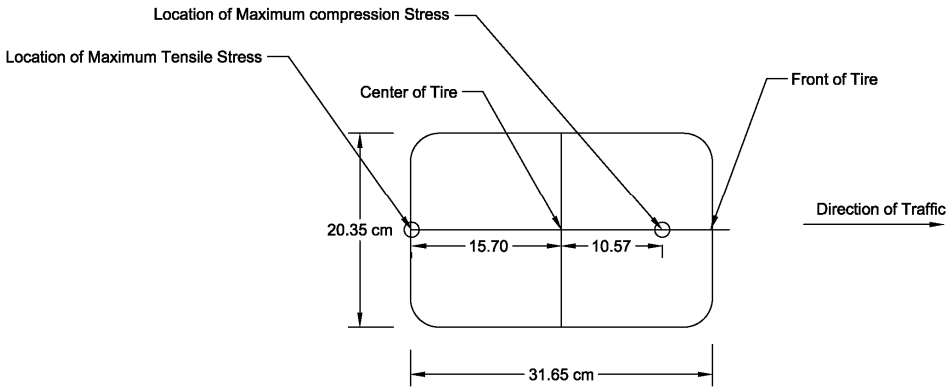

Figure B.37 Location of the maximum tensile and maximum compression stresses at the surface of the pavement along the central longitudinal axis of the tire imprint.

Table B.11 presents the maximum tensile stress values and the corresponding tensile strength values. This table shows that the pavement tensile strength at 60°C (140°F) is less than the corresponding maximum tensile stress and, therefore, the section would fail in tension under the analyzed conditions at 60°C (140°F). At 20°C (68°F), the tensile strength is higher than the corresponding maximum tensile stress and, therefore, failure is not anticipated.

Table B.11 Comparison of peak tensile stress and tensile strength for 60°C (140°F) and 20°C (68°F) with the coefficient of friction of 0.55.

Analysis Case	Tensile Stress kPa (psi)	Tensile Strength kPa (psi)	Critical Tensile Ratio	Fail or Pass
Z=0, T=60°C (140°F), v=8 km/h (5 mph), μ=0.55	647 (94)	431 (63)	1.50	Fail
Z=0, T=60°C(140°F), v=40.2 km/h (25 mph), μ=0.55	608 (88)	458 (66)	1.33	Fail
Z=0, T=60°C (140°F), v=88.5 km/h (55 mph), μ=0.55	586 (85)	473 (69)	1.23	Fail
Z=0, T=20°C(68°F), v=8 km/h (5 mph), μ=0.55	263 (38)	1200 (174)	0.22	Pass
Z=0, T=20°C (68°F), v=40.2 km/h (25 mph), μ=0.55	181 (26)	3000 (435)	0.06	Pass
Z=0, T=20°C (68°F), v=88.5 km/h (55 mph), μ=0.55	193 (28)	4320 (627)	0.04	Pass

6.3.2. Effect of Temperature on Tensile Failure

Asphalt concrete is a viscoelastic material. Therefore, the tensile stress and strength of asphalt concrete are expected to be highly temperature-dependent. Figure B.38 shows the variation of the tensile stress levels at various temperatures at the constant speed of 8 km/hr (5 mph) with the friction coefficient of 0.55 between a braking wheel and asphalt surface. As shown in Figure B.38, the tensile stress increases with an increase in temperature. Conversely, as is shown in Figure B.39, the tensile strength of the asphalt concrete decreases with an increase in temperature. The tensile strength of the asphalt concrete at the low temperature, 5°C (41°F), is significantly higher than the tensile strength at the higher temperature, 60°C (140°F).

Table B.12 presents a comparison of the maximum tensile stress values and the tensile strength values at different temperatures for a wheel moving at 8 km/hr (5 mph) with the coefficient of friction between the tire and the pavement of 0.55. As shown in Table B.12, the surface layer of the pavement structure will crack in tension at 60°C (140°F) with the CTR of 1.5.

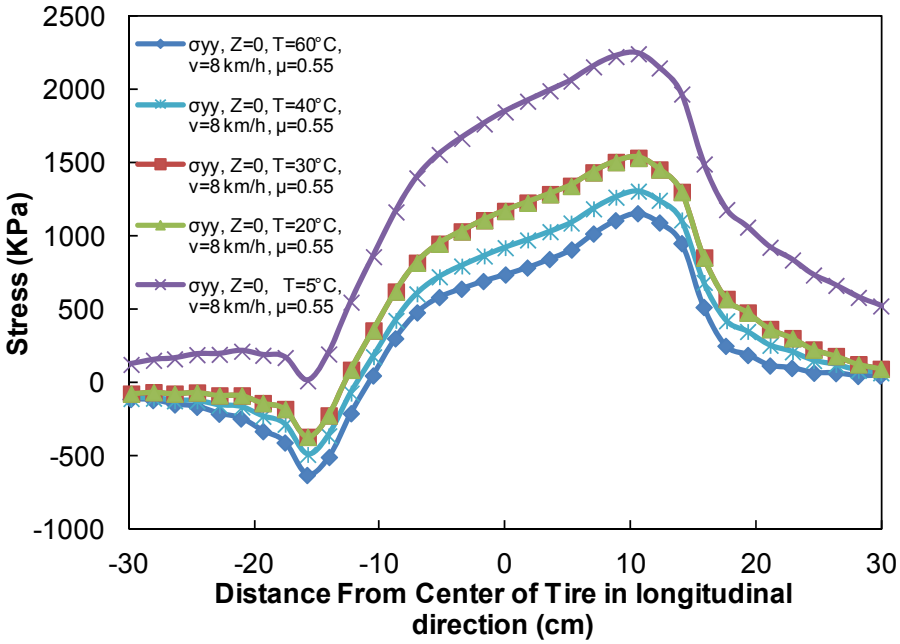

Figure B.38 Horizontal stress (σ_{yy}) on surface of the pavement due to braking wheel.

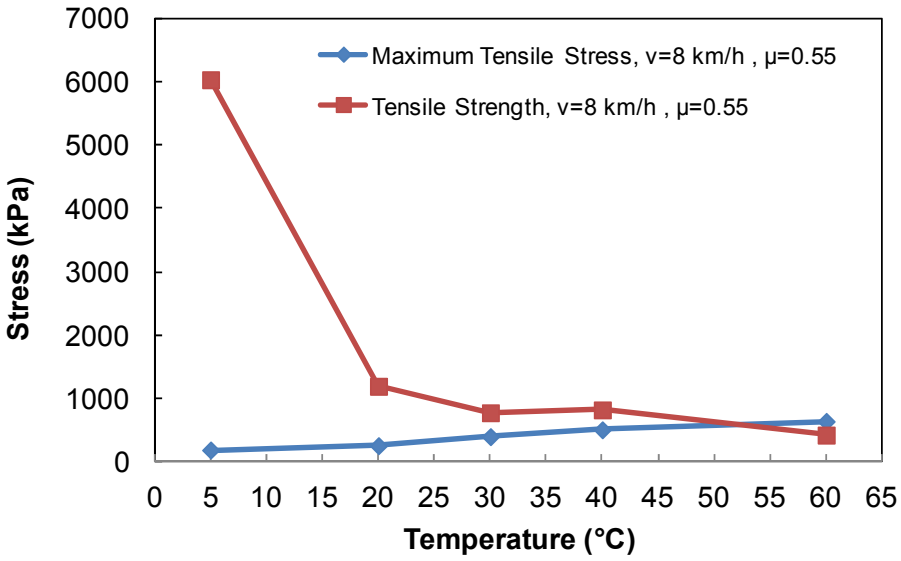

Figure B.39 Tensile strength and tensile stress versus temperature.

Table B.12 Comparison of peak tensile stress and tensile strength for 8 km/hr (5 mph) and coefficient of friction of 0.55 at different temperatures.

Analysis Case	Tensile Stress kPa (psi)	Tensile Strength kPa (psi)	CTR	Fail or Pass
Z=0, T=60°C (140°F), v=8 km/h (5 mph), μ=0.55	647 (94)	431 (63)	1.5	Fail
Z=0, T=40°C(104°F) , v=8 km/h (5 mph), μ=0.55	514 (74)	828 (120)	0.62	Pass
Z=0, T=30°C (86°F), v=8 km/h (5 mph), μ=0.55	406 (59)	783 (114)	0.51	Pass
Z=0, T=20°C (68°F), v=8 km/h (5 mph), μ=0.55	263 (38)	1200 (174)	0.22	Pass
Z=0, T=5°C (41°F), v=8 km/h (5 mph), μ=0.55	195 (28)	6034 (875)	0.03	Pass

6.3.3. Effect of Friction Coefficient on Tensile Failure

Friction is the force that resists the relative motion of bodies. The coefficients of friction can be derived from the stopping distance and speed of the vehicle. Three friction coefficients of 0.35, 0.45 and 0.55 were investigated in this study. Figure B.40 indicates that the tensile stress on the surface of the pavement due to a braking wheel decreases with decreasing friction coefficients. Figure B.41 presents a comparison of the tensile strength and stress for the different

friction coefficients. As shown, the pavement surface layer would fail due to a braking wheel with friction coefficients of 0.55 and 0.45 and would pass the design criteria for 0.35.

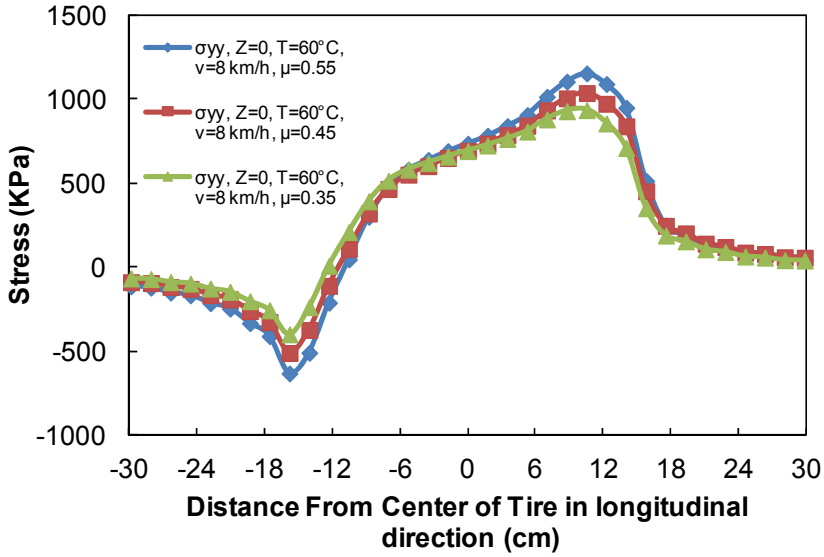

Figure B.40 Horizontal stress (σ_{yy}) in the surface of a pavement due to the shear force of braking wheel.

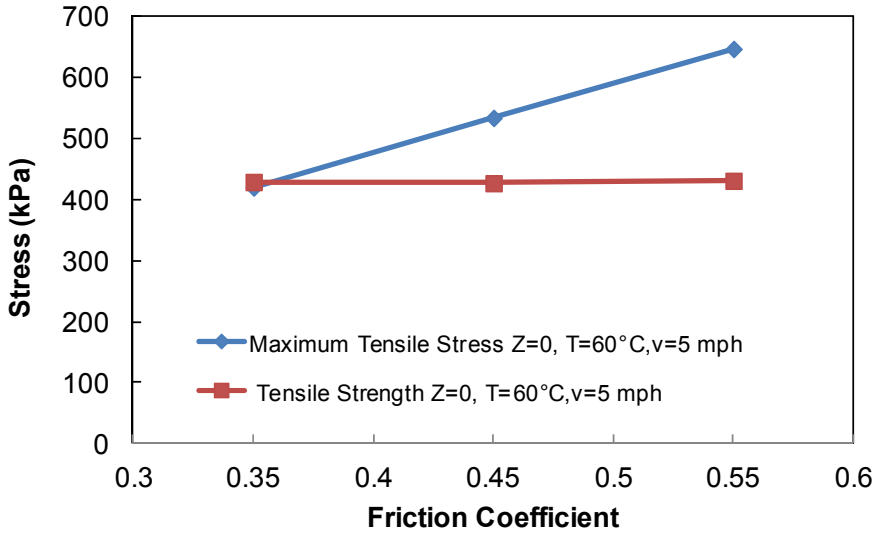

Figure B.41 Tensile strength and tensile stress with respect to friction coefficient.

To consider the effects of both the speed of the vehicle and the friction coefficient on the tensile strength and tensile stress, three different combinations of speeds and friction coefficients at 60°C (140°F) were studied: v = 8 km/hr (5mph), μ = 0.35); v = 40.2 km/hr (25 mph), μ = 0.45; and v = 88.5 km/hr (55 mph), μ = 0.55. The horizontal tensile stress values, which are shown in

Figure B.42, for the aforementioned analysis conditions, demonstrate that the horizontal tensile stress increases with increases in the friction coefficient and speed.

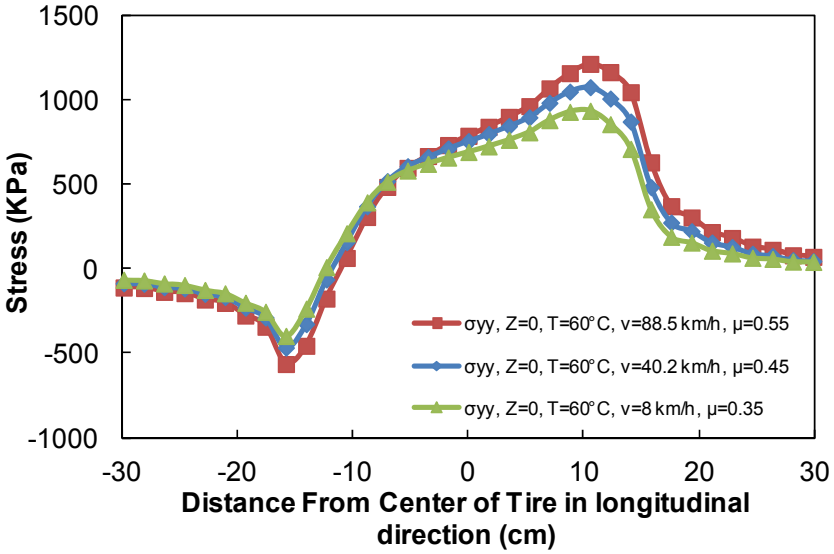

Figure B.42 Horizontal stress (σ_{yy}) on surface of the pavement due to braking tire at 60°C with different friction coefficients and speeds.

Table B.13 shows that with the same friction coefficient of 0.45, the difference between the tensile strength and tensile stress at the speed of 40.2 km/hr (25 mph) is smaller than the difference between the tensile stress and tensile strength at the speed of 8 km/hr (5 mph). In addition, at the friction coefficient of 0.55, the CTR is higher for the speed of 8 km/hr (5 mph) than the speed of 88.5 km/hr (55 mph). Therefore, in all cases, the lower speed produces a higher CTR.

Table B.13 Comparison of peak tensile stress and tensile strength at 60°C with different speeds and friction coefficients.

Analysis Case	Tensile Stress kPa (psi)	Tensile Strength kPa (psi)	CTR	Fail or Pass
Z=0, T=60°C (140°F), v=8 km/h (5 mph), μ=0.55	647 (94)	431 (63)	1.50	Fail
Z=0, T=60°C (140°F), v=88.5 km/h (55 mph), μ=0.55	586 (85)	473 (69)	1.24	Fail
Z=0, T=60°C (140°F),v= 8 km/h (5 mph), μ=0.45	534 (78)	428 (62)	1.25	Fail
Z=0, T=60°C (140°F), v=40.2 km/h (25 mph), μ=0.45	495 (72)	450 (65)	1.10	Fail
Z=0, T=60°C (140°F), v=8 km/h (5 mph), μ=0.35	420 (61)	429 (62)	0.97	Pass

The contours of the principal horizontal stress on the surface of the pavement structure are presented in Figure B.43. The pavement structure was analyzed at 60°C (140°F) with a wheel moving at the speed of 8 km/hr (5 mph) in the braking state. The friction coefficient between the wheel and the pavement surface was 0.55.

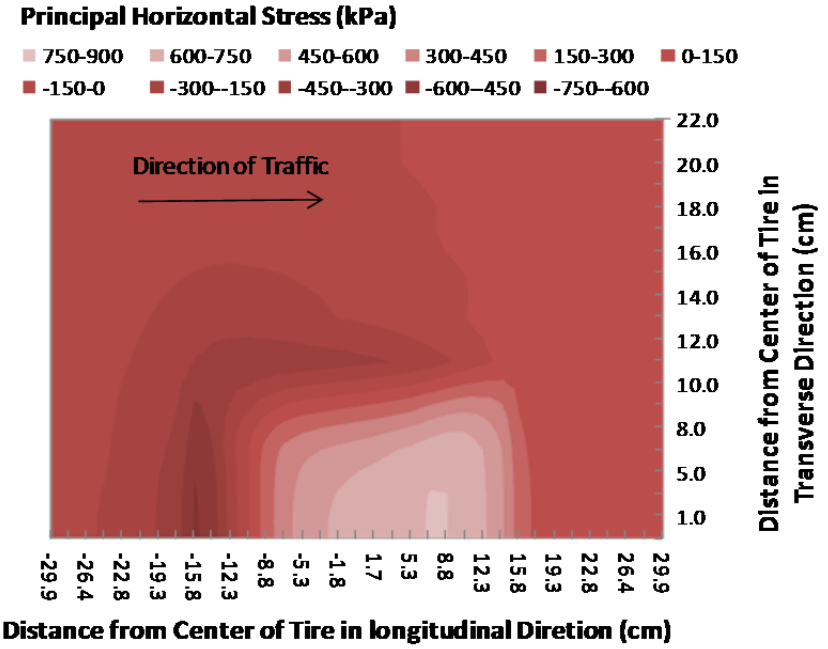

Figure B.43 Principal horizontal stress on surface of the pavement with bonded interface due to braking wheel at 60°C (140°F), 8 km/hr (5 mph), and friction coefficient of 0.55. Note: half of the tire imprint is shown due to symmetry.

6.4. Debonded Pavement Analysis

To study the behavior of a debonded surface layer in a multilayered pavement structure, a model was developed using the LVECD computer program in which the debonded interface is represented as a thin layer with a very low modulus of elasticity between the asphalt layers. The analyzed pavement structure is shown in Figure B.44, and the material properties are shown in Table B.14. A 1-mm thick elastic layer with the modulus of elasticity of 1 kPa and Poisson's ratio of 0.499 was modeled between the S9.5B asphalt surface layer and the I19B layer. The pavement was analyzed in two load cases of a rolling wheel and a braking wheel with the coefficient of friction of 0.55 between the tire and the pavement surface. The load was an 80-kN (18 kips) standard axle load moving at a speed of 8 km/hour (5 mph). The tire load was applied using a single tire configuration with 827.4 kPa (120 psi) tire pressure at the temperature of 60°C (140°F).

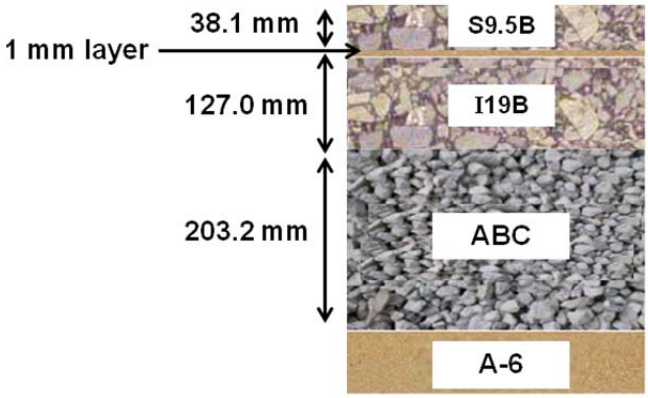

Figure B.44 Cross-section of pavement structure with a debonded surface layer.

Table B.14 Layer thicknesses and material properties for pavement structure.

Pavement Layer	Type	Layer Thickness cm (in.)	Poisson's Ratio	Layer Modulus MPa (ksi)
Asphalt Concrete	S9.5B	3.81 (1.5)	0.35	Based on Mastercurve Data (Table B.3)
Elastic Layer	Debonded	0.1 (0.04)	0.499	0.001 (1.45E-4)
Asphalt Concrete	I19B	12.70 (5)	0.35	Based on Mastercurve Data (Table B.3)
Base	ABC	20.32 (8)	0.40	270.63 (39.25)
Subgrade	A6	Infinite	0.45	68.5 (10)

6.4.1. Stress Distribution in Debonded Pavement Due to a Rolling Wheel

Figure B.45 shows the stress distribution on the surface of a debonded pavement due to a rolling wheel moving at the speed of 8 km/hour (5 mph).

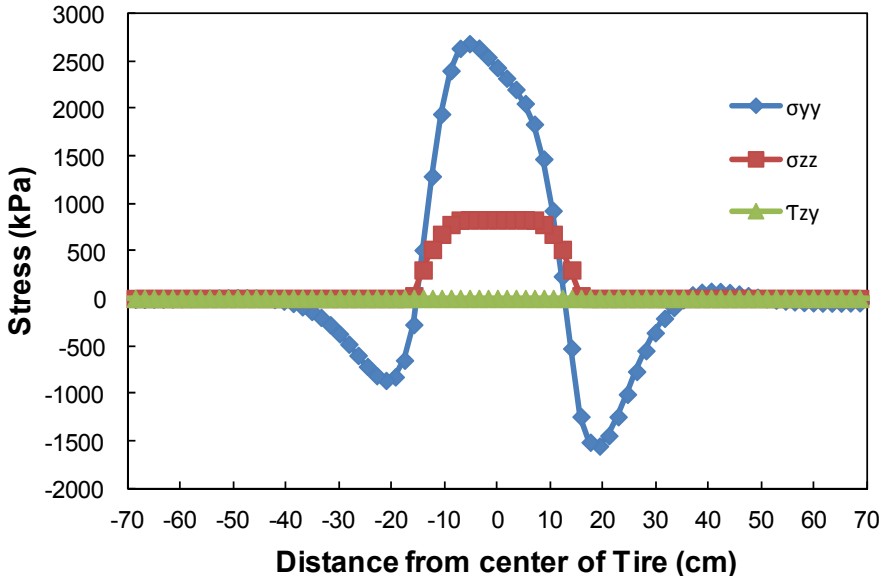

Figure B.45 Stresses on surface of debonded pavement along central longitudinal axis of wheel imprint due to a rolling wheel: 8 km/hr (5 mph) and 60°C (140°F).

The coefficient of friction between the tire and the pavement was assumed to be zero in this analysis case. As shown in Figure B.45, the shear stress on the surface of the pavement is zero ($\tau_{zy} = 0$), which is due to the rolling state of the wheel. The maximum normal stress (σ_{zz}) on the surface of the pavement is 827.4 kPa (120 psi), which is equal to the assumed tire pressure. The maximum horizontal tensile stress of 1,550 kPa (225 psi) occurs at 19.3 cm (7.6 in.) from the center of the wheel imprint in front of the wheel. The tensile stress behind the wheel is 825 kPa (119.6 psi) at 19.3 cm from the center of the wheel in the opposite direction of the traffic.

Using Equation (12), the tensile strength of the HMA pavement at 60°C (140°F) with a vehicle moving at the speed of 8 km/hr (5 mph) was predicted to be 430 kPa (62.3 psi). The strain rate used in Equation (12) was calculated using the bilinear method shown in Figure B.34. A comparison of the tensile stress on the surface of the debonded pavement and the tensile strength shows that the tensile stress values are much higher than the tensile strength values. Therefore, the debonded pavement would crack in front and behind the wheel due to a rolling wheel at the speed of 8 km/hr (5 mph) and at the temperature of 60°C (140°F).

The contours of the principal horizontal stress on the surface of the pavement with the debonded interface between the pavement layers are shown in Figure B.46. As shown, a rolling wheel moving over a debonded surface asphalt layer causes a circular tensile stress around the wheel and can result in the delamination distress in the debonded pavement.

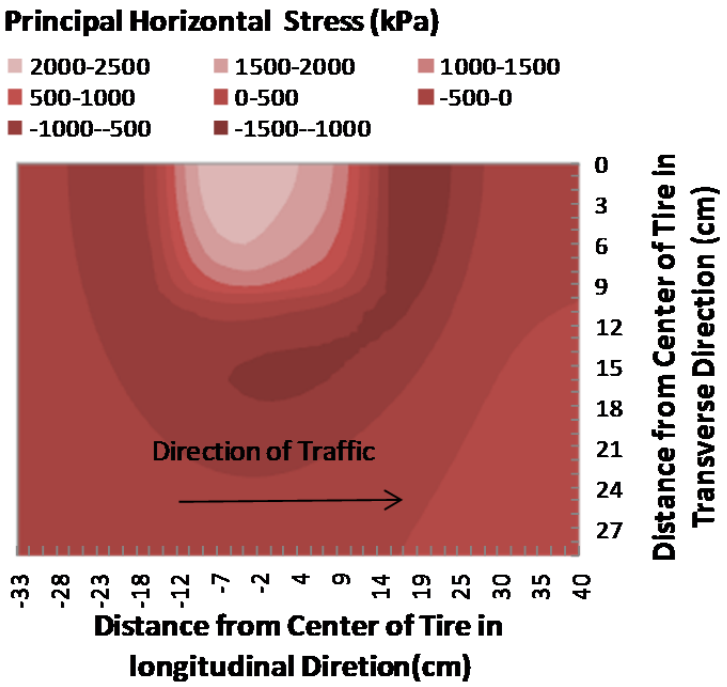

Figure B.46 Principal horizontal stress on the surface of pavement with debonded interface due to rolling wheel at 8 km/hr (5 mph) and at 60°C (140°F). Note: half of the tire imprint is shown due to symmetry.

The stresses due to the rolling wheel at the interface between the two debonded asphalt layers (stresses at the bottom of the top layer) are presented in Figure B.47. The maximum normal stress (σ_{zz}) at the interface is 736 kPa (106 psi) and the shear stress between the asphalt layers at the interface is zero, which indicates that no shear transfer occurred between the surface layer and the underlying layer.

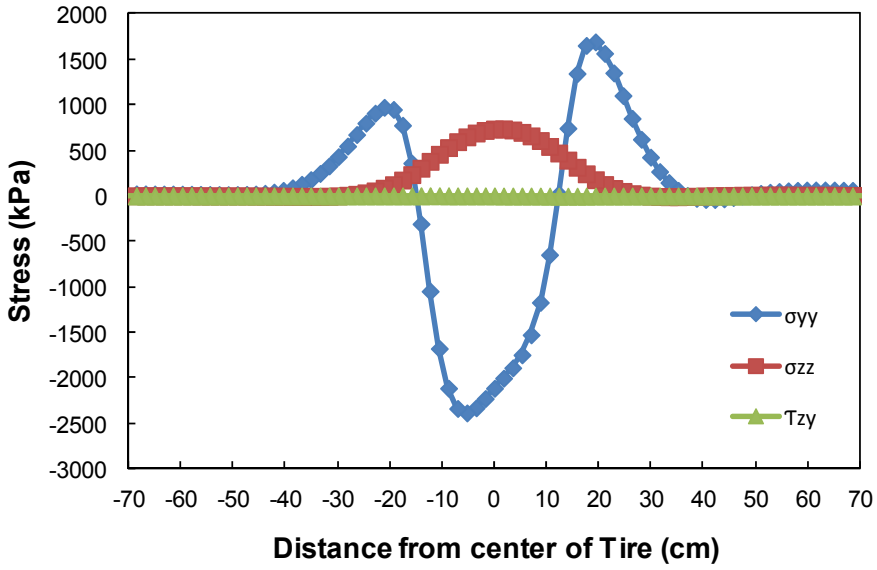

Figure B.47 Stress distribution at interface of debonded pavement layers due to rolling wheel along central longitudinal axis of tire: 8 km/hr (5 mph) and 60°C (140°F).

The maximum horizontal tensile stress at the bottom of the surface layer is shown in Figure B.47 at 5.2 cm from the center of the tire in the opposite direction of the traffic. The horizontal tensile stress at the bottom of the surface layer is 2,328 kPa (337.6 psi), which is much higher than the tensile strength of the HMA, and it caused a vertical crack at the bottom of the pavement 5.2 cm (2.05 in.) from the center of the tire.

Figure B.48 shows the horizontal stresses on the surface of the pavement and at the bottom of the top layer at the debonded interface due to a rolling wheel. The compressive horizontal stress (σ_{yy}) on the surface of the pavement at the center of the tire imprint and the tensile horizontal stress at the interface between the debonded asphalt layers at the center of the tire imprint indicate the bending of the surface asphalt layer separately as a beam. The bending of the surface layer introduced large horizontal tensile stresses in front of the tire imprint and behind the tire imprint due to the negative moment at the surface asphalt layer.

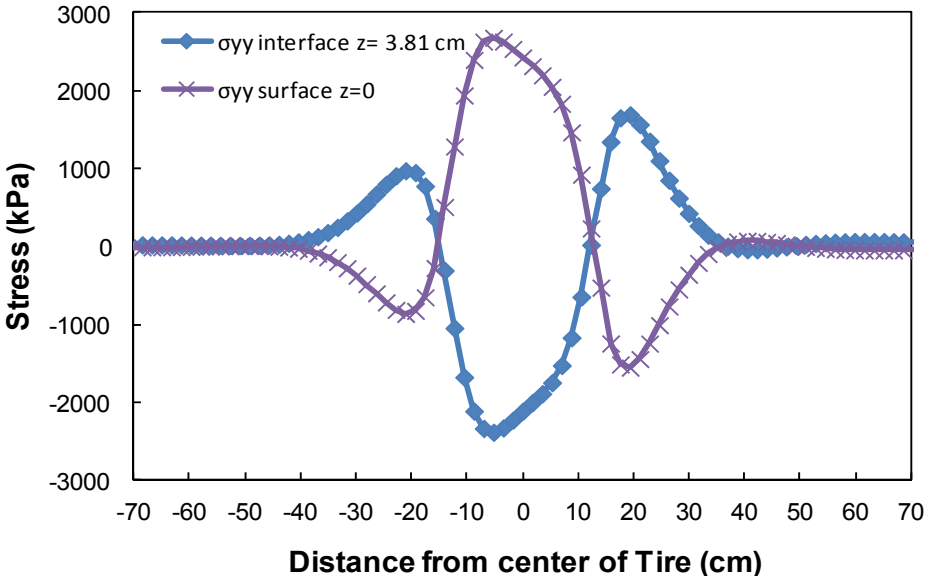

Figure B.48 Horizontal stresses (σ_{yy}) at the top (surface) and bottom (interface) of debonded surface asphalt layer along central longitudinal axis of the wheel. Note: tensile stress is negative.

Figure B.49 shows the approximate locations of the tensile cracks due to a rolling wheel in a schematic debonded pavement section.

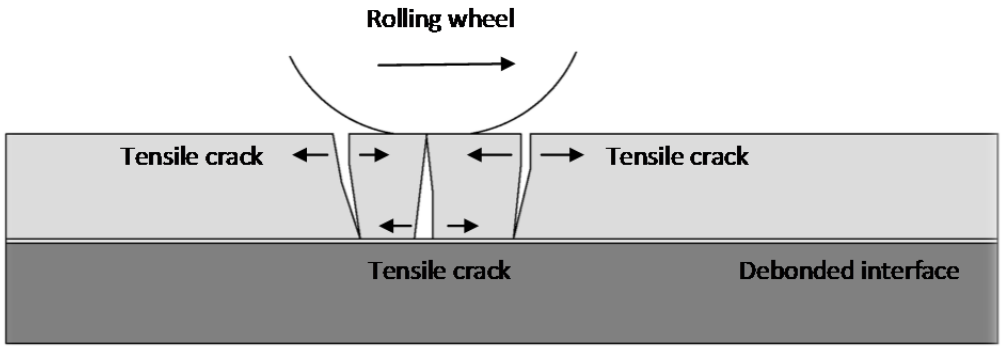

Figure B.49 Schematic tensile cracks in debonded surface layer due to rolling wheel.

Figure B.50 presents the stresses on the surface of the bonded pavement section with the structure shown in Figure B.19 (i.e., without the thin debonded layer) due to a rolling wheel moving with the speed of 8 km/hr (5 mph) at 60°C (140°F). The load is an 80-kN (18 kips) standard axle load applied in a single tire configuration with 827.4 kPa (120 psi) tire pressure. As shown in Figure B.50, the shear stress at the surface of the pavement is zero (rolling wheel condition) and the horizontal tensile stress in front of the tire is about 64 kPa (9.2 psi), which is lower than the tensile strength of the asphalt concrete. The horizontal compressive stress at the surface of the pavement is 720 kPa (104.4 psi), which is located 7 cm (2.75 in.) from the center of the tire in the opposite direction of the traffic.

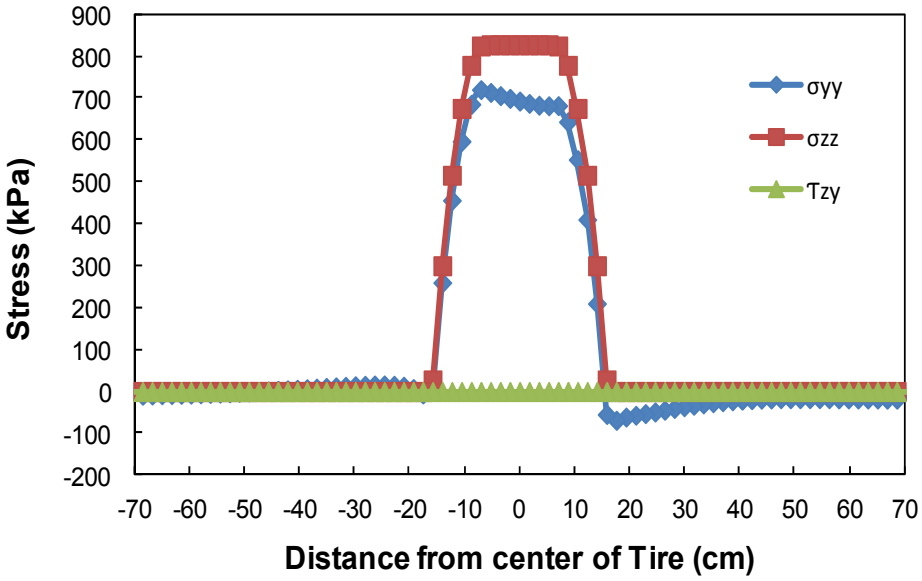

Figure B.50 Stresses at surface of pavement due to rolling wheel on bonded pavement along central longitudinal axis of the wheel: 60°C (140°F) and 8 km/hr (5 mph).

Figure B.51 shows the stresses at the interface between the surface layer and the underlying asphalt layer of the bonded pavement due to a rolling wheel. At the interface, only horizontal compression stress developed, and there is no horizontal tensile stress, which indicates the complete interaction between the asphalt layers as a composite structure. The shear stress at the interface was introduced due to the bending of the bonded pavement layers.

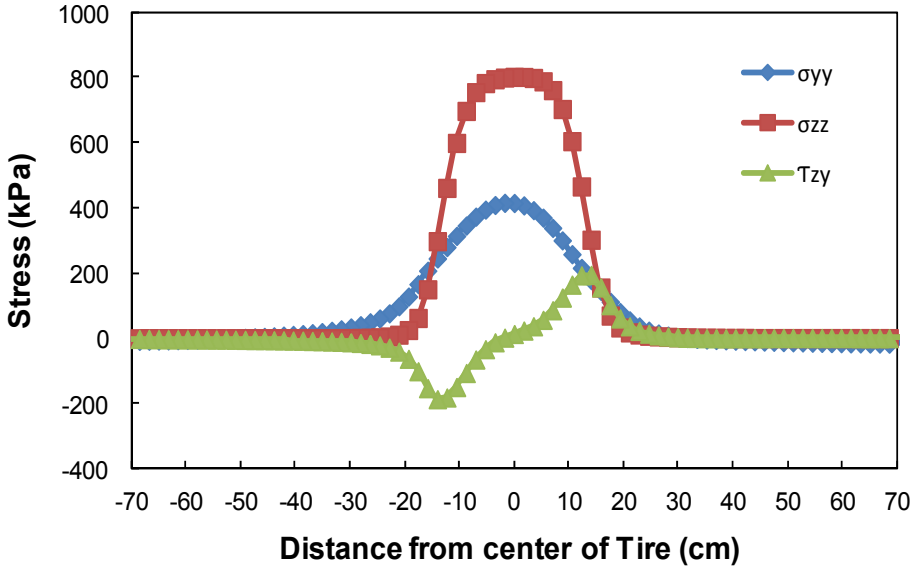

Figure B.51 Stresses at interface due to rolling wheel on bonded pavement along central longitudinal axis of the tire imprint: 60°C (140°F) and 8 km/hr (5 mph).

6.4.2. Stress in the Debonded Pavement with a Wheel in the Braking State

Figure B.52 shows the stresses at the surface of the pavement due to a wheel in the braking state moving at the speed of 8 km/hr (5 mph) with the coefficient of friction of 0.55 between the tire and pavement at 60°C (140°F). The load is an 80-kN (18 kips) standard axle load applied in a single tire configuration with 827.4 kPa (120 psi) tire pressure. The maximum shear stress (τ_{zy}) at the surface of the pavement is 455 kPa (66 psi) and the maximum vertical stress (σ_{yy}) is 827 kPa (120 psi), which is equal to the tire pressure.

As shown in Figure B.52, the maximum horizontal tensile stress (σ_{yy}) on the surface of the pavement behind the tire is 1,676 kPa (243 psi) and in front of the tire is 811 kPa (117.6 psi), which are higher levels than the tensile strength of the pavement, which is 446 kPa (64.7 psi). Therefore, a braking wheel moving over debonded pavement may cause vertical tensile cracks on the surface of the pavement in front of the tire and behind the tire.

Figure B.53 shows the principal horizontal stress on the surface of the debonded pavement due to a braking wheel moving at the speed of 8 km/hr (5 mph) with the coefficient of friction of 0.55 between the tire and pavement at 60°C (140°F). As is shown, the braking wheel causes tensile cracks around the wheel on the surface of the pavement.

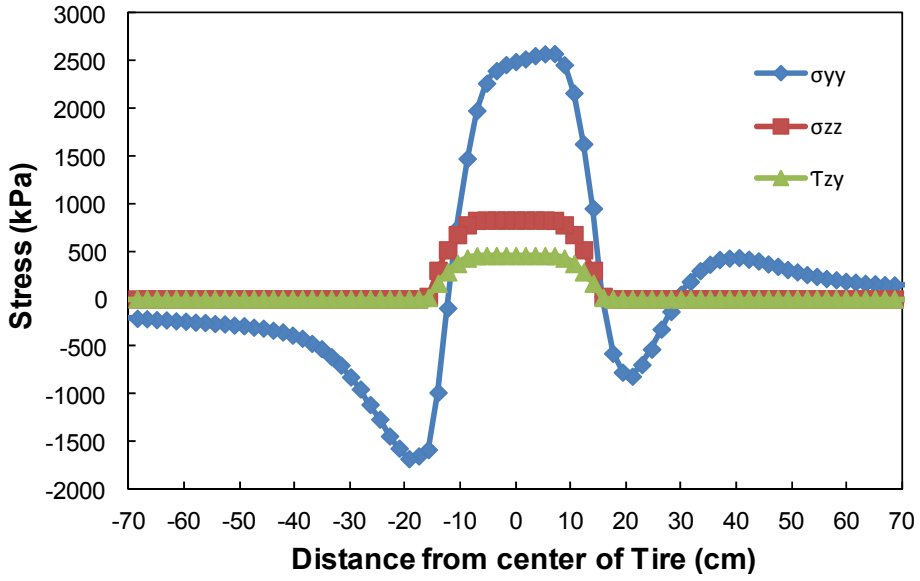

Figure B.52 Stresses on surface of debonded pavement due to braking wheel along central longitudinal axis of the tire: 60°C (140°F), 8 km/hr (5 mph), and 0.55 friction coefficient.

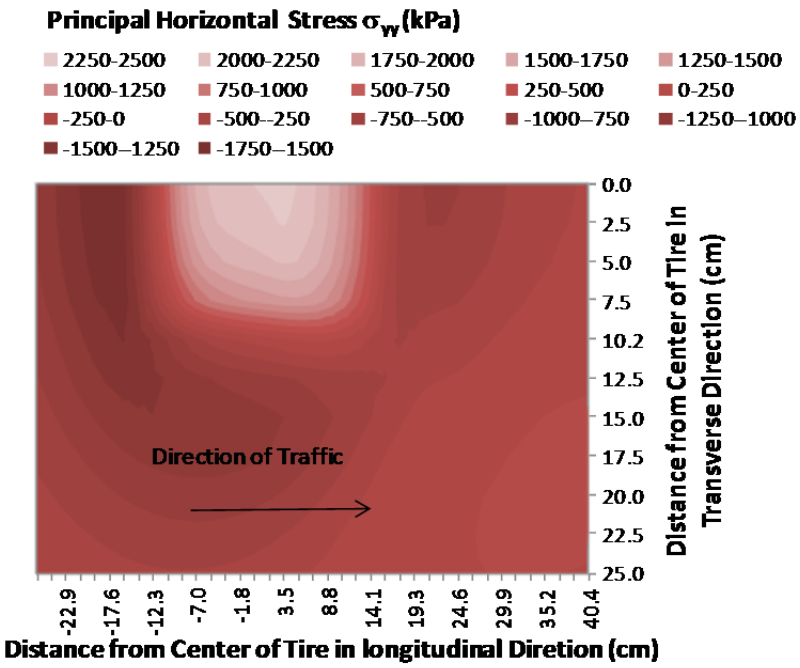

Figure B.53 Principal horizontal stress on surface of pavement with debonded interface due to braking wheel: 60°C (140°F), 8 km/hr (5 mph), and friction coefficient of 0.55. Note: half of the tire imprint is shown due to symmetry.

At the bottom of the surface layer, the maximum horizontal tensile stress occurs at 3.5 cm from the center of the tire in the opposite direction of the traffic, as shown in Figure B.54. This horizontal tensile stress can cause vertical cracks at the bottom of the surface layer (top-down cracking).

According to Chen (2010), crescent-shaped surface cracks that occur soon after the construction of HMA, as shown in Figure B.55, are possibly due to a debonded interface, which can be the result of improper tack coat application. A comparison of Figure B.55 and the principal horizontal stress shown in Figure B.53 shows the similarity of the crack patterns around the braking wheel to the maximum tensile principal horizontal stress. It can be concluded that a braking wheel moving on a debonded surface layer will cause a slippage crack behind the wheel and crescent-shaped surface cracks around the wheel.

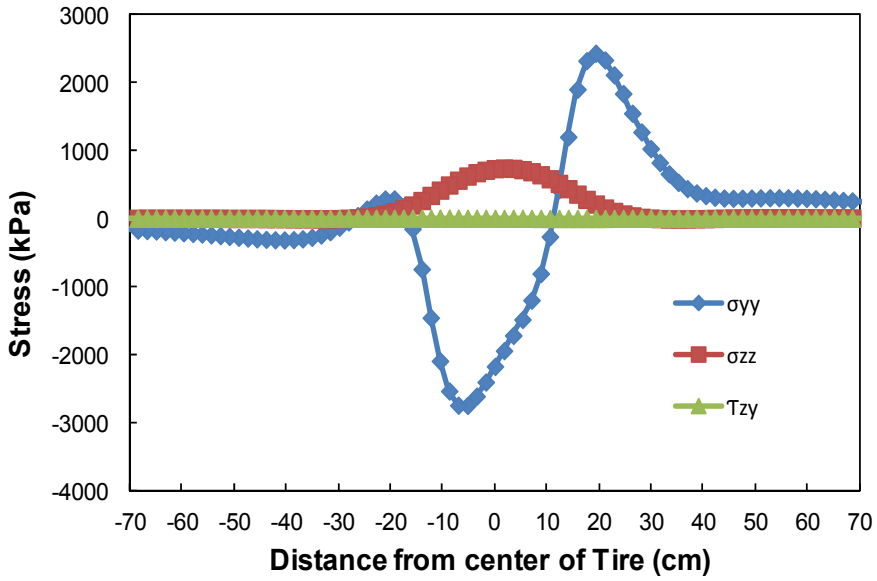

Figure B.54 Stresses at interface of debonded pavement due to braking wheel along central longitudinal axis of the wheel: 60°C (140°F), 8 km/hr (5 mph), and 0.55 friction coefficient.

Figure B.55 Premature slippage failure with crescent-shaped cracks after one day of traffic (Chen 2010).

APPENDIX C: Experimental Program

1. Materials

1.1. Asphalt Mixture

The RS9.5B mixture, which is the mixture type most commonly used in North Carolina, was used for this study. This mixture was mixed at a production plant and sampled during construction. The aggregate structure of the RS9.5B mix is coarse 9.5 mm nominal maximum aggregate size (NMAS) composed of 27 percent #78 coarse aggregate, 33 percent washed screenings, 10 percent fractionated reclaimed asphalt pavement (RAP) retained on a 6.35-mm (1/4-in.) screen, and 30 percent fractionated RAP passing a 6.35-mm (1/4-in.) screen. The total asphalt content is 5.6 percent by weight of the total mix. The blended aggregate gradation is shown in Figure C.1.

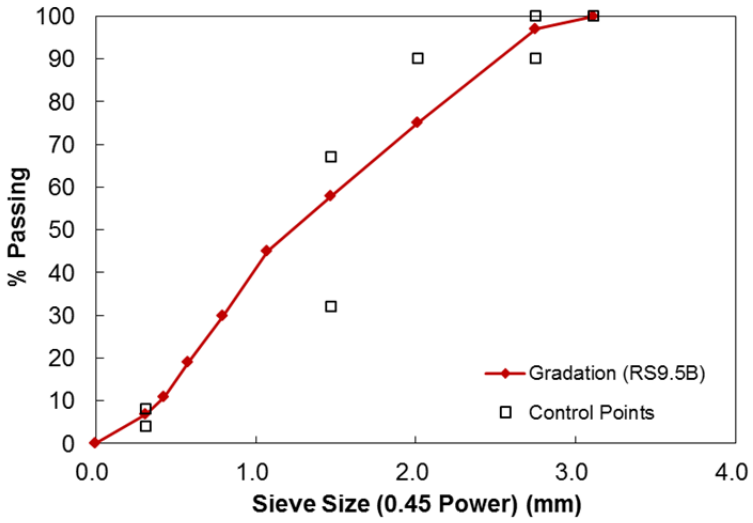

Figure C.1 Aggregate gradation chart of RS9.5B mixture.

The loose mixture was reheated and compacted after a separation process developed at North Carolina State University (NCSU) in order to reduce the specimen-to-specimen variability.

1.2. Tack Coat Materials and Surface Conditions

In this study, four types of tack coat material, CRS-2, CRS-1h, NTCRS-1hM (trackless tack coat), and no tack coat, were used. Residue recovery tests and evaporation tests were conducted and density measurements were taken to investigate the fundamental properties of each tack coat emulsion. The results of the residue recovery tests were used to determine the actual applied tack coat rate (i.e., residual application rate) that remained after the water in the asphalt emulsion evaporated. That is, the residue content determined from the residue recovery tests was used to calculate the actual weight of the tack coat that was applied to the bottom layer of the sample after the water in the asphalt emulsion had evaporated using the densities of each emulsion.

After each test sample was placed on a sensitive balance, the tack coat materials were applied to the bottom layer of the sample using a paint brush. The tack coat application rate of 0.181 L/m^2 (0.04 gal/yd^2), which is the application rate commonly used in North Carolina, was

used in this study. The tack coat application rate is the volume unit per unit area in this stage of the sample fabrication process. For this study, the application rate was converted to the weight (g) of the tack coat for gyratory specimens that were 150 mm in diameter using the densities of each asphalt emulsion. The application of the tack coat was performed quickly to ensure an accurate weight measurement because the tack coat starts curing immediately after its application. The samples on which the tack coat was applied were cured for various curing periods based on the results of the evaporation test for each tack coat material. In this study, a non-milled surface condition was used.

2. Asphalt Emulsion Residue Recovery

Asphalt residue needs to be recovered because it is important for understanding the actual applied rate of the tack coat that remains after the water in the asphalt emulsion has evaporated. For example, results from shear tests using samples with tack coat materials at the interface of asphalt specimens are affected by the rate and characteristics of asphalt residue. The tack coat residual rates that usually are used in laboratory applications differ from the tack coat application rates used in the field. The tack coat residual rate is the amount of actual asphalt binder that remains after the water that is retained in the asphalt emulsion has evaporated, whereas the tack coat application rate is the amount of liquefied asphalt that is sprayed by the distributor (California Department of Transportation 2009). However, if an asphalt binder (i.e., PG 64-22) is utilized as a tack coat material, the residual rate of the tack coat material applied on the pavement surface is equivalent to the applied application rate. It should be noted that the application rate of 0.181 L/m^2 (0.04 gal/yd^2) used in this study is not the tack coat residual rate but the tack coat application rate commonly used in North Carolina in the field.

The standard methods for residue recovery are described in the American Society for Testing and Materials (ASTM) D7497 and ASTM D6934 standards. ASTM D7497 specifies 60 grams of emulsion poured into a 1-mm thick silicon mold. Then, the sample is placed into an air-forced oven at 25°C for 24 hours and an extra 24 hours at 60°C. This procedure takes two days. Other methods have been proposed to reduce the recovery time, such as the Texas method (Prapaitrakul et al. 2010) and rapid recovery procedure using a rolling thin film oven (Takamura et al. 2000). In the Texas method, the sample's thickness is reduced to 0.381 mm (0.015 in.), and the residue recovery is carried out in an air-forced oven at 60°C for six hours. In the Takamura method, 35 grams of emulsion are poured into individual bottles. The samples are dried at 85°C for 75 minutes with a forced air flow of 4 liter/minute. Then, the bottles are placed in an oven at 135°C for 15 minutes. Other techniques used for emulsion residue recovery include the Belgian procedure 08-34, Spanish method NLT 147, distillation according to ASTM D244/EN 1431, and an ethanol precipitation method.

In this study, residue recovery was conducted based on ASTM D6934. In this method, 50 ±0.1 grams of asphalt emulsion heated to 50°C ±3.0°C are poured into each of three open-top beakers made of glass or metal. Then, the samples are placed in an air-forced oven at 163°C ±3.0°C for two hours. At the end of this period, each beaker is removed from the oven and its contents are stirred thoroughly using glass rods. The samples are put back into the oven for one hour and then allowed to cool to room temperature. Finally, the percentage of residue is calculated by weighing the samples using the following equation:

$$\text{Residue, \%} = 2(A - B) \quad (14)$$

where

A = weight of beaker, rod, and residue (g), and

B = tare weight of beaker and rod (g).

The residue recovery tests were carried out for the three study emulsions, CRS-2, CRS-1h, and NTCRS-1hM (trackless tack coat) used in this research. Figure C.2 shows the test samples in the oven.

Table C.1 provides the results of the asphalt residue recovery tests for the study emulsions.

Figure C.2 Asphalt residue recovery test samples in oven.

Table C.1 Asphalt residue recovery test results for study emulsions.

Type	Replicate	A (g)	B (g)	Residue (%)	Average (%)
CRS-2	1	127.2	94.1	66.2	66.4
	2	126.7	93.5	66.4	
	3	127.0	93.7	66.6	
CRS-1h	1	123.2	93.7	59.0	59.1
	2	123.2	93.6	59.2	
	3	123.4	93.9	59.0	
NTCRS-1hM (Trackless)	1	124.5	93.8	61.4	61.2
	2	124.0	93.5	61.0	
	3	124.3	93.7	61.2	

3. Asphalt Emulsion Curing Time

In this study, understanding the curing procedure and time is important to finding the appropriate compaction time for the top layer after the tack coat emulsion has been applied to the bottom layer of the asphalt test sample. The emulsion curing process takes two steps: breaking and curing (Im 2013). The breaking process is when the emulsion changes from a dispersed form into an asphalt form. In other words, breaking is characterized by the separation of the liquid asphalt and water into two separate phases. Curing is when the water evaporates from the emulsion.

An evaporation test typically is performed to help determine the curing time that is required for each emulsion to reach its asymptotic percentage of water loss. In this research, each type of emulsion was placed in an environmental chamber at 25°C for the evaporation tests. The test temperature was determined based on the normal ambient temperature in the NCSU laboratory. Three replicates for each emulsion were prepared and subjected to the same test conditions. The tack coat application rate of 0.181 L/m^2 (0.04 gal/yd^2) was distributed uniformly in a 140-mm diameter container at 25°C. Figure C.3 shows the evaporation test samples in the environmental chamber. The curing time was determined when the percentage of water loss (% water loss) reached asymptotic trends, that is, the point at which no more water loss occurred.

Figure C.3 Evaporation test samples in environmental chamber.

Figure C.4 shows the curing time results for the three study emulsions. Figure C.4 indicates that the each emulsion reached its asymptotic percentage of water loss (curing value) in approximately 30 minutes. In addition, Figure C.4 (a) illustrates that the CRS-2 emulsion contains a larger quantity of asphalt residue than the other two emulsion types after the water evaporated. Thus, the water loss percentages of the CRS-2 emulsions are lower than those of the CRS-1h and NTCRS-1hM emulsions, as shown in Figure C.4 (b).

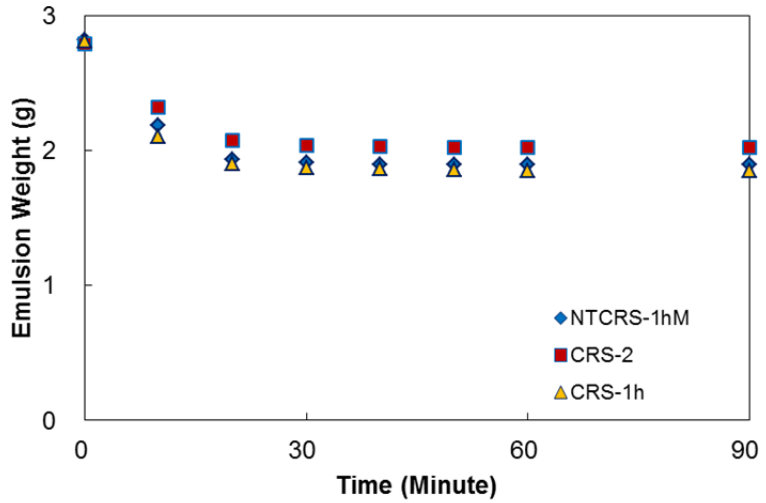

(a)

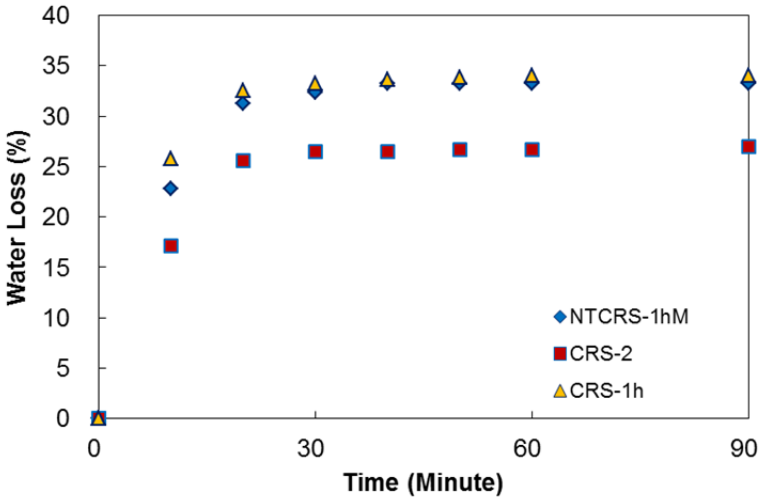

(b)

Figure C.4 Results of curing time for study emulsions: (a) emulsion weight versus time and (b) water loss versus time.

4. Density of Emulsified Asphalt

The density of the emulsified asphalt was determined in order to convert the volume unit per unit area of the tack coat application rate (or the tack coat residual application rate) to the weight unit per unit area. These tests were performed according to ASTM D6937. The density values obtained from these tests were used for laboratory sample fabrication because knowing the weight of the tack coat (g) is required for this process.

After each test sample was placed on a sensitive balance, the tack coat material was applied to the bottom layer of the sample using a paint brush. In the case of the CRS-2 emulsion, the tack coat application rate of 0.181 L/m^2 (0.04 gal/yd^2) of volume unit per unit area used in this stage of the sample fabrication process was converted to the tack coat application of 3.22

grams for gyratory specimens that were 150 mm in diameter using 1.010 (kg/L) as the density of the asphalt emulsion. Table C.2 presents the material properties of the study emulsions.

Table C.2 Material properties of study emulsions.

Property	Type of Emulsion		
	CRS-2	CRS-1h	NTCRS-1hM (Trackless)
Residual Asphalt Content (%)	66.4	59.1	61.2
Density (kg/L)	1.010	1.016	1.018
Application Weight of Tack Coat (g)	3.22	3.25	3.26
Base Binder	PG 58-22	PG 64-22	PG 64-22 Modified
Tack Coat Application Rate (L/m^2)	0.181 (0.04 gal/yd^2)		
Residual Application Rate (L/m^2)	0.120 (0.027 gal/yd^2)	0.107 (0.024 gal/yd^2)	0.111 (0.025gal/yd^2)
Curing Time (Minutes)	30		

5. Theoretical Maximum Specific Gravity (G_{mm})

The theoretical maximum specific gravity (G_{mm}) is the specific gravity (excluding air voids) in a mixture that is used to calculate the air void content for an asphalt concrete specimen. The maximum specific gravity is determined using samples in a loose mixture condition. The mixture should be loose and broken up so that the fine aggregate is separated into particles smaller than 6.25 mm (0.25 in.), taking care not to fracture the aggregate. The minimum required sample sizes (by weight) are presented in Table C.3. The maximum specific gravity (G_{mm}) measurements were taken for the RS9.5B mixture and were later used for laboratory specimen fabrication following the standard specifications found in ASTM D2041. The maximum specific gravity of 2.424 was obtained from these measurements.

Table C.3 Mass requirements for maximum specific gravity measurements.

Nominal Maximum Aggregate Size	Minimum Sample Size (g)
37.5 mm or greater	5,000
19 mm to 25 mm	2,500
12.5 mm or smaller	1,500

The test procedure for obtaining the maximum specific gravity measurements is as follows:

1) Cure the laboratory-prepared samples in an oven at 135°C ±5°C (275°F ±9°F) for a minimum of two hours or until constant mass is achieved.
2) After the G_{mm} samples cool, separate the aggregate particles into particle sizes that are smaller than 6.25 mm (0.25 in.), as illustrated in Figure C.5.
3) Measure the dry weight of the loose mix and record it as A.

4) Put the loose mix inside a pycnometer and fill the pycnometer with water to half the distance between the mix level and the top level.
5) Apply 3.7 kPa (0.54 psi) of vacuum for 15 minutes.
6) Remove the vacuum and fill the pycnometer with water. Measure the weight of the pycnometer, water, and loose mix, and record as E.
7) Remove the water and loose mix from the pycnometer. Refill the pycnometer with water and record the weight of the pycnometer and water as D.
8) Calculate the G_{mm} using the following equation:

$$G_{mm} = \frac{A}{A + D - E} \tag{15}$$

Figure C.5 Test-ready separated sample.

6. Dynamic Modulus (|E*|) Testing

Dynamic modulus (|E*|) tests were conducted for the RS9.5B mixture, which was later used for lab testing, in order to obtain the basic viscoelastic properties, i.e., the dynamic modulus values and time-temperature (t-T) shift factors. Asphalt concrete in the linear viscoelastic range is known to be thermorheologically simple material. The effects of time and temperature can be combined into a joint parameter, i.e., reduced time/frequency, f_R, using the t-T shift factor (a_T).

In this study, three replicates were used for the dynamic modulus tests. The specimens were compacted using a Servopac Superpave Gyratory Compactor, manufactured by IPC Global of Australia, to dimensions of 178 mm in height and 150 mm in diameter. To obtain specimens of uniform quality for testing, especially in terms of air void content, these samples were cored and trimmed to a height of 150 mm and a diameter of 75 mm. After obtaining specimens with the appropriate dimensions, air void measurements were taken via the Core-Lok method. Table C.4 presents the air void content results for the specimens used in the dynamic modulus tests. It should be noted that air void contents used for dynamic modulus tests should coincide with air void contents used for shear tests, which are between 5.5 percent and 6.5 percent, with a target air void content of 6.0 percent.

Table C.4 Air void content results for dynamic modulus tests.

Sample ID	Bag Weight (g)	Sample Weight Before Sealing (g)	Sealed Sample Weight in Water (g)	Sample Weight After Water Submersion (g)	Density of Water (g/cm^3) for Temperature Correction	Maximum Specific Gravity	Bulk-Specific Gravity (g/cm^3)	Air Voids (%)
DMT-T1	27.6	1511.7	840.6	1511.7	0.997448	2.424	2.273	6.2
DMT-T2	27.5	1546.7	862.9	1546.7	0.997448	2.424	2.282	5.9
DMT-T3	27.7	1530.7	853	1530.7	0.997448	2.424	2.279	6.0

Prior to testing, steel end plates were glued to the specimen using DEVCON steel putty. To ensure that the specimens were properly aligned, a special gluing jig was employed so that the end plates were parallel, thus minimizing any eccentricity that might occur during the test. Measurements of axial deformations were taken at 90° intervals over the middle 100 mm of the specimens using loose-core linear variable displacement transducers (LVDTs). Load, crosshead movement, and specimen deformation data were acquired using a 16-bit National Instruments data acquisition board and collected using LabVIEW software. Note: The data acquisition rate varies depending on the nature of the test so that the appropriate amount of data can be acquired for analysis. An MTS closed-loop servo-hydraulic loading frame with an 8.9-kN (2000-lb) load cell was used for the tests. An environmental chamber, equipped with liquid nitrogen coolant and a feedback system, was used to control and maintain the test temperature. Figure C.6 (a) shows the gluing jig and Figure C.6 (b) shows the entire test set-up installed in the MTS machine.

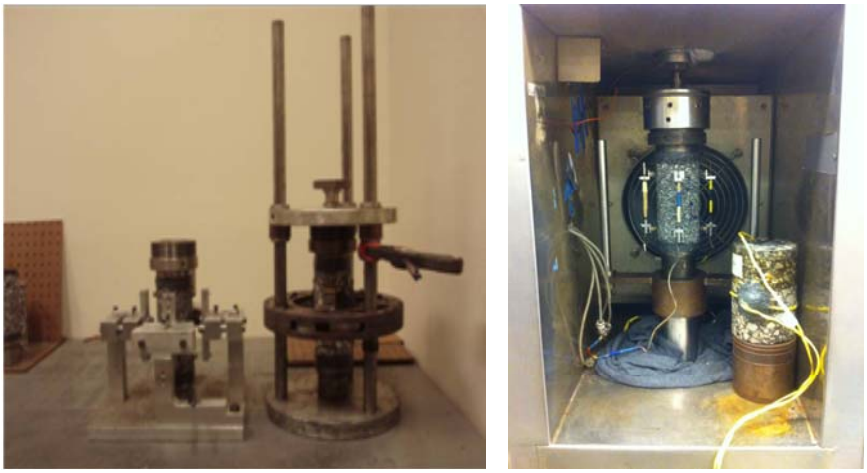

(a) (b)

Figure C.6 (a) Gluing jig and (b) entire dynamic modulus test set-up.

The dynamic modulus tests were performed in stress-controlled mode. The tests were performed at frequencies of 25, 10, 5, 1, 0.5, and 0.1 Hz and temperatures of -10°C, 5°C, 20°C, 40°C, and 54°C. The load level was adjusted for each condition to produce total strain amplitudes of about 50 to 75 micro-strains, which are within the linear viscoelastic range.

Figure C.7 presents the results for the three replicates of the RS9.5B mixture at several different temperature/frequency combinations. The data at various temperatures were shifted with respect to time until the curves merged into a single smooth function. That is, the data were shifted horizontally onto an arbitrarily selected reference temperature curve to form a single curve, the mastercurve, which can be used to describe the constitutive behavior of asphalt concrete over a wide range of temperatures and frequencies.

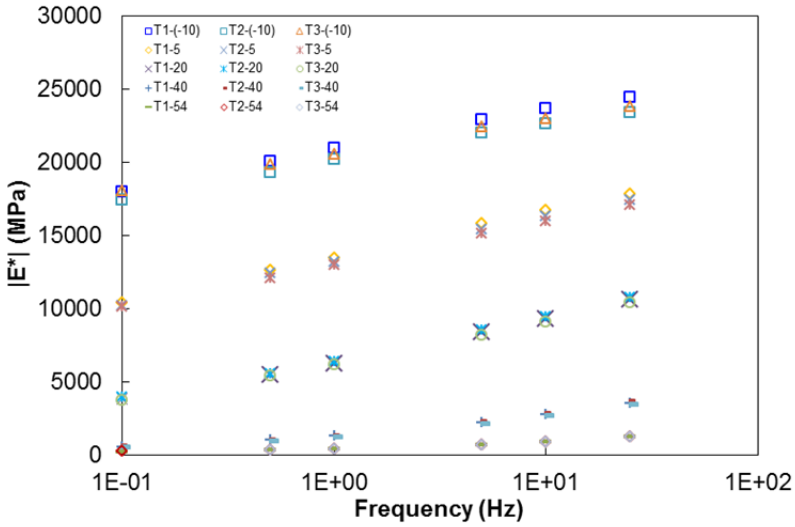

Figure C.7 Typical unshifted dynamic modulus values for three replicates of RS9.5B mixture.

The t-T shift factor is the amount of horizontal shift in log scale that is required to create a continuous curve. For thermorheologically simply materials, the amount of shifting is dependent only on the temperature chosen as the reference temperature and, therefore, varies by temperature, as shown in Figure C.8 for the three replicates of the RS9.5B mixture.

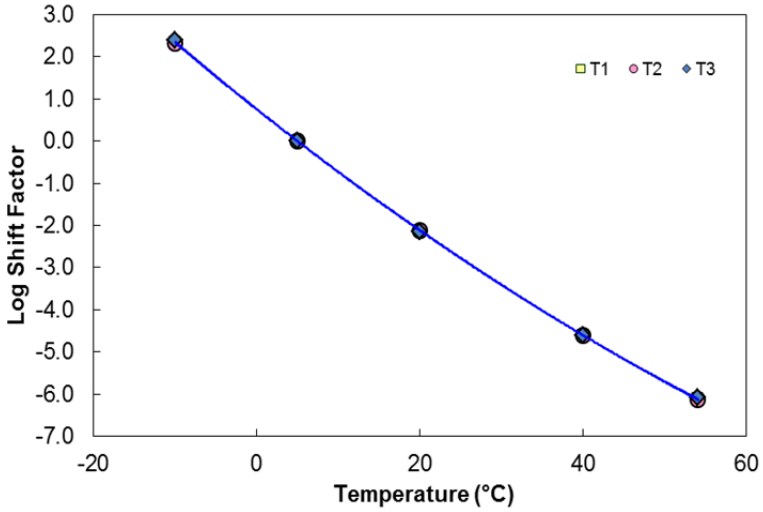

Figure C.8 Time-temperature shift factor function for three replicates of RS9.5B mixture.

Table C.5 presents the averaged t-T shift factor function coefficients for the RS9.5B mixture. The t-T shift factor function coefficients presented in Table C.5 were used later for the horizontal shifting of the interface shear bond strength data using the Modified Advanced Shear Tester (MAST) at several different temperatures and constant displacement control rates. Figure C.9 presents the dynamic modulus mastercurve for the RS9.5B mixture.

Table C.5 Averaged fitting coefficients of time-temperature shift factor function.

Parameters	RS9.5B
α_1	0.0005055
α_2	-0.1544783
α_3	0.7597547

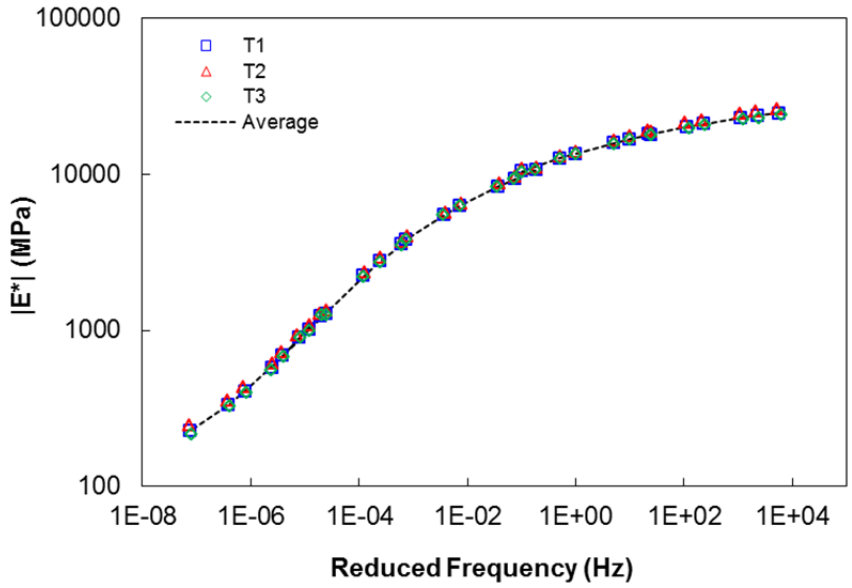

Figure C.9 Dynamic modulus mastercurve for RS9.5B mixture.

As mentioned before, the t-T shift factor is a function of temperature only and is independent of strain level (Chehab et al. 2002). Moreover, the following relationship between the elastic modulus (*E*) and shear modulus (*G*) is valid: E (t, T) = α·G (t, T). In this relationship, α represents the constant, which is related to Poisson's ratio, ν (t, T). However, the effect of the constant α is not so strong that the t-T shift factors obtained from the dynamic modulus tests in axial mode would work for shear mode. Later, the t-T shift factors obtained from the dynamic modulus tests within the linear viscoelastic range were used to construct the mastercurve between shear strength and log reduced shear strain rate.

7. Modified Advanced Shear Tester (MAST)

The MAST was designed to investigate the shear properties of uniform asphalt mixtures as well as interlayer interfaces, and to resolve the problems inherent of many of the devices currently used for shear testing. Such problems could produce highly variable results that could

lead to the need for complex biaxial load frames and elaborate sample preparation. The MAST was developed after reviewing numerous interface performance test methods, as stated in Appendix A.

The MAST was designed in such a way that it not only can test different specimen geometries, such as cylindrical and square-shaped specimens, but it also can acquire digital image correlation (DIC) images from the surface of the specimen at areas close to the interface. Figure C.10 presents drawings of the MAST, which is a direct shear apparatus that is capable of testing 152.4-mm (6-in.) and 101.6-mm (4-in.) square-shaped specimens as well as 101.6-mm (4-in.) diameter cylindrical specimens for direct shear. This device can conduct not only simple shear bond strength tests but also shear fatigue resistance tests under different environmental conditions (e.g., load- or displacement-control mode at various temperatures).

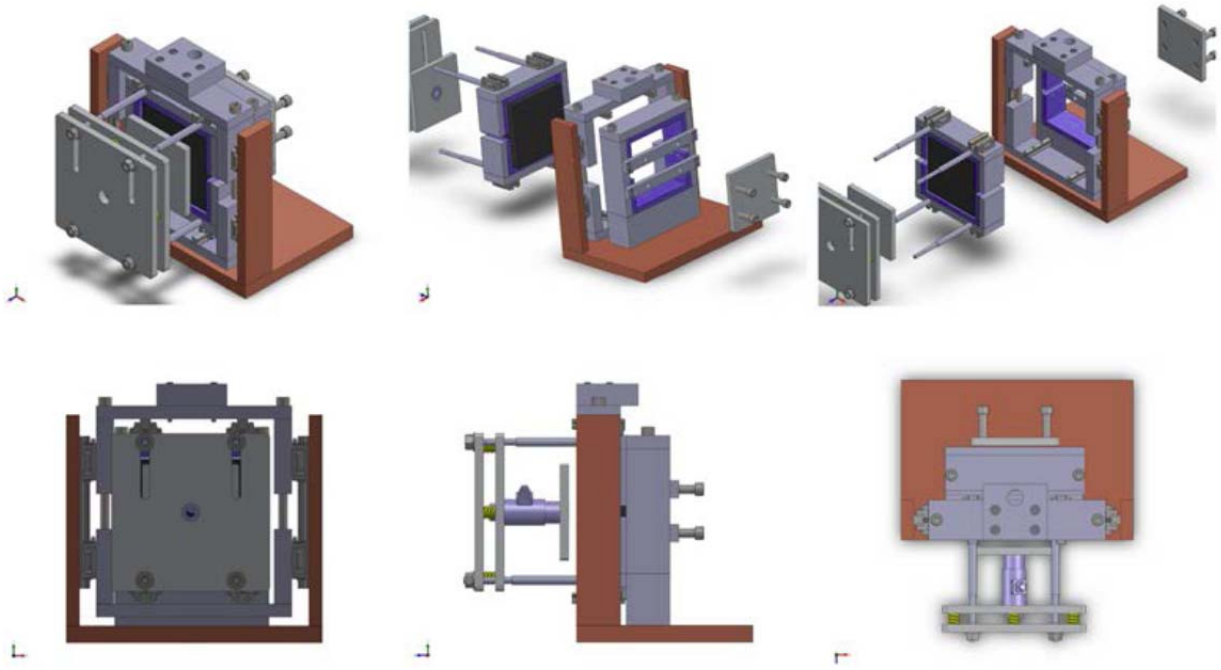

Figure C.10 Drawings of Modified Advanced Shear Tester (MAST).

One of the distinctive features of the MAST is its ability to control the initial normal confining stress that is applied to a specimen: the operator simply tightens a set of bolts while monitoring the load level during testing using an in-line load cell. The application method used for normal confining stresses was inspired by Adam Zofka's shearing device (Zofka et al. 2015), the Advanced Shear Tester (AST), shown in Figure C.11. Zofka et al. (2015) demonstrated that laboratory tests could simulate the states of stress that are encountered under moving vehicle loading conditions in the field. If the conditions are not simulated, then the measured responses from the tests could be unreliable. Thus, Zofka et al. (2015) introduced the concept of constant normal load (CNL) and constant normal stiffness (CNS) in their study. The authors clarified that, although the CNL condition is the more realistic of the two conditions, as the normal stress remains relatively constant during the shearing process, the CNS condition is actually more appropriate as a test condition, as the normal stress changes considerably during the shearing process. It is worth noting that normal stress is not always constant at the top of the asphalt layer due to moving vehicle loads, especially in the case of heavy vehicles at slow speeds over thin

pavement layers. In addition, the CNL condition might not fully explain the dilation phenomenon in asphalt materials. Therefore, Zofka et al. (2015) contend that, although the CNL condition is commonly found in layered asphalt pavements, the CNS condition might be as suitable as the CNL condition in certain cases, thereby better simulating actual field conditions. Therefore, the authors demonstrated that their AST device might have a unique feature in terms of CNS mode that differentiates it from other devices.

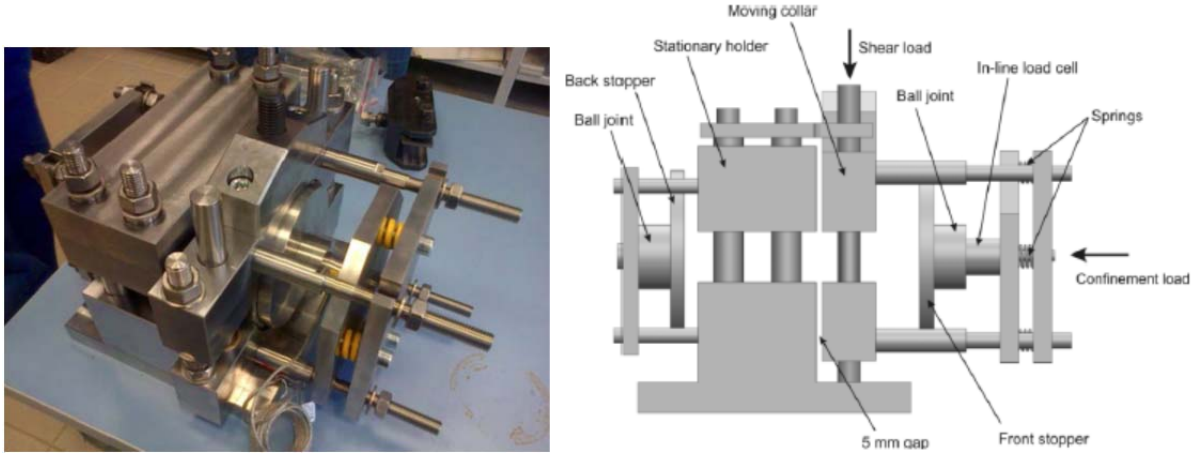

Figure C.11 Advanced Shear Tester (AST).

The NCSU research team modified the AST design slightly to remove possible friction that could occur among the different components involved in applying the normal confining stress, yet still retain all the benefits of the AST. Previous research results by Canestrari et al. (2005) indicate that normal loads or confining stresses can have a substantial effect on asphalt specimen shear test results, so this feature of the MAST provides a distinct advantage over many of the current devices used for shear testing.

The results of the comprehensive shear bond strength tests performed by the MAST on the laboratory-fabricated samples and the results of the computational analysis are used later to determine the critical conditions for the debonding distress.

8. Laboratory Specimen Fabrication

8.1. Superpave Gyratory-Based Shear Test Protocol

The MAST originally was intended for a specimen composed of two symmetrical asphalt layers obtained from slabs compacted by a steel wheel compactor to examine the interface shear bond strength. However, gyratory-based shear test specimens with a double layer were developed for this study. This procedure is as follows.

In order to produce the desired MAST specimen, the first stage of fabrication is to create a one-layered cylindrical specimen that is 150 mm (6 in.) in diameter and 50.8 mm (2 in.) in height using the Servopac Superpave Gyratory Compactor, manufactured by IPC Global of Australia. Once hot mix asphalt (HMA) has been poured into the gyratory compactor mold, the compactor compacts the mixture to a height of 50.8 mm (2 in.). After cooling, a tack coat is applied uniformly to achieve a consistent thickness on the top of the bottom layer. This process involves using a paint brush to apply the tack coat with an application rate of 0.181 L/m^2 (0.04 gal/yd^2) after placing the specimen on a sensitive balance. The specimen is then cured for various

curing periods as determined by the evaporation test (curing time test) for each emulsion type. During the curing period, the water evaporates, leaving only residual asphalt on the surface.

After curing, the same compaction process used for the bottom layer is repeated on top of the bottom layer in order to produce the upper asphalt concrete layer that has a thickness of 50.8 mm (2 in.). At this time, the bottom layer, where the tack coat has been applied and has already cured, is placed into the gyratory compactor mold again. The amounts of the bottom and top layer mixtures are measured prior to compaction to ensure a constant air void content and specimen thickness between the two layers. When the top layer is compacted, a cold mold is used because it best simulates field conditions during compaction. Hasiba (2012) observed that, although the compaction process was intended originally to be conducted using a hot mold that reaches the compaction temperature of a mixture to prevent the loss of heat during compaction, a hot mold that is used for compaction of the second layer in a two-layer compaction process allows the binder in the asphalt mixture and applied tack coat to provide the layer interface with higher bond strength during shear testing due to the heat.

After compacting the upper layer, the specimens are sealed in bags and placed in an unlit cabinet to reduce the aging effects. Then, in order to maintain consistent air void distribution, thereby obtaining specimens of uniform quality for testing, the specimens are cored and cut to a height of 76.2 mm (3 in.) and a diameter of 101.6 mm (4 in.) before testing. Figure C.12 shows the specimen preparation steps.

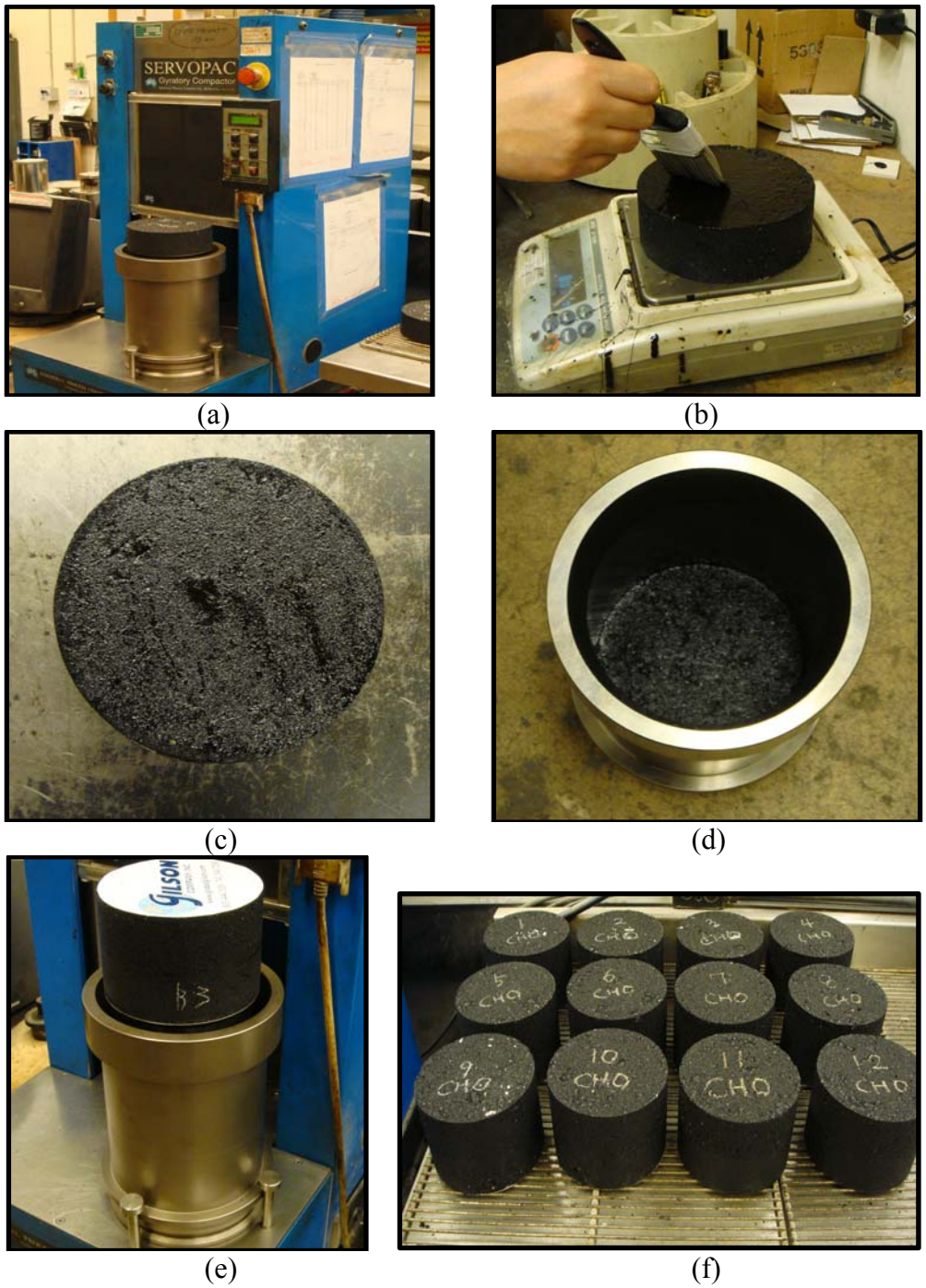

Figure C.12 Specimen preparation steps: (a) compaction of bottom layer, (b) tack coat application, (c) curing process, (d) placement of the bottom layer in the mold, (e) compaction of top and bottom layers, and (f) completed gyratory-compacted specimens.

8.2. Air Void Study of MAST Samples

MAST specimens need to have the same characteristics for both layers, especially in terms of air void content. Therefore, effort to make the air void content the same for both layers was required for this study. After obtaining specimens of the appropriate dimensions, i.e., height of 38.1 mm (1.5 in.) and diameter of 101.6 mm (4 in.) for both layers, air void measurements were taken via the CoreLok method. Table C.6 presents the air void content for each layer. The air void contents for the top and bottom layers are similar.

Table C.6 Air void content data for MAST specimens.

Design Air Void (%)	Layer	Dimension (mm)		
		150 (D) × 50.8 (H)*	150 (D) × 50.8 (H)	101.6 (D) × 38.1 (H)
7.5	Bottom	6.9	6.0	5.3
	Top	-	7.2	5.0
8.0	Bottom	7.5	6.8	5.6
	Top	-	7.8	5.3
8.5	Bottom	7.9	7.2	6.1
	Top	-	8.3	5.9

- ** Before compaction of top layer*
- *D: diameter, H: height*
- *Gray shaded column: target air voids*

It should be noted that the air void contents for shear testing using the MAST are between 5.5 percent and 6.5 percent, with a target air void of 6.0 percent. A relationship was found for the air void contents between the gyratory samples and the MAST samples. Based on this relationship, the design air void content of 8.5 percent for the gyratory samples was used in order to reach the target air void content of 6.0 percent.

Next, verification of the air void study results was conducted, as presented in Table C.7. Figure C.13 presents the dimensions and air void contents of the MAST samples.

Table C.7 Verification of air void study results.

No.	**Sample ID**	**Bag Weight (g)**	**Sample Weight Before Sealing (g)**	**Sealed Sample Weight in Water (g)**	**Sample Weight After Water Submersion (g)**	**Density of Water (g/cm^3) for Temperature Correction**	**Maximum Specific Gravity**	**Bulk-Specific Gravity (g/cm^3)**	**Target Air Voids (%)**
1	Top 8.5%	27.4	671.8	370.8	671.8	0.997327	2.424	2.278	6.0
	Bottom 8.5%	27.4	642.2	353.7	642.2	0.997327	2.424	2.274	6.2
2	Top 8.5%	27.5	651.0	359.5	651.0	0.997327	2.424	2.281	5.9
	Bottom 8.5%	27.3	650.7	358.4	650.7	0.997327	2.424	2.273	6.2

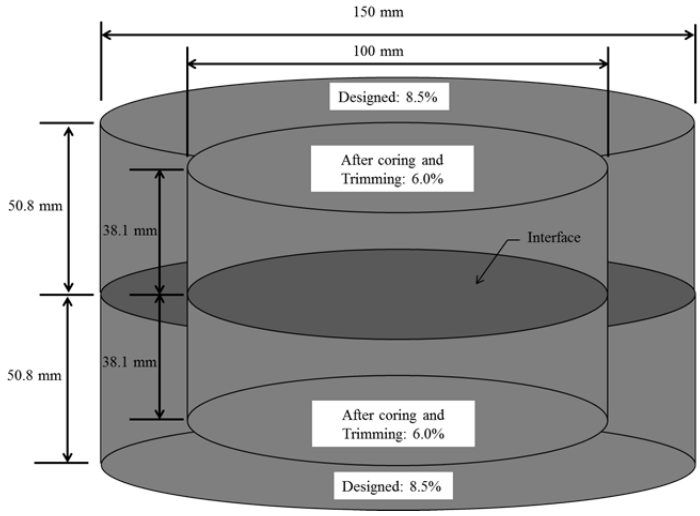

Figure C.13 Dimensions and air void contents of MAST sample.

9. Simulation of Debonding Distress Mechanisms

9.1. Loading Rate

Table C.8 provides a summary of available shear test devices and their test procedures as obtained from the literature. Based on the loading rates presented in Table C.8, the base loading rate of 50.8 mm/min (2 in./min) was selected for this study. This rate is commonly used in monotonic shear testing, i.e., controlled crosshead (CX) strain tests. Two additional loading rates, 0.508 mm/min (0.02 in./min) and 5.08 mm/min (0.2 in./min), which are hundred times and ten times slower, respectively, than the base loading rate, were selected for this study as well.

Table C.8 Shear test devices and test procedures (Bernier et al. 2012).

Year	Author	Gap Width (mm)	Loading Rate (mm/min)	Normal Stress (kPa)	Temperature (°C)
Monotonic Unconfined Shear					
1979	Leutner	1	50.8	0	20
2004	Raab and Partl		50.8	0	20
2004	Scholar et al.	4.8	19.1, 50.8	0	25~60
2005	Vacin et al.		50.8	0	22
2006	Tashman et al.	4.76	50.8	0	25
2008	Collop et al.	5	20	0	20
2007	Ascher et al.	1	50	0	25
Superpave Shear Tester					
1994	Sousa			0~100	(-10)~70
1998	Romero and Mogawer		4200 kPa/min		40~58
2005	Mohammad et al.	Agg. Dependent	12.6 kPa/min		22~55
Monotonic Shear					
1978	Uzan		2.5	4.9~490	25~55
1999	Romanoschi	5	12	138~522	15~35
2005	Canestrari et al.	Agg. Dependent	2.5, 50.8	0~400	20~40
2005	West et al.	6.35	50.8	0~138	10~60
2008	Al-Qadi et al.		12	0	10~30
2009	Mohammad	12.7	2.54	0~138	25
2010	Raab et al.	0~5	50	0	20
2012	Zofka et al.	5	1	85~340	22
Shear Fatigue					
1999	Romanoschi			138~522	25
2006	Diakhaté	Agg. Dependent	1 Hz Sinusoidal		5
2007	Ascher et al.	0-15	Sweep	0~750	(-10)~50
2012	Zofka et al.	5	Load-Control	170	35

9.2. Temperature

The selection of proper test temperatures is an important decision because asphalt material is very sensitive to temperature/time. The temperatures chosen for laboratory testing, especially the high temperatures, should represent the field conditions because debonding problems usually occur at high temperatures. To identify the temperature test conditions for this study, the highest pavement temperature data at a depth of 3.81 cm (1.5 in.) below the surface course, as provided by the Enhanced Integrated Climatic Model (EICM) for the Raleigh, North Carolina area, were utilized, as shown in Figure C.14. The highest pavement temperature at a depth of 3.81 cm (1.5 in.) in the Raleigh area was 52.78°C (127°F). In order to encompass this highest temperature, 53°C (127.4°F) was chosen as the high temperature for the lab tests in this study. The low temperature for lab testing was selected as 5°C, which is the temperature used in the Layered ViscoElastic pavement analysis for Critical Distresses (LVECD) model simulations.

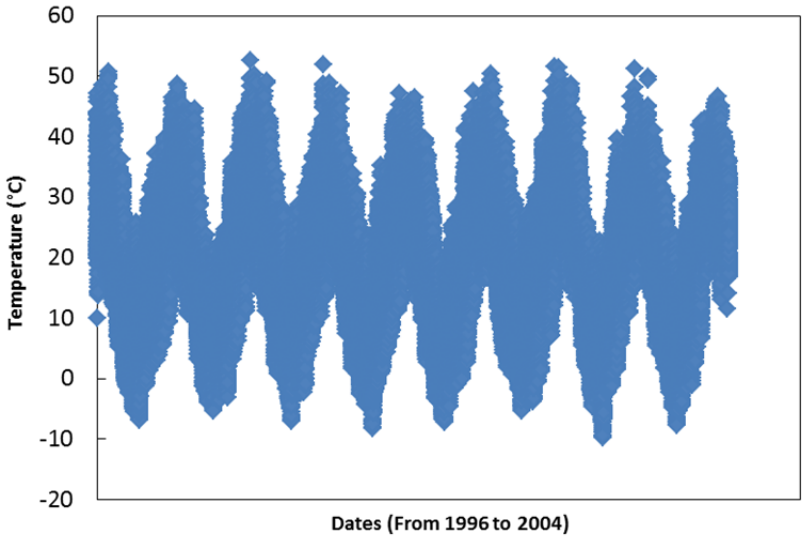

Figure C.14 Pavement temperature data at 3.81 cm (1.5 in.) below the surface course (EICM).

In order to satisfy the t-T superposition principle, it is important to observe the overlaps of reduced strain rates from adjacent temperatures, as shown in Figure C.15. The number of temperatures and the temperatures that should be used depend on the t-T shift factor. In this study, the t-T shift factors obtained from the dynamic modulus tests on the RS9.5B mixture were used for the horizontal shifting. The test temperatures were determined according to the following scheme. For example, the lowest reduced strain rate at 5°C was used initially to find the other temperatures in this study. Then, this rate was divided by the highest strain rate at an unknown temperature. After that, a shift factor function was necessary to solve for the unknown temperature. By repeating this process, lastly, two more temperatures, 19°C and 35°C, were chosen as intermediate temperatures to satisfy the t-TS principle. In other words, intermediate temperatures were designed to ensure overlaps in the reduced strain rates between adjacent temperatures. The validity of the t-TS principle can be checked by comparing the shear strength values determined from two adjacent temperatures, but at the same reduced strain rates.

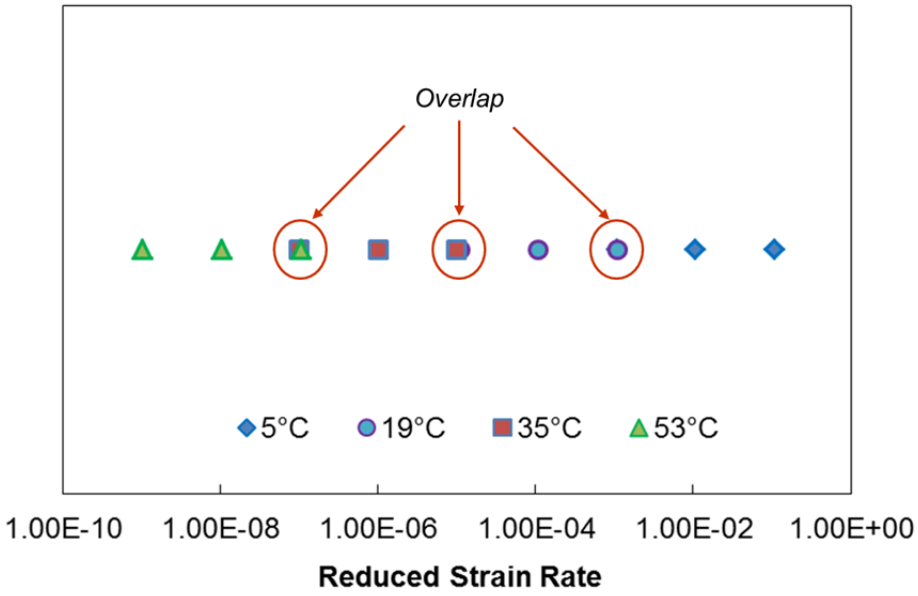

Figure C.15 Ranges of reduced strain rate for each temperature.

9.3. Normal Confining Stress

The spectrum of normal confining stresses that is used to evaluate shear bond strength using shear test devices encompasses zero to full passive confinement. Recent studies conducted by various researchers (Mohammad et al. 2012, West et al. 2005, and Canestrari and Santagata 2005) indicate that the interface bond strength increases with the application of a normal confining stress in conjunction with other test parameters, such as rate of loading and temperature.

In this study, the shear strength levels for different normal stress magnitudes and temperatures were computed with a displacement rate of 2.5 mm/min for the cationic emulsion using the Canestrari et al. (2013) equations, as shown in Figure C.16. According to Figure C.16, a normal confining stress has a significant effect on the interface bond strength. In other words, Figure C.16 shows shear strength as a linear function of the normal confining stress (normal stress) at each temperature.

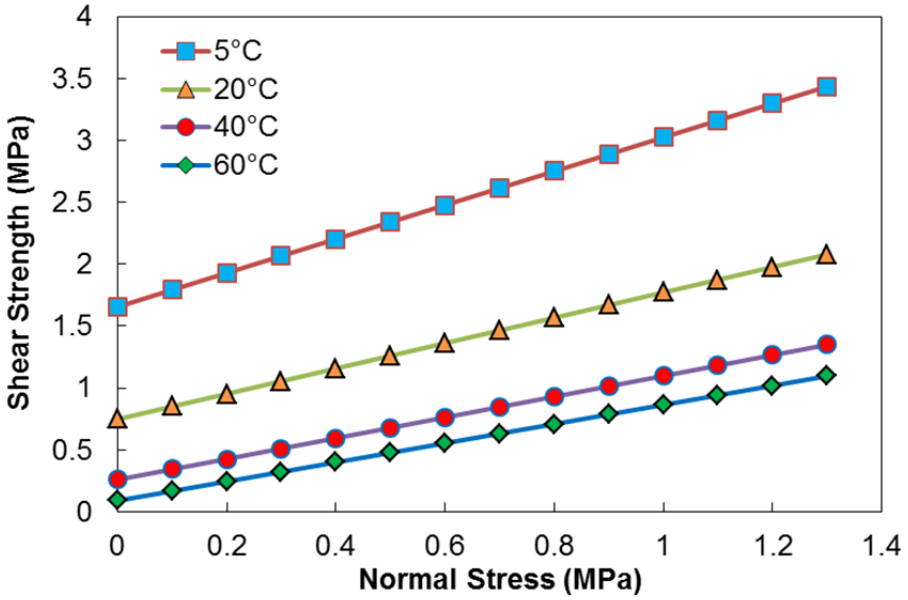

Figure C.16 Shear strength versus normal confining stress (normal stress) for 100-mm (4 in.) samples, 2.5 mm/min rate of loading, and cationic emulsion, based on equations by Canestrari et al. (2013).

However, the question remains as to the level of normal confining stress that should be used in direct shear testing to evaluate the interface bond strength. A mechanistic methodology is necessary to provide guidance for the selection of the appropriate level of normal confining stress. In order to determine the appropriate confining stress level, it is necessary to understand and quantify the pavement responses computed using the LVECD program for the various conditions of the three different pavement structures (thin, intermediate, and thick). The state of the stress and strain in the pavement section should be reflected in the selection of the appropriate level of the normal confining stress.

The location of the MSR $(\tau_{max}/\tau_s)_{max}$ under braking condition was found to be on the central longitudinal axis of the tire all the time for all the conditions under consideration, although the distance from the center of the tire imprint on the central longitudinal axis may vary slightly (see Appendix B). Therefore, the shear and normal stress levels on the central longitudinal axis of the tire under braking conditions, where critical behavior is found to occur at the layer interface, are considered in this study. As shown in Figure B.24 in Appendix B, the LVECD analysis was used to find the magnitude of the normal stress that corresponds to the location of the MSR. Using the method illustrated in Figure B.24, the ranges of normal stress that correspond to the location of the MSR for each rolling resistance coefficient for the conditions under consideration in this study were determined. Then, the range for the rolling resistance coefficient of 0.55 under the braking condition was confirmed as a critical condition. The normal stress levels were developed for the rolling resistance coefficient of 0.55 for all the conditions under consideration in this study, as presented in Table C.9.

Table C.9 shows that the normal confining stress (normal stress) ranges from 162.63 kPa (23.59 psi) to 278.28 kPa (40.36 psi). In order to encompass the range of normal confining stresses, three normal confining stress levels of 68.95 kPa (10 psi), 275.79 kPa (40 psi), and

482.63 kPa (70 psi) were chosen for the experimental program in this study. Table C.9 also shows that the normal stress increases as the temperature increases, whereas it decreases with an increase in speed. Furthermore, as the load level increases, the normal stress decreases. The thin pavement structure has the largest magnitude of normal stress of the three structures.

Table C.9 Magnitude of normal stress that corresponds to the location of the maximum shear ratio under the rolling resistance coefficient of 0.55 (braking condition).

Normal Stress (kPa)	Thin Pavement								
Temperature (°C)	53.4 kN (12 kips)			80 kN (18 kips)			106.8 kN (24 kips)		
	8 km/hr (5 mph)	40 km/hr (25 mph)	88 km/hr (55 mph)	8 km/hr (5 mph)	40 km/hr (25 mph)	88 km/hr (55 mph)	8 km/hr (5 mph)	40 km/hr (25 mph)	88 km/hr (55 mph)
5	196.46	193.33	190.21	180.12	176.66	173.03	170.46	166.61	162.63
20	223.27	211.88	208.09	210.38	198.74	194.05	203.18	190.93	185.67
40	271.23	258.59	251.91	257.42	247.67	241.78	244.83	237.93	233.58
60	278.28	276.18	273.06	259.69	258.50	255.05	247.11	240.98	239.48
Normal Stress (kPa)	Intermediate Pavement								
Temperature (°C)	53.4 kN (12 kips)			80 kN (18 kips)			106.8 kN (24 kips)		
	8 km/hr (5 mph)	40 km/hr (25 mph)	88 km/hr (55 mph)	8 km/hr (5 mph)	40 km/hr (25 mph)	88 km/hr (55 mph)	8 km/hr (5 mph)	40 km/hr (25 mph)	88 km/hr (55 mph)
5	237.11	236.34	235.40	212.06	211.18	210.11	194.10	193.10	191.91
20	244.42	241.52	240.60	220.83	217.38	215.91	204.09	200.21	198.57
40	256.82	253.10	251.62	235.93	231.48	229.58	220.66	215.84	213.89
60	262.24	261.26	260.59	241.77	240.77	240.18	225.70	224.91	224.66
Normal Stress (kPa)	Thick Pavement								
Temperature (°C)	53.4 kN (12 kips)			80 kN (18 kips)			106.8 kN (24 kips)		
	8 km/hr (5 mph)	40 km/hr (25 mph)	88 km/hr (55 mph)	8 km/hr (5 mph)	40 km/hr (25 mph)	88 km/hr (55 mph)	8 km/hr (5 mph)	40 km/hr (25 mph)	88 km/hr (55 mph)
5	253.83	252.19	250.10	229.60	228.67	228.38	210.64	210.12	210.10
20	254.21	253.86	253.67	230.34	228.95	228.89	210.93	210.30	210.20
40	254.29	254.08	253.91	231.46	230.66	229.98	214.63	212.75	212.45
60	256.71	255.67	255.60	235.61	234.04	233.59	219.33	217.37	217.06

The shear test conditions of importance used in this study are summarized in Table C.10.

Table C.10 Summary of shear test conditions.

Testing Conditions	
Mixture Type	RS9.5B (6% air void)
Specimen Dimension (mm)	Diameter: 101.6 (4 in.), Height: 76.2 (3 in.)
Testing Mode	Monotonic
Loading Rate (mm/min)	0.508 (0.02 in./min), 5.08 (0.2 in./min), 50.8 (2 in./min)
Normal Confining Stress (kPa)	68.95 (10 psi), 275.79 (40 psi), 482.63 (70 psi)
Temperature (°C)	5 (41°F), 19 (66.2°F), 35 (95°F), 53 (127.4°F)
Interlayer Material	CRS-2, CRS-1h, NTCRS-1hM (Trackless), No tack coat
Tack Coat Application Rate	0.181 L/m^2 (0.04 gal/yd^2)
Surface Condition	Non-milled

10. Application of Digital Image Correlation (DIC) Method

In this study, an effective digital image correlation (DIC) measurement system, which is a noncontact, full-field displacement/strain measurement technique, was used for the interface shear bond strength tests. These tests were performed using cylindrical laboratory-fabricated specimens composed of two symmetrical asphalt layers to capture the failure behavior at the layer interface. The DIC technique was used instead of conventional LVDTs due to the limitations for contact associated with the LVDT mounting method.

The DIC system includes a charge coupled device (CCD) digital camera, an illumination device with very low heat emission, an image frame grabber, computer, and software for image correlation analysis. In this study, a commercial package from Correlated Solutions Inc., VIC-2D, designed for two-dimensional digital image correlations, was used for the image correlation analysis. Figure C.17 presents the DIC test set-up used in this study.

Figure C.17 DIC test set-up.

A DIC system can be employed to compute the relative displacements and strains at the layer interface through the comparison of images of a deformed specimen with the images of an initial, undeformed reference specimen using advanced mathematical techniques. To implement the image correlation analysis of the differences between the initial image and the deformed images, the reference undeformed image was divided into small subsets, and then the corresponding locations of these subsets in the deformed images were tracked by matching their pixel grayscale levels, as shown in Figure C.18. By tracking the location of the subsets, the horizontal and vertical displacements of the center point of each subset in the pixels were determined at different stages in the testing (Seo et al. 2002).

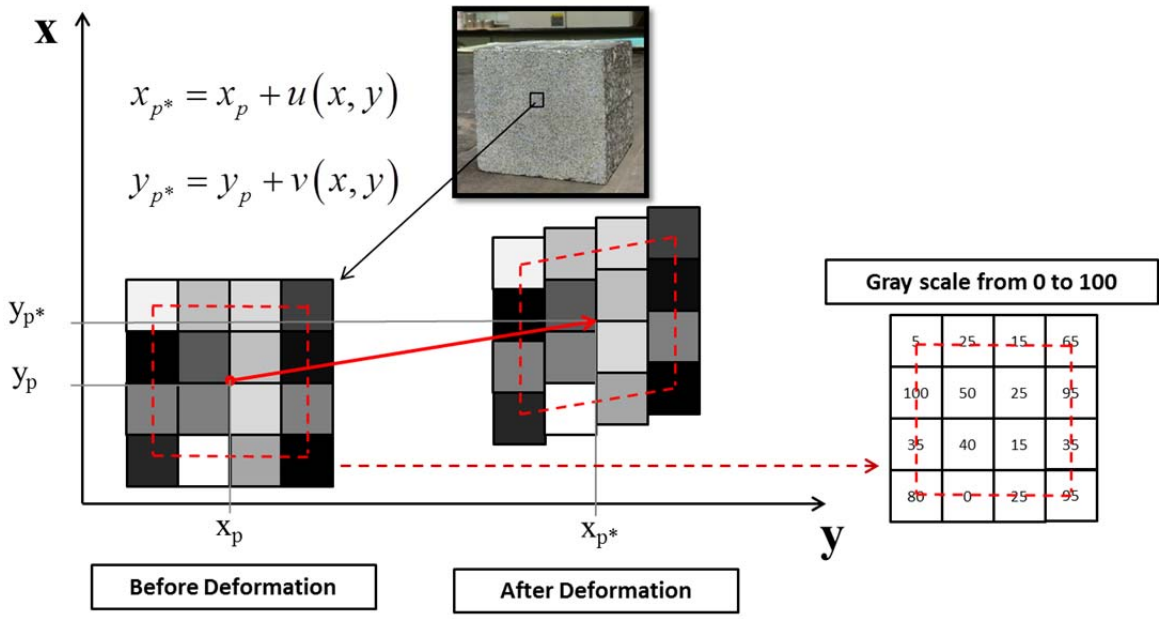

Figure C.18 Image correlation analysis of the differences between the initial image and the deformed image.

In order to perform image correlation analysis, a uniform-sized speckle pattern with a white background and black dots should be marked onto the area of interest of the specimen. However, due to the difficulty associated with applying a desired pattern onto the curved surface of a cylindrical specimen, in this study, paper with the desired speckled pattern density that incorporated black and white dots was attached to the steel shoes.

The optimal distance between the digital camera and the surface of the specimen placed in the temperature chamber was found to be 45 cm to obtain the best image resolution, in accordance with the study by Chehab et al. (2007). This distance was kept constant for all the tests in this study in order to capture the same image resolution for all of the specimens. Then, the camera was positioned perpendicular to the specimen with the desired speckled pattern comprised of black and white dots. The CCD digital camera obtained undeformed and deformed images at the layer interface using the fastest image acquisition rate of 15 frames per second during the interface shear bond strength tests.

11. Interface Shear Bond Strength Test

In this study, the MAST was used to evaluate the interface shear bond strength of cylindrical laboratory-fabricated specimens composed of two symmetrical asphalt layers. Prior to the shear tests, steel shoes were glued to the prepared MAST specimens using DEVCON steel putty. Extreme care was taken to clean both the shoes and the specimen completely before each glue application to prevent failure at the glued area. To increase the bond between the shoes and the specimen, each shoe has grooves. To ensure the specimens are properly aligned, a special gluing jig, shown in Figure C.19, was employed so that the shoes were parallel, thus minimizing any eccentricity that might occur during the test.

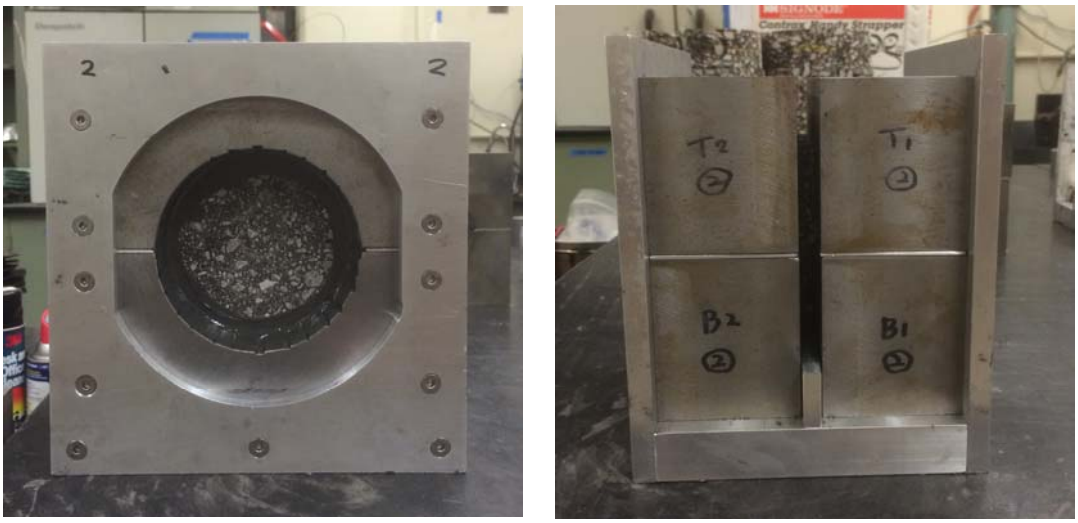

Figure C.19 Gluing jig for MAST samples.

An MTS closed-loop servo-hydraulic loading frame with a 89-kN (20,000-lb) load cell was used for the interface shear bond strength tests. An environmental chamber, equipped with liquid nitrogen coolant and a feedback system, was used to control and maintain the test temperature. Load, crosshead movement, and normal confining stress data were acquired using a 16-bit National Instruments data acquisition board and collected using LabVIEW software.

The interface shear bond strength tests were performed in constant displacement-control mode to measure the maximum shear load and corresponding shear displacement in order to evaluate the interface shear bond strength of the specimen. The tests were performed in tension mode until failure occurred in the specimen. The tests were conducted at three loading rates, four temperatures, and three normal confining stresses. Prior to testing, samples were conditioned in an environmental chamber to maintain the test temperature for three hours. The normal confining stress level was confirmed if the desired confining stress level was achieved. After the check, the specimen was sheared under a constant crosshead displacement rate loading until the failure.

12. Field Tack Coat Bond Strength Evaluation

Currently, there is no standard test method for the *in situ* bond strength evaluation of tack coat materials. During the past decade, several devices have been developed by researchers for the on-site measurement of tack coat bond strength. To evaluate the performance of the existing tack coat bond strength measurement instruments, i.e., TACKY and ATacker™, field tests were performed in collaboration with the North Carolina Department of Transportation (NCDOT). The research team performed four tensile bond strength tests, one shear bond strength test, and one torsion bond strength test using ATacker™. The TACKY tests were performed on the broken tack coat of the asphalt surface, and the tack coat application rate was investigated in the field. The test section used for the

bond strength evaluation tests was approximately a quarter mile of the Martin Pond Road overlay project. A photograph and overhead view of the test section are shown in Figure C.20.

(a) (b)

Figure C.20 Test location: (a) photograph and (b) bird's eye view.

12.1. Tack Coat Application Rate Test

The tack coat application rate was measured by placing six 20.32 × 20.32 cm^2 (8×8 $in.^2$) steel plates on the surface of the existing asphalt pavement before the application of the tack coat by the distribution truck. The steel plates were weighed before and after the application of the tack coat on the pavement surface to measure the applied tack coat weight. Figure C.21 shows the steel plates before and after the application of the tack coat to the asphalt surface.

(a) (b)

Figure C.21 Steel plates placed on the surface of asphalt pavement for measurement of tack coat application rate: (a) before tack coat application and (b) after tack coat application.

The tack coat used in this project was CRS-1 emulsion with the target application rate of 0.27 L/m^2 (0.06 gal/yd^2). The tack coat application on the asphalt surface, as illustrated in Figure C.22, was uneven. Figure C.22 shows the tack-coated asphalt surface immediately after the distribution truck had passed. Table C.11 presents the measured tack coat

application rates. As shown in Table C.11, the measured tack coat application rates for the test plates are lower than the target application rate and vary significantly among the different steel plates.

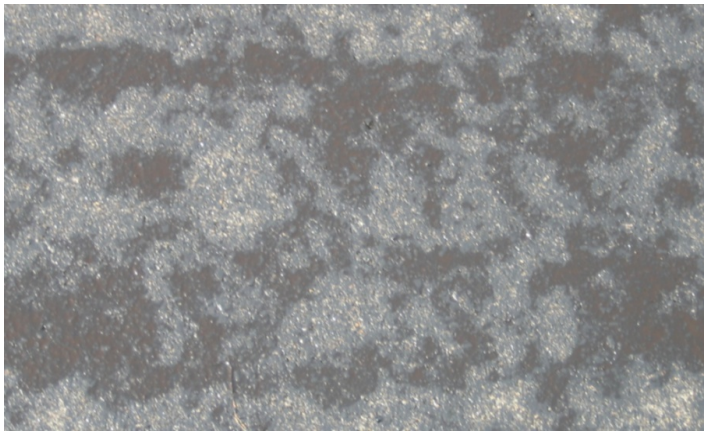

Figure C.22 Distributed tack coat on existing asphalt surface.

Table C.11 Measured tack coat application rates.

Plate No.	Measured Application Rate, L/m^2 (gal/yd^2)
#1	0.18 (0.041)
#2	0.067 (0.015)
#3	0.081 (0.018)
#4	0.063 (0.014)
#5	0.09 (0.020)
#6	0.058 (0.013)

12.2. ATacker™ Tests

The ATacker™ test instrument was used to measure the bond strength of the tack coat (CRS-1 emulsion) in shear, tension, and torsion modes in the field. ATacker™ applies direct tension, torsion, or shear to an aluminum plate that is bonded to the existing asphalt surface by a tack coat. In this study, due to the inadequate bond strength between the aluminum plate and the tack-coated asphalt surface, moisture-bearing foam was attached to the aluminum plate using double-sided tape to increase the bond strength between the aluminum plate and tack-coated asphalt surface. Moisture-bearing foam was chosen based on the recommendation by Mohammad et al. (2012).

12.2.1. ATacker™ Tension Bond Strength Test

The test apparatus, materials, and procedure for the ATacker™ tension bond strength tests are shown in Figure C.23 and described in the following sections.

Apparatus

- ATacker™ with 127-mm (5-inch) circular aluminum contact plate
- Handheld noncontact infrared thermometer with an accuracy of ± 1°C (± 2°F)
- Thermometer capable of measuring ambient temperature from -15°C (5°F) to 50°C (122°F)
- Thermocouple to measure the contact surface temperature (test temperature) at the time of the application of the tensile load
- Heater (infrared lamp) capable of applying uniform heat to the test area
- 27.2 kg (60 lb) of weight
- Utility cutting knife

Materials

- Moisture-bearing foam
- Double-sided tape

ATacker™ tensile test procedure

- Cut a circular piece of double-sided tape 127 mm (5 in.) in diameter and attach the double-sided tape to the aluminum contact plate of the testing apparatus.
- Cut a circular piece of moisture-bearing foam 127 mm (5 in.) in diameter and attach the moisture-bearing foam to the double-sided tape.
- Make a hole in the moisture-bearing foam using the hole on the contact plate for placing the thermocouple.
- Fasten the contact plate to the test device using nuts.
- Select a test section of the pavement that is coated with the tack coat and mark the test area.
- Heat the tack coat surface using an infrared heat lamp to 80°C (176°F) for approximately 15 minutes and measure the surface temperature using an infrared thermometer.
- Position the test device over the test section.
- Place approximately 27.2 kg (60 lb) of weight on the machine.
- Place the contact plate on the tack-coated surface by rotating the ATacker™ lever clockwise, apply 22.7 kg (50 lb) compression load to the surface, and hold in place for one minute.
- Measure the contact surface temperature continuously using the thermocouple that is placed into the prepared hole on the plate.
- Perform the test at the designated temperature by rotating the lever counter-clockwise with constant speed.

The procedure for cutting the adhesive tape and gluing the moisture-bearing foam to the aluminum plate took about five minutes for the first test. However, for the subsequent tests, removing the glue and the moisture-bearing foam from the aluminum plate and cleaning the plate took more than five minutes. The total time of the test depended on how fast the pavement temperature reaches to the target test temperature of the tack-coated pavement, which was measured by the thermocouple.

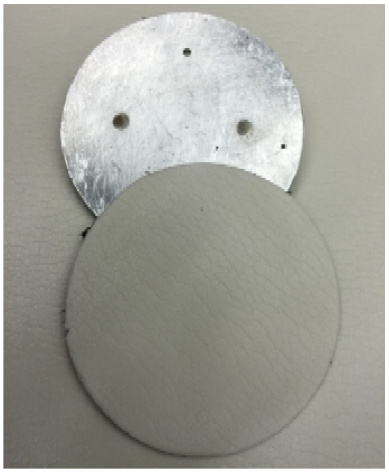

(a) Cut moisture-bearing foam.

(b) Attach double-sided tape to aluminum plate.

(c) Heat the asphalt surface.

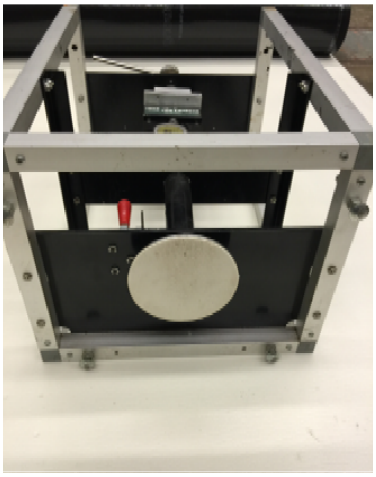

(d) Attach aluminum plate to ATacker.™

(e) Measure the pavement temperature.

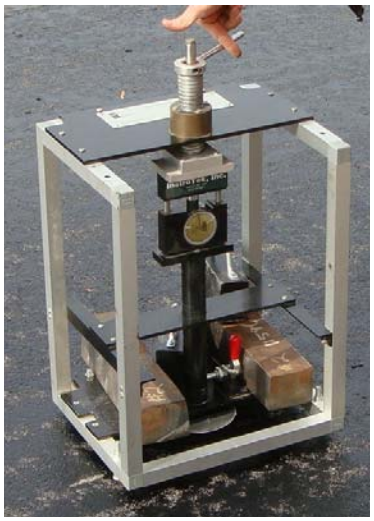

(f) Apply tensile load.

Figure C.23 Procedure for ATackerTM tensile bond strength test.

12.2.2. ATacker^{TM} Torsion Bond Strength Test

The ATacker^{TM} torsion bond strength test apparatus, materials, and procedures are presented in the following section.

Apparatus

- ATacker^{TM} with 127-mm (5-in.) circular aluminum contact plate
- Torque wrench with 16.9-N.m (150-lbf.in) capacity
- Handheld noncontact infrared thermometer with an accuracy of ± 1°C (± 2°F)
- Thermometer capable of measuring ambient temperature from -15°C (5°F) to 50°C (122°F)
- Thermocouple to measure contact surface temperature
- Heater (infrared lamp) capable of applying uniform heat to the test area
- 27.2 kg (60 lb) of weight
- Utility cutting knife

Materials

- Moisture-bearing foam
- Double-sided tape

ATacker^{TM} torsion test procedure

- Cut a circular piece of double-sided tape 127 mm (5 in.) in diameter and attach the double-sided tape to the aluminum contact plate of the testing apparatus.
- Cut a circular piece of moisture-bearing foam 127 mm (5 in.) in diameter and attach the moisture-bearing foam to the double-sided tape.
- Make a hole in the moisture-bearing foam using the hole on the contact plate for placing the thermocouple.
- Fasten the contact plate to the test device using nuts.

- Select a test section of the pavement that is coated with the tack coat and mark the area.
- Heat the tack-coated surface with a heat lamp to 80°C (176°F) for 15 minutes and measure the surface temperature using an infrared thermometer.
- Position the test device over the test section.
- Place approximately 27.2 kg (60 lb) of weight on the machine.
- Place the contact plate on the tack-coated surface by rotating the ATacker™ torsion lever clockwise, apply 16.9 kg (50 lb) compression load to the surface, and hold in place for one minute.
- Measure the contact surface temperature continuously using a thermocouple that is placed into the prepared hole on the plate.
- Release the rotation stop lever of the ATacker™ device.
- Adjust the gauge of the torque wrench to zero and apply torque to the torsion lever until failure. Rotate the rotation lever with a constant speed by controlling the rotation time.

Figure C.24 shows the ATacker™ torsion test set-up.

Figure C.24 ATacker™ torsion test set-up.

12.2.3. ATacker™ Shear Bond Strength Test

For the shear bond strength tests, the ATacker™ apparatus was placed horizontally on the tack-coated asphalt surface and 27.2 kg (60 lb) of weight was used to prevent the horizontal movement of the ATacker™. The procedure, apparatus, and materials used for the shear tests are as follows.

Apparatus

- ATacker™ with L-shaped 127×127 mm^2 (5×5 in.^{2}) aluminum contact plate
- Handheld noncontact infrared thermometer with an accuracy of ± 1°C (± 2°F)
- Thermometer capable of measuring ambient temperature: -15°C (5°F) to (122°F) 50°C
- Thermocouple to measure the contact surface temperature
- Heater (infrared lamp) capable of applying uniform heat to the test area
- 27.2 kg (60 lb) of weight
- Utility cutting knife

Materials

- Moisture-bearing foam
- Double-sided tape

ATacker™ shear test procedure

- Cut a square piece of double-sided tape 127×127 mm^2 (5×5 in.^{2}) and attach the double-sided tape to the L-shaped contact plate of the test apparatus.
- Cut a square piece of the moisture-bearing foam to 127×127 mm^2 (5×5 in.^{2}) and attach the moisture-bearing foam to the double-sided tape.
- Make a hole in the moisture-bearing foam using the hole on the contact plate for placement of the thermocouple.
- Select a test section of the pavement that is coated with tack coat and mark the section.
- Heat the tack-coated surface using an infrared heating lamp to 80°C (176°F) and allow the tack coat to cure for approximately 15 minutes.
- Measure the surface temperature using an infrared thermometer.
- Position the test device horizontally over the test section.
- Place approximately 27.2 kg (60 lb) of weight on the machine.
- Fasten the contact plate to the test device using nuts.
- Place the contact plate on the tack coat surface, apply 22.6 kg (50 lb) of weight, and hold in place for approximately one minute.
- Measure the contact surface temperature continuously using the thermocouple that is placed into the prepared hole on the plate.
- Perform the test at the designated temperature by rotating the torsion lever counter-clockwise with constant speed.

Figure C.25 shows the ATacker™ shear bond strength test set-up. The results of the ATacker ™ tension, torsion, and shear tests are presented in Table C.12, Table C.13, and Table C.14, respectively.

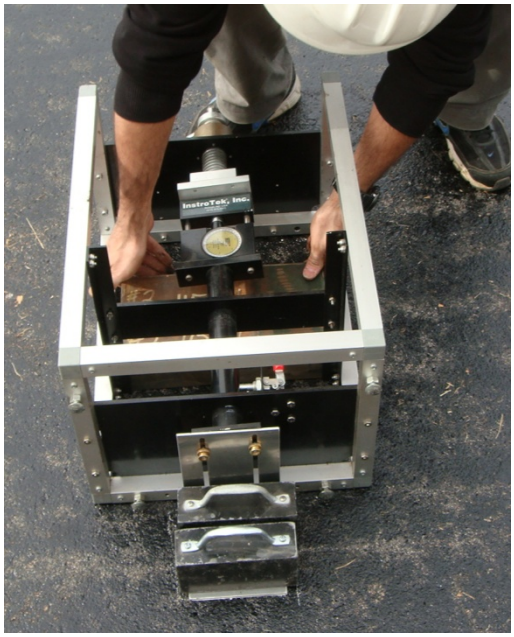

Figure C.25 ATacker ™ shear bond strength test set-up.

Table C.12 ATacker ™ tension test results.

Shear Test	Pavement Temperature, °C (°F)	Pavement Temperature at Time of Test °C (°F)	Bond Strength kPa (psi)
Tension #1	65 (150)	30 (86)	5.26 (0.764)
Tension #2	78 (173)	27 (82)	11.59 (1.681)
Tension #3	60 (140)	27 (82)	6.32 (0.917)
Tension #4	71 (160)	32 (90)	5.97 (0.866)

Table C.13 ATacker ™ torsion test results.

Shear Test	Pavement Temperature, °C (°F)	Pavement Temperature at Time of Test °C (°F)	Bond Strength kPa (psi)
Torsion #1	87 (190)	27 (82)	11.8 (1.711)

Table C.14 ATacker ™ shear test results.

Shear Test	Pavement Temperature, °C (°F)	Pavement Temperature at Time of Test °C (°F)	Bond Strength KPa (psi)
Shea r#1	93 (200)	30 (86)	3.3 (0.48)

The ATacker ™ tack coat bond strength test results are presented in Figure C.26. As shown, the data are scattered and the R-square value is low for the function fitted to the tensile bond strength test data.

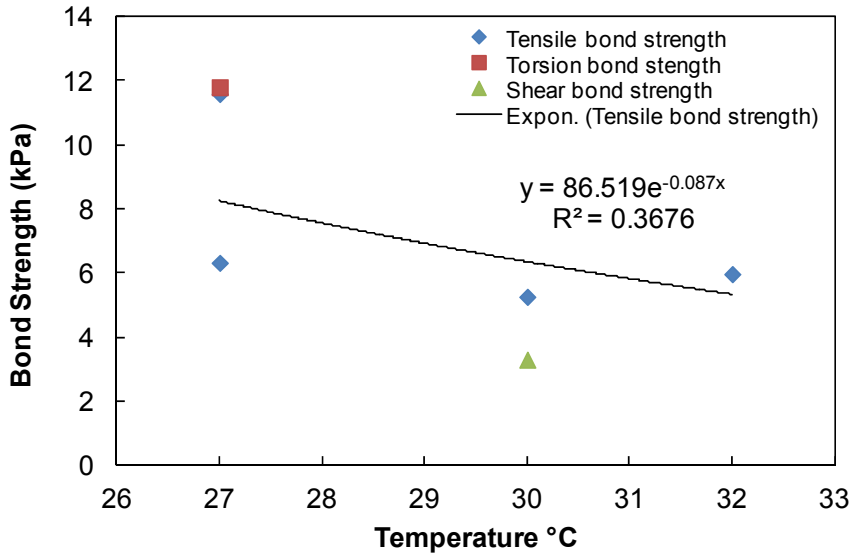

Figure C.26 ATacker ™ *in situ* tack coat bond strength test results.

12.2.4. Summary of ATacker ™ Evaluation

Based on the test results, the ATacker™ performance is summarized as follows:

- A proper bond could not be achieved between the ATacker™ contact plate and the tack-coated asphalt surface due to the roughness of the asphalt surface. A bond between the contact plate and the points with the highest texture peaks on the pavement surface could be achieved. Therefore, the bond strength values measured at different locations on the asphalt surface were not necessarily representative of the tack coat properties. The lack of complete contact between the device's contact plate and the tack coat applied on the milled asphalt surface would be more obvious than that on unmilled pavement surface.
- Due to the uneven tack coat application, the locations of the tested areas on the pavement surface affected the test results. That is, performing the tests at different locations produced inconsistent test results.

Based on the tests results, ATacker™ is not recommended for measuring the bond strength of tack coat materials applied on an asphalt surface.

12.3. TACKY Test

The so-called TACKY test device was developed to measure the resistance of a tack-coated surface against a rolling wheel. Figure C.27 shows the TACKY device and its parts. TACKY tests should be performed on a tack-coated surface after the tack coat has broken. During the TACKY field evaluation test in this study, due to the load cell's high capacity, the load cell did not show any load measurement or sensitivity. In order to obtain a reasonable result from the TACKY test, a more sensitive load cell is needed. In addition, the TACKY test procedure was not suitable to measure the bond strength of modified tack coats, such as trackless emulsion, which are designed to minimize the tracking of the tack coat by the hauling trucks after the breaking of the tack coat. The running time for the TACKY test was less than five minutes. To perform TACKY tests at different temperatures, the path of the rolling wheel should have been heated using a proper heating instrument. Unfortunately, the heating pad that was designed for the TACKY tests could not heat the asphalt surface properly, and the tests were performed at ambient temperature.

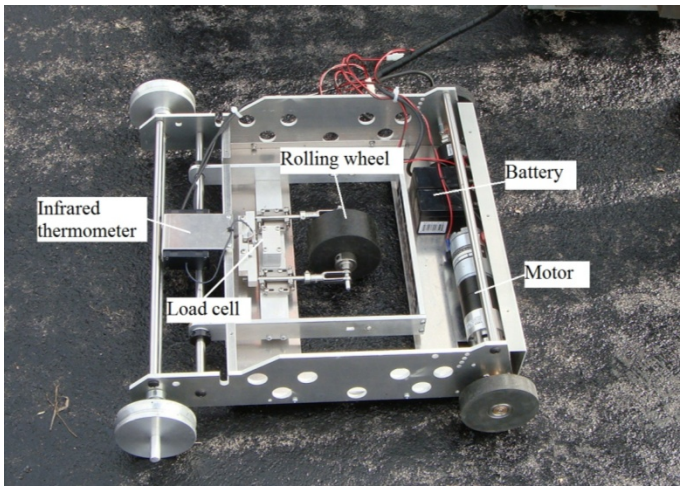

Figure C.27 TACKY test device.

12.3.1. Summary of TACKY Evaluation

The TACKY tests did not provide any useful data. The following observations were made during the TACKY tests.

- Due to the low bond strength between the broken tack coat and the rolling wheel of the TACKY device, it was not possible to obtain any reasonable results from the TACKY tests performed in the field.
- The TACKY device was not suitable for measuring the bond strength of modified tack coats, such as Trackless, which are designed to minimize the tracking of the tack coats by the hauling truck tires.

- It was not possible to heat the test area uniformly at the construction site using the heating pad designed for the TACKY device. Therefore, it was not possible to perform the tests at different temperatures.
- A proper bond strength could not be developed between the rolling wheel of the TACKY device and the tack coat applied on a rough asphalt surface.

Based on these observations, the prototype TACKY in its current state is not recommended as a standard field tack coat evaluation method. Further research is needed to improve TACKY's performance.

13. Pneumatic Adhesion Tensile Testing Instrument (PATTI) Tests

Due to the observed difficulty to develop a proper bond strength between the previously mentioned test instruments' contact surfaces and the existing tack-coated asphalt surface, the research team decided to place an aluminum plate on the existing asphalt surface prior to the application of the tack coat in the field and perform the bond strength tests in the lab using samples collected on the aluminum plate.

The Pneumatic Adhesion Tensile Testing Instrument (PATTI) was selected to measure the tensile bond strength of a tack coat applied on an aluminum plate *in situ*. PATTI is an ASTM D4145 Type IV adhesion tester. The ASTM D4145 standard covers the procedures to measure the pull-off strength of a coating system from metal substrates (ASTM D4541). The major advantage of the PATTI test is that it is a standard procedure. In addition, PATTI tests can be performed in a controlled environment (i.e., temperature and humidity) in a climate chamber and can be performed in the field. ASTM D4145 adhesion tester type IV is a self-aligning automated PATTI that has a control module, detaching assemblies or pistons, and a pressurized air source, as shown in Figure C.28.

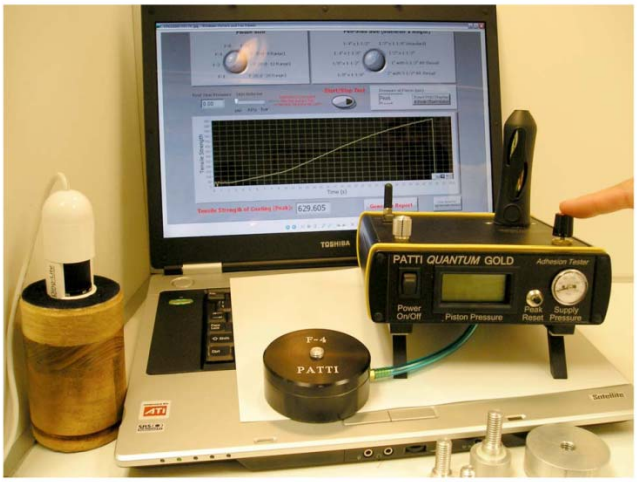

(a)

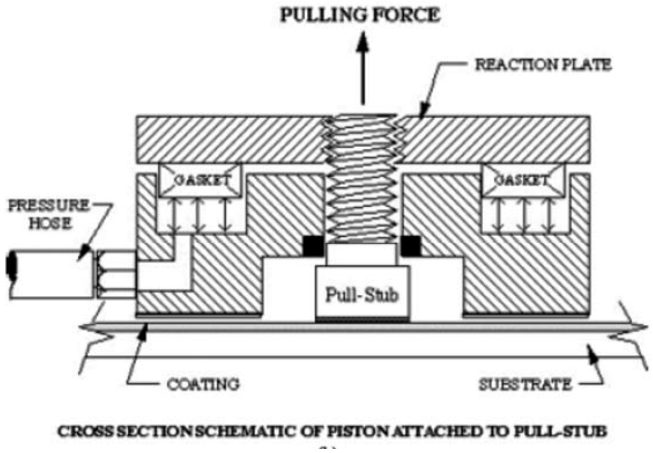

(b)

Figure C.28 (a) Type IV self-alignment adhesion tester (PATTI) and (b) schematic of PATTI piston (ASTM D4145 2009).

The PATTI test pullout stub used in this study has a diameter of 12.5 mm (0.5 in.). The pistons are available in several different sizes and load ranges. See Appendix E for details regarding the PATTI test results.

13.1. PATTI Test Procedure

This section describes the apparatus and procedures for testing tack coat bond strength using PATTI. The tack coat samples can be applied on an aluminum plate with a paint brush in the laboratory or acquired in the field by placing an aluminum test plate on the existing asphalt surface before the tack coat is applied by the distribution truck.

Apparatus

- Aluminum plate: The plate should be a solid aluminum plate with a minimum thickness of 6.4 mm (0.25 in.), which should be large enough to accommodate the specified number of test replicates.
- PATTI: Type IV adhesion tester, as defined in ASTM D4541, should be used for the test.
- Air supply: Self-contained air cylinders, shop (bottled) air, or air from an automatic pump.
- Pullout stub: 12.5-mm (0.5-in.) diameter standard pullout stub.
- Forced draft oven: Forced draft oven for heating the pullout stubs.
- Environmental chamber: A chamber that is capable of maintaining the temperature between 0°C and 75°C for the conditioning of the test samples.
- Weight: 1.31-kg (2.89-lb) weight to place on the pullout stubs as the initial pressure.
- Ultrasonic cleaner: An ultrasonic cleaner to remove residual particles from the pullout stubs prior to testing according to AASHTO TP-91 (2011).

Procedure

- Obtain a tack coat sample for testing either by placing the aluminum plate on the existing asphalt surface prior to the application of the tack coat at the construction site or by applying a tack coat with the specified application rate using a paint brush in the laboratory.
- Cure the tack coat sample for one hour in an oven at 60°C.
- Heat the pullout stubs to the application temperature of 80°C in a forced draft oven.
- Place the heated pullout stubs on the tack coat sample on the aluminum plate and place a 1.31-kg (2.89-lb) weight on the stub to maintain full contact between the stub and tack coat. Maintain the load for two minutes. Pressure is applied at the ambient temperature of the laboratory.
- Place the aluminum plate with the applied emulsion and the pullout stubs in the environmental chamber at the test temperature for one hour of conditioning.
- Place the pressure ring around the pullout stub.
- Screw the pressure plate onto the pullout stub.
- Test the samples using PATTI following the standard procedure.
- Record the maximum pullout tension and observe the failure mode.

APPENDIX D: Test Results and Discussion

1. Interlayer Shear Stiffness Calculation

As stated in Appendix A, Section A.6, the interlayer shear stiffness can be assumed to be a characteristic value that can be used to measure the level of interlayer bonding. Mohammad et al. (2012) used the interlayer shear stiffness to evaluate interface shear characteristics in the NCHRP Project 9-40.

Figure D.1 (a) and (b) illustrate the interlayer shear stiffness calculation method using the test data sets of tests performed under identical conditions. In this study, two methods were considered to calculate the interlayer shear stiffness. The first method, shown in Figure D.1 (a), is to use the crosshead linear variable differential transducer (LVDT) displacement to peak interface shear stress and the peak shear stress amplitude in an interface shear stress-displacement curve. The second method, shown in Figure D.1 (b), is to use the displacement calculated by a digital image correlation (DIC) system instead of using crosshead LVDT displacement. That is, the interlayer shear stiffness is the slope of an interface shear stress-displacement curve.

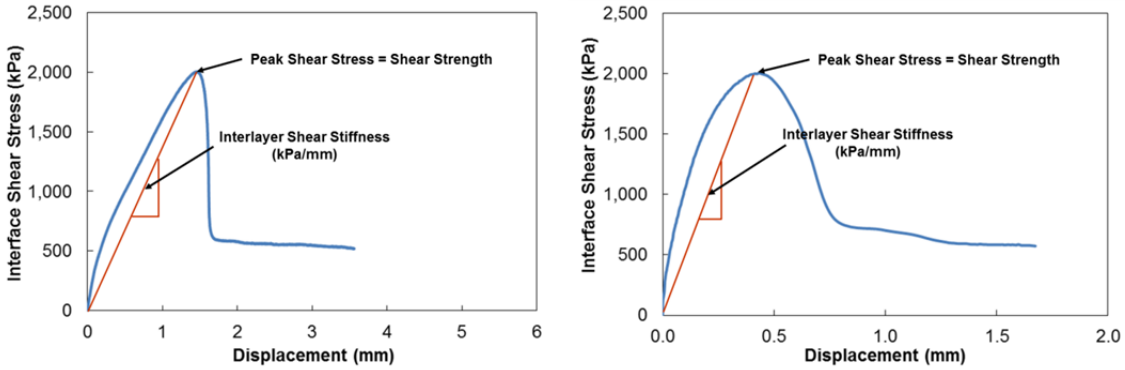

(a) (b)

Figure D.1 Typical interface shear stress versus displacement curves: (a) interface shear stress-crosshead LVDT displacement curve and (b) interface shear stress-DIC displacement curve. Test conditions: 5.08 mm/min (0.2 in./min), 19°C, 482.63 kPa (70 psi) normal confining stress, and CRS-2 emulsion.

Figure D.2 (a) and (b) respectively provide interlayer shear stiffness values determined by use of the crosshead LVDT displacement and DIC displacement at different test conditions using specimens with CRS-2 emulsion at the layer interface under 482.63 kPa (70 psi) normal confining stress. The numbers in the figures indicate the interlayer shear stiffness value for each test condition. Figure D.2 also shows that as the temperature decreases, the interlayer shear stiffness value increases. In addition, as the loading rate increases, the interlayer shear stiffness value increases as well. The interlayer shear stiffness

determined by DIC displacement has a higher value than that determined by crosshead LVDT displacement.

Two limiting values for the interlayer shear stiffness were identified by Al Hakim (2002). If the interlayer shear stiffness is below 10^{-2} MPa/mm, the level of interlayer bonding represents the perfect slippage condition (complete debonding), whereas if it is above 10^{2} MPa/mm, the level of interlayer bonding represents the perfect bonding condition. Therefore, based on this observation, the interlayer shear stiffness values presented in Figure D.2 show that the level of interlayer bonding is somewhere between slippage and perfect bonding.

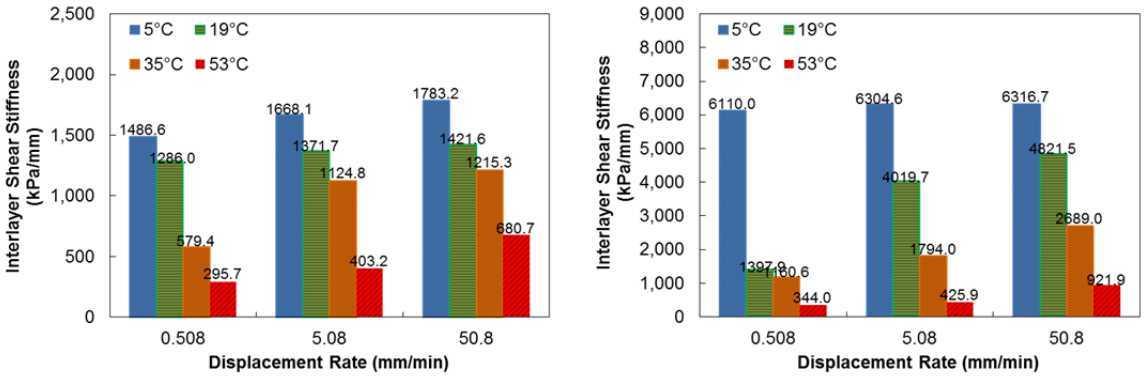

Figure D.2 Interlayer shear stiffness values at different test conditions determined by (a) crosshead LVDT displacement and (b) DIC displacement. Test conditions: CRS-2 emulsion, 482.63 kPa (70 psi) normal confining stress.

2. Determination of Crosshead LVDT Strain Rate

The crosshead LVDT displacement rates can be converted to crosshead LVDT shear strain rates using the gap width between the two platens of the Modified Advanced Shear Tester (MAST) in order to develop a shear strength mastercurve using reduced strain rate. As mentioned in Appendix C, Section C.7, the gap width between shearing platens is 8 mm. This conversion was achieved by dividing the constant crosshead LVDT displacement rate used in the shear strength tests by the gap width between the shearing platens. Table D.1 presents the crosshead LVDT displacement rates and their corresponding crosshead LVDT shear strain rates derived using the described method.

Table D.1 Transformation of crosshead LVDT displacement rate into crosshead LVDT shear strain rate.

Displacement Rate (mm/min)	Shear Strain Rate
50.8 (2 in./min)	0.11
5.08 (0.2 in./min)	0.01
0.508 (0.02 in./min)	0.001

Figure D.3 presents the interface shear bond strength values at four different temperatures and the crosshead LVDT strain rates that were converted from the crosshead LVDT displacement rates in semi-log scale. It is well known that shear strength increases at low temperature/high loading rate combinations, as confirmed in Figure D.3.

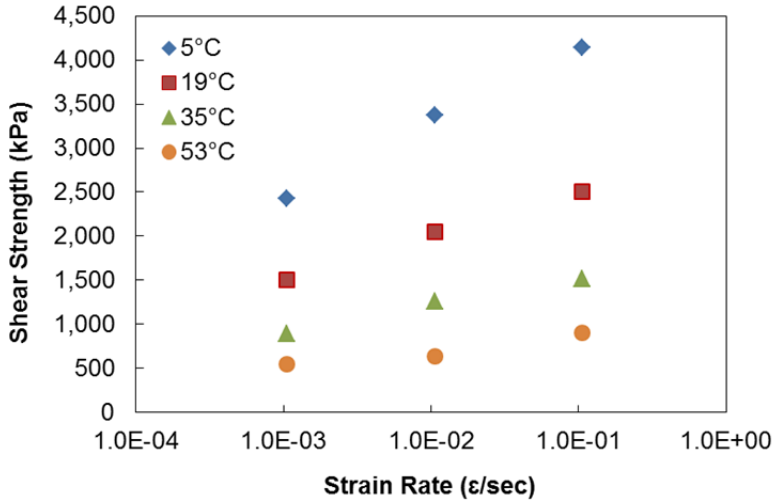

Figure D.3 Interface shear strength versus crosshead LVDT shear strain rate at different test conditions in semi-log scale. Test conditions: CRS-2 emulsion, 482.63 kPa (70 psi) normal confining stress.

In these shear tests, the effects of strain rate and temperature can be combined into a joint parameter, i.e., reduced shear strain rate, $\dot{\gamma}_R$, using the time-temperature (t-T) shift factor (a_T) determined from dynamic modulus tests of the RS9.5B mixture, as shown in Equation (16).

$$\dot{\gamma}_R = \dot{\gamma} \times a_T \tag{16}$$

where

$\dot{\gamma}_R$ = reduced shear strain rate,

$\dot{\gamma}$ = shear strain rate, and

a_T = shift factor.

3. Determination of DIC Strain Rate

3.1. Effects of Machine Compliance Issues

Strain values that are measured from on-specimen LVDTs are lower than those measured from crosshead LVDTs due to machine compliance issues, i.e., the deformation of certain machine components throughout the loading frame. The effects of machine compliance problems are compounded at low temperatures and high strain rates due to the increase in the material's stiffness.

Chehab et al. (2002) observed that an on-specimen strain history is nonlinear due to machine compliance issues, whereas the crosshead strain rate remains constant throughout the test. Moreover, they found through observations of their experimental tests and theoretical derivation that the on-specimen strain rate follows a pure power law until failure of the specimen (or up to a certain strain/time). That is, the data that deviate from a pure power law cannot be utilized for the application of the time-temperature superposition (t-TS) principle in the growing damage state, as shown in Figure D.4. The detailed theoretical derivation of this observation can be found in Chehab et al. (2002).

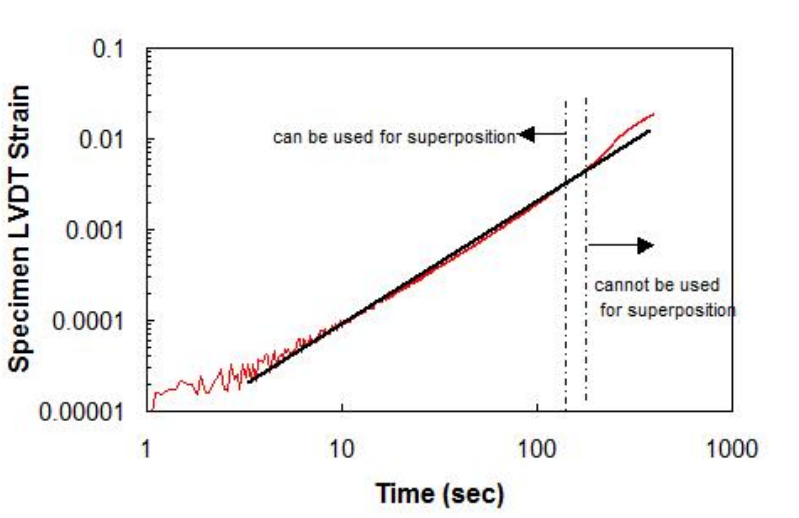

Figure D.4 On-specimen LVDT strain deviation from a pure power law (linear on log-log scales) (Chehab et al. 2002).

3.2. DIC Strain Rate

Figure D.5 presents a typical strain history for crosshead and DIC strain measurements, which demonstrates the effects of machine compliance issues on the specimen strain rate. As shown in Figure D.5, the crosshead strain rate remains constant, whereas the DIC strain rate is not constant but nonlinear.

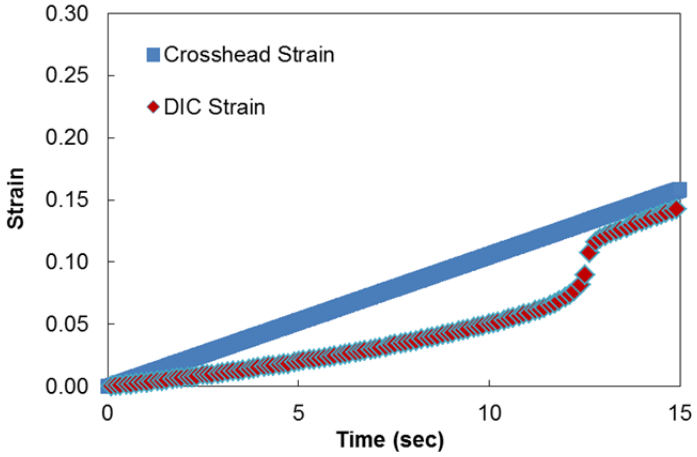

Figure D.5 Comparison between crosshead strain and DIC strain for interface shear bond strength test conducted at 5.08 mm/min (0.2 in./min), 35°C, 68.95 kPa (10 psi) normal confining stress, and CRS-2 emulsion.

In this study, the DIC strain rate was determined using the method suggested by Chehab et al. (2002). That is, the data that deviated from a pure power law were not used to determine the DIC shear strain rate, as presented in Figure D.6.

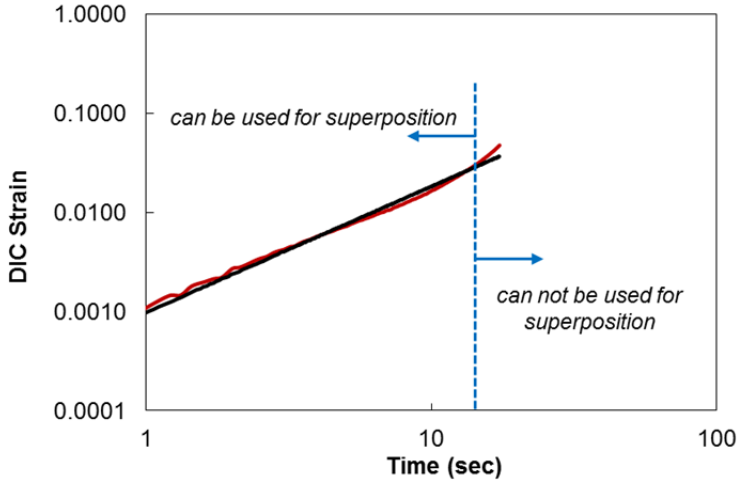

Figure D.6 DIC strain deviation from a pure power law (linear on log-log scales).

Table D.2 shows the crosshead strain rates and DIC strain rates for the different test conditions. In Table D.2, C/D stands for the ratio of the crosshead strain rate to the DIC strain rate. The C/D ratio could explain the effects of machine compliance problems and the validity of the t-TS principle. As shown in Table D.2, the C/D ratio decreases with an increase in temperature as the effects of the machine compliance issues decrease at high temperatures and low strain rates due to the decreased stiffness of the material. Table D.2

explains that, in order to satisfy the t-TS principle, it is important to observe the overlaps of the reduced strain rates from two adjacent temperatures as well as the cells highlighted in gray need to show similar C/D ratio values. As presented in Figure D.7, the DIC strain rates are always lower than the crosshead strain rates due to machine compliance problems.

Table D.2 Crosshead strain rate and DIC strain rate: CRS-2 emulsion, 482.63 kPa (70 psi) normal confining stress.

Temperature	Loading Rate (mm/min)	Crosshead		DIC		C/D
		Strain Rate (ε/sec)	Red. Strain Rate	Strain Rate (ε/sec)	Red. Strain Rate	
5°C	50.8	0.1058333	1.06E-01	0.01277923	1.28E-02	8.282
	5.08	0.0105833	1.06E-02	0.00129586	1.30E-03	8.167
	0.508	0.0010583	1.06E-03	0.00016967	1.70E-04	6.238
19°C	50.8	0.1058333	1.08E-03	0.01720343	1.75E-04	6.152
	5.08	0.0105833	1.08E-04	0.00223034	2.27E-05	4.745
	0.508	0.0010583	1.08E-05	0.00042469	4.32E-06	2.492
35°C	50.8	0.1058333	9.93E-06	0.04214525	3.95E-06	2.511
	5.08	0.0105833	9.93E-07	0.00467760	4.39E-07	2.263
	0.508	0.0010583	9.93E-08	0.00065324	6.13E-08	1.620
53°C	50.8	0.1058333	1.04E-07	0.07145647	7.02E-08	1.481
	5.08	0.0105833	1.04E-08	0.00843925	8.29E-09	1.254
	0.508	0.0010583	1.04E-09	0.00087981	8.64E-10	1.203

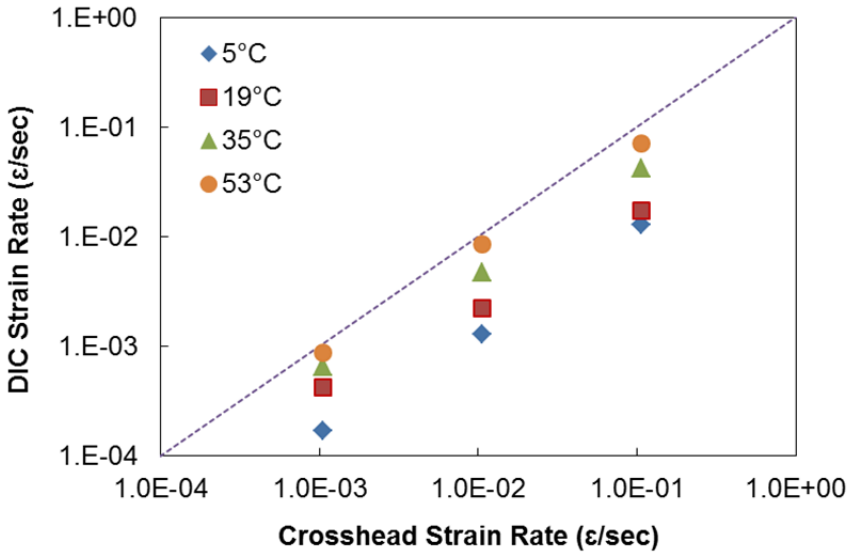

Figure D.7 Comparison between crosshead strain rate and DIC strain rate: CRS-2 emulsion, 482.63 kPa (70 psi) normal confining stress.

4. Validation of Time-Temperature Superposition Principle for Interlayer System with Tack Coat

Asphalt concrete is well known as thermorheologically simple (TRS) material if it is constrained within the linear viscoelastic range. The effects of time and temperature on TRS materials can be combined into a single parameter, i.e., reduced time/frequency, using the time-temperature (t-T) shift factor (a_T) whereby the data at various temperatures are shifted with respect to time until the curves merge into a single smooth function, which allows for the horizontal shifting of the data onto an arbitrarily selected reference temperature curve to form a single curve, the mastercurve. Any material for which a single mastercurve can be formed by such a shifting method is considered TRS material. The t-TS principle is a well-known characteristic of TRS materials.

The constitutive behavior of asphalt concrete depends on the loading rate and the temperature, so numerous tests are necessary to characterize the properties used for performance modeling of asphalt concrete pavements. However, if the concept of t-TS is valid even with growing damage, the number of tests can be reduced significantly for the prediction of asphalt concrete behavior for a wide range of temperatures. This advantage of the t-TS principle has made it appealing to several researchers (Yun et al. 2010 and Chehab et al. 2002) to try to extend the t-TS principle to materials outside of the linear viscoelastic range, even failure conditions.

This study investigated whether or not asphalt concrete material with a tack coat as an interlayer system is TRS material in shear failure mode by conducting shear tests using the Modified Advanced Shear Tester (MAST) at different loading rates and temperatures. To check the applicability of the t-TS principle in shear failure mode for a wide range of test conditions, as Chehab et al. (2002) suggested in their study of the t-TS principle as it applies to asphalt concrete with growing damage in tension, the number of test conditions was increased and the number of test replicates was minimized, instead of conducting many more test replicates over a narrow range of test conditions.

4.1. Phase 1: Verification of Time-Temperature Superposition Principle for Shear Strength

The applicability of the t-TS principle for shear strength was validated in this study using samples fabricated with each study emulsion at the layer interface and specific normal confining stress, as presented in Table D.3. To prove the t-TS principle, eight reduced strain rates were chosen to ensure overlap in the reduced strain rates between adjacent temperatures. These reduced strain rates are 0.508 mm/min (53°C), 50.8 mm/min (53°C), 0.508 mm/min (35°C), 50.8 mm/min (35°C), 0.508 mm/min (19°C), 50.8 mm/min (19°C), 0.508 mm/min (5°C), and 50.8 mm/min (5°C).

Table D.3 Shear strength test combinations for each phase.

Tack Coat	Normal Confining Stress		
	68.95 kPa (10 psi)	275.79 kPa (40 psi)	482.63 kPa (70 psi)
CRS-2	Phase 2	Phase 2	Phase 1
CRS-1h	Phase 2	Phase 2	Phase 1
NTCRS-1hM (Trackless)	Phase 2	Phase 1	Phase 2
No Tack Coat	Phase 1	Phase 2	Phase 2

Superposition using DIC Strain Rate

The shear strength data at various temperatures can be shifted horizontally onto an arbitrarily selected reference temperature to form a single curve, which is called the mastercurve, assuming that the t-TS principle is valid even in shear failure mode. In this study, 5°C was chosen as the reference temperature. Figure D.8 through Figure D.11 show the interface shear strength with respect to the reduced DIC strain rate for the samples with each study emulsion at the layer interface under the specific normal confining stresses. The validity of the t-TS principle was confirmed by comparing the shear strength values determined from two adjacent temperatures but at the same reduced DIC strain rates. One representative curve, which can be termed the *shear strength mastercurve*, is presented in Figure D.8 through Figure D.11. These figures also show that the shear strength mastercurve follows a power form and is a function of shear strain rate and temperature, thereby demonstrating that the t-TS principle is valid for shear strength using dynamic modulus shift factors. It is worth noting that the t-T shift factors determined from the dynamic modulus tests were used successfully to develop the shear strength mastercurve.

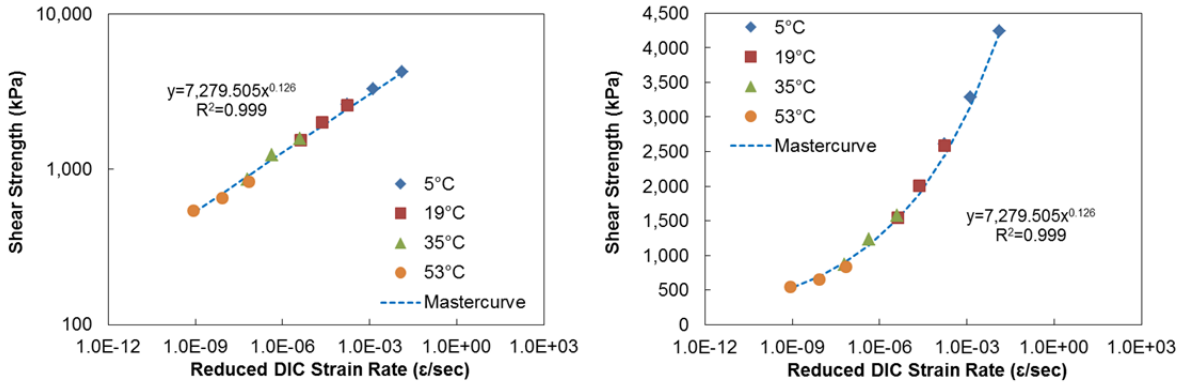

(a) (b)

Figure D.8 Verification of t-TS principle for shear strength and mastercurves using DIC strain rate (CRS-2 emulsion and 482.63 kPa (70 psi) normal confining stress): (a) log-log scale and (b) semi-log scale.

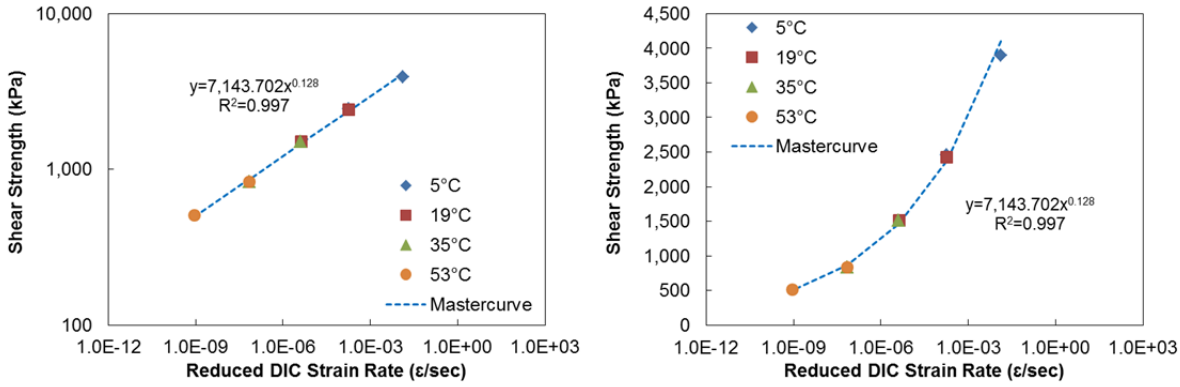

(a) (b)

Figure D.9 Verification of t-TS principle for shear strength and mastercurves using DIC strain rate (CRS-1h emulsion and 482.63 kPa (70 psi) normal confining stress): (a) log-log scale and (b) semi-log scale.

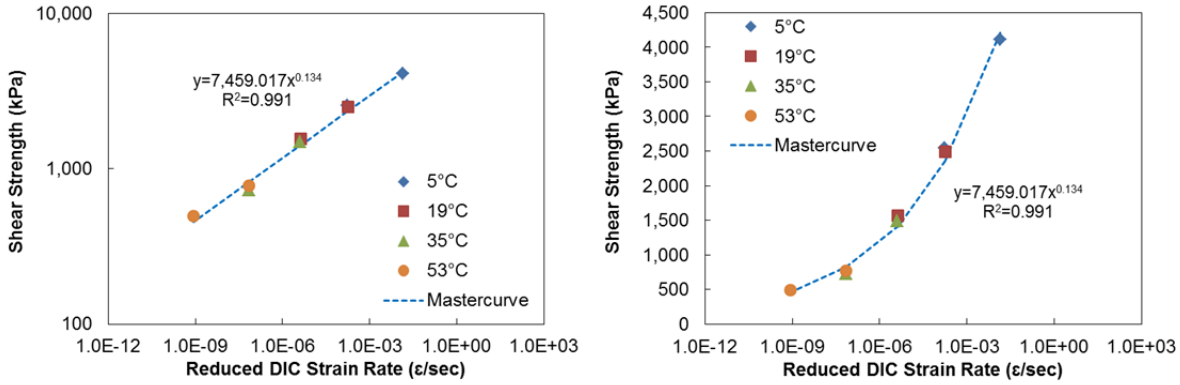

(a) (b)

Figure D.10 Verification of t-TS principle for shear strength and mastercurves using DIC strain rate (NTCRS-1hM (Trackless) emulsion and 275.79 kPa (40 psi) normal confining stress): (a) log-log scale and (b) semi-log scale.

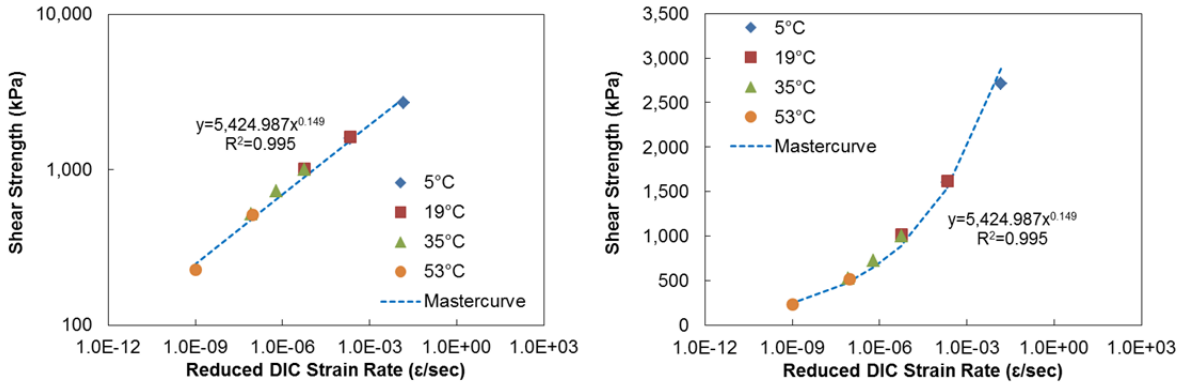

(a) (b)

Figure D.11 Verification of t-TS principle for shear strength and mastercurves using DIC strain rate (No tack coat and 68.95 kPa (10 psi) normal confining stress): (a) log-log scale and (b) semi-log scale.

Superposition using Crosshead Strain Rate

Figure D.12 through Figure D.15 show that the t-TS principle for shear strength is also valid using the crosshead strain rate.

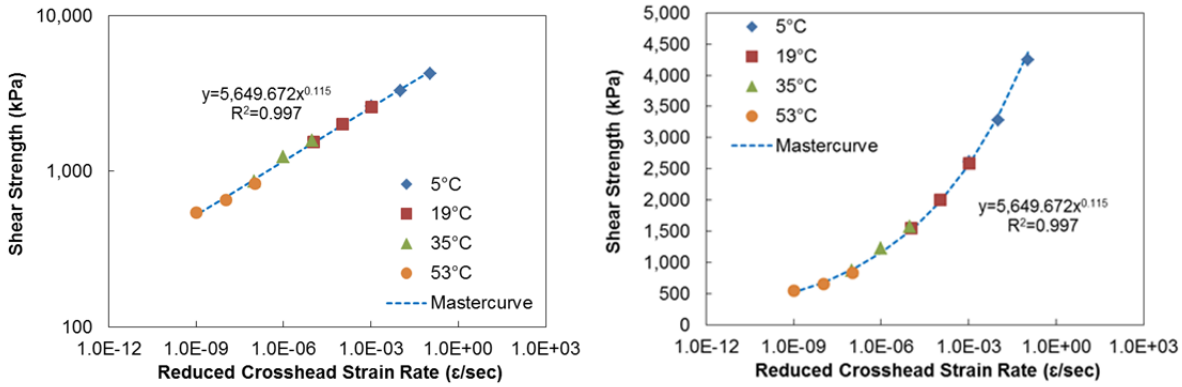

(a) (b)

Figure D.12 Verification of t-TS principle for shear strength and mastercurves using crosshead strain rate (CRS-2 emulsion and 482.63 kPa (70 psi) normal confining stress): (a) log-log scale and (b) semi-log scale.

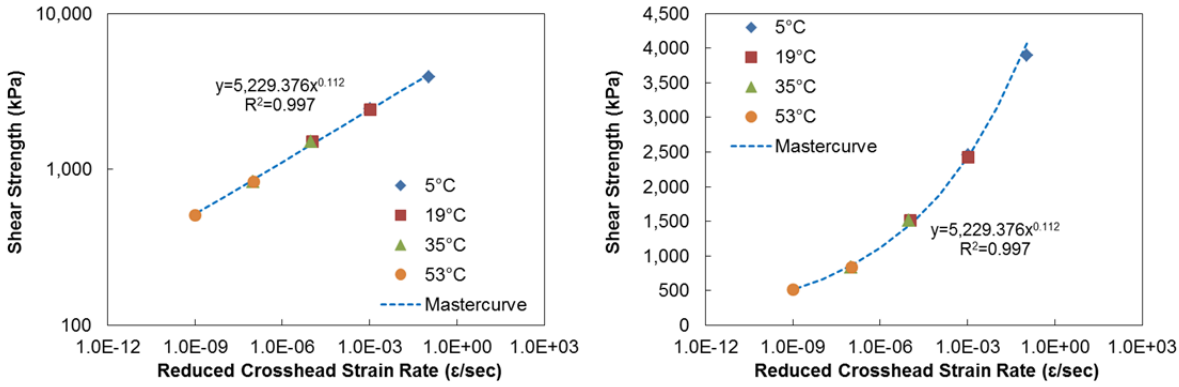

(a) (b)

Figure D.13 Verification of t-TS principle for shear strength and mastercurves using crosshead strain rate (CRS-1h emulsion and 482.63 kPa (70 psi) normal confining stress): (a) log-log scale and (b) semi-log scale.

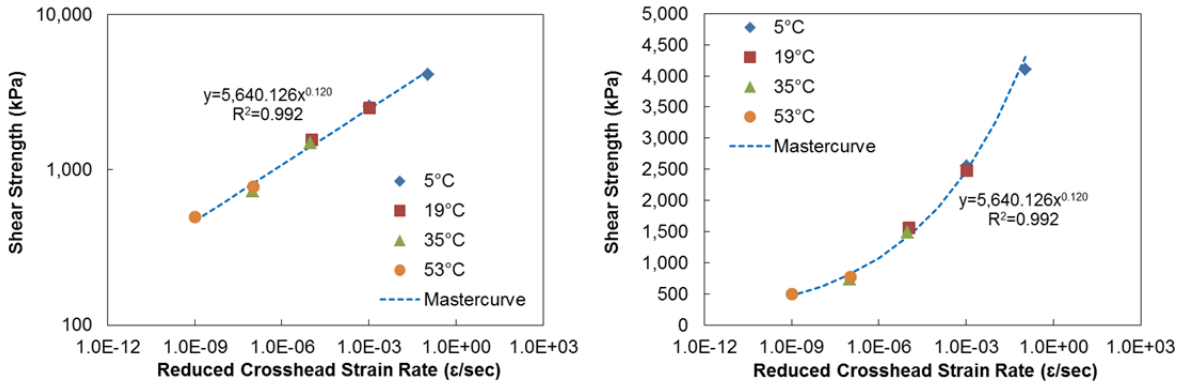

(a) (b)

Figure D.14 Verification of t-TS principle for shear strength and mastercurves using crosshead strain rate (NTCRS-1hM (Trackless) emulsion and 275.79 kPa (40 psi) normal confining stress): (a) log-log scale and (b) semi-log scale.

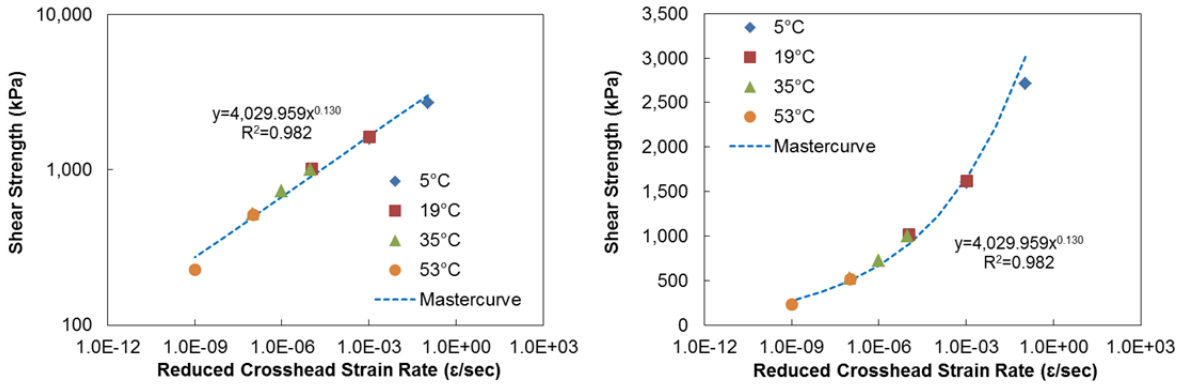

(a) (b)

Figure D.15 Verification of t-TS principle for shear strength and mastercurves using crosshead strain rate (No tack coat and 68.95 kPa (10 psi) normal confining stress): (a) log-log scale and (b) semi-log scale.

4.2. Phase 1: Verification of Time-Temperature Superposition Principle for Interlayer Shear Stiffness

In this section, the t-TS principle is proven to be valid also for the interlayer shear stiffness, which is assumed to be a characteristic value that can be used to measure the level of interlayer bonding. As previously stated in Appendix D, Section D.1, two calculation methods are available to determine the interlayer shear stiffness. The first method is to use the crosshead LVDT displacement to peak interface shear stress and the peak shear stress amplitude in an interface shear stress-displacement curve, and the second method is to use the displacement calculated by the DIC system.

The applicability of the t-TS principle was attempted to be proven for the interlayer shear stiffness as determined by these two calculation methods described in Appendix D, Section D.1. Figure D.16 shows that if the crosshead LVDT displacement to peak interface shear stress and the peak shear stress amplitude are used to calculate the interlayer shear stiffness value in an interface shear stress-displacement curve, the t-TS principle is not valid for the interlayer shear stiffness due to the effects of machine compliance issues, i.e., contributions from certain machine components throughout the loading frame to the overall displacement. Moreover, even though DIC displacement instead of crosshead LVDT displacement was used for the interlayer shear stiffness calculations, the applicability of the t-TS principle is still not valid for the interlayer shear stiffness, as shown in Figure D.17 and Figure D.18.

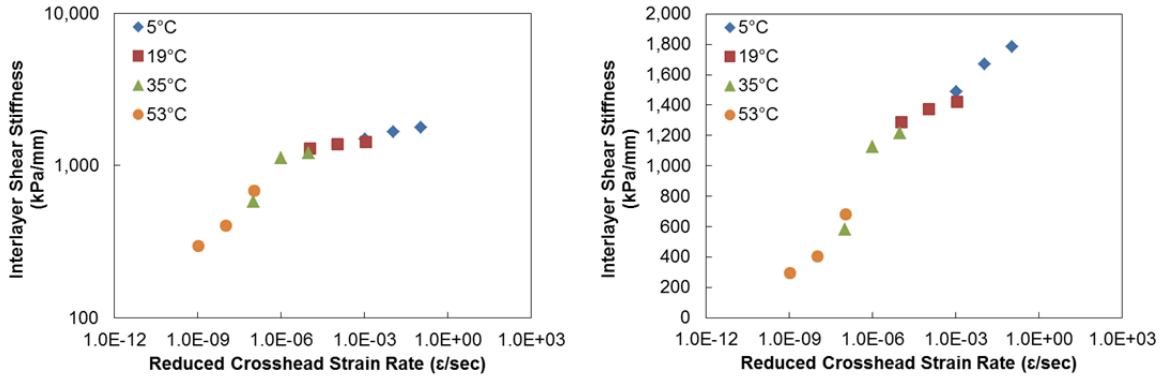

(a) (b)

Figure D.16 Non-applicability of t-TS principle for interlayer shear stiffness using crosshead LVDT displacement (CRS-2 emulsion and 482.63 kPa (70 psi) normal confining stress): (a) log-log scale and (b) semi-log scale.

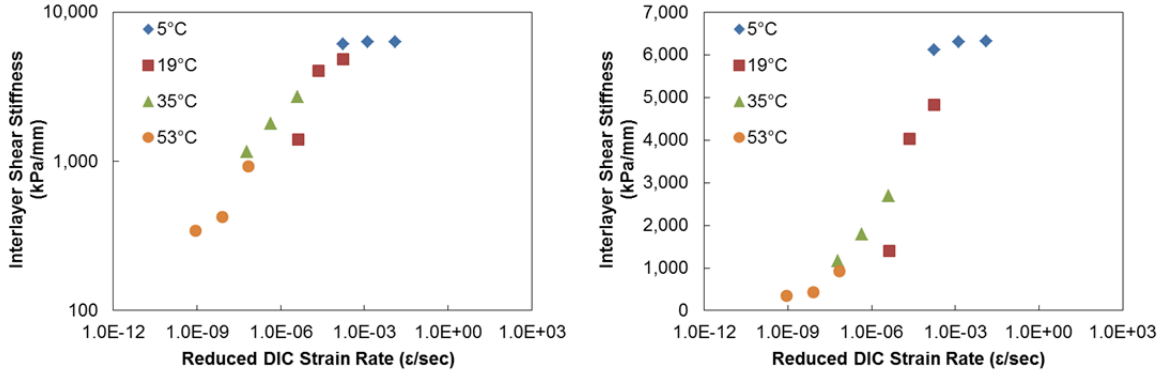

(a) (b)

Figure D.17 Non-applicability of t-TS principle for interlayer shear stiffness using DIC displacement (CRS-2 emulsion and 482.63 kPa (70 psi) normal confining stress): (a) log-log scale and (b) semi-log scale.

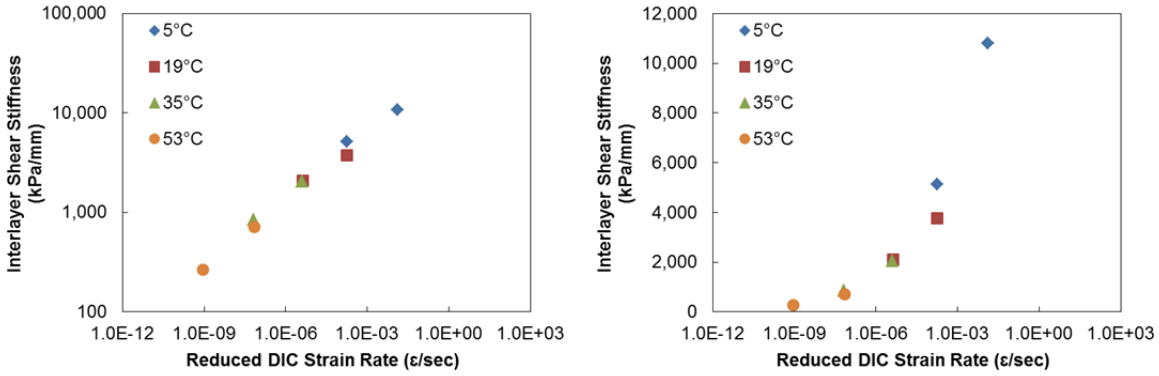

(a) (b)

Figure D.18 Non-applicability of t-TS principle for interlayer shear stiffness using DIC displacement (CRS-1h emulsion and 482.63 kPa (70 psi) normal confining stress): (a) log-log scale and (b) semi-log scale.

In this study, a new calculation method for determining the interlayer shear stiffness is proposed based on the idea that the data that deviates from a pure power law cannot be utilized for the application of the t-TS principle in the growing damage state (Chehab et al. 2002). Thus, DIC displacement following a pure power law until failure of the specimen and the corresponding shear stress amplitude in an interface shear stress-displacement curve were used to calculate the interlayer shear stiffness values. Figure D.19 illustrates the proposed calculation method for determining the interlayer shear stiffness to make the t-TS principle applicable for the damage state.

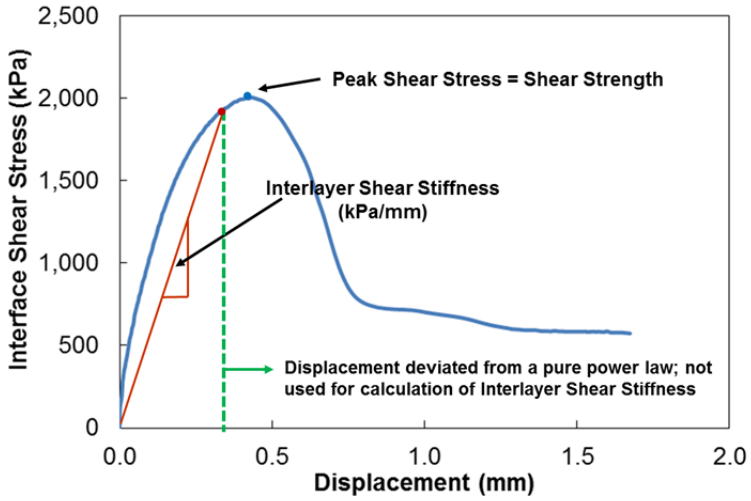

Figure D.19 New calculation method for determination of interlayer shear stiffness.

Consequently, when DIC displacement following a pure power law until failure of the specimen and the corresponding shear stress amplitude were used for the interlayer shear stiffness calculation, the applicability of the t-TS principle was verified for the interlayer shear stiffness, as shown in Figure D.20 through Figure D.23.

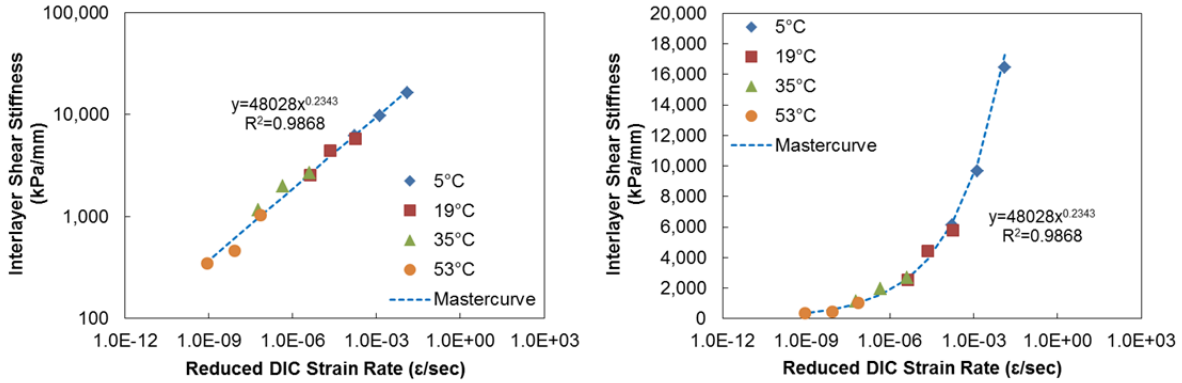

(a) (b)

Figure D.20 Verification of t-TS principle for interlayer shear stiffness using DIC displacement following a pure power law (CRS-2 emulsion and 482.63 kPa (70 psi) normal confining stress): (a) log-log scale and (b) semi-log scale.

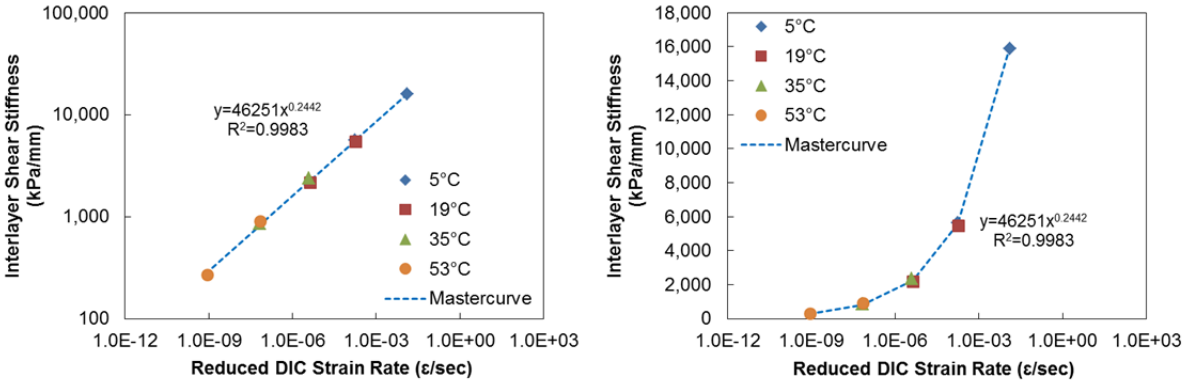

(a) (b)

Figure D.21 Verification of t-TS principle for interlayer shear stiffness using DIC displacement following a pure power law (CRS-1h emulsion and 482.63 kPa (70 psi) normal confining stress): (a) log-log scale and (b) semi-log scale.

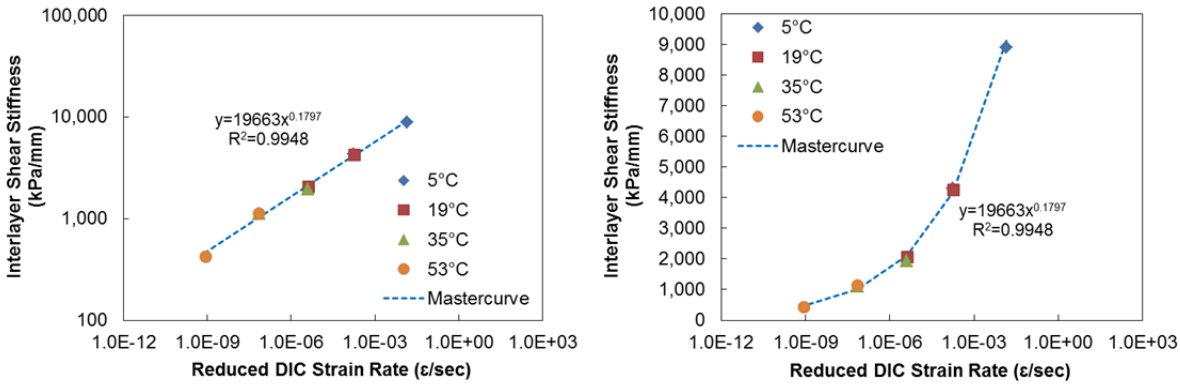

(a) (b)

Figure D.22 Verification of t-TS principle for interlayer shear stiffness using DIC displacement following a pure power law (NTCRS-1hM (Trackless) emulsion and 275.79 kPa (40 psi) normal confining stress): (a) log-log scale and (b) semi-log scale.

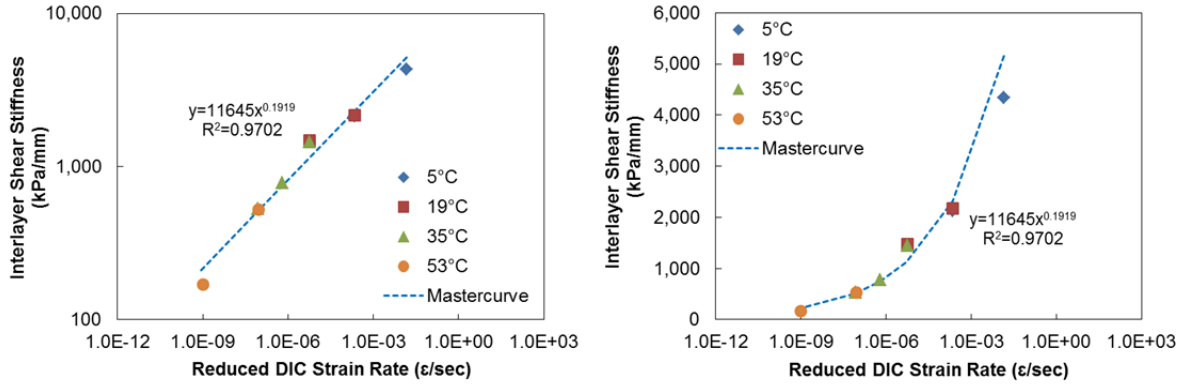

(a) (b)

Figure D.23 Verification of t-TS principle for interlayer shear stiffness using DIC displacement following a pure power law (No tack coat and 68.95 kPa (10 psi) normal confining stress): (a) log-log scale and (b) semi-log scale.

4.3. Phase 2: Development of Shear Strength Mastercurve

The main purpose of the application of the t-TS principle is to develop a shear strength mastercurve as a function of reduced strain rate at a desired reference temperature. Developing such a mastercurve enables the strength of a material at any strain rate and temperature combination to be determined.

In Phase 1, the t-TS principle's applicability for shear strength was proven to be valid for specimens with different tack coat materials at the layer interface. In this Phase 2 section, the shear strength mastercurve is developed for the remaining test combinations presented in Table D.3, using four reduced strain rates. Thus, less effort is needed to develop shear

strength mastercurves for the remaining test combinations in Phase 2. The test conditions are as follows:

- Reduced strain rates: 0.508 mm/min (53°C), 5.08 mm/min (35°C), 50.8 mm/min (19°C), 50.8 mm/min (5°C)
- Total number of tests: 4 reduced strain rates × 8 tack coat/normal confining stress combinations = 32 tests

4.3.1. Effect of Loading Rate and Temperature

Figure D.24 presents the shear strength mastercurves developed at various confining stresses using samples with the four study emulsions at the layer interface. It is well known that shear strength increases at high reduced strain rates (low temperature/high strain rate combinations). As shown in Figure D.24, the strength mastercurves indicate the increase in shear strength as the reduced strain rate increases.

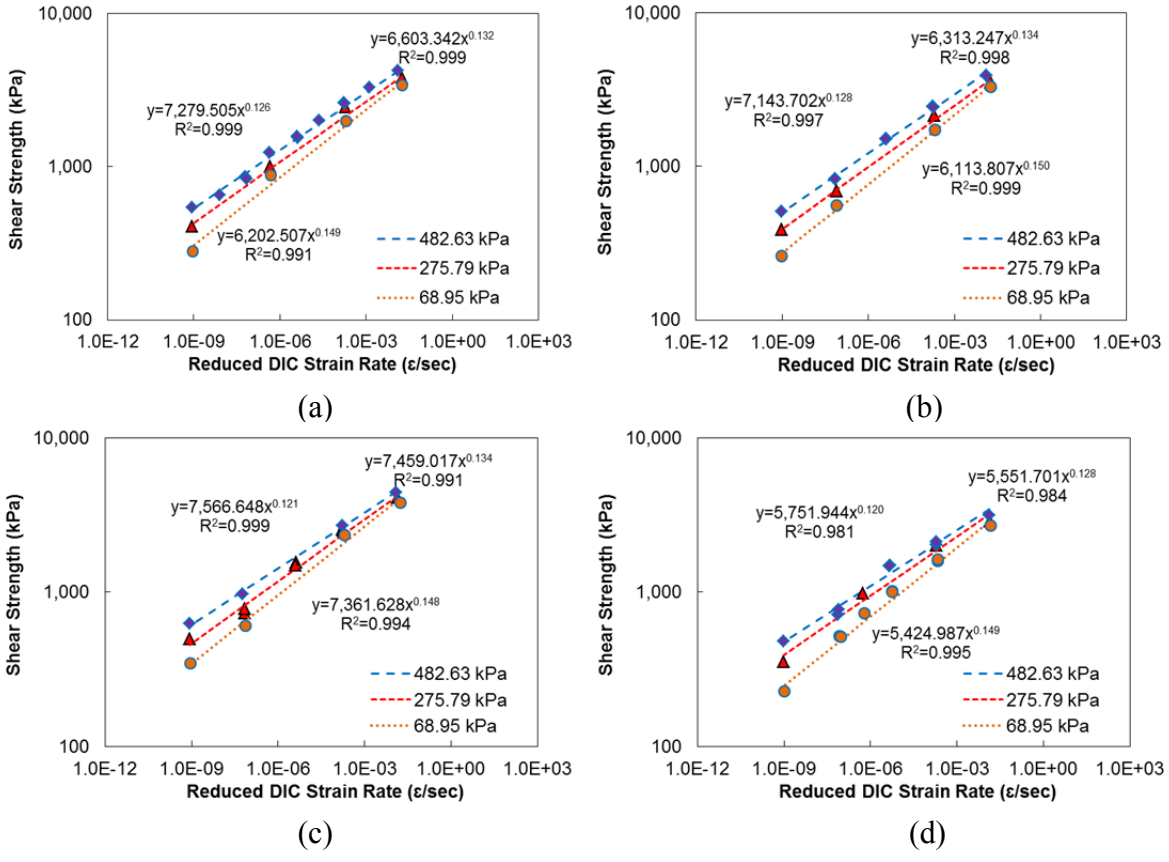

Figure D.24 Shear strength mastercurves developed at various confining stresses: (a) CRS-2 emulsion, (b) CRS-1h emulsion, (c) NTCRS-1hM (Trackless) emulsion, and (d) no tack coat. Note: The numbers in the legends represent the normal confining stresses used in this study.

4.3.2. Effect of Normal Confining Stress

Figure D.24 also indicates that the shear strength obviously increases with the application of a normal confining stress at low reduced strain rates (i.e., high temperature/low strain rate combinations). That is, shear strength clearly is affected by the effect of the normal confining stress, whereas the effect of the normal confining stress is less for high reduced strain rates, i.e., when the temperature is low and/or the strain rate is fast. Generally, the greater the normal confining stress, the greater the shear strength, which can be observed more obviously at the low reduced strain rate (i.e., high temperature/low strain rate).

4.3.3. Effect of Tack Coat Type

Four types of tack coat material were tested in this research: CRS-2, CRS-1h, NTCRS-1hM (trackless) emulsions, and no tack coat. Figure D.25 shows the effects of the different tack coats on the shear strength values determined at three different normal confining stresses. Among the emulsified tack coats, the NTCRS-1hM (trackless) emulsion exhibits the highest interface shear strength, followed by the CRS-2 and CRS-1h emulsions, and no tack coat, as shown in Figure D.25. The figure also shows that the CRS-2 emulsion has slightly higher strength values than the CRS-1h emulsion, because the CRS-2 samples contain a larger quantity of asphalt residue at the layer interface than the CRS-1h samples.

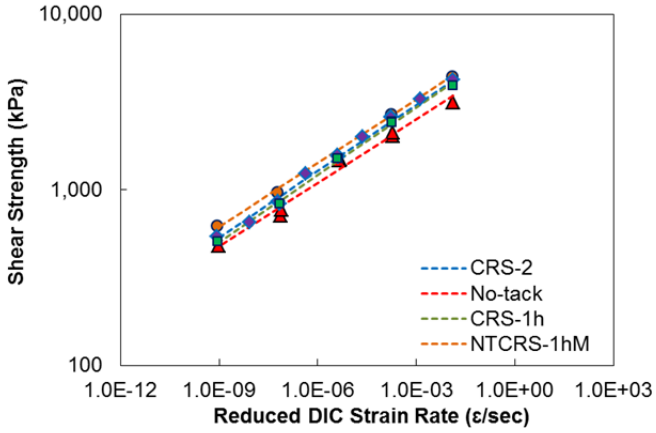

(a)

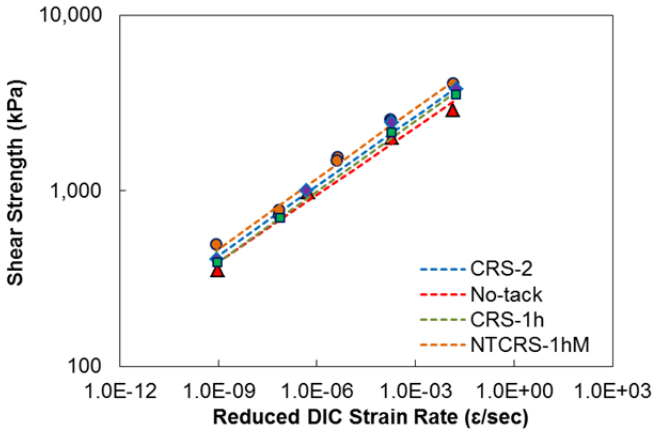

(b)

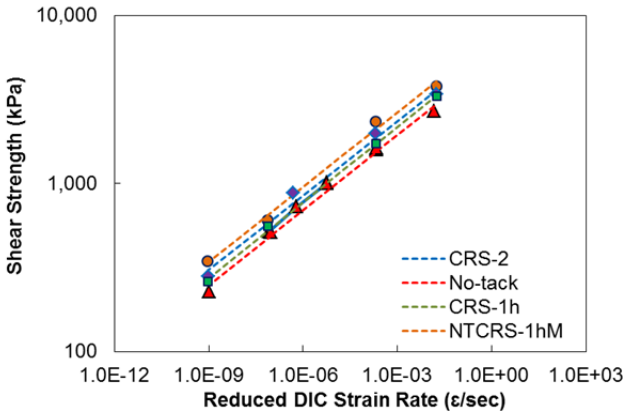

(c)

Figure D.25 Effects of different tack coat materials on shear strength: (a) 482.63 kPa (70 psi) confining stress, (b) 275.79 kPa (40 psi) confining stress, and (c) 68.95 kPa (10 psi) confining stress.

5. Validation of Time-Temperature Superposition Principle for Interlayer System with GlasGrid

The applicability of the t-TS principle for shear strength was proven to be valid using double-layered asphalt specimens fabricated with tack coat materials at the layer interface and the t-T shift factors measured from dynamic modulus tests of the test mixtures. In this section, the validation of the t-TS principle is extended to the shear strength of GlasGrid-reinforced asphalt concrete specimens with two different types of tack coat, PG 64-22 binder and SS-1 emulsion, between the layers. Basically, the same approach that was taken in the case of asphalt concrete specimens with only a tack coat at the layer interface was applied to verify the t-TS principle in shear failure mode. The shear loading rates, i.e., 0.508 mm/min and 5.08 mm/min, were selected from the fastest and the slowest shear loading rates used for the previous tests on the double-layered asphalt concrete specimens with tack coat materials at the layer interface. The temperature of 5°C was selected as the low temperature for these shear strength tests. The other test temperatures were determined based on the scheme described in Section 3.5.2. In other words, four temperatures and two shear loading rates were determined in such a way that the reduced strain rates for the different loading rates at adjacent temperatures were the same. For this task, RS12.5B loose mixture was used. The RS12.5B mixture is not produced or used in North Carolina, so this mixture was obtained from an asphalt plant in Virginia. This mixture is composed of 12.5 mm NMAS granite aggregate, 30 percent RAP, and 5.3 percent PG 64-22 binder. The detailed blended aggregate gradation is shown in Figure D.26.

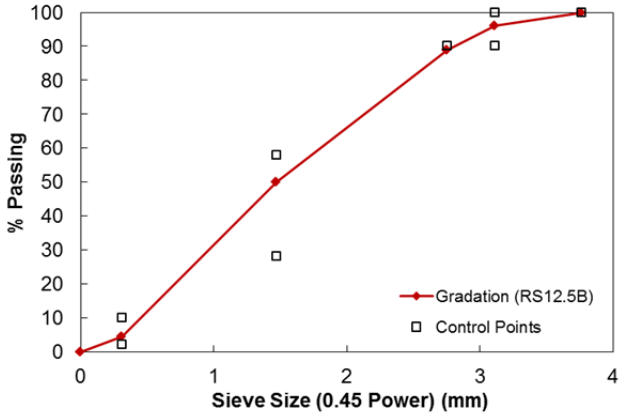

Figure D.26 Aggregate gradation chart of RS12.5B mixture.

PG 64-22 binder and SS-1 emulsion were used as the tack coat materials, with a residual application rate of 0.199 L/m^2 (0.044 gal/yd^2). Table D.4 presents the residual asphalt content and application rate for each tack coat used in this task.

Table D.4 Residual asphalt contents and application rates.

Property	Type of Tack Coat	
	PG 64-22	SS-1
Residual Asphalt Content (%)	100	71.43
Tack Coat Application Rate (L/m^2)	0.199 ($0.044\ gal/yd^2$)	0.279 L/m^2 ($0.062\ gal/yd^2$)
Residual Application Rate (L/m^2)	0.199 ($0.044\ gal/yd^2$)	0.199 ($0.044\ gal/yd^2$)

Two types of geogrids, GlasGrid® 8501 and GlasGrid® 8511, were used for the reinforcement of the HMA interlayers in this task. These geogrids were supplied by Saint-Gobain ADFORS America. GlasGrid® 8501 and GlasGrid® 8511 are self-adhesive glass fiber grids with 12.5-mm (0.5 in.) and 25-mm (1 in.) grid openings, respectively, and are impregnated with acrylic polymer resin. GlasGrid is well known as a geosynthetic material that can be used to control reflective cracking in asphalt pavements by retarding crack propagation.

For specimen fabrication, a double-layered slab was compacted using a standard roller compactor from Cooper Technology. For this process, once the mixture had been poured into the slab compactor mold, the compactor compacted the mixture to a height of 50.8 mm (2 in.) using vibrations. After the mixture had cooled down, a grid was embedded into the top of the bottom layer, and then a tack coat was applied uniformly to achieve a consistent thickness on the top of the bottom layer and the grid. For the case of the specimens with the asphalt binder tack coat, i.e., PG 64-22 binder, the top layer was compacted immediately after the tack coat application, but for the specimens with the SS-1 emulsion tack coat, a 24-hour curing period was allowed prior to compaction of the top layer. In order to produce the upper asphalt layer with a height of 50.8 mm (2 in.), the same compaction process was repeated on top of the bottom layer. Then, the double-layered slab was cut and trimmed to a width of 152.4 mm (6 in.) and a height of 76.2 mm (3 in.) before testing. Two specimens could be obtained from one slab. These slabs were constructed using a combination of GlasGrid® 8501(12.5-mm) and PG 64-22 binder and GlasGrid® 8511(25-mm) and SS-1 emulsion. Figure D.27 shows the MAST square-shaped specimen preparation steps.

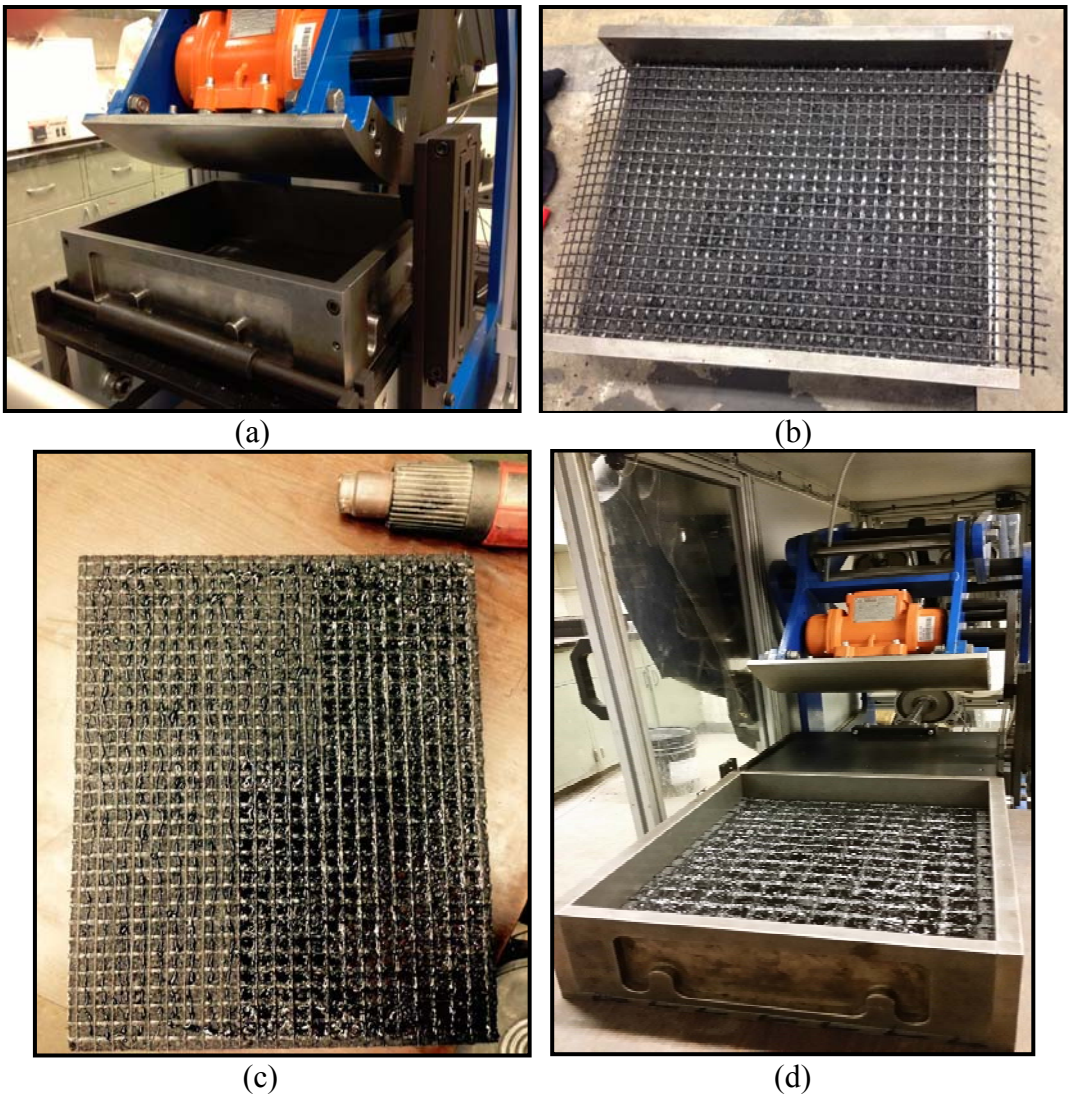

Figure D.27 MAST square-shaped specimen preparation steps: (a) compaction of bottom layer, (b) GlasGrid installation, (c) tack coat application, and (d) compaction of top and bottom layers.

The interface shear bond strength tests were conducted using the MAST and DIC system in constant displacement-control mode, thereby measuring a maximum shear load and its corresponding shear displacement to evaluate the interface shear bond strength. The tests were performed at different loading rates and temperatures until the specimen failed. Shear loading rates of 0.508 mm/min (0.02 in./min) and 5.08 mm/min (2 in./min) were used to shear the specimens at different temperatures with normal confining pressure of 275.79 kPa (40 psi). Prior to testing, the specimens were speckled with a uniform-sized speckle pattern to allow for image correlation analysis and then glued to steel shoes that were designed for

152.4 mm (6 in.) square-shaped specimens, as presented in Figure D.28. The shear test conditions used for the GlasGrid-reinforced specimens are summarized in Table D.5.

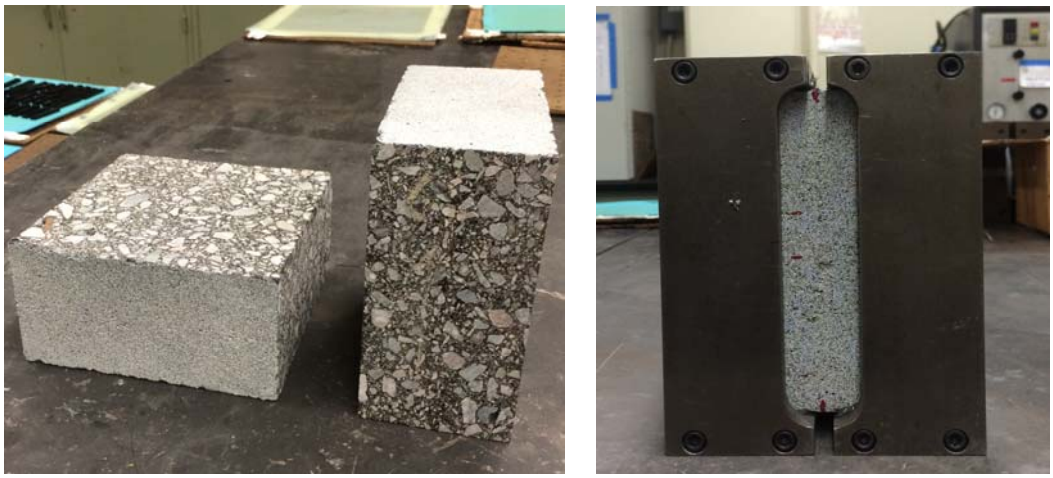

(a) (b)

Figure D.28 (a) Speckled pattern on specimens and (b) specimen glued to steel shoes.

Table D.5 Summary of shear test conditions used for GlasGrid-reinforced specimens.

Testing Conditions	
Mixture Type	RS12.5B (6% air void)
Specimen Dimension (mm)	Square Shape: 152.4 (6 in.) × 152.4 (6 in.), Height: 76.2 (3 in.)
Testing Mode	Monotonic
Loading Rate (mm/min)	0.508 (0.02 in./min), 50.8 (2 in./min)
Normal Confining Stress (kPa)	275.79 (40 psi)
Temperature (°C)	5 (41°F), 18 (64.4°F), 32 (89.6°F), 48 (118.4°F)
Interlayer Material	PG 64-22 binder/12.5 mm GlasGrid® 8501, SS-1 emulsion/25 mm GlasGrid® 8511
Application Rate (Residual)	0.199 L/m^2 (0.044 gal/yd^2)

Dynamic modulus (|E*|) tests were conducted for the RS12.5B mixture used for this task at frequencies of 25, 10, 5, 1, 0.5, and 0.1 Hz and temperatures of 5°C, 20°C, and 40°C. Figure D.29 presents the dynamic modulus test results for the RS12.5B mixture. As implemented for the verification of the t-TS principle for asphalt concrete specimens with tack coats at the layer interface, the t-T shift factors determined from the dynamic modulus tests were used for the horizontal shifting of the shear strength data obtained at various

temperatures and loading rates onto a selected reference temperature. The temperature of 5°C was chosen as the reference temperature. Table D.6 presents the coefficients of the t-T shift factor function for the RS12.5B mixture.

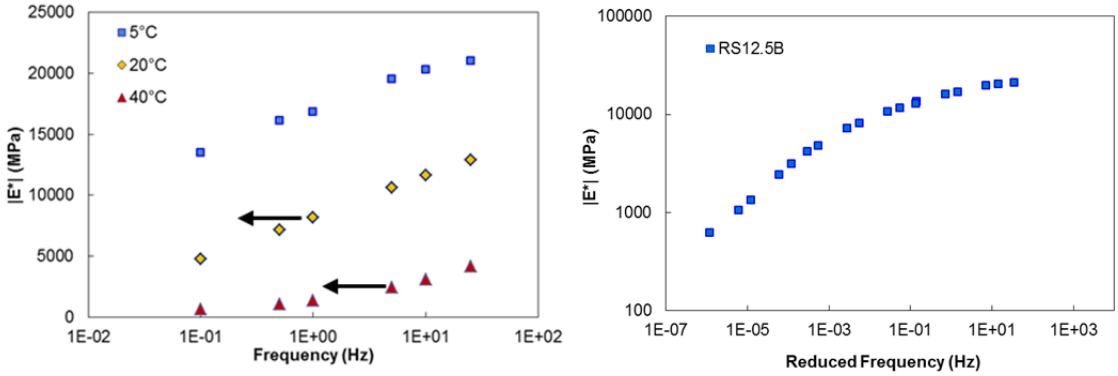

(a) (b)

Figure D.29 Dynamic modulus test results for RS12.5B mixture: (a) unshifted dynamic modulus values and (b) dynamic modulus mastercurve.

Table D.6 Fitting coefficients of time-temperature shift factor function.

Parameters	RS12.5B
α_1	0.0004926
α_2	-0.1626845
α_3	0.8011076

It is worth noting that the interface shear strength values determined from two adjacent temperatures but at the same reduced strain rate would be assumed to be the same in order to verify the applicability of the t-TS principle for the shear strength values of GlasGrid-reinforced asphalt concrete specimens. In other words, the verification of the t-TS principle should be able to be confirmed by comparing the interface shear strength values determined from two adjacent temperatures but at the same reduced strain rates. However, as presented in Figure D.30, the application of the t-T shift factors obtained from the dynamic modulus tests of the RS12.5B mixture did not allow overlaps of the interface shear strength values between two adjacent temperatures but at the same reduced strain rates due to the presence of the GlasGrid embedded between the two layers, thereby disobeying the laws of TRS material behavior at the layer interface in shear failure mode.

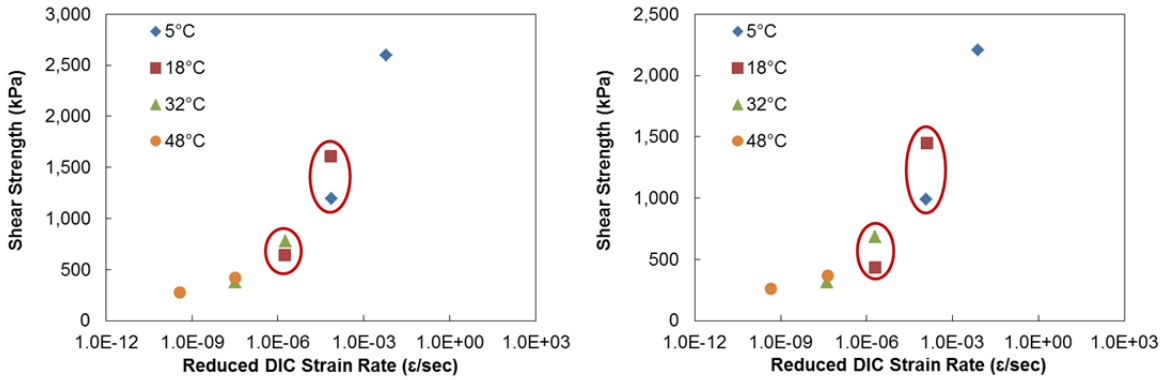

(a) (b)

Figure D.30 Non-applicability of t-TS principle: (a) 12.5 mm GlasGrid with PG 64-22 binder and (b) 25 mm GlasGrid with SS-1 emulsion.

Hence, as an alternative strategy, a new approach was attempted in order to verify the t-TS principle as it applies to the shear strength of GlasGrid-reinforced asphalt concrete specimens using the t-T shift factors of the PG binder and the residue of the SS-1 emulsion. For this purpose, complex shear rheometer (DSR) tests were conducted using an AR-G2 DSR to measure the dynamic shear modulus (|G*|) and to determine the t-T shift factors of the asphalt binder and the emulsion residue. These mechanical tests were performed using frequency sweep tests at one percent shear strain amplitude at 5°C, 20°C, and 35°C and a range of 0.1 Hz to 30 Hz loading frequencies. The frequency sweep tests were designed to construct mastercurves of the complex shear modulus (G*) values and to obtain the t-T shift factors for the binder and emulsion residue used in this study. Figure D.31 (a) and (b) show the complex shear modulus mastercurves for each tack coat type and t-T shift factor functions of the PG 64-22 asphalt binder and SS-1 emulsion residue, including a comparison with the t-T shift factor function of the RS12.5 mixture, respectively. Figure D.31 (b) clearly shows that the mixture shift factors are noticeably different from the tack coat shift factors. Table D.7 presents the coefficients of the t-T shift factor functions for the PG binder and SS-1 emulsion residue.

Table D.7 Fitting coefficients of time-temperature shift factor function.

Parameters	PG 64-22	SS-1 Residue
α_1	0.0008560	0.0007990
α_2	-0.1497080	-0.1498350
α_3	0.7271400	0.7292000

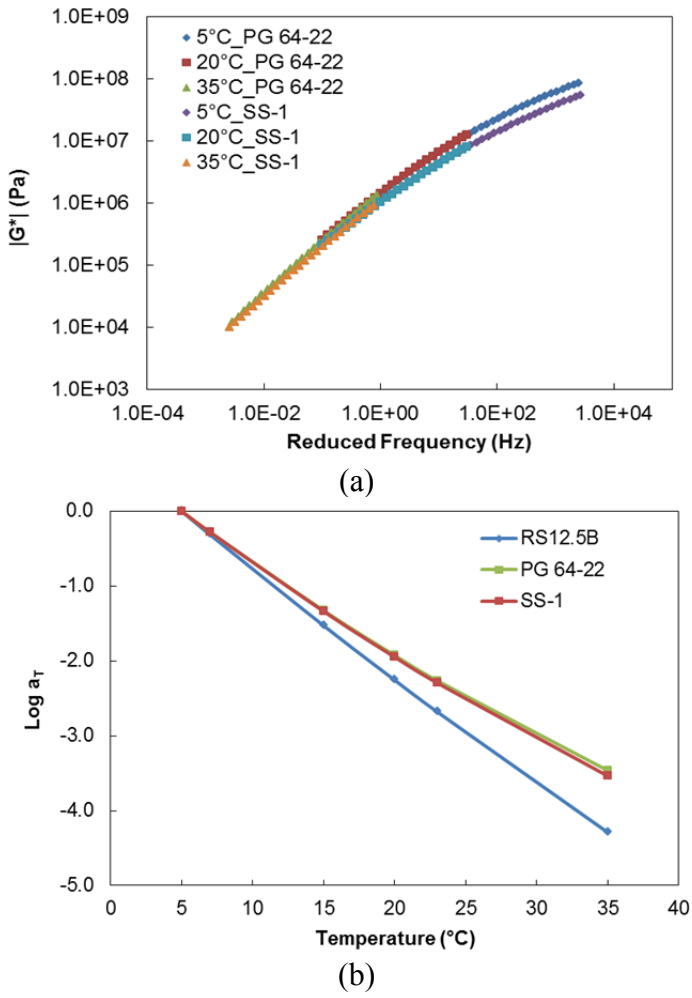

Figure D.31 (a) Complex shear modulus mastercurves for each material and (b) time-temperature shift factor functions for each material.

Basically, the temperatures used for the interface shear strength tests were redetermined based on the t-T shift factors of the PG binder and SS-1 emulsion residue by means of the scheme previously described in Section 3.5.2. Then, the shear tests also needed to be conducted again at the determined test temperatures. However, this approach would require a more extensive testing effort. Instead, if a single smooth curve could be constructed, as the existing strength data sets tested at various temperatures are shifted horizontally with respect to the strain rate onto a selected reference temperature using the t-T shift factors of the binder and residue, then the t-TS principle would be valid in shear failure mode.

As shown in Figure D.32 and Figure D.33, a single mastercurve was constructed successfully for the interface shear strength values of the GlasGrid-reinforced asphalt concrete specimens using the t-T shift factors of the PG binder and SS-1 emulsion residue, respectively, indicating that the t-TS principle is valid for the shear strength of GlasGrid-reinforced asphalt concrete specimens as long as the t-T shift factors of the binder between

the layers are used instead of the mixture t-T shift factors. This observation is different from the one made in Section 4.2.1 for shear strengths of non-reinforced asphalt concrte specimens where the mixture t-T shift factors were successfully used to develop the shear strength mastercurves. This difference could be originated from the greater effects of tack coat on the behavior of GlasGrid-reinforced asphalt concrete specimens than on the behavior of non-reinforced asphalt concrete specimens due to a larger amount of applied residual tack coats and more pronounced discontinuity between the asphalt layers in the GlasGrid-reinforced asphalt concrete specimens.

For comparative purposes regarding the interface shear strength between the GlasGrid-reinforced asphalt concrete specimens with different interlayer conditions, Figure D.34 shows that the shear strength of the specimens with PG binder and 12.5 mm GlasGrid at the layer interface outperforms the shear strength of the specimens with SS-1 emulsion and 25 mm GlasGrid at all reduced stain rates. This behavior is expected given that the complex shear modulus (G*) of PG 64-22 binder is known to outperform that of SS-1 emulsion, as shown in Figure D.31 (a). Essentially, assuming that the quality of the tack coat used at the layer interface is the same for the two specimens, the specimens with the larger GlasGrid opening size would be expected to have higher shear strength values, because these specimens have much larger asphalt-to-asphalt contact areas and fewer ribs between the top and bottom layers. Nevertheless, the fact that the specimens with a combination of the smaller opening size and better quality tack coat have higher shear strength values indicates that the quality of the tack coat plays a more important role than the opening size of the GlasGrid in terms of the shear strength of the interface.

In addition, as shown in Figure D.35, the applicability of the t-TS principle was verified for the interlayer shear stiffness of GlasGrid-reinforced asphalt concrete specimens determined using the method described in Figure D.19.

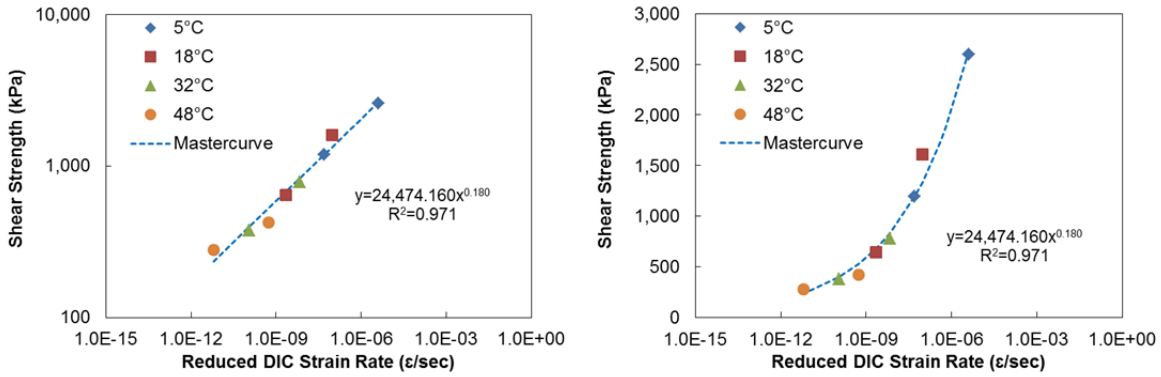

(a) (b)

Figure D.32 Verification of t-TS principle for shear strength of GlasGrid-reinforced asphalt concrete specimens (12.5-mm) with PG 64-22 binder at the layer interface: (a) log-log scale and (b) semi-log scale.

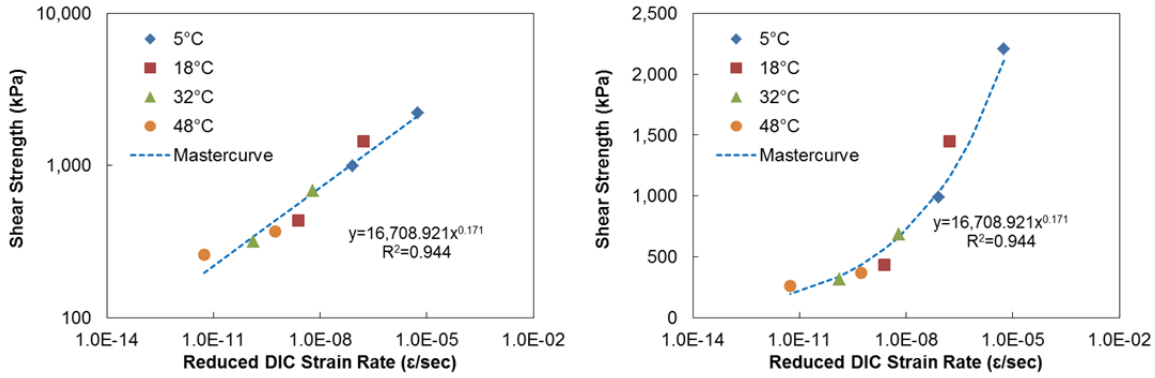

(a) (b)

Figure D.33 Verification of t-TS principle for shear strength of GlasGrid-reinforced asphalt concrete specimens (25-mm) with SS-1 emulsion at the layer interface: (a) log-log scale and (b) semi-log scale.

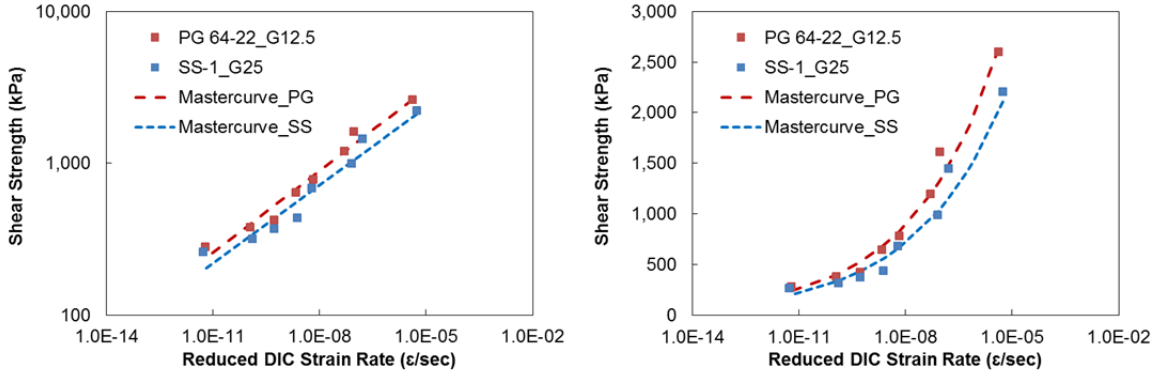

(a) (b)

Figure D.34 Comparison of shear strength values between GlasGrid-reinforced asphalt concrete specimens with different interlayer conditions: (a) log-log scale and (b) semi-log scale.

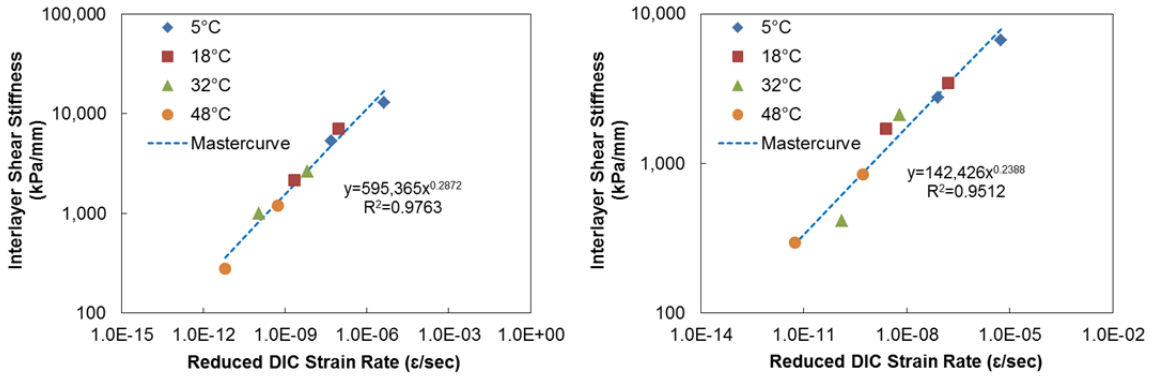

(a) (b)

Figure D.35 Verification of t-TS principle for interlayer shear stiffness of GlasGrid-reinforced asphalt concrete specimens: (a) 12.5 mm GlasGrid with PG 64-22 binder and (b) 25 mm GlasGrid with SS-1 emulsion.

In this section, one notable point is that deficiency of the shear bond strength with respect to the GlasGrid-reinforced asphalt concrete specimens was detected as compared with the shear strength of specimens with only a tack coat (i.e., CRS-2, CRS-1h, and Trackless) at the layer interface; therefore, additional shear tests were conducted using the specimens composed only of PG asphalt binder as a tack coat under the test conditions of 50.8 mm/min (2 in./min) loading rate, 18°C, and normal confining stress of 275.79 kPa (40 psi). Figure D.36 indicates that the presence of GlasGrid at the layer interface led to some degree of deficiency in shear strength; however, further research is needed to verify with certainty that the presence of the geosynthetic materials at the layer interface actually caused the deficiency in shear strength. Therefore, additional shear strength tests were conducted using specimens with various geosynthetic materials, as described in the next section.

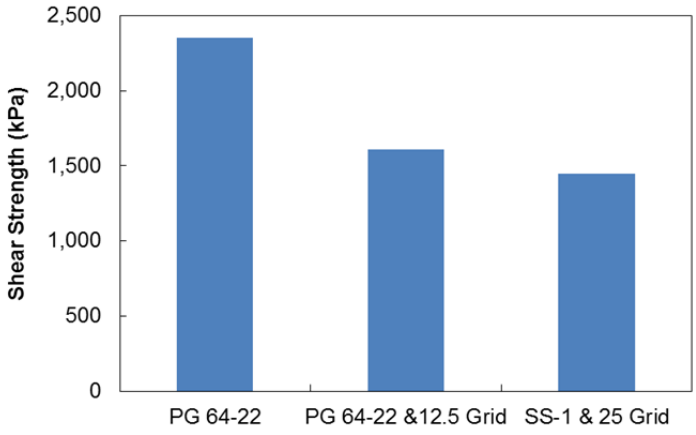

Figure D.36 Shear strength deficiency of GlasGrid-reinforced asphalt concrete specimens.

6. Effect of Geosynthetic Interlayer Materials on Shear Bond Strength

The shear resistance properties, especially the deficiency of the shear bond strength, of two-layered asphalt concrete specimens with three different types of geosynthetic material at the layer interface were investigated using the MAST under the test conditions of 20°C, 50.8 mm/min (2 in./min) loading rate, and unconfinement. The types and properties of the geosynthetic materials used in this study are summarized in Table D.8. For all of the geosynthetic materials, PG 64-22 asphalt binder was used as the tack coat at the layer interface. The control condition was composed only of CRS-2 emulsion with an optimal application rate of 0.181 L/m^2 (0.04 gal/yd^2) at the layer interface as the tack coat. Table D.9 presents the properties of the emulsion used in this task.

A number of 152.4-mm (6-in.) diameter field cores for each geosynthetic material were obtained from test sections constructed under the North Carolina Department of Transportation (NCDOT) HWY-2012-02 research project. Detailed field construction information can be found in Wargo (2015).

Lab-fabricated specimens were prepared using the RS9.5B loose mixture described in Chapter 3. In order to produce a double-layered slab, a slab compactor was used, and the same specimen fabrication process outlined in Appendix D, Section D.5 was repeated with only the replacement of the interlayer materials. During this process, the tack coat application rates for each geosynthetic material were maintained with the same target application rate intended for field construction. The target application rates were selected based on each geosynthetic material manufacturer's optimal recommendation. During the construction process, the measurements of the tack coat application rates were taken by placing 304.8-mm (12-in.) square steel plates on the surface and then removing them prior to the placement of the interlayer. The target application rates and measured application rates can be found in Table D.10. The results of the measurements indicate a highly significant difference between the target application rate and the measured rate. For the field cores, the target application rate for each geosynthetic material was intended to be used, but in practice the measured application rate was applied.

Table D.8 Geosynthetic material properties (Wargo 2015).

Property	TruPave	GlasPave	Petromat
Geosynthetic Type	Paving Mat	Paving Mat	Paving Fabric
Description	nonwoven blend of fiberglass and polyester fibers	continuous fiberglass fibers coated in an elastomeric compound embedded between two polyester textiles	nonwoven polypropylene
Tensile Strength (MD)	40 lb/in. (ASTM D5035)	170 lb/in. (ASTM D5035)	101 lb/in. (ASTM D4632)
Tensile Elongation	<5% (ASTM D5035)	3.5% (ASTM D5035)	5% (ASTM D4632)
Mass/Unit Area (ASTM D5261)	4.1 oz/yd^2	4.0 oz/yd^2	4.1 oz/yd^2
Asphalt Retention (ASTM D6140)	0.18 gal/yd^2	0.10 gal/yd^2	0.20 gal/yd^2
Melting Point (ASTM D-276)	>446ºF	>450ºF	320ºF

Table D.9 Material properties of CRS-2 emulsion.

Property	CRS-2
Residual Asphalt Content (%)	65.21
Base Binder	PG 58-22
Tack Coat Application Rate (L/m^2)	0.181 (0.04 gal/yd^2)
Residual Application Rate (L/m^2)	0.118 (0.026 gal/yd^2)

Table D.10 Comparison of target application rate and measured application rate for field cores (Wargo 2015).

Section Name	TruPave	GlasPave	Petromat	Control (CRS-2)
Target Application Rate (gal/yd^2)	0.20	0.17	0.25	0.04
Measured Application Rate (gal/yd^2)	0.075	0.078	0.0813	0.036

Prior to testing, both the field cores and lab-fabricated specimens were cut and trimmed to a width of 101.6 mm (4 in.) and a height of 76.2 mm (3 in.) and then were glued to steel shoes designed for 101.6-mm (4-in.) square-shaped specimens. The shear tests were conducted using these laboratory-fabricated specimens and field cores.

Figure D.37 shows the shear bond strength values of the specimens with different interlayer conditions. As shown in Figure D.37, the shear strength values are very similar for the two replicates. As expected, the laboratory-fabricated specimens have higher shear strength values than the field cores. The results of the laboratory-fabricated specimens show that the control condition, CRS-2, has the highest shear strength values followed by Petromat, Glaspave, and Trupave. One notable fact is that the shear strength values of Petromat and Trupave field cores are much lower than the shear strength values of laboratory-fabricated specimens. This deficiency of the shear bond strength is supported by deficient tack coat application rates in the field cores, as compared with the manufacturers' optimal recommendation rates; thus, this might lead to different raking system among Glaspave, Petromat, and Trupave in the shear strength results of the field cores and the laboratory-fabricated specimens.

Collop et al. (2009) found minimum limits for shear bond strength for surface/binder (S/B) course interface specimens and binder course/base interface (B/B) specimens through a literature review, as shown in Table D.11. The shear bond strength values were investigated under the test conditions of 50.8 mm/min (2 in./min) loading rate, 20°C, and unconfinement. These minimum limits are those suggested for use in European countries and were applied to the shear strength data in this study, as shown in Figure D.37. Obviously, only the field cores from the control section satisfied all the minimum limits for shear bond strength proposed by different researchers.

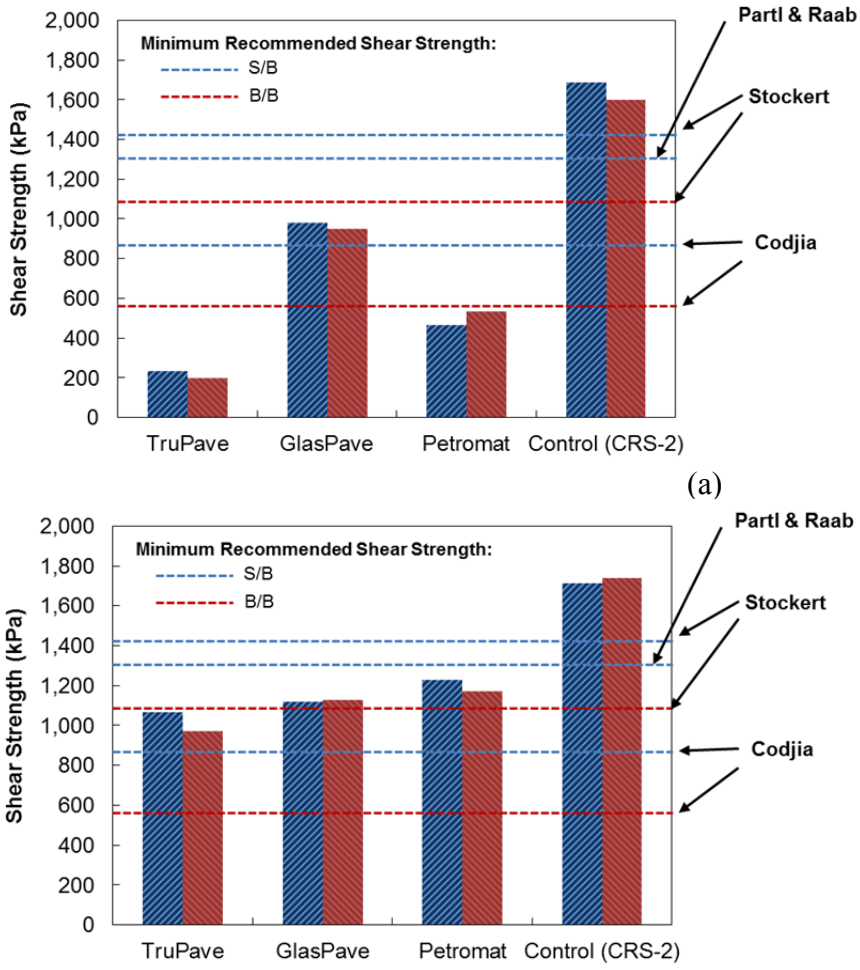

Figure D.37 Comparison of shear bond strength values among specimens with different interlayer conditions: (a) field cores and (b) laboratory-fabricated specimens.

Table D.11 Proposed minimum limits of shear bond strength (Collop et al. 2009).

Source	Test Equipment	Specimen Size (mm diameter)	Displacement Rate (mm/min)	Shear Strength (MPa)	
				S/B	B/B
Codjia	Leutner	150	50.8	0.85 (123 psi)	0.57 (83 psi)
Partl and Raab	LPDS	150	50.8	1.3 (189 psi)	-
Stockert	Leutner	150	50.8	1.41 (204 psi)	1.13 (164 psi)

In addition, Figure D.37 proves that the presence of geosynthetic materials at the layer interface leads to a significant reduction (approximately 38%~44%) in shear bond strength. When geosynthetic materials are installed at the layer interface, the adhesion between the layers could be adversely affected if the tack coat material is not applied properly. Consequently, their use can create discontinuities at the interface and act as stress concentrators. If the reduction in shear bond strength occurs in the field, it might cause poor bonding or debonding between adjacent asphalt concrete layers and subsequently activate distress mechanisms that could lead to total failure of the pavement structure. Hence, a proper adhesive bond between the structural layers is crucial to prevent pavement distresses, such as slippage cracking or delamination, when utilizing geosynthetic interlayer materials. Further, the use of geosynthetic materials especially at the layer interface requires a high quality bond as well as specifications for the threshold of shear bond strength. In other words, particularly careful selection of the tack coat as the bonding material is essential when geosynthetic materials are used at the layer interface, even more so than relying only on empirical methods and manufacturers' recommendations. Even though a tack coat is used only at the layer interface as a bonding material, great attention must be paid to the selection of the tack coat. Also, further research is required to establish the specifications for a minimum limit for shear bond strength to provide acceptable field performance, which would require more shear tests using both field cores and laboratory-fabricated specimens composed of various types of interlayer systems.

7. Comparison of Normal Confining Stresses Determined from Different Shear Strength Prediction Equations

In this section, the LVECD program was used to compare the normal confining stress level determined using the shear strength values predicted from the equations proposed by Canestrari et al. (2013) and that determined from the shear strength prediction model equation (Equation (2)) developed in this study. Figure D.38 shows that the shear strength values determined from the Equation (2) developed in this study (shown in Figure D.38 (b)) are higher than the shear strength values determined from the Canestrari et al. (2013) equations (shown in Figure D.38 (a)). This result is due to the fact that Canestrari et al. (2013) equations were developed using the shear strength data from field cores, whereas Equation (2) was developed using the shear strengths measured from specimens fabricated under well controlled laboratory settings. Also, the properties of tack coat materials used in the two studies are different.

Figure D.38 presents that, although the shear strength values computed from the two different prediction models are quite different, the location of the MSR at the layer interface under the braking condition is the same. Moreover, the normal and shear stresses do not change between the two cases because identical pavement structures were used in the LVECD simulations. Consequently, the proper confining stress level derermined from the shear strength data measured in this study is the same as the one determined by the Canestrari et al. equations. It is also found that the range of confining stress to be used in the confined shear strength tests remains the same whether the shear strength equations proposed by Canestrari et al. (2013) are used or Equation (2) is used.

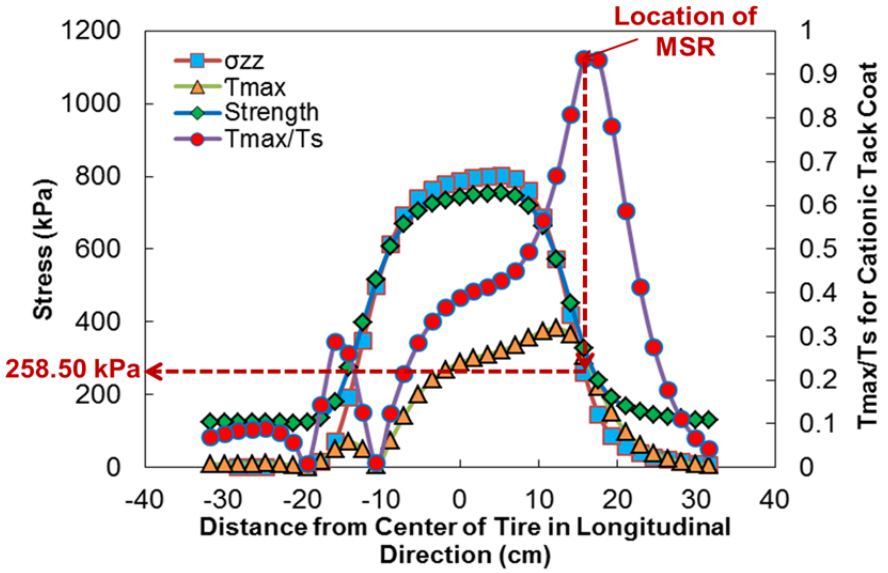

(a)

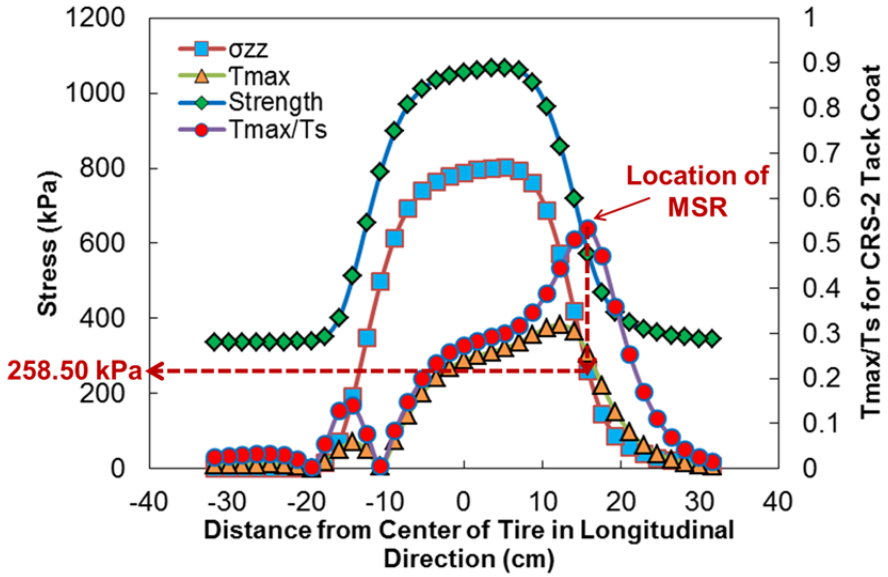

(b)

Figure D.38 Shear ratio, shear strength, and shear and normal stress levels in the longitudinal direction under the central axis of the tire at the layer interface: (a) normal confining stress as determined using the shear strength equations proposed by Canestrari et al. (2013) and (b) normal confining stress as determined using Equation (2) developed in this study. Conditions: thin pavement, 80 kN (18 kips), 40 km/hour (25 mph), 60°C, at 3.81 cm (1.5 in.) depth, braking condition (rolling resistance coefficient of 0.55).

8. Maximum Shear Ratios for Asphalt Concrete Layers with Different Tack Coat Materials at the Layer Interface

This section provides an analysis framework to evaluate the debonding potential at the asphalt concrete layer interface. This analysis framework includes procedures for the prediction of the interface shear strength using the model equation developed in this study, the calculation of the shear stress for the given conditions using the layered viscoelastic pavement analysis for critical distresses (LVECD) program, and the determination of the MSR as a shear failure criterion.

The asphalt concrete layers in the three pavement structures were assumed to be tacked using the four different tack coat materials, i.e., no tack coat, CRS-2, CRS-1h, and NTCRS-1hM emulsions, in order to evaluate the debonding potential at the layer interface under wheel loading. It is noted that the computational simulation conditions and parameters used in the LVECD program are identical to those used in the earlier simulations in this study, except that the material properties of the typical surface layer are substituted by the specific material properties used in the experimental tests of this study. The states of the stress and strain at the layer interface were analyzed for the various conditions using the LVECD program. Figure D.39 presents the normal and shear stress distributions at the layer interface under braking conditions, respectively, as determined from the LVECD program analysis.

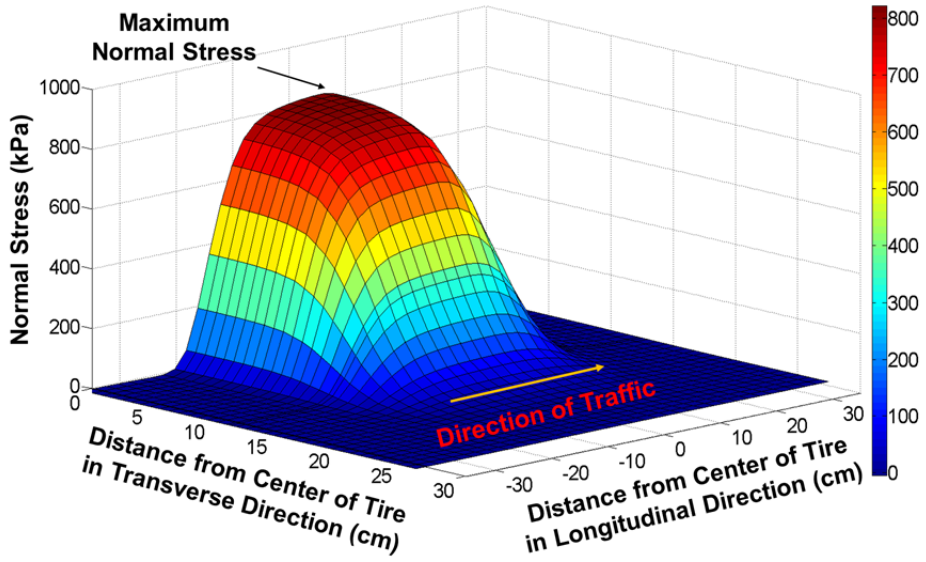

(a)

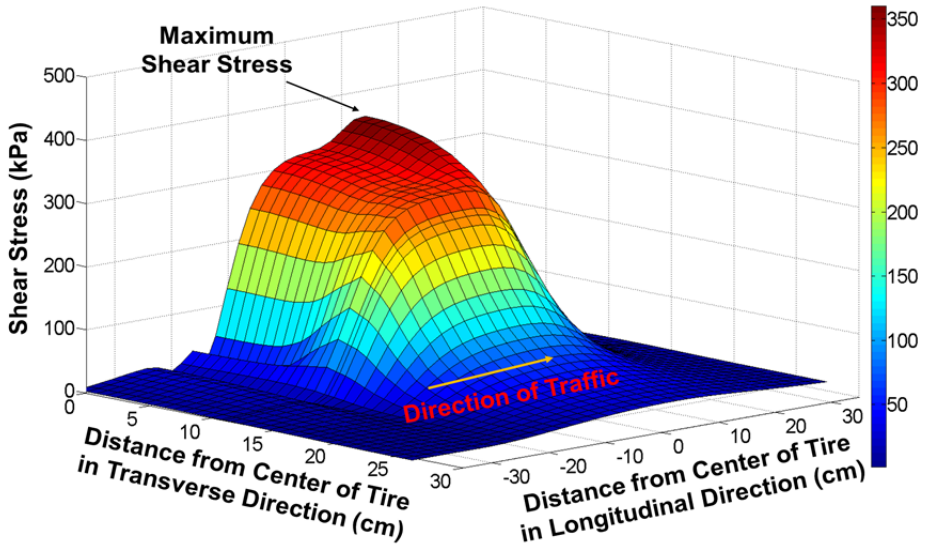

(b)

Figure D.39 Single tire stress distribution at the layer interface: (a) normal stress and (b) shear stress for thin pavement, 106.8 kN (24 kips), 8 km/hour (5 mph), 60°C, at 3.81 cm (1.5 in.) depth under braking condition. Note: The rolling resistance coefficient of 0.55 under the braking condition was used in the analysis.

Then, the shear bond strength levels (τ_s) for each point under consideration at the layer interface were computed from the prediction model equation developed in this research, which in turn enabled the prediction of the shear strength for an asphalt concrete layer with a specific tack coat material at the layer interface at any strain rate and temperature combination as well as at any normal confining stress. In other words, the shear bond strength levels (τ_s) at the layer interface with each tack coat material were computed using the shear strength prediction model equation, and the normal stress and shear strain rates determined from the LVECD program analysis, as presented in Figure D.40.

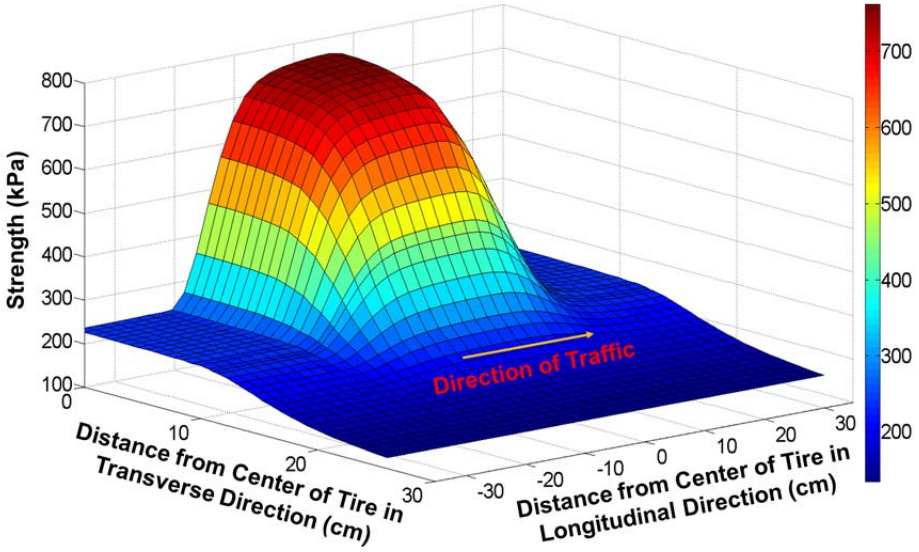

(a)

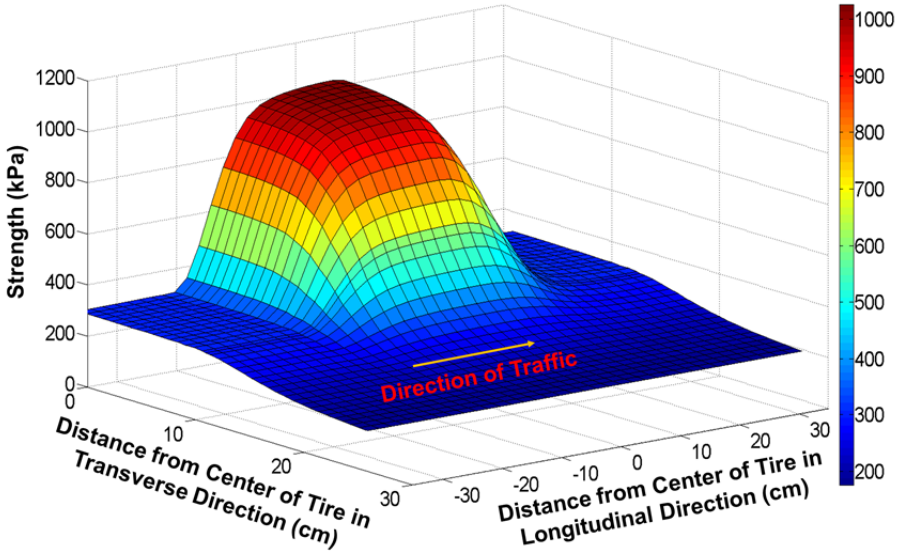

(b)

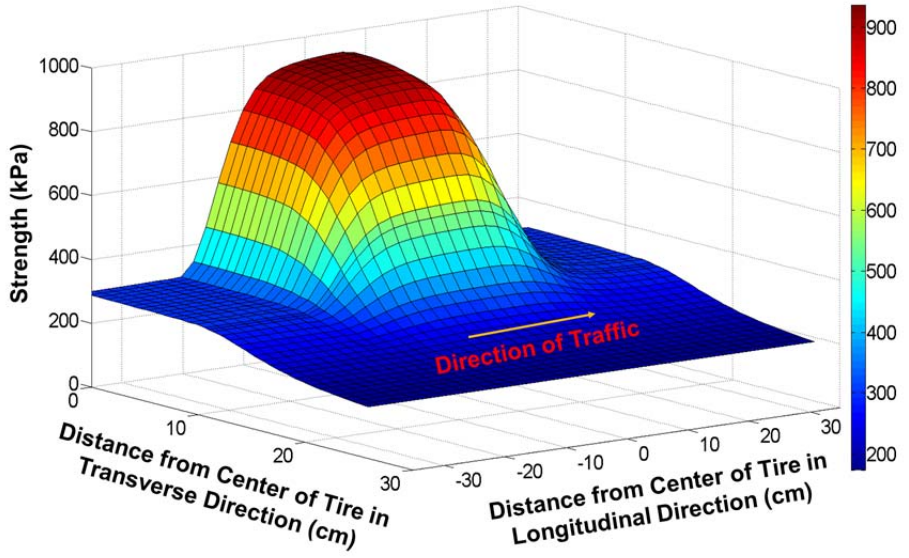

(c)

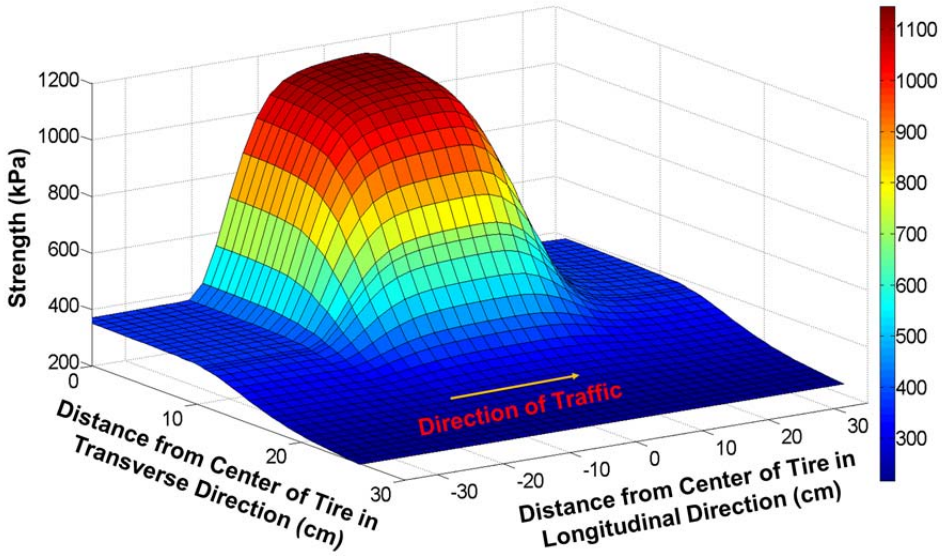

(d)

Figure D.40 Shear bond strength distribution at the layer interface: (a) no tack coat, (b) CRS-2 emulsion, (c) CRS-1h emulsion, and (d) NTCRS-1hM emulsion. Conditions: thin pavement, 106.8 kN (24 kips), 8 km/hour (5 mph), 60°C, at 3.81 cm (1.5 in.) depth under braking condition (rolling resistance coefficient of 0.55).

Lastly, a profile of the shear stress ratio, which is the ratio of the computed shear stress (τ_{max}) to the shear bond strength (τ_s) under the tire at the asphalt concrete layer interface, was determined to evaluate the MSR, which then could be used to determine the integrity of the interface bond.

Figure D.41 through Figure D.44 present example distributions of the shear ratios under the tire at the asphalt concrete layer interface for the different tack coat conditions. For all the conditions considered in this study, the MSR under the braking condition occurred right in front of the tire on the central longitudinal axis all the time, although the distance from the center of the tire imprint along the central longitudinal axis may vary slightly, as confirmed in Section 2.1.2. Moreover, the shear ratio contours shown in Figure D.41 through Figure D.44 indicate apparently that high shear ratios were observed to be around the front of the tire due to the braking force.

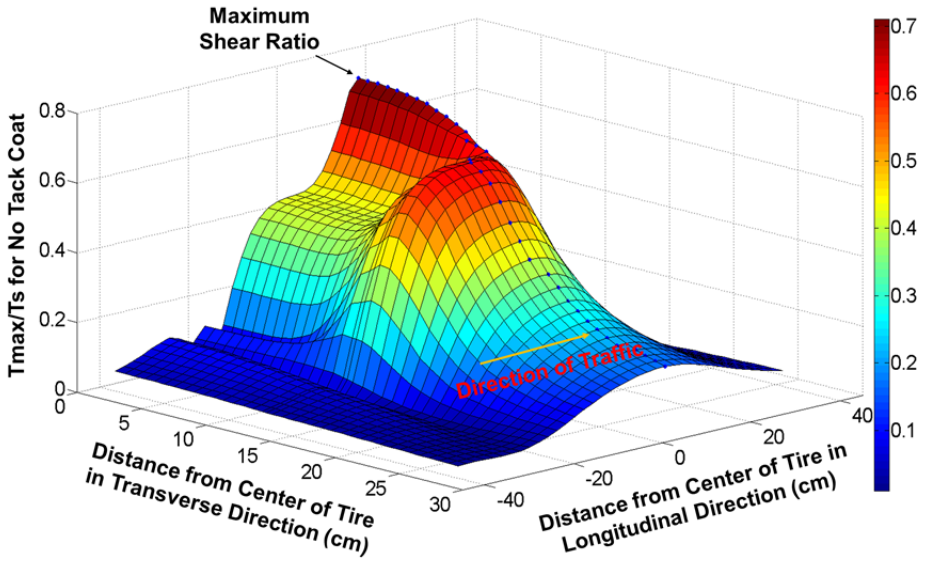

(a)

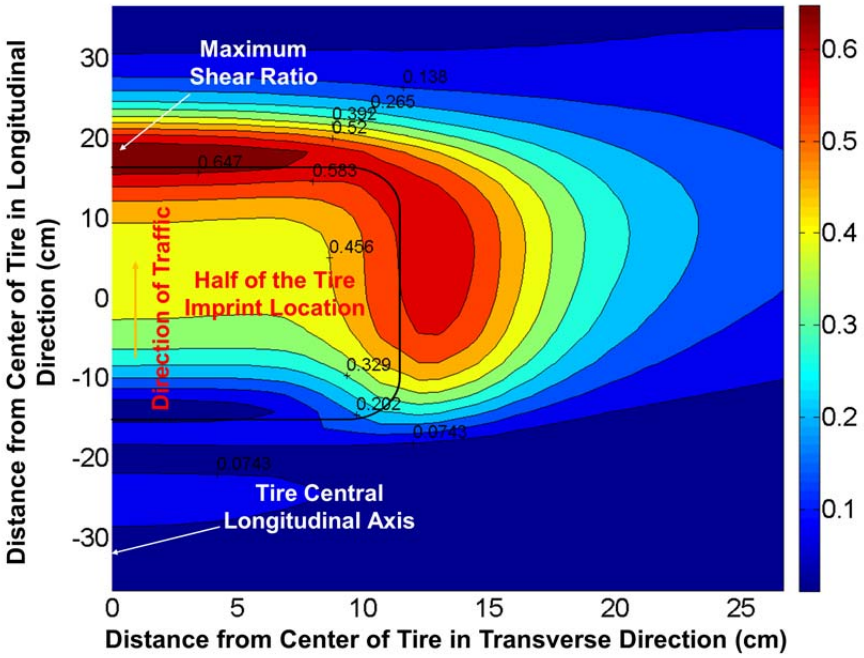

(b)

Figure D.41 (a) Shear ratio profile and (b) shear ratio contours under the tire at the layer interface. Conditions: thin pavement, 106.8 kN (24 kips) axle load, 8 km/hour (5 mph), 60°C, no tack coat, braking condition (rolling resistance coefficient of 0.55).

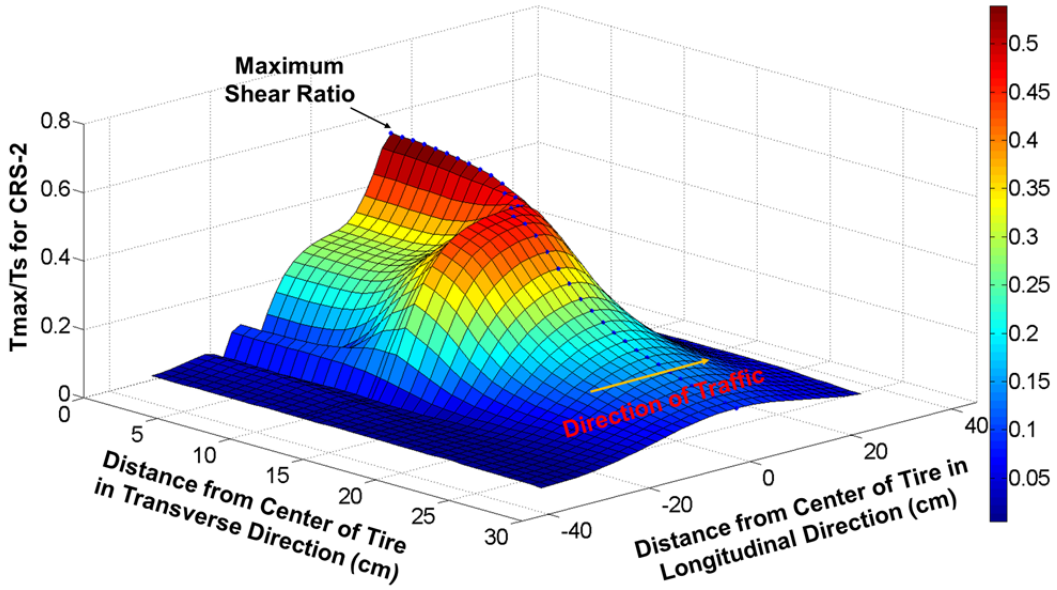

(a)

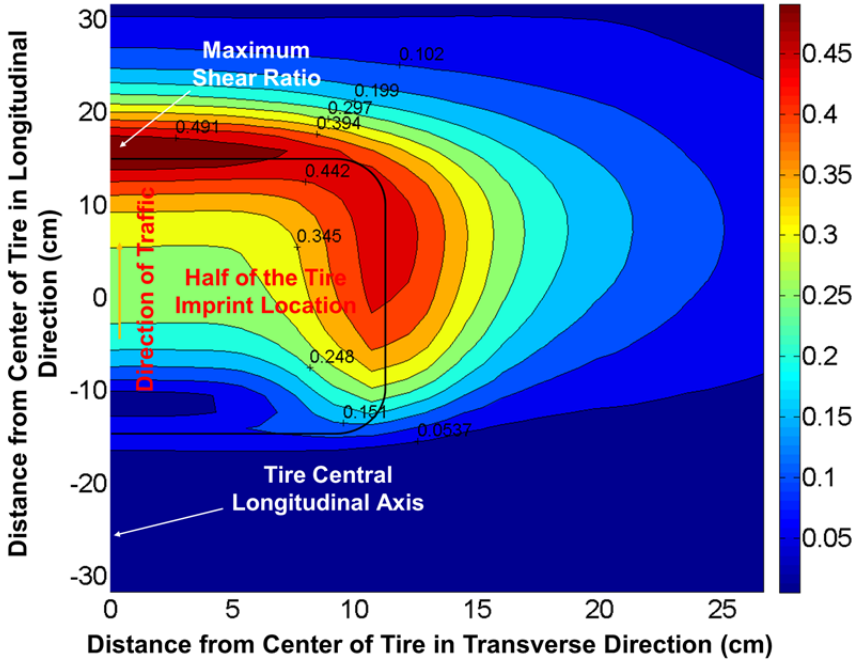

(b)

Figure D.42 (a) Shear ratio profile and (b) shear ratio contours under the tire at the layer interface. Conditions: intermediate pavement, 80 kN (18 kips) axle load, 40 km/hour (25 mph), 60°C, CRS-2, braking condition (rolling resistance coefficient of 0.55).

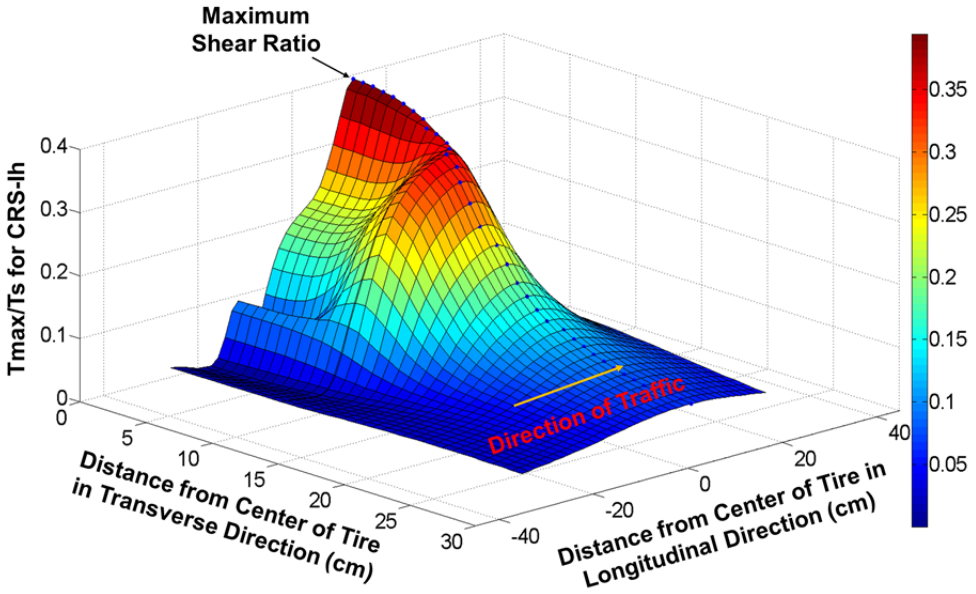

(a)

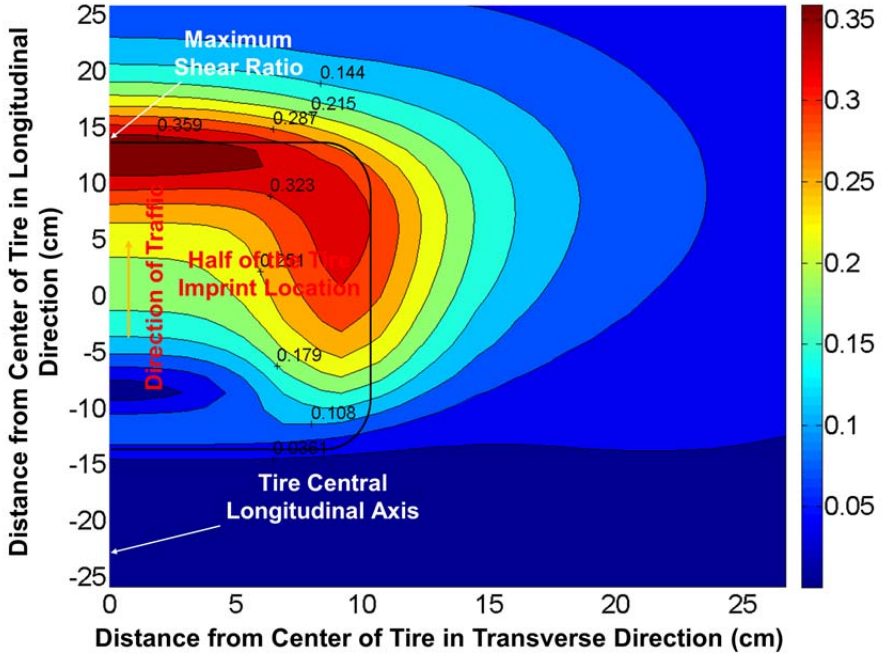

(b)

Figure D.43 (a) Shear ratio profile and (b) shear ratio contours under the tire at the layer interface. Conditions: thick pavement, 53.4 kN (12 kips) axle load, 88 km/hour (55 mph), 40°C, CRS-1h, braking condition (rolling resistance coefficient of 0.55).

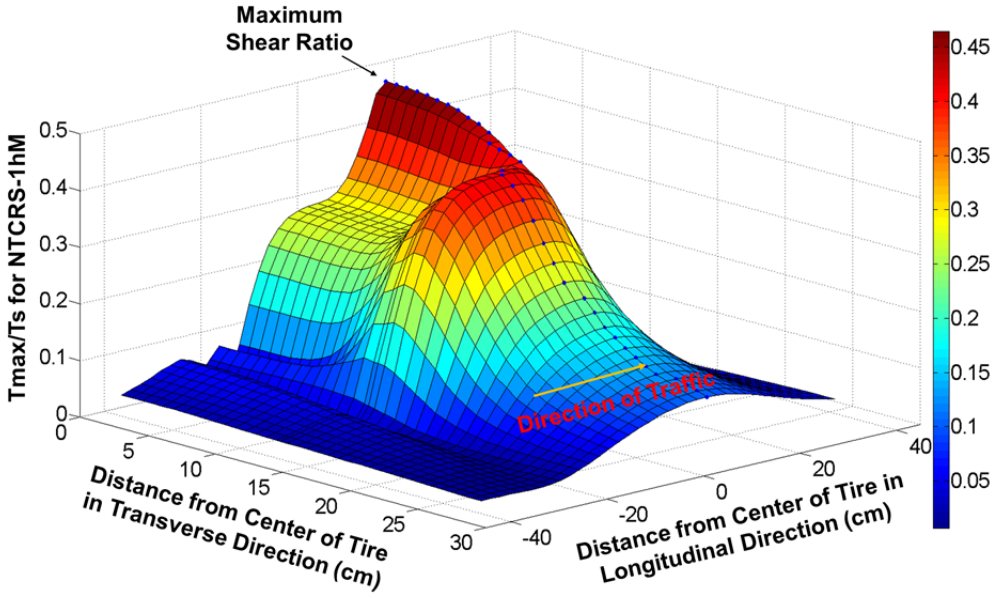

(a)

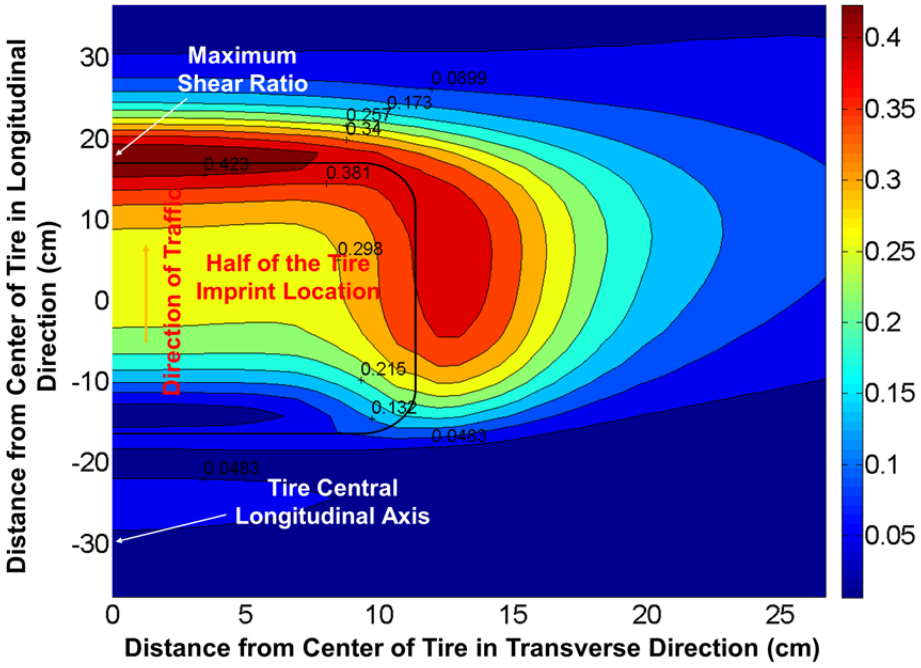

(b)

Figure D.44 (a) Shear ratio profile and (b) shear ratio contours under the tire at the layer interface. Conditions: thin pavement, 106.8 kN (24 kips) axle load, 8 km/hour (5 mph), 60°C, NTCRS-1hM, braking condition (rolling resistance coefficient of 0.55).

The MSRs for asphalt concrete layers with different tack coat materials at the layer interface under the 'only rolling' resistance coefficient of 0.55 for the braking condition are tabulated in Table D.12 through Table D.15. The rolling resistance coefficient of 0.55 was used because it provides the most critical shear stress values compared to the other coefficients under consideration (i.e., 0.35 and 0.45).

One noteworthy point that can be observed from Table D.12 through Table D.15 is that all the MSRs are less than 1.0, which indicates no shear failure at the asphalt concrete layer interface. However, this outcome does not fully represent the critical states under realistic loading conditions in service because the computational simulations performed in this research consider only one single braking action. The debonding distress in the field might occur under repeated braking conditions or at a single braking action, depending on the speed and weight of the vehicle. Therefore, a MSR that is close to 1.0 implies a much high potential for the interface debonding due to repeated braking between the asphalt concrete layers. Consequently, an asphalt concrete layer with no tack coat at the layer interface has a much higher potential for the interface debonding distress because it has higher MSR values than the other conditions in Table D.12 through Table D.15.

Figure D.45 through Figure D.56 show the MSRs for asphalt concrete layers with different tack coat materials at the layer interface for different temperatures, speed levels, axle loads, and pavement structures. In the legends of these figures, the first number is the vehicle speed, the second number is the axle load, and the third notation is the thickness of the asphalt pavement (*TN*, *I*, and *TK* refer to thin, intermediate, and thick pavement structures, respectively). According to the MSR results presented in these figures, a slower speed clearly corresponds to a higher shear ratio. That is, although both the shear stress and shear strength values increase as the vehicle speed increases, the shear ratio could be higher at a slower speed than at a faster speed because the rate of reduction in shear strength as the speed decreases is much greater than that of shear stress. Also, the MSR increases with an increase in temperature. Moreover, as the axle load increases, the MSR increases as well. It should be noted that these figures indicate that the higher temperature, lower speed, and heavier axle load are critical conditions with respect to the debonding distress at the asphalt concrete layer interface. Furthermore, the thin pavement structure shows higher MSR values and therefore is more vulnerable to the interface debonding distress than the other structures, except for the case of 60°C. Table D.12 through Table D.15 indicate that in the MSR comparisons for the different structure types, the MSR deceases except for the case of 60°C, as shown in Figure D.57 (a). This result is due to the fact that the effect of the different structure types in terms of stress gradually diminishes with an increase in temperature; thus, this effect is not clear, especially at 60°C, as shown in Figure D.57 (c). Moreover, in contrast to the other temperatures, at 60°C the magnitude of the shear stress at the location of the MSR in the thin pavement is even less than it is in the thick pavement.

As aforementioned in Section 4.3.3 of this appendix, the NTCRS-1hM (trackless tack coat) emulsion has the highest shear strength of all the emulsion types, thereby obtaining a better bond at the layer interface than the other emulsions. Consequently, all the pavement structures with the NTCRS-1hM emulsion at the asphalt concrete layer interface as a tack coat exhibited better resistance to debonding with lower MSRs than the pavements with the

other tack coat conditions, as expected. Therefore, Figure D.45 through Figure D.56 indicate that a high quality tack coat could reduce the possibility of the debonding distress and they also confirm the need for a tack coat between the asphalt structural layers.

Table D.12 Maximum shear ratios for no tack coat condition at the asphalt concrete layer interface.

Maximum Shear Ratio	Thin Pavement								
Temperature (°C)	53.4 kN (12 kips)			80 kN (18 kips)			106.8 kN (24 kips)		
	8 km/hr (5 mph)	40 km/hr (25 mph)	88 km/hr (55 mph)	8 km/hr (5 mph)	40 km/hr (25 mph)	88 km/hr (55 mph)	8 km/hr (5 mph)	40 km/hr (25 mph)	88 km/hr (55 mph)
5	0.30160	0.26300	0.21190	0.37870	0.31870	0.24540	0.43650	0.36100	0.30930
20	0.50460	0.41170	0.38000	0.59380	0.49360	0.45210	0.65820	0.61190	0.51140
40	0.60690	0.57490	0.56620	0.62650	0.61280	0.60450	0.67910	0.66850	0.65010
60	0.62710	0.61720	0.59720	0.64280	0.63710	0.62760	0.71070	0.69940	0.68760
Maximum Shear Ratio	Intermediate Pavement								
Temperature (°C)	53.4 kN (12 kips)			80 kN (18 kips)			106.8 kN (24 kips)		
	8 km/hr (5 mph)	40 km/hr (25 mph)	88 km/hr (55 mph)	8 km/hr (5 mph)	40 km/hr (25 mph)	88 km/hr (55 mph)	8 km/hr (5 mph)	40 km/hr (25 mph)	88 km/hr (55 mph)
5	0.23610	0.20230	0.15720	0.26560	0.22680	0.18110	0.30570	0.25350	0.20180
20	0.41120	0.35340	0.29960	0.45620	0.39390	0.33170	0.50950	0.43910	0.37160
40	0.59150	0.54490	0.52220	0.62660	0.58960	0.56520	0.68970	0.65250	0.62590
60	0.64810	0.63850	0.61150	0.66750	0.65890	0.64840	0.73750	0.72850	0.71630
Maximum Shear Ratio	Thick Pavement								
Temperature (°C)	53.4 kN (12 kips)			80 kN (18 kips)			106.8 kN (24 kips)		
	8 km/hr (5 mph)	40 km/hr (25 mph)	88 km/hr (55 mph)	8 km/hr (5 mph)	40 km/hr (25 mph)	88 km/hr (55 mph)	8 km/hr (5 mph)	40 km/hr (25 mph)	88 km/hr (55 mph)
5	0.20900	0.17390	0.13590	0.22380	0.18620	0.15230	0.24370	0.20170	0.16390
20	0.34980	0.29740	0.25450	0.37210	0.31670	0.27060	0.40470	0.34740	0.29950
40	0.55480	0.49460	0.46650	0.58200	0.52440	0.49280	0.63870	0.57400	0.53870
60	0.66380	0.64690	0.62480	0.68750	0.66990	0.65710	0.76200	0.75150	0.74180

Table D.13 Maximum shear ratios for CRS-2 emulsion condition at the asphalt concrete layer interface.

Maximum Shear Ratio	Thin Pavement								
Temperature (°C)	53.4 kN (12 kips)			80 kN (18 kips)			106.8 kN (24 kips)		
	8 km/hr (5 mph)	40 km/hr (25 mph)	88 km/hr (55 mph)	8 km/hr (5 mph)	40 km/hr (25 mph)	88 km/hr (55 mph)	8 km/hr (5 mph)	40 km/hr (25 mph)	88 km/hr (55 mph)
5	0.23860	0.20770	0.16950	0.29990	0.25350	0.19680	0.33990	0.28350	0.24250
20	0.39610	0.32340	0.29890	0.46690	0.38820	0.35600	0.50030	0.46790	0.39400
40	0.48540	0.45490	0.44660	0.50130	0.48540	0.47720	0.50990	0.50240	0.48920
60	0.51940	0.50540	0.48430	0.53200	0.52210	0.51050	0.53790	0.52770	0.51790
Maximum Shear Ratio	Intermediate Pavement								
Temperature (°C)	53.4 kN (12 kips)			80 kN (18 kips)			106.8 kN (24 kips)		
	8 km/hr (5 mph)	40 km/hr (25 mph)	88 km/hr (55 mph)	8 km/hr (5 mph)	40 km/hr (25 mph)	88 km/hr (55 mph)	8 km/hr (5 mph)	40 km/hr (25 mph)	88 km/hr (55 mph)
5	0.18520	0.15760	0.12180	0.20910	0.17740	0.14040	0.23470	0.19370	0.15350
20	0.32290	0.27680	0.23460	0.35880	0.30920	0.26040	0.38650	0.33480	0.28490
40	0.47610	0.43440	0.41470	0.50390	0.46990	0.44890	0.51980	0.49190	0.47210
60	0.53610	0.52380	0.49740	0.55170	0.53950	0.52800	0.55880	0.55070	0.54080
Maximum Shear Ratio	Thick Pavement								
Temperature (°C)	53.4 kN (12 kips)			80 kN (18 kips)			106.8 kN (24 kips)		
	8 km/hr (5 mph)	40 km/hr (25 mph)	88 km/hr (55 mph)	8 km/hr (5 mph)	40 km/hr (25 mph)	88 km/hr (55 mph)	8 km/hr (5 mph)	40 km/hr (25 mph)	88 km/hr (55 mph)
5	0.16070	0.13370	0.10490	0.17220	0.14330	0.11750	0.18080	0.15070	0.12350
20	0.27460	0.23270	0.19720	0.29260	0.24840	0.20960	0.30650	0.26070	0.22240
40	0.44660	0.39440	0.37060	0.46820	0.41820	0.39160	0.48180	0.43280	0.40640
60	0.54920	0.53180	0.51070	0.56780	0.54930	0.53690	0.57760	0.56890	0.56110

Table D.14 Maximum shear ratios for CRS-1h emulsion condition at the asphalt concrete layer interface.

Maximum Shear Ratio	Thin Pavement								
Temperature (°C)	53.4 kN (12 kips)			80 kN (18 kips)			106.8 kN (24 kips)		
	8 km/hr (5 mph)	40 km/hr (25 mph)	88 km/hr (55 mph)	8 km/hr (5 mph)	40 km/hr (25 mph)	88 km/hr (55 mph)	8 km/hr (5 mph)	40 km/hr (25 mph)	88 km/hr (55 mph)
5	0.24980	0.21790	0.17660	0.27710	0.26440	0.20460	0.35490	0.29530	0.25280
20	0.41880	0.34060	0.31430	0.49280	0.40820	0.37380	0.52750	0.49190	0.41310
40	0.51770	0.48420	0.47480	0.53380	0.51600	0.50670	0.54200	0.53330	0.51890
60	0.55360	0.53910	0.51680	0.56550	0.55550	0.54350	0.57060	0.56030	0.55020
Maximum Shear Ratio	Intermediate Pavement								
Temperature (°C)	53.4 kN (12 kips)			80 kN (18 kips)			106.8 kN (24 kips)		
	8 km/hr (5 mph)	40 km/hr (25 mph)	88 km/hr (55 mph)	8 km/hr (5 mph)	40 km/hr (25 mph)	88 km/hr (55 mph)	8 km/hr (5 mph)	40 km/hr (25 mph)	88 km/hr (55 mph)
5	0.19530	0.16720	0.13010	0.21980	0.18750	0.14980	0.24610	0.20370	0.16320
20	0.34270	0.29320	0.24810	0.37950	0.32650	0.27440	0.40780	0.35250	0.29950
40	0.50680	0.46220	0.44110	0.53500	0.49850	0.47610	0.55080	0.52070	0.49960
60	0.57030	0.55750	0.52950	0.58550	0.57280	0.56070	0.59190	0.58350	0.57320
Maximum Shear Ratio	Thick Pavement								
Temperature (°C)	53.4 kN (12 kips)			80 kN (18 kips)			106.8 kN (24 kips)		
	8 km/hr (5 mph)	40 km/hr (25 mph)	88 km/hr (55 mph)	8 km/hr (5 mph)	40 km/hr (25 mph)	88 km/hr (55 mph)	8 km/hr (5 mph)	40 km/hr (25 mph)	88 km/hr (55 mph)
5	0.17300	0.14370	0.11240	0.18530	0.15390	0.12590	0.19450	0.16170	0.13210
20	0.29180	0.24740	0.21160	0.30990	0.26370	0.22510	0.32380	0.27590	0.23830
40	0.47530	0.41980	0.39440	0.4968	0.44360	0.41530	0.51010	0.45810	0.43000
60	0.58380	0.56550	0.54330	0.60220	0.58270	0.56960	0.61130	0.60220	0.59400

Table D.15 Maximum shear ratios for NTCRS-1hM (Trackless) emulsion condition at the asphalt concrete layer interface.

Maximum Shear Ratio	Thin Pavement								
Temperature (°C)	53.4 kN (12 kips)			80 kN (18 kips)			106.8 kN (24 kips)		
	8 km/hr (5 mph)	40 km/hr (25 mph)	88 km/hr (55 mph)	8 km/hr (5 mph)	40 km/hr (25 mph)	88 km/hr (55 mph)	8 km/hr (5 mph)	40 km/hr (25 mph)	88 km/hr (55 mph)
5	0.21280	0.18630	0.15180	0.23580	0.22560	0.17580	0.30120	0.25190	0.21640
20	0.35120	0.28760	0.26600	0.41260	0.34400	0.31590	0.44150	0.41310	0.34890
40	0.42760	0.40220	0.39530	0.44060	0.42820	0.42160	0.44710	0.44230	0.43160
60	0.45160	0.44140	0.42460	0.46090	0.45430	0.44570	0.46480	0.45800	0.45080
Maximum Shear Ratio	Intermediate Pavement								
Temperature (°C)	53.4 kN (12 kips)			80 kN (18 kips)			106.8 kN (24 kips)		
	8 km/hr (5 mph)	40 km/hr (25 mph)	88 km/hr (55 mph)	8 km/hr (5 mph)	40 km/hr (25 mph)	88 km/hr (55 mph)	8 km/hr (5 mph)	40 km/hr (25 mph)	88 km/hr (55 mph)
5	0.16640	0.14310	0.11210	0.18680	0.16040	0.12890	0.20870	0.17420	0.14040
20	0.28660	0.24640	0.20950	0.31720	0.27410	0.23160	0.34070	0.29590	0.25250
40	0.41730	0.38220	0.36550	0.44030	0.41210	0.39430	0.45310	0.43020	0.41360
60	0.46510	0.45580	0.43420	0.47710	0.46820	0.45920	0.48200	0.47660	0.46900
Maximum Shear Ratio	Thick Pavement								
Temperature (°C)	53.4 kN (12 kips)			80 kN (18 kips)			106.8 kN (24 kips)		
	8 km/hr (5 mph)	40 km/hr (25 mph)	88 km/hr (55 mph)	8 km/hr (5 mph)	40 km/hr (25 mph)	88 km/hr (55 mph)	8 km/hr (5 mph)	40 km/hr (25 mph)	88 km/hr (55 mph)
5	0.14730	0.12300	0.09680	0.15770	0.13160	0.10820	0.16540	0.13820	0.11360
20	0.24400	0.20830	0.17910	0.25890	0.22200	0.19040	0.27040	0.23220	0.20140
40	0.39120	0.34700	0.32670	0.4087	0.36660	0.34390	0.41940	0.37830	0.35590
60	0.47600	0.46200	0.44460	0.49060	0.47580	0.46570	0.49780	0.49130	0.48500

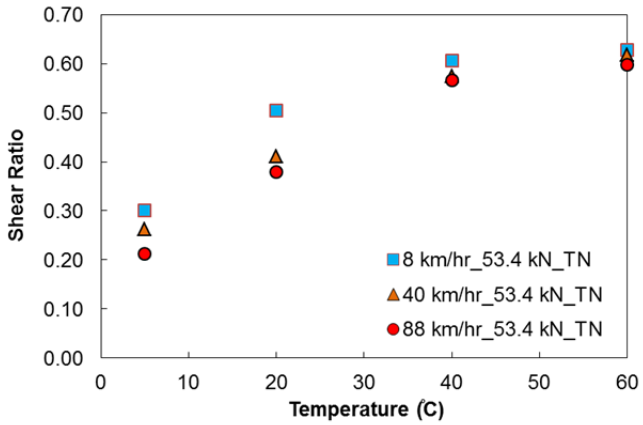

(a)

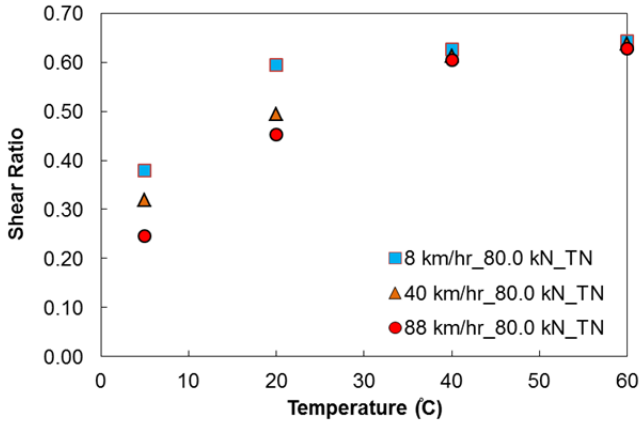

(b)

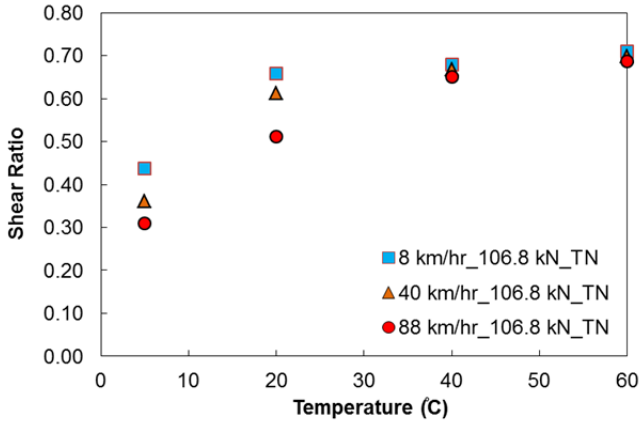

(c)

Figure D.45 Maximum shear ratios for no tack coat condition at the asphalt concrete layer interface for thin pavement structure: (a) 53.4-kN (12-kip) axle load, (b) 80-kN (18-kip) axle load, and (c) 106.8-kN (24-kip) axle load.

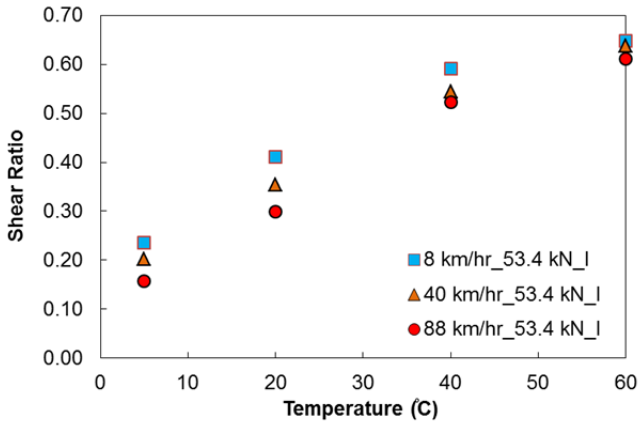

(a)

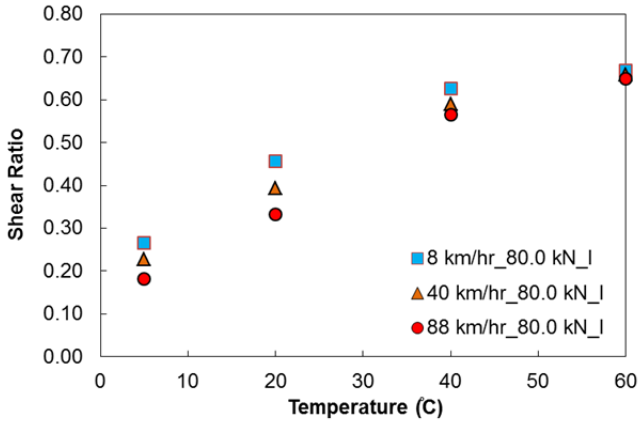

(b)

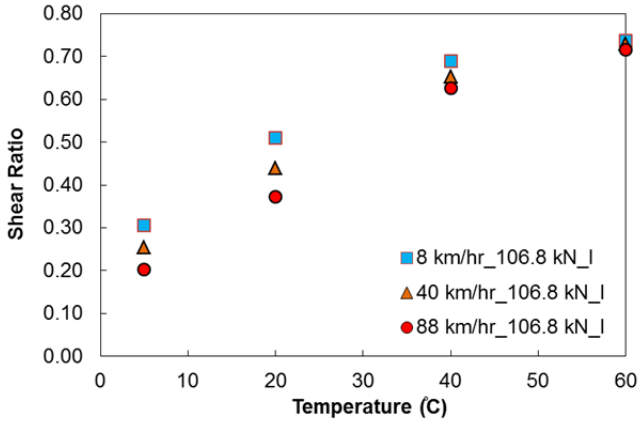

(c)

Figure D.46 Maximum shear ratios for no tack coat condition at the asphalt concrete layer interface for intermediate pavement structure: (a) 53.4-kN (12-kip) axle load, (b) 80-kN (18-kip) axle load, and (c) 106.8-kN (24-kip) axle load.

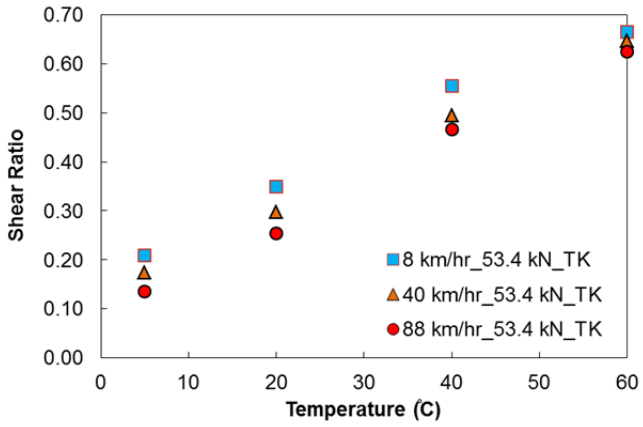

(a)

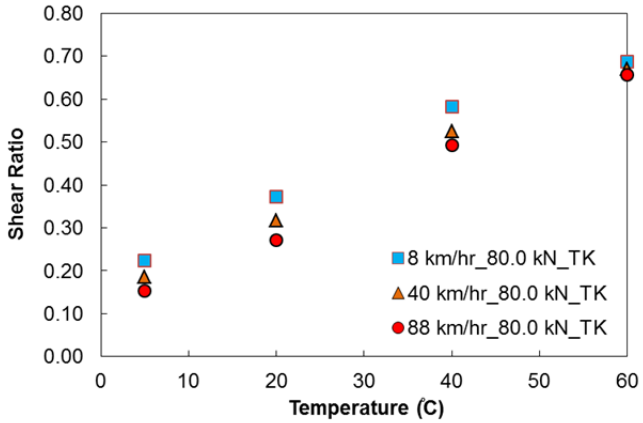

(b)

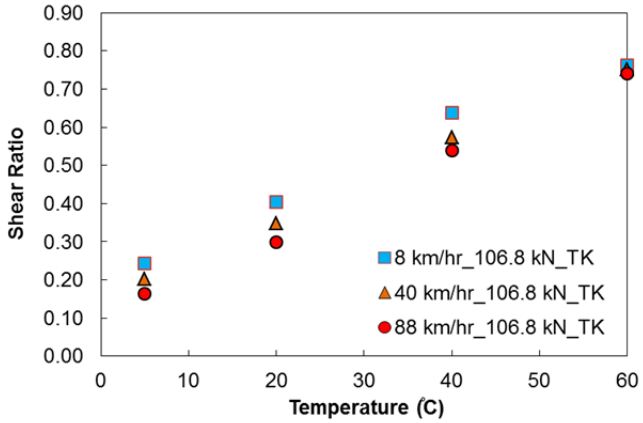

(c)

Figure D.47 Maximum shear ratios for no tack coat condition at the asphalt concrete layer interface for thick pavement structure: (a) 53.4-kN (12-kip) axle load, (b) 80-kN (18-kip) axle load, and (c) 106.8-kN (24-kip) axle load.

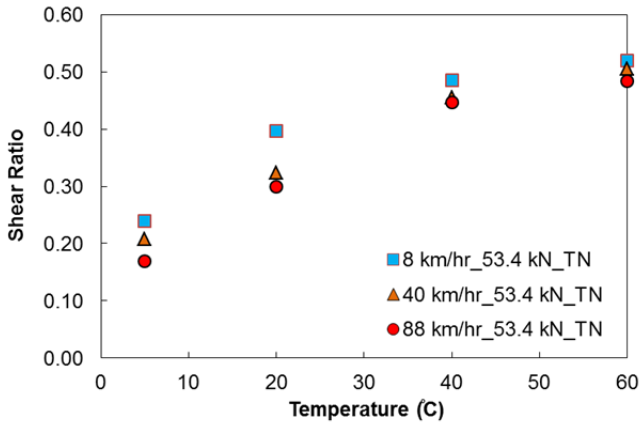

(a)

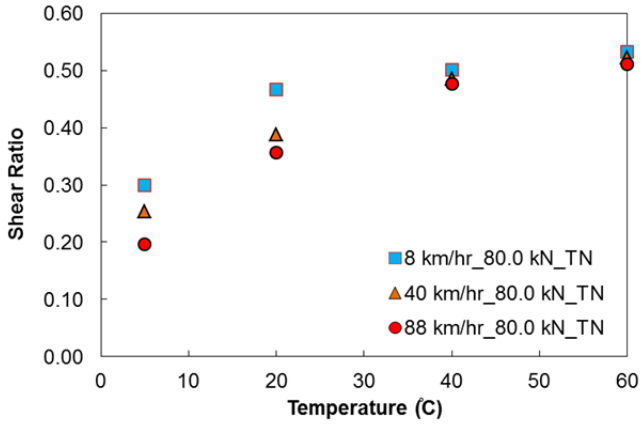

(b)

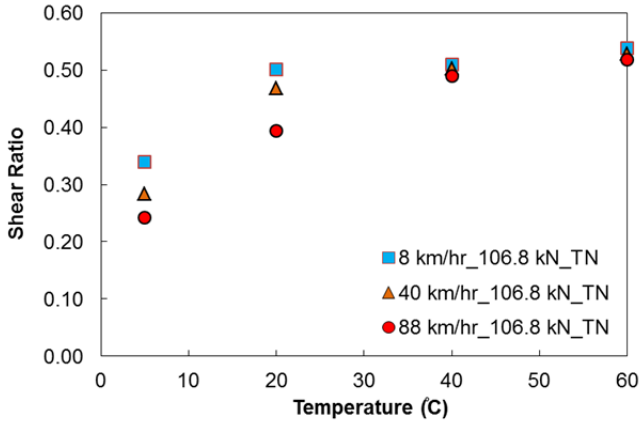

(c)

Figure D.48 Maximum shear ratios for CRS-2 emulsion condition at the asphalt concrete layer interface for thin pavement structure: (a) 53.4-kN (12-kip) axle load, (b) 80-kN (18-kip) axle load, and (c) 106.8-kN (24-kip) axle load.

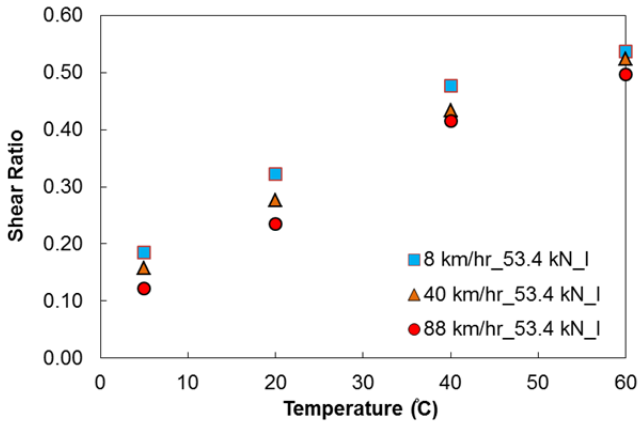

(a)

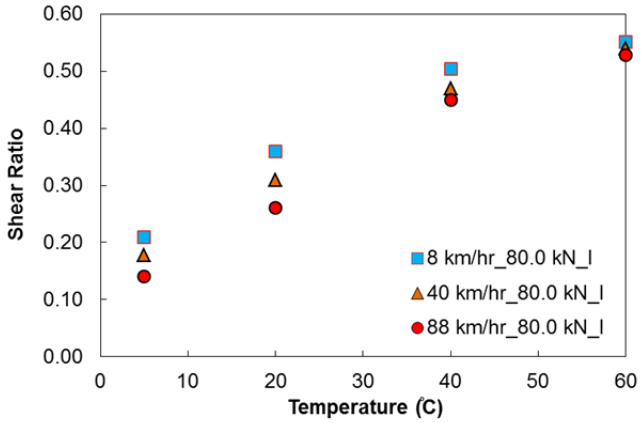

(b)

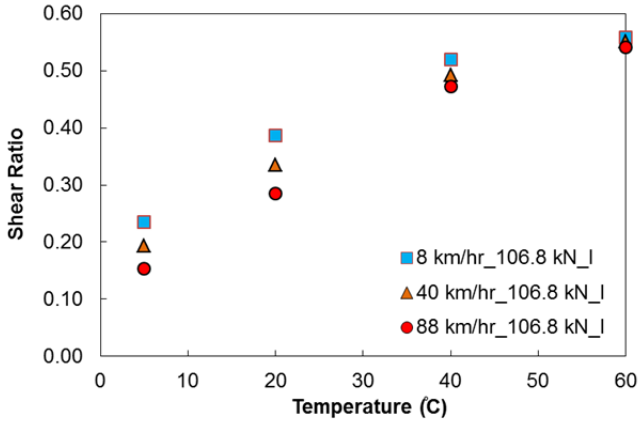

(c)

Figure D.49 Maximum shear ratios for CRS-2 emulsion condition at the asphalt concrete layer interface for intermediate pavement structure: (a) 53.4-kN (12-kip) axle load, (b) 80-kN (18-kip) axle load, and (c) 106.8-kN (24-kip) axle load.

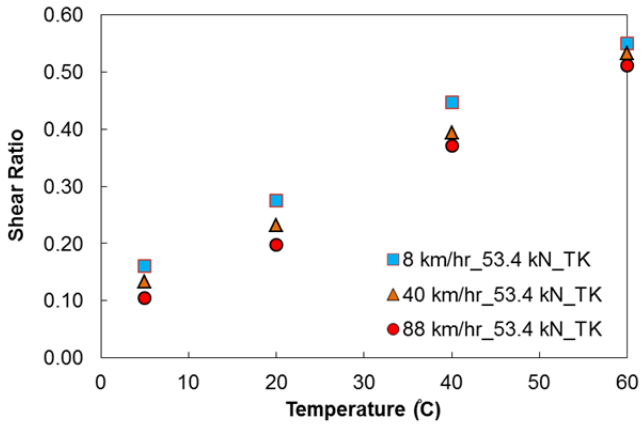

(a)

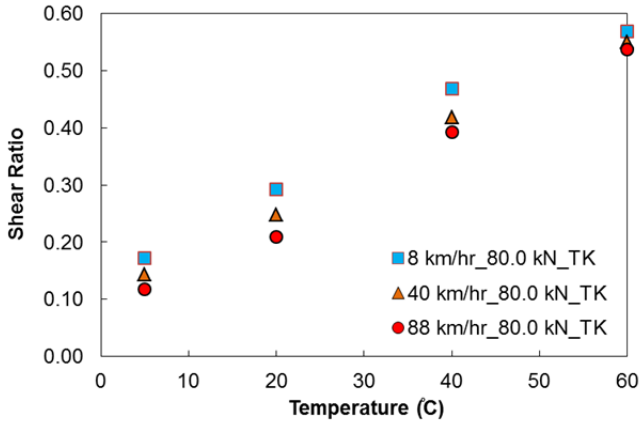

(b)

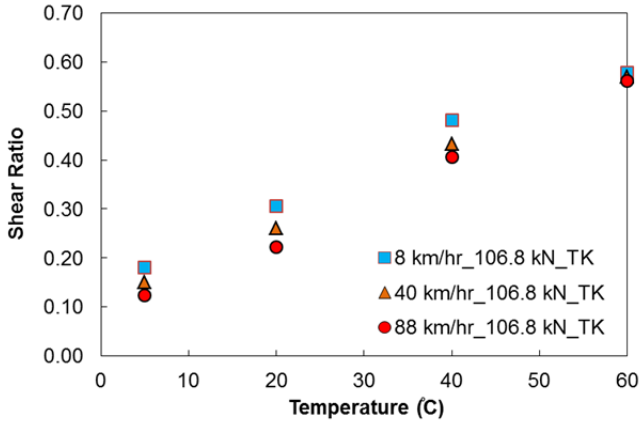

(c)

Figure D.50 Maximum shear ratios for CRS-2 emulsion condition at the asphalt concrete layer interface for thick pavement structure: (a) 53.4-kN (12-kip) axle load, (b) 80-kN (18-kip) axle load, and (c) 106.8-kN (24-kip) axle load.

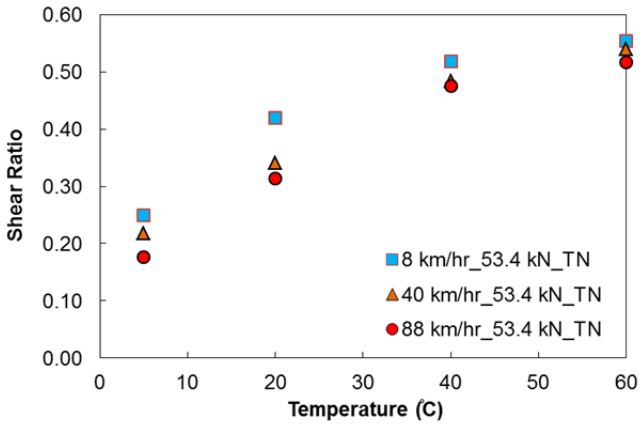

(a)

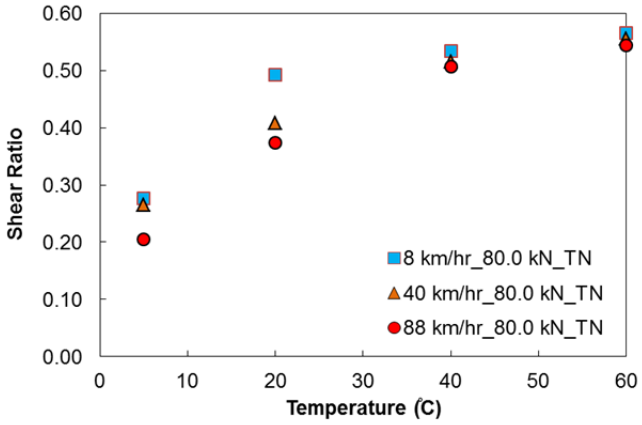

(b)

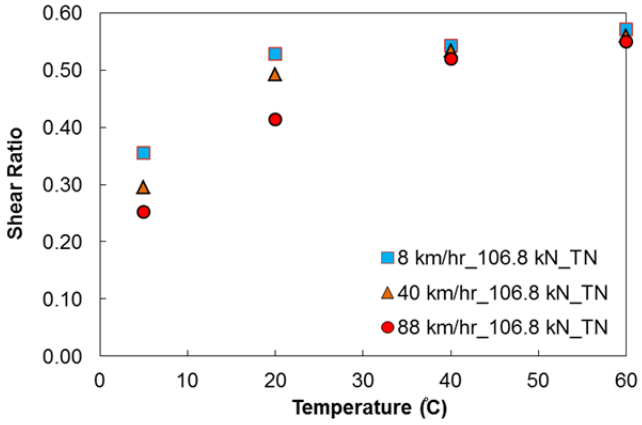

(c)

Figure D.51 Maximum shear ratios for CRS-1h emulsion condition at the asphalt concrete layer interface for thin pavement structure: (a) 53.4-kN (12-kip) axle load, (b) 80-kN (18-kip) axle load, and (c) 106.8-kN (24-kip) axle load.

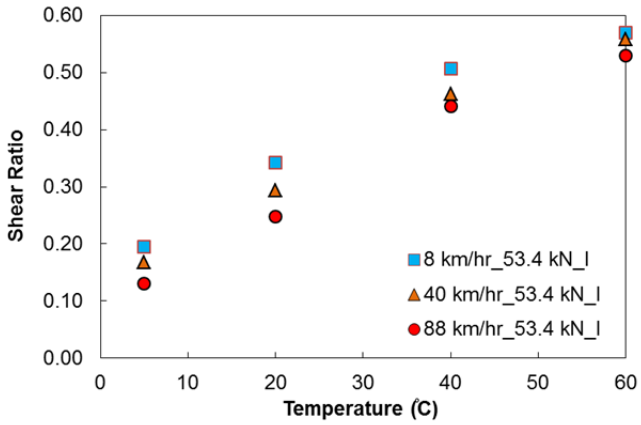

(a)

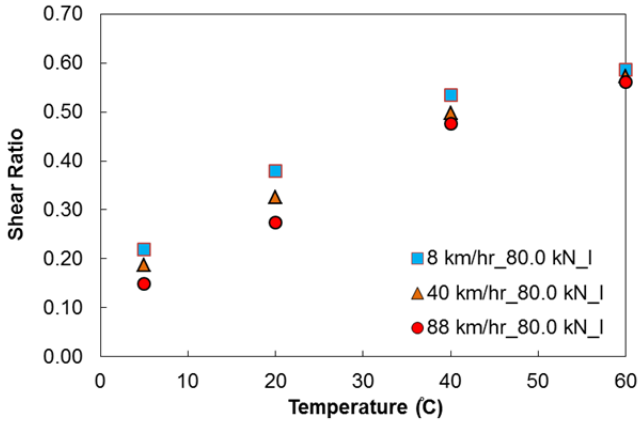

(b)

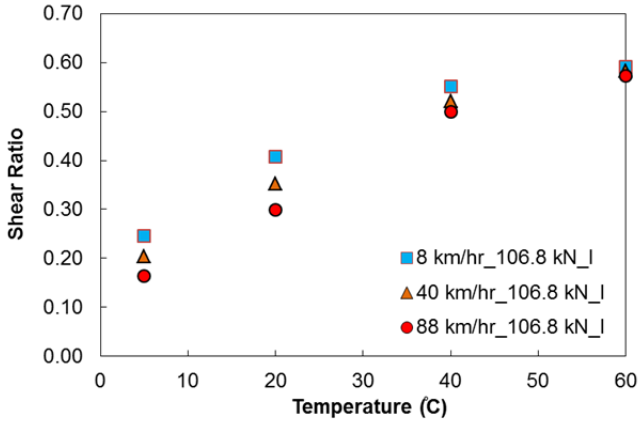

(c)

Figure D.52 Maximum shear ratios for CRS-1h emulsion condition at the asphalt concrete layer interface for intermediate pavement structure: (a) 53.4-kN (12-kip) axle load, (b) 80-kN (18-kip) axle load, and (c) 106.8-kN (24-kip) axle load.

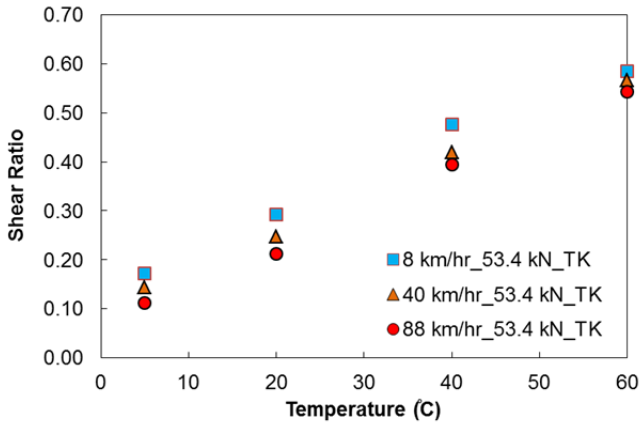

(a)

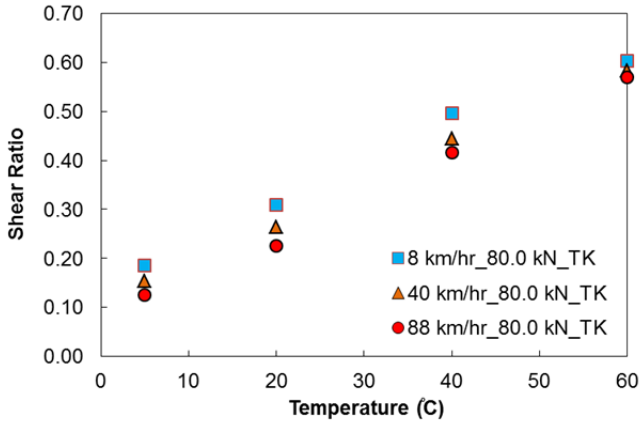

(b)

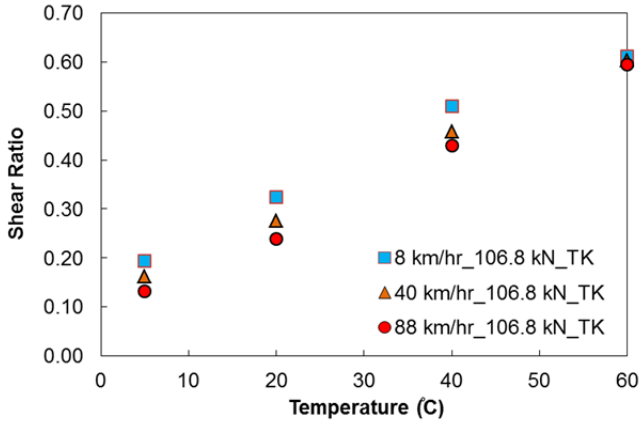

(c)

Figure D.53 Maximum shear ratios for CRS-1h emulsion condition at the asphalt concrete layer interface for thick pavement structure: (a) 53.4-kN (12-kip) axle load, (b) 80-kN (18-kip) axle load, and (c) 106.8-kN (24-kip) axle load.

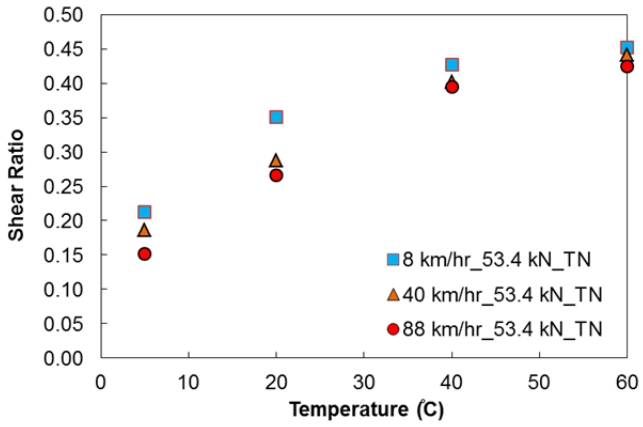

(a)

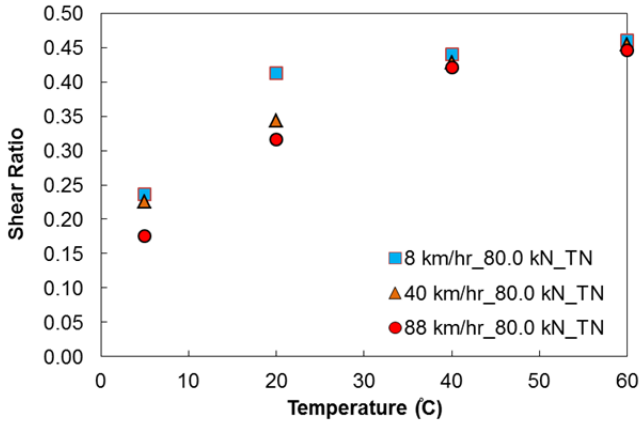

(b)

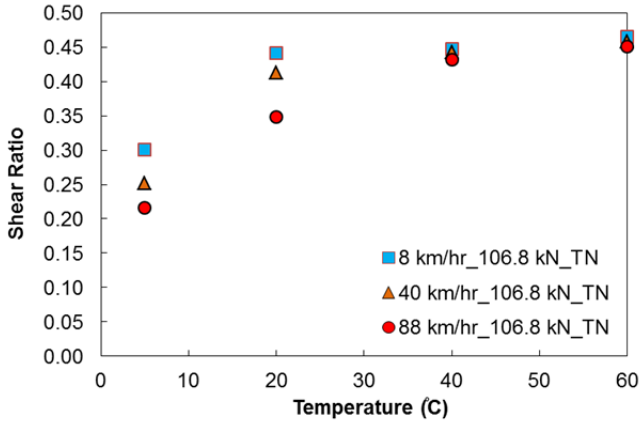

(c)

Figure D.54 Maximum shear ratios for NTCRS-1hM (Trackless) emulsion condition at the asphalt concrete layer interface for thin pavement structure: (a) 53.4-kN (12-kip) axle load, (b) 80-kN (18-kip) axle load, and (c) 106.8-kN (24-kip) axle load.

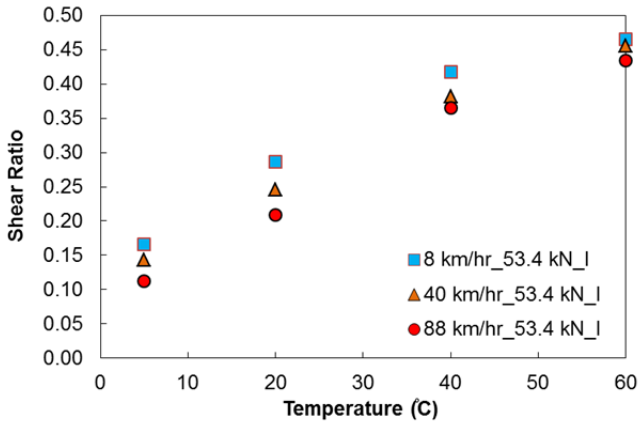

(a)

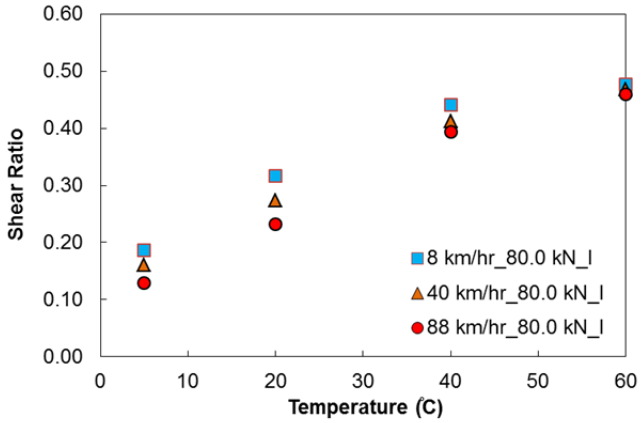

(b)

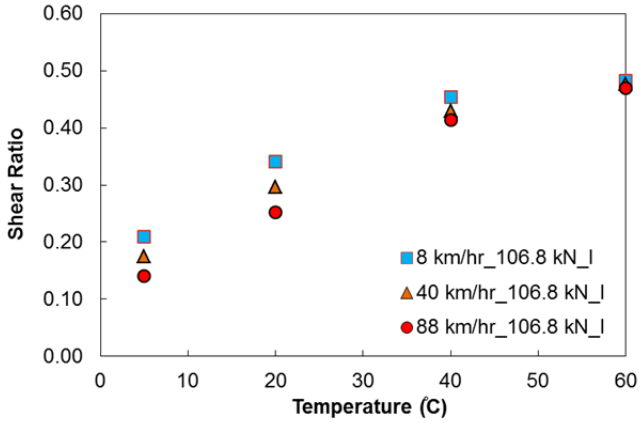

(c)

Figure D.55 Maximum shear ratios for NTCRS-1hM (Trackless) emulsion condition at the asphalt concrete layer interface intermediate pavement structure: (a) 53.4-kN (12-kip) axle load, (b) 80-kN (18-kip) axle load, and (c) 106.8-kN (24-kip) axle load.

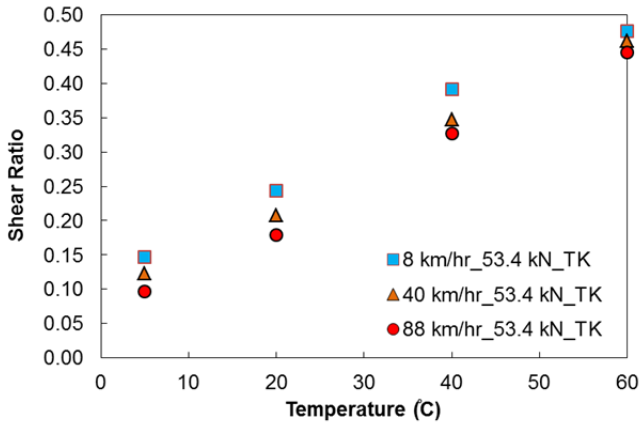

(a)

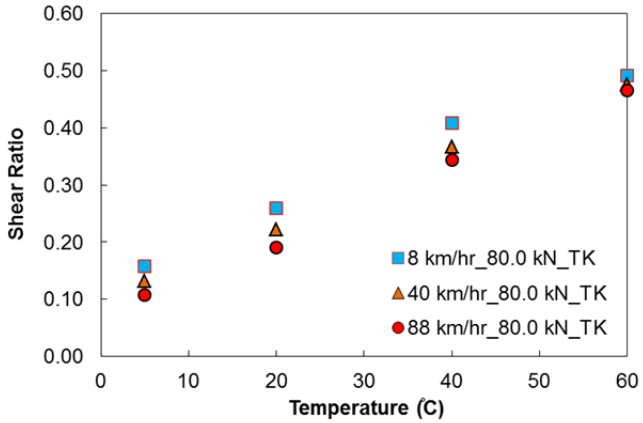

(b)

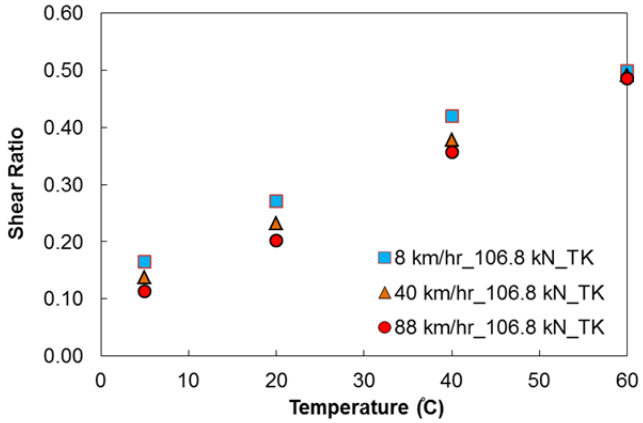

(c)

Figure D.56 Maximum shear ratios for NTCRS-1hM (Trackless) emulsion condition at the asphalt concrete layer interface for thick pavement structure: (a) 53.4-kN (12-kip) axle load, (b) 80-kN (18-kip) axle load, and (c) 106.8-kN (24-kip) axle load.

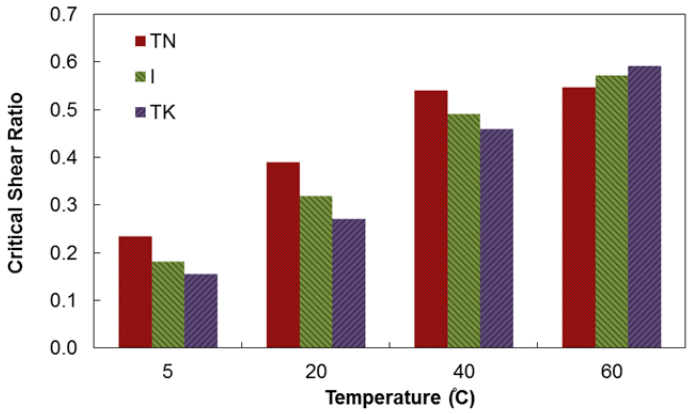

(a)

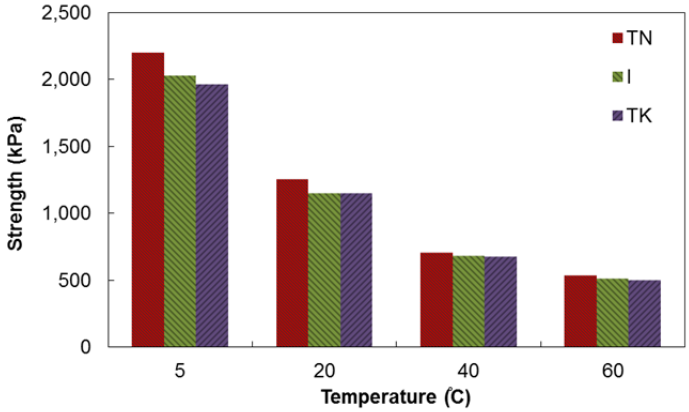

(b)

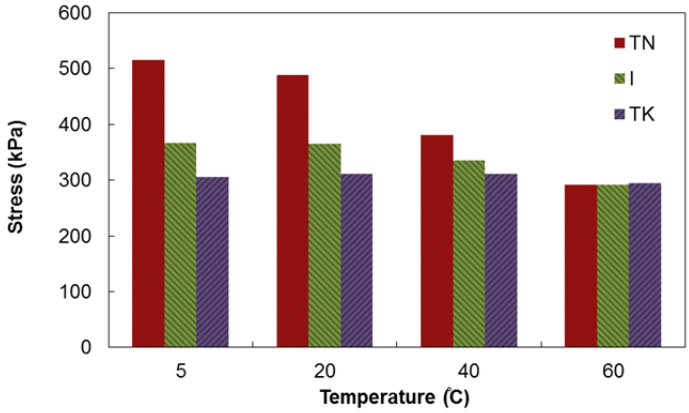

(c)

Figure D.57 (a) Maximum shear ratio, (b) shear strength, and (c) shear stress for CRS-2 emulsion at 53.4 kN (12 kips) and 8 km/hr (5 mph).

9. Pneumatic Adhesion Tensile Testing Instrument (PATTI) Test Results

This section presents the results of the PATTI tests for two emulsions, CRS-2 and CRS-1h, at four temperatures: 5°C, 19°C, 35°C, and 53°C. All tests were performed in an environmental chamber after one hour of conditioning at each test temperature. Figure D.58 shows the temperature conditioning of an emulsion sample in the environmental chamber. Paper was placed around the pullout stubs to prevent the emulsion adhering to the bottom of the PATTI pressure ring.

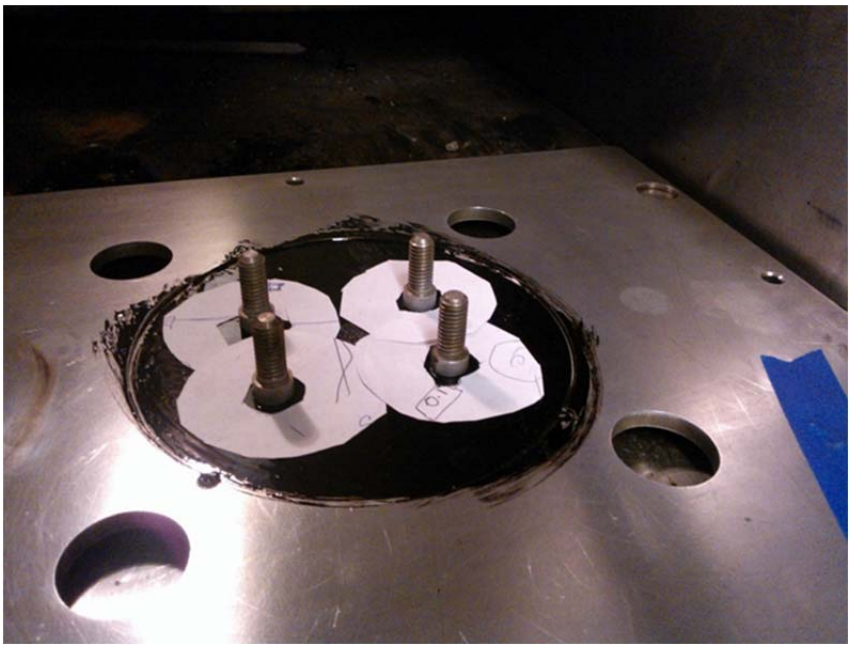

Figure D.58 Tack coat emulsion applied on aluminum plate with pullout stubs in the environmental chamber.

As shown in Figure D.59, failure occurred in the binder (i.e., cohesion failure of the emulsion) for all of the tested samples.

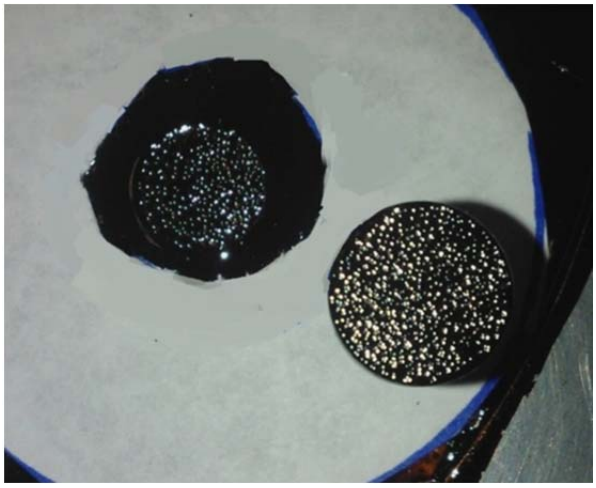

Figure D.59 Failure mode of the PATTI test samples (i.e., cohesion failure of the emulsion).

Figure D.60 shows the results of the PATTI pullout tests for the CRS-1h and CRS-2 emulsions on an aluminum plate. The CRS-1h emulsion shows higher tensile strength values than the CRS-2 emulsion. The PATTI test results and the test procedure indicate a promising method that can be used to evaluate the bond strength of different tack coat materials for quality control or design purposes.

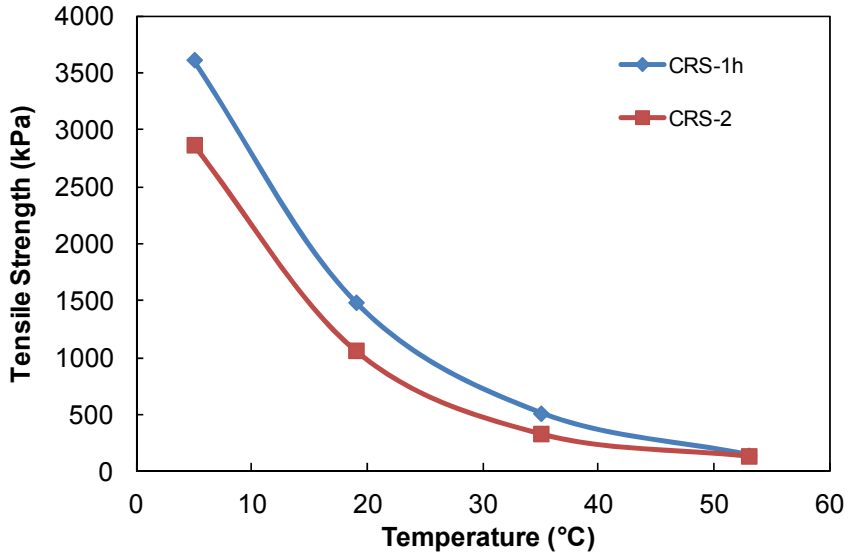

Figure D.60 PATTI tensile bond strength results for CRS-2 and CRS-1h emulsions versus temperature with emulsion application rate of 0.18 L/m^2 (0.04 gal/yd^2) on an aluminum plate.

Figure D.61 presents the stress versus time plots for the CRS-1h emulsion PATTI test at four temperatures: 5°C, 19°C, 35°C, and 53°C. According to the ASTM D4541 standard, the loading rate for the PATTI tests should be around 689.47 kPa/s (100 psi/s).

The PATTI bond strength values and the loading rates for the CRS-1 and CRS-2 emulsions are presented in Table D.16 and Table D.17, respectively.

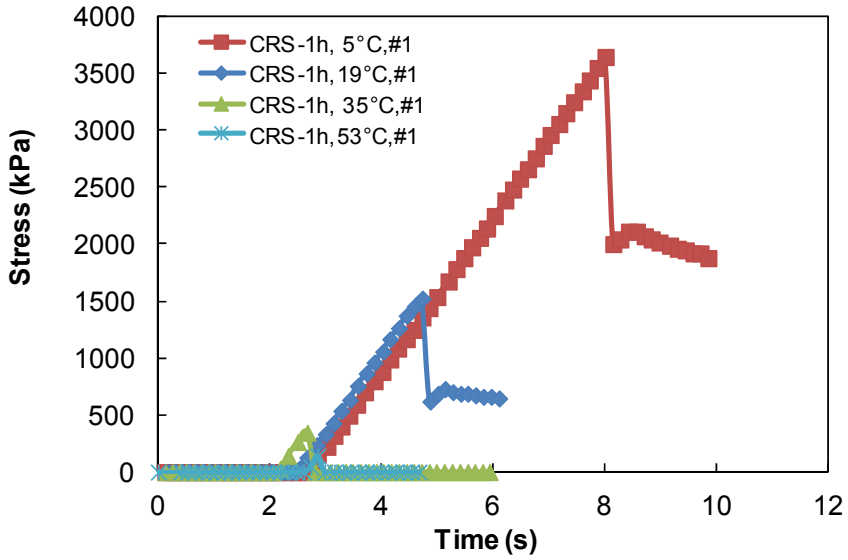

Figure D.61 Tensile stress versus time at four temperatures of 5°C, 19°C, 35°C, and 53°C with emulsion application rate of 0.18 L/m^2 (0.04 gal/yd^2) CRS-1h.

Table D.16 Bond strength values and stress rates for tensile bond strength PATTI tests for CRS-1h emulsion.

Test Number	Emulsion Type	Temperature (°C)							
		5		19		35		53	
		Strength (psi) kPa	Stress Rate (psi/s) kPa/s	Strength (psi) kPa	Stress Rate (psi/s) kPa/s	Strength (psi) kPa	Stress Rate (psi/s) kPa/s	Strength (psi) kPa	Stress Rate (psi/s) kPa/s
#1	CRS-1h	(528.4) 3643.4	(98.8) 681.5	(220.8) 1522.4	(100.6) 693.9	(50.1) 345.5	(103.9) 716.1	(20.3) 140.3	(111.1) 766.3
#2	CRS-1h	(534.4) 3684.5	(97.9) 675.3	(226.8) 1563.4	(101.6) 700.5	(70.0) 482.4	(99.7) 687.3	(20.3) 140.3	(88.0) 606.7
#3	CRS-1h	(550.3) 3794.0	(97.8) 674.1	(179.1) 1235.0	(95.3) 656.8	(103.7) 715.0	(98.4) 678.7		
#4	CRS-1h	(484.8) 3342.4	(93.8) 646.5	(236.7) 1631.9	(100.0) 689.7				
Average		(524.5) 3616.1	(97.1) 669.3	(215.8) 1488.2	(99.4) 685.2	(74.6) 514.3	(100.7) 694.0	(20.3) 140.3	(99.6) 686.5

Table D.17 Bond strength values and stress rates for tensile bond strength PATTI tests for CRS-2 emulsion.

Test Number	Emulsion Type	Temperature (°C)							
		5		19		35		53	
		Strength (psi) kPa	Stress Rate (psi/s) kPa/s	Strength (psi) kPa	Stress Rate (psi/s) kPa/s	Strength (psi) kPa	Stress Rate (psi/s) kPa/s	Strength (psi) kPa	Stress Rate (psi/s) kPa/s
#1	CRS-2	(468.9) 3232.9	(107.8) 743.4	(155.3) 1070.8	(94.8) 653.6	(54.1) 372.9	(88.8) 612.1	(26.3) 181.3	(112.6) 776.4
#2	CRS-2	(363.7) 2507.6	(104.8) 722.6	(175.2) 1207.6	(91.6) 631.3	(30.3) 208.7	(87.3) 602.1	(20.3) 140.3	(95.3) 656.8
#3	CRS-2			(133.5) 920.3	(95.3) 656.8	(36.2) 249.7	(103.8) 716.0	(14.4) 99.2	(95.3) 656.8
#4	CRS-2					(62.0) 427.6	(92.3) 636.5		
Average		(416.3) 2870.3	(106.3) 733.0	(154.6) 1066.2	(93.9) 647.2	(45.7) 314.8	(93.1) 641.7	(20.3) 140.3	(101.0) 696.7

Figure D.62 shows the semi-log plot for stress versus temperature for the CRS-2 and CRS-1h asphalt emulsions. The prediction functions used to predict the tensile bond strengths of the tack coats applied to an aluminum plate are shown in Figure D.62.

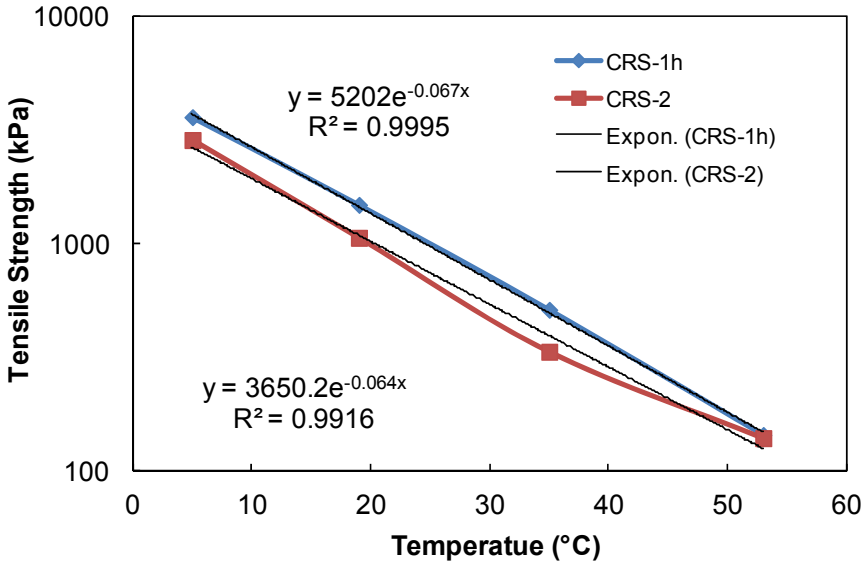

Figure D.62 PATTI test prediction equations.

Knowing the temperature, the bond strengths of the tested emulsions were predicted by Equations (17) and (18) for the CRS-1h and CRS-2 emulsions, respectively.

$$TBS_{CRS-1h} = 5202e^{-0.067T} \quad (17)$$

$$TBS_{CRS-2} = 3650.2e^{-0.064T} \quad (18)$$

where

TBS = tensile (PATTI) bond strength (kPa) and
T = temperature (°C).

10. Prediction of the Interface Shear Strength between Asphalt Layers

The tensile bond strength PATTI test results were compared to the results of the interface shear strength tests of the laboratory gyratory-compacted specimens. To measure the interface shear strength between the asphalt layers, two layers of asphalt samples were compacted with the same asphalt emulsions used in the PATTI tests as the bonding agent between the two asphalt layers. The interface shear strengths of the compacted samples were measured by the direct shear test device developed at North Carolina State University, i.e., the MAST. The MAST shear strength tests were performed in displacement mode. Conversely, the PATTI tensile bond strength test is a load-controlled test method. Therefore, in order to compare the results of the two experiments, i.e., MAST and PATTI tests, the stress rates of the MAST tests needed to be predicted using a proper approximation method.

The chord method shown in Figure D.63 was used in this study to approximate the stress rates of the MAST tests. In the chord method, the slope of the chord between the points within 2.5 percent and 45 percent of the shear strength on the shear stress versus time graph was assumed as the stress rate for the shear strength test. In the region below 45 percent of the shear strength, the development of cracks was assumed to be minimal, the material was assumed to be in the elastic range, and the deformation was assumed to be linear.

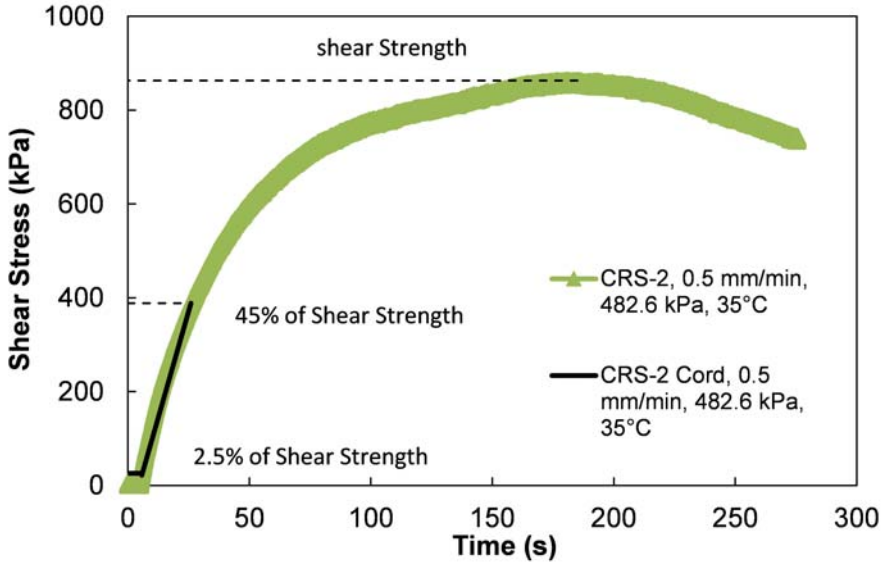

Figure D.63 Chord method for CRS-2 emulsion with displacement rate of 0.508 mm/min (0.02 in./min) and 482.6 kPa (70 psi) confinement at 35°C (95°F) based on MAST test results.

The stress rates for the CRS-2 emulsion MAST tests at different temperatures with 5.08 mm/min (0.2 in./min) strain rate are shown in Figure D.64. As shown, the slopes of the stress rate lines at different temperatures with the same strain rate are very close.

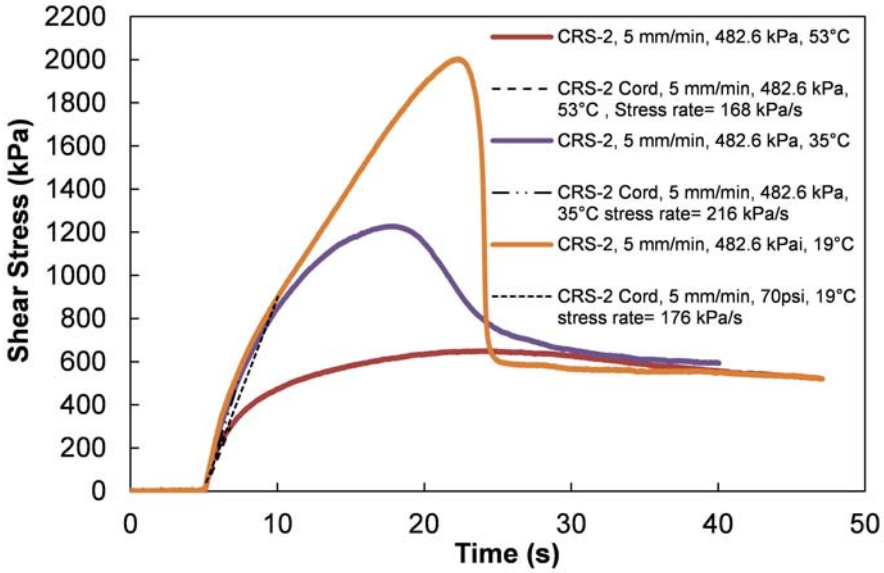

Figure D.64 Typical stress rate calculation by chord method for CRS-2 emulsion at overhead strain rate of 5.08 mm/min (0.2 in./min), confinement pressure of 482.6 kPa (70 psi), based on MAST test results.

The calculated stress rates for the CRS-2 and CRS-1h emulsions at the temperatures of 5°C, 19°C, 35°C, and 53°C with the different strain rates are presented in Table D.18 and Table D.19, respectively.

Table D.18 Stress rates for MAST shear strength tests at normal confinement of 482.6 kPa (70 psi) for CRS-2 emulsion.

Temperature °C (°F)	Crosshead Displacement Rate mm/min (in./min)	Strain Rate ε/sec (DIC)	Stress Rate kPa/s (psi/s) Chord method	Reduced. Strain Rate ε/sec	Strength kPa (psi)
5 (41)	50.8 (2)	1.278E-02	1510 (219)	1.278E-02	4240 (615)
	5.08 (0.2)	1.296E-03	181 (25.26)	1.296E-03	3279 (475.6)
	0.508 (0.02)	1.697E-04	17.2 (2.5)	1.697E-04	2611 (378.8)
19 (66.2)	50.8 (2)	1.720E-02	1175 (170.4)	1.749E-04	2580 (374.2)
	5.08 (0.2)	2.230E-03	176 (25.52)	2.267E-05	2004 (291)
	0.508 (0.02)	4.247E-04	24.5 (3.5)	4.317E-06	1543 (223.8)
35 (95)	50.8 (2)	4.215E-02	2273 (330)	3.953E-06	1570 (227.8)
	5.08 (0.2)	4.678E-03	216 (31.3)	4.388E-07	1229 (178)
	0.508 (0.02)	6.532E-04	18.2 (2.64)	6.128E-08	863 (125.2)
53 (127.4)	50.8 (2)	7.146E-02	2276 (330)	7.020E-08	835 (121.1)
	5.08 (0.2)	8.439E-03	168 (24.3)	8.290E-09	651 (94.4)
	0.508 (0.02)	8.798E-04	16 (2.3)	8.643E-10	541 (78.5)

Table D.19 Stress rates for MAST shear strength tests at normal confinement of 482.6 kPa (70 psi) for CRS-1h emulsion.

Temperature °C (°F)	Crosshead Displacement Rate mm/min (in./min)	Strain Rate ε/sec (DIC)	Stress Rate kPa/s (psi/s) Chord method	Reduced. Strain Rate ε/sec	Strength kPa (psi)
5 (41)	50.8 (2)	1.31E-02	1688 (244.8)	1.31E-02	3900 (565.6)
	0.508 (0.02)	1.76E-04	24 (3.5)	1.76E-04	2452 (355.6)
19 (66.2)	50.8 (2)	1.79E-02	1195 (173.3)	1.82E-04	2421 (351.1)
	0.508 (0.02)	4.29E-04	18 (2.6)	4.36E-06	1508 (218.7)
35 (95)	50.8 (2)	4.23E-02	1974 (286.3)	3.97E-06	1511 (219.1)
	0.508 (0.02)	7.25E-04	16 (2.3)	6.80E-08	829 (120)
53 (127.4)	50.8 (2)	7.15E-02	2016 (292.4)	7.03E-08	834 (121)
	0.508 (0.02)	9.45E-04	11 (1.6)	9.29E-10	509 (73.8)

The relationship between the strain rate and stress rate for each temperature was developed by plotting the stress rates versus the strain rates as shown in Figure D.65 and Figure D.66 for the two emulsions, respectively.

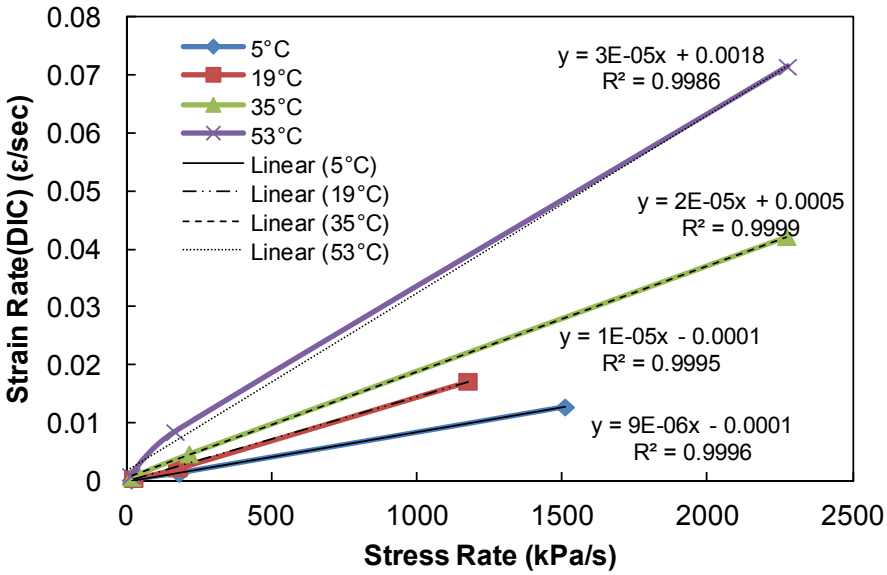

Figure D.65 Stress rate and strain rate relationship at different temperatures for CRS-2 emulsion at normal confinement pressure of 482.6 kPa (70 psi).

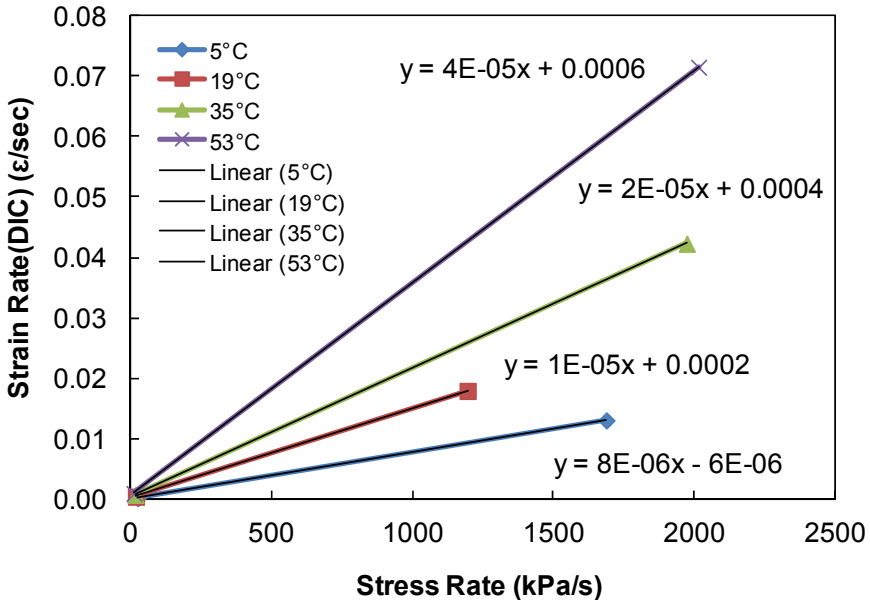

Figure D.66 Stress rate and strain rate relationship at different temperatures for CRS-1h emulsion at normal confinement pressure of 482.6 kPa (70 psi).

Using Equations (19), (20), (21), and (22), the strain rates at 5°C, 19°C, 35°C, and 53°C were predicted for the given stress rates for the CRS-2 emulsion.

$$\dot{\gamma}_{53,crs-2} = 0.00003 \times \dot{\sigma} + 0.0018 \quad (19)$$

$$\dot{\gamma}_{35,crs-2} = 0.00002 \times \dot{\sigma} + 0.0005 \quad (20)$$

$$\dot{\gamma}_{19.crs-2} = 0.00001 \times \dot{\sigma} - 0.0001 \quad (21)$$

$$\dot{\gamma}_{5,crs-2} = 0.000009 \times \dot{\sigma} - 0.0001 \quad (22)$$

where

$\dot{\gamma}_{crs-2}$ = strain rate for CRS-2 emulsion at 5°C, 19°C, 35°C, and 53°C (ε/sec) and

$\dot{\sigma}$ = stress rate (kPa/s).

Using Equations (23), (24), (25), and (26), the strain rates at 5°C, 19°C, 35°C, and 53°C were predicted for the given stress rates for the CRS-1h emulsion.

$$\dot{\gamma}_{53,crs-1h} = 0.00004 \times \dot{\sigma} + 0.0006 \quad (23)$$

$$\dot{\gamma}_{35,crs-1h} = 0.00002 \times \dot{\sigma} + 0.0004 \quad (24)$$

$$\dot{\gamma}_{19,crs-1h} = 0.00001 \times \dot{\sigma} + 0.0002 \quad (25)$$

$$\dot{\gamma}_{5,crs-1h} = 0.000008 \times \dot{\sigma} - 0.000006 \quad (26)$$

where

$\dot{\gamma}_{crs-1h}$ = strain rate at 5°C, 19°C, 35°C, and 53°C (ε/sec) and

$\dot{\sigma}$ = stress rate (kPa/s).

The stress rates for the CRS-1h and CRS-2 emulsions used for the PATTI tests at different temperatures are shown in Table D.16 and Table D.17, respectively. Using the average stress rate for each temperature, the shear strain rate at each temperature was calculated using Equations (19), (20) , (21), and (22) for the CRS-2 emulsion and by Equations (23), (24), (25), and (26) for the CRS-1h emulsion. The calculated strain rates are presented in Table D.20 and Table D.21 for the two emulsions, respectively.

The strain rate that corresponds to each temperature in the PATTI tests was divided by the shift factor for that temperature (asphalt mixture shift factor) to calculate the reduced strain rates. The interface shear strength for the CRS-2 emulsion was calculated using Equation (27) developed for the MAST shear tests. Equation (27) was developed for shear tests performed by the MAST on two-layered asphalt specimens with CRS-2 emulsion as the bonding agent between the asphalt layers. The shear strength values that correspond to the calculated reduced strain rates with normal confinement of 482.6 kPa (70 psi) are presented in Table D.20.

$$\tau_{f,crs-2} = (2.6116 \times \bar{\gamma}^{0.0685}) \times \sigma_c + 6140.4 \times \bar{\gamma}^{0.1564} + 0.18 \times \sigma_c \quad (27)$$

where

$\tau_{f,crs-2}$ = MAST interface shear strength (kPa),

$\bar{\gamma}$ = reduced strain rate (ε/sec), and

σ_c = confinement pressure (kPa).

The shear strength values for the CRS-1h emulsion at different reduced strain rates were calculated by the following Equation (28). The shear strength results are shown in Table D.21 with the normal confinement of 482.6 kPa (70 psi).

$$\tau_{f,crs-1h} = (1.8174 \times \dot{\gamma}^{0.0562}) \times \sigma_c + 6075.3 \times \dot{\gamma}^{0.1566} + 0.16 \times \sigma_c \quad (28)$$

where

$\tau_{f,crs-1h}$ = MAST interface shear strength (kPa),

$\dot{\gamma}$ = reduced strain rate (ε/sec), and

σ_c = confinement pressure (kPa).

Table D.20 PATTI tensile bond strength values versus e corresponding interface shear strength values calculated for CRS-2 emulsion.

Temperature °C (°F)	PATTI stress rate from (Table D.17) (psi) kPa	Tensile bond strength (PATTI) (Table D.17) (psi) kPa	Strain rate (ε/sec) by Equations (19), (20), (21) and (22)	Reduced strain rate (ε/sec) using mixture shift factor	Shear strength with normal confinement of 482 kPa (70 psi) by Equation (27) (psi) kPa
5 (41)	(106) 730.8	(416.3) 2870.3	6.48E-03	6.48E-03	(546.3) 3766
19 (66.2)	(93) 641.2	(154.6) 1066.2	6.31E-03	6.42E-05	(303) 2089
35 (95)	(93) 641.2	(45.7) 314.8	1.33E-02	1.25E-06	(190.2) 1311
53 (127.4)	(101) 696.4	(20.3) 140.3	2.27E-02	2.23E-08	(123.2) 849

Table D.21 PATTI tensile bond strength values versus corresponding interface shear strength values calculated for CRS-1h emulsion.

Temperature (°C)	Stress rate from (Table D.16) (psi) kPa	Tensile bond strength (Table D.16) (psi) kPa	Strain rate (ε/sec) by Equations (23), (24), (25), and (26)	Reduced strain rate (ε/sec) using mixture shift factor	Shear strength with normal confinement of 482 kPa (70 psi) by Equation (28) (psi) kPa
5 (41)	(97.1) 669.3	(524.5) 3616.1	5.35E-03	5.35E-03	(501.1) 3455
19 (66.2)	(99.4) 685.2	(215.8) 1488.2	7.05E-03	7.17E-05	(281.6) 1942
35 (95)	(100.7) 694.0	(74.6) 514.3	1.43E-02	1.34E-06	(176.6) 1218
53 (127.4)	(99.6) 686.5	(20.3) 140.3	2.81E-02	2.76E-08	(114) 786

The tensile bond strength values versus the interface shear strength values with the normal confinement of 482.6 kPa (70 psi) for the CRS-2 and CRS-1h emulsions are plotted in Figure D.67. Equation (29) was developed to predict the interface shear strength using the CRS-2 emulsion as a function of the tensile bond strength of the CRS-2 emulsion at the confinement pressure of 482 kPa (70 psi). Equation (30) was used to predict the CRS-1h emulsion interface shear strength as a function of the tensile bond strength of the CRS-1h emulsion measured by PATTI.

$$SBS_{CRS-2} = (-74.43 \times TBS_{CRS-2}^{-0.77}) \times 482.63 + 0.127 \times TBS_{CRS-2}^{1.2289} + 482.63 \times 3.2986 \quad (29)$$

where

SBS_{CRS-2} = shear bond strength (kPa) and
TBS_{CRS-2} = tensile bond strength (PATTI) (kPa).

$$SBS_{CRS-1h} = (-1.5 \times TBS_{CRS-1h}^{-19.07}) \times 482.63 + 3.09 \times TBS_{CRS-1h}^{0.8324} + 482.63 \times 1.28 \quad (30)$$

where

SBS_{CRS-1h} = shear bond strength (kPa) and
TBS_{CRS-1h} = tensile bond strength (PATTI) (kPa).

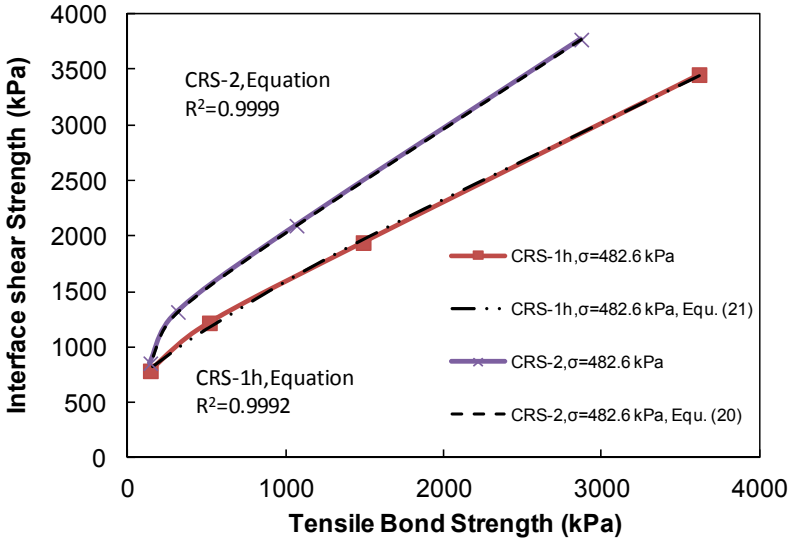

Figure D.67 Interface shear strength versus tensile bond strength.

Due to the lack of strain rates for the interface shear strength tests at confining pressures other than 482.6 kPa (70 psi), the developed strain rates for the confinement pressure of 482.6 kPa (70 psi) presented in Table D.20 and Table D.21 were used to calculate the interface shear strength values at the other confining pressures using Equations (27) and (28). The calculated interface shear strength values versus the tensile bond strength values for the CRS-2 and CRS-1h emulsions at the confining pressures of 482.6 kPa (70 psi), 275.8 kPa (40 psi), and 69 kPa (10 psi) are shown in Figure D.68 and Figure D.69 for the CRS-2 and CRS-1h emulsions, respectively.

The interface shear strength was predicted for the CRS-2 and CRS-1h emulsions using Equations (31) and (32).

$$SBS_{CRS-2} = (-19.2263 \times TBS_{CRS-2}{}^{-0.01}) \times \sigma_c + 10.9189 \times TBS_{CRS-2}{}^{0.6975} + \sigma_c \times 19.1952 \qquad (31)$$

where

SBS_{CRS-2} = interface shear strength for CRS-2 emulsion (kPa),
TBS_{CRS-2} = tensile bond strength (PATTI) for CRS-2 emulsion (kPa), and
σ_c = normal stress in shear test.

$$SBS_{CRS-1h} = (-1.5 \times TBS_{CRS-1h}{}^{-19.0764}) \times \sigma_c + 5.405 \times TBS_{CRS-1h}{}^{0.762} + \sigma_c \times 1.233 \qquad (32)$$

where

SBS_{CRS-1h} = interface shear strength for CRS-1h emulsion (kPa),
TBS_{CRS-1h} = tensile bond strength (PATTI) for CRS-1h emulsion (kPa), and
σ_c = normal stress in shear test.

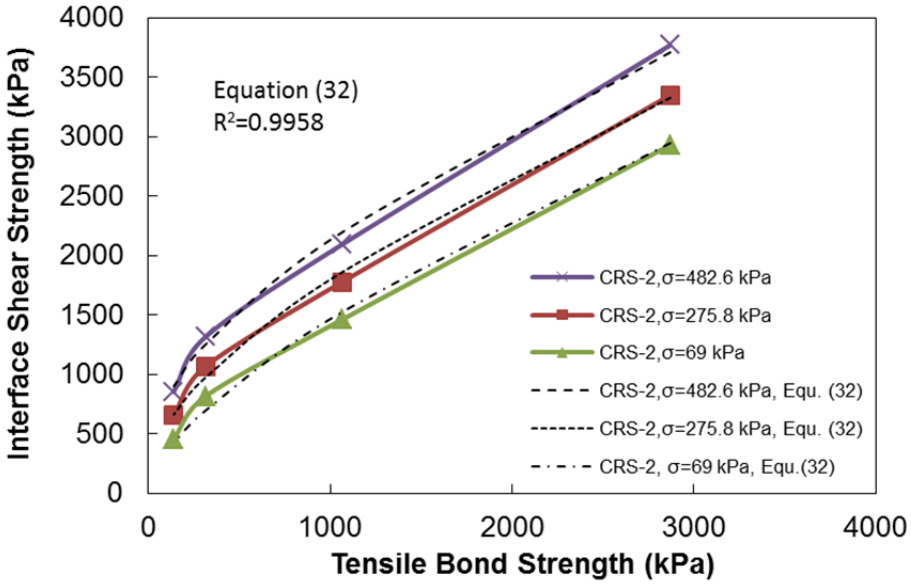

Figure D.68 Interface shear strength versus tensile bond strength for CRS-2 emulsion.

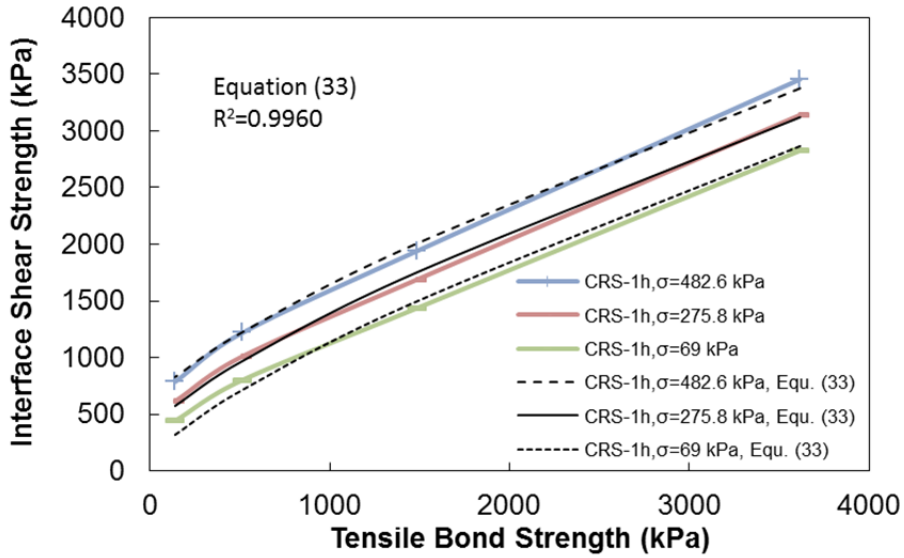

Figure D.69 Interface shear strength versus tensile bond strength for CRS-1h emulsion.

11. Summary of interface shear strength prediction method

In order to predict tack coat performance in the field, it was proposed in this study to collect tack coat samples on aluminum plates placed on the existing asphalt surface before the application of the tack coat by the distribution trucks. The PATTI was used to measure the tensile bond strength of the tack coat samples collected on the aluminum plates. The PATTI test is a standard test procedure and the test can be performed in a controlled laboratory environment (i.e., temperature and humidity). Equations were developed to correlate the shear strength values of the asphalt interfaces between two layers of laboratory-compacted asphalt mix and the tensile

bond strength values of the tack coat used between the asphalt layers measured by the PATTI test.

APPENDIX E: *In Situ* Quality Control Methodology for Tack Coat Materials

1. Minimum Required Bitumen Bond Strength (BBS)

The need for a standard *in situ* quality control method to ensure the appropriate application of tack coats to existing asphalt surface layers has led to extensive research over the last decade. Several test methods and test devices have been proposed by researchers (Karshenas 2015, Mohammad et al. 2012, and Tashman et al. 2006) to evaluate the bond strength of tack coats in the field immediately after application. Among these researchers, Karshenas (2015) used the pneumatic adhesion tensile testing instrument (PATTI) test to evaluate the bitumen bond strength (BBS) of tack coats applied to aluminum plates. The PATTI test is an adhesion test typically used in the paint industry and is standardized in ASTM D4541. This test is also referred to as the *bitumen bond strength test*, or *BBS test*. Karshenas (2015) placed aluminum plates on an existing asphalt surface layer prior to the application of the tack coat from distribution trucks at a construction site and performed BBS tests in the laboratory or in the field using samples collected on the aluminum plates and pull-stubs with a diameter of 12.5 mm (0.5 in.). Karshenas (2015) concluded that his PATTI test (BBS test) results and test procedures offer a promising method that can be used to evaluate the BBS of tack coat materials for quality control or design purposes.

In this study, the PATTI test procedures proposed by Karshenas (2015) were used to develop an *in situ* quality control methodology for tack coat materials. This quality control methodology requires PATTI tests to be performed in the field using tack coat samples applied from distribution trucks and collected on aluminum plates. In order to develop this *in situ* quality control methodology for tack coats, a minimum required BBS value of the tack coat applied to the aluminum plates needed to be established. This minimum required BBS value should be able to provide acceptable field performance.

In this section, two different tack coat materials, i.e., CRS-2 and CRS-1h emulsions, are used to demonstrate how the *in situ* quality control methodology is established. To establish the minimum required BBS value for each emulsion, the shear bond strength value proposed by Partl and Raab (1999) was adopted. Partl and Raab (1999) performed direct shear tests to investigate the shear bond strength between asphalt layers under the test conditions of 50.8 mm/min (2 in./min) loading rate, 20°C, and unconfinement using a layer parallel direct shear (LPDS) device. Based on their results, they then proposed the minimum shear bond strength value of 1,300 kPa (189 psi), which is the value required to provide acceptable field performance to meet a Swiss specification.

Conversion of the minimum shear bond strength value into the required BBS values for the two emulsions was done using Equation (33) and Equation (34), which were proposed by Karshenas (2015) for CRS-2 and CRS-1h emulsions, respectively. Detailed information about the derivation of Equation (33) and Equation (34) can be found in Karshenas (2015).

$$\tau_{f,\ CRS-2} = (-19.2263 \times BBS_{CRS-2}^{\ -0.01}) \times \sigma_c + 10.9189 \times BBS_{CRS-2}^{\ 0.6975} + \sigma_c \times 19.1952 \qquad (33)$$

where

$\tau_{f,\ CRS-2}$ = shear bond strength at the layer interface with CRS-2 emulsion, kPa,
BBS_{CRS-2} = bitumen bond strength of CRS-2 emulsion measured by PATTI, kPa, and
σ_c = normal confining stress, kPa.

$$\tau_{f,\ CRS-1h} = (-1.5 \times BBS_{CRS-1h}^{-19.0764}) \times \sigma_c + 5.405 \times BBS_{CRS-1h}^{0.762} + \sigma_c \times 1.233 \quad (34)$$

where
$\tau_{f,\ CRS-1h}$ = shear bond strength at the layer interface with CRS-1h emulsion, kPa,
BBS_{CRS-1h} = bitumen bond strength of CRS-1h emulsion measured by PATTI, kPa, and
σ_c = normal confining stress, kPa.

To convert the shear bond strength value of 1,300 kPa (189 psi) proposed by Partl and Raab (1999) into the required BBS values, σ_c was set to zero in Equation (33) and Equation (34) because Partl and Raab used direct shear tests under the unconfined condition. Therefore, Equation (33) and Equation (34) can be simplified for the unconfined condition and rearranged to obtain the required BBS values for the two emulsions from the minimum shear bond strength as

$$BBS_{CRS-2} = \left(\frac{\tau_{f,\ CRS-2}}{10.9189} \right)^{\frac{1}{0.6975}} \quad (35)$$

$$BBS_{CRS-1h} = \left(\frac{\tau_{f,\ CRS-1h}}{5.405} \right)^{\frac{1}{0.762}} \quad (36)$$

Next, the shear bond strength terms, $\tau_{f,\ CRS-2}$ and $\tau_{f,\ CRS-2}$, were substituted with 1,300 kPa (189 psi) in Equation (35) and Equation (36), and the minimum required BBS values for CRS-2 and CRS-1h emulsions were found to be 946 kPa and 1330 kPa, respectively.

2. Determination of PATTI Test Temperature

The minimum required BBS value should be compared with the BBS value measured in the field using PATTI tests to determine whether or not the tack coat is applied properly to the existing asphalt surface layer. However, it is noted that the PATTI test conditions should correspond to the direct shear test conditions that were used in the tests performed by Partl and Raab (1999) in terms of loading rate and temperature. The reduced strain rate was used to determine the PATTI test conditions that are equivalent to the conditions applied to the direct shear strength tests performed by Partl and Raab (1999). The reduced strain rate is determined using the reduced time instead of physical time in calculating the strain rate. It is noted that the t-TS principle should be verified for both shear bond strength values and BBS values in order to

employ the reduced strain rate concept. The t-TS principle was proven to be valid for the shear strength in Section 4.2.1; however, the validation of the t-TS princilple for the BBS values could not be done in this study due to the lack of BBS data at varying temperatures. Further research is required to verify the t-TS principle for the BBS values measured from the PATTI tests. In the remaining section, it is assumed that the t-TS principle is valid for the BBS values to demonstrate the entire procedure.

The crosshead LVDT displacement rate of 50.8 mm/min (2 in./min) that Partl and Raab (1999) used for their direct shear tests was converted to the crosshead LVDT strain rate using the gap width between the yoke and the pneumatic clamp of the LPDS device. This conversion was achieved by dividing the constant crosshead LVDT displacement rate by the 2-mm gap between the yoke and the pneumatic clamp. The reduced crosshead LVDT strain rate was then calculated by multiplying the converted crosshead LVDT strain rate by the t-T shift factors of the CRS-2 and CRS-1h emulsion residues at 20°C. In this study, the t-T shift factors of the CRS-1h emulsion residue were not available and therefore the t-T shift factors of the CRS-2 emulsion residue were used to calculate the reduced crosshead LVDT strain rate. Figure E.1 presents the t-T shift factor function of the CRS-2 emulsion residue. Consequently, the reduced crosshead LVDT strain rate of 0.00488 was obtained from this calculation. This reduced strain rate should be consistent with the reduced strain rate determined under the PATTI test conditions.

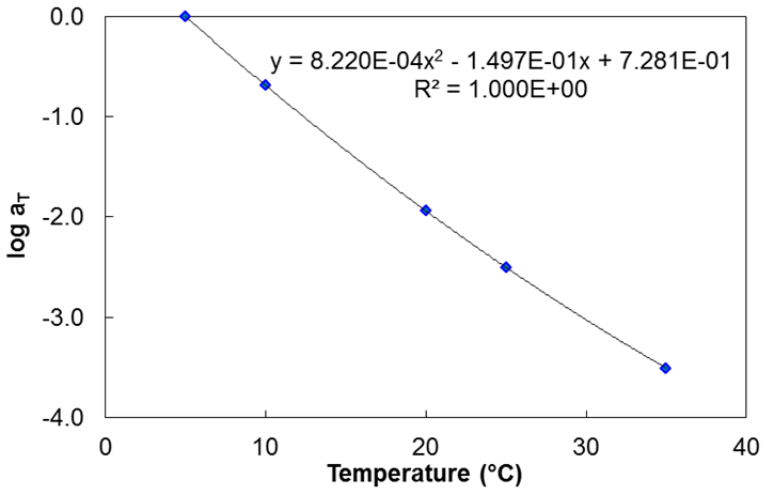

Figure E.1 Time-temperature shift factor function for CRS-2 emulsion residue.

The ASTM D4541 standard specifies that the loading rate for the PATTI test should be maintained around 689.47 kPa/sec (100 psi/sec). Thus, only the temperature condition for the PATTI test can be adjusted to match the reduced crosshead LVDT strain rate of 0.00488 determined from the direct shear test. The direct shear test was performed in constant displacement-control mode, whereas the PATTI test was performed in constant load-control mode. Therefore, the strain rate for the PATTI test in constant load-control mode needs to be predicted using a proper approximation method. For this prediction, this study used the methodology suggested by Karshenas (2015).

First, stress rates were determined from the direct shear test results at different temperatures using the chord method (Karshenas 2015). Then, the relationship between the crosshead LVDT strain rate used for the direct shear test and the stress rate determined by the

chord method for each temperature was developed by plotting the stress rates versus the strain rates. Lastly, the strain rate for the PATTI test at each temperature was predicted using the stress rate of 689.47 kPa/sec (100 psi/sec) for each temperature.

The temperature for the PATTI test that makes the reduced strain rate for the PATTI test consistent with the reduced strain rate for the direct shear test was found using the t-T shift factors of the CRS-2 emulsion residue. The test temperature turned out to be 11.5°C. Moreover, the temperature sensitivity of the PATTI test was investigated using the t-T shift factors for the three different tack coats, as presented in Table E.1. Consequently, the temperature of 12°C that was decided for the PATTI test could be used for the *in situ* quality control of tack coats based on the temperature sensitivity results. The fitting coefficients of the t-T shift factor functions for the PG 64-22 binder and SS-1 emulsion residue used for the temperature sensitivity analysis can be found in Table D.7.

Table E.1 Temperature sensitivity results of PATTI tests for different tack coats.

Tack Coat	PATTI Test Temperature (°C)
CRS-2 emulsion	11.5
SS-1 emulsion	11.6
PG 64-22 binder	11.4

3. In Situ Quality Control Procedures

This section presents the recommended procedures for the *in situ* quality control of tack coat materials using PATTI tests. The presented procedures are able to ensure the appropriate quality of tack coats. The *in situ* quality control procedures are as follows.

- Obtain tack coat samples for the PATTI tests by placing aluminum plates on the existing asphalt surface layer prior to the application of the tack coat from the distribution trucks at the construction site.
- Cure the tack coat samples using an infrared heat lamp. The curing time depends on the tack coat types, e.g., RS (rapid setting), MS (medium setting), SS (slow setting), and QS (quick setting) tack coats. For example, the RS emulsion needs approximately 30 minutes at 60°C for complete curing.
- Heat the pull-stubs (diameter of 12.5 mm (0.5 in.)) to the application temperature of 60°C using an infrared heat lamp and place the heated pull-stubs on the tack coat samples.
- Place a weight of approximately 50 ±1.0 g on top of the pull-stubs in order to ensure full contact between the pull-stubs and the tack coat samples (AASHTO TP-91 2013).
- Condition the tack coat samples in a portable environmental chamber to maintain the test temperature of 12°C.
- Conduct the PATTI tests (at least three replicates) in the chamber once the desired test temperature is reached.
- Compare the measured *in situ* BBS values with the minimum required BBS value. If the measured *in situ* BBS value is higher than the minimum required BBS value, the tack coat is expected to provide acceptable field performance. For example, if the *in situ* BBS value for the CRS-2 tack coat was measured to be 1,100 kPa at 12°C, the tack coat will provide acceptable field performance because the *in situ* BBS value is higher than the minimum required BBS value of 946 kPa. However, for the opposite case, where the

measured *in situ* BBS value is lower than the minimum required BBS value, then the agency can penalize the contractor for failure to meet the construction specification.

APPENDIX F: Tensile Bond Strength Test Results (PATTI)

The results of the Pneumatic Adhesion Tensile Testing Instrument (PATTI) tensile bond strength tests in terms of time are presented in the following figures.

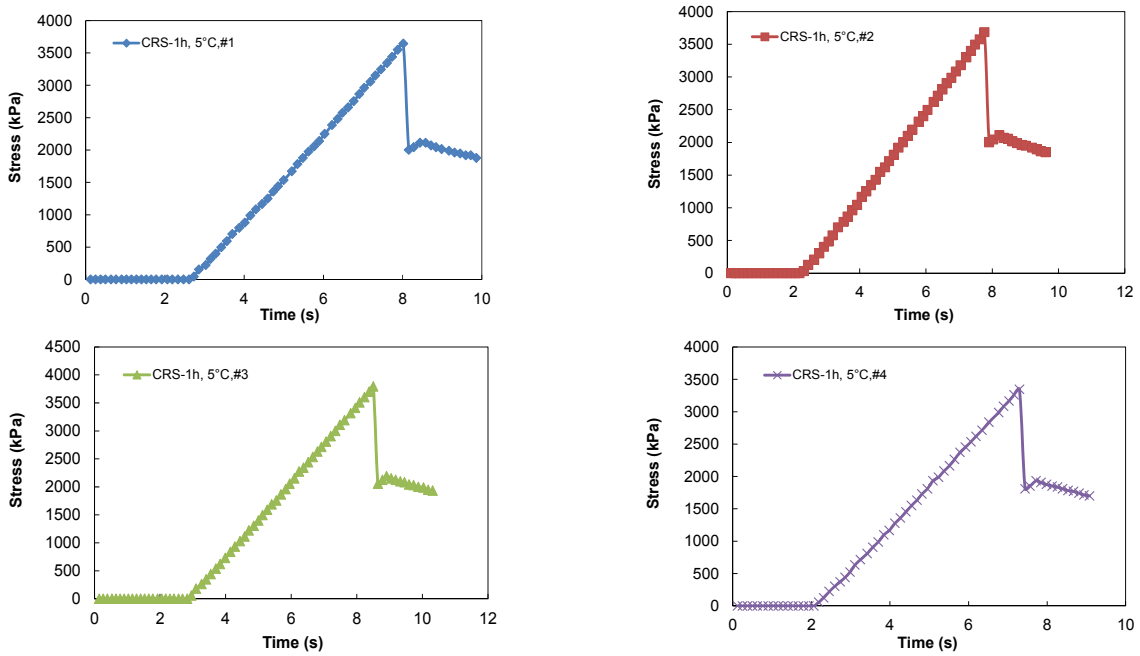

Figure F.1 CRS-1h emulsion tensile bond strength at 5°C (41°F).

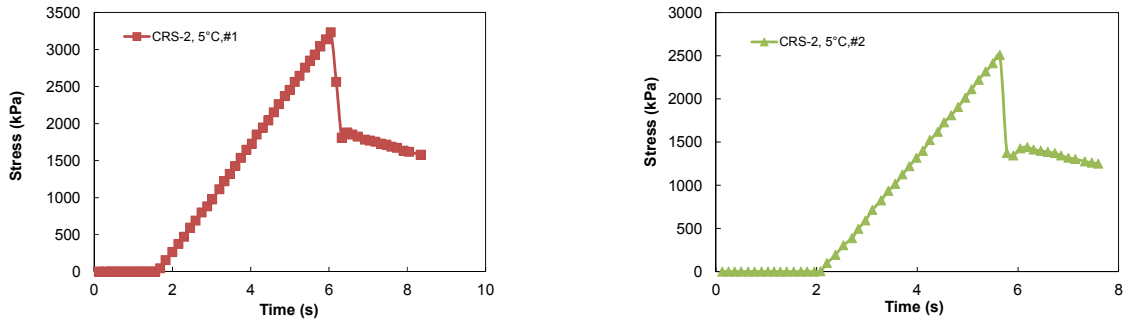

Figure F.2 CRS-2 emulsion tensile bond strength at 5°C (41°F).

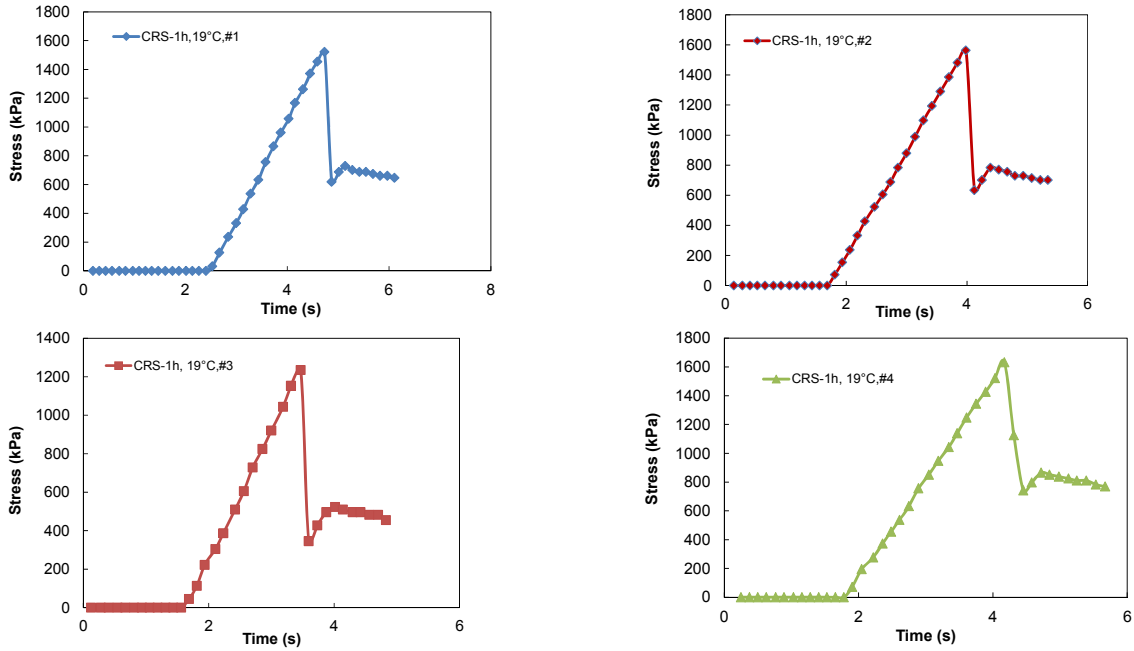

Figure F.3 CRS-1h emulsion tensile bond strength at 19°C (66.2°F).

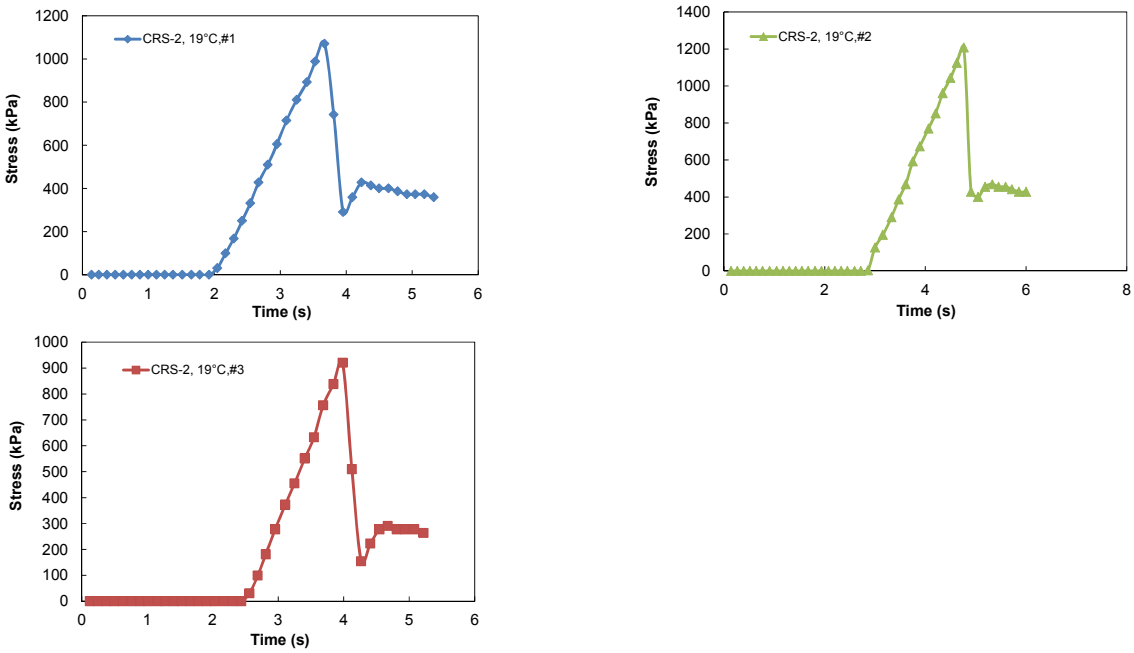

Figure F.4 CRS-2 emulsion tensile bond strength at 19°C (66.2°F).

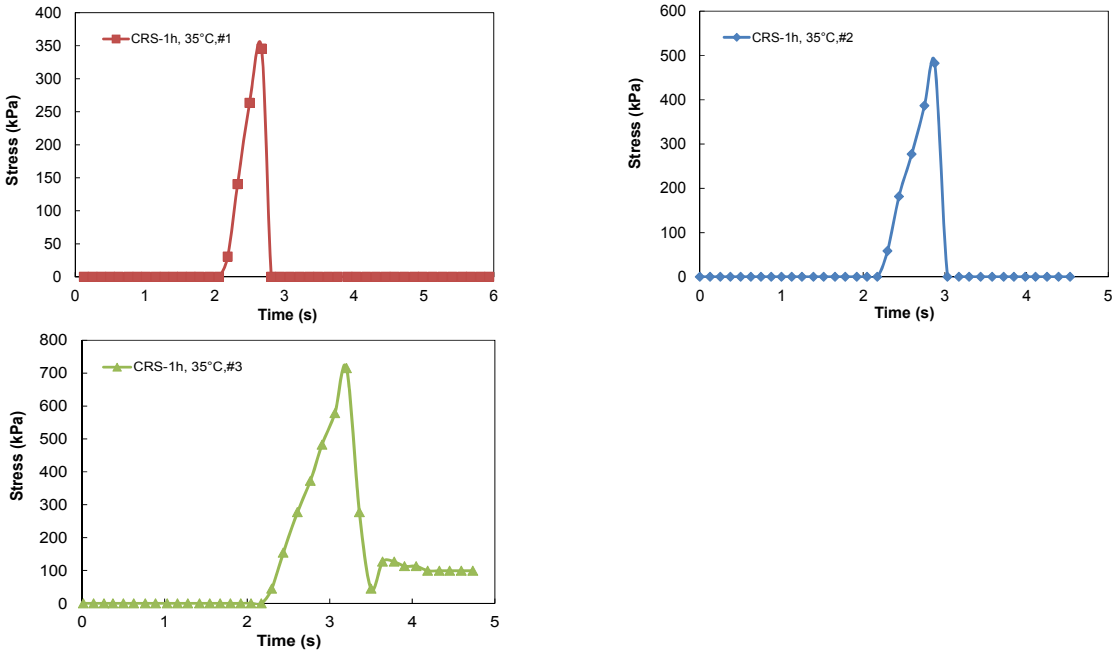

Figure F.5 CRS-1h emulsion tensile bond strength at 35°C (95°F).

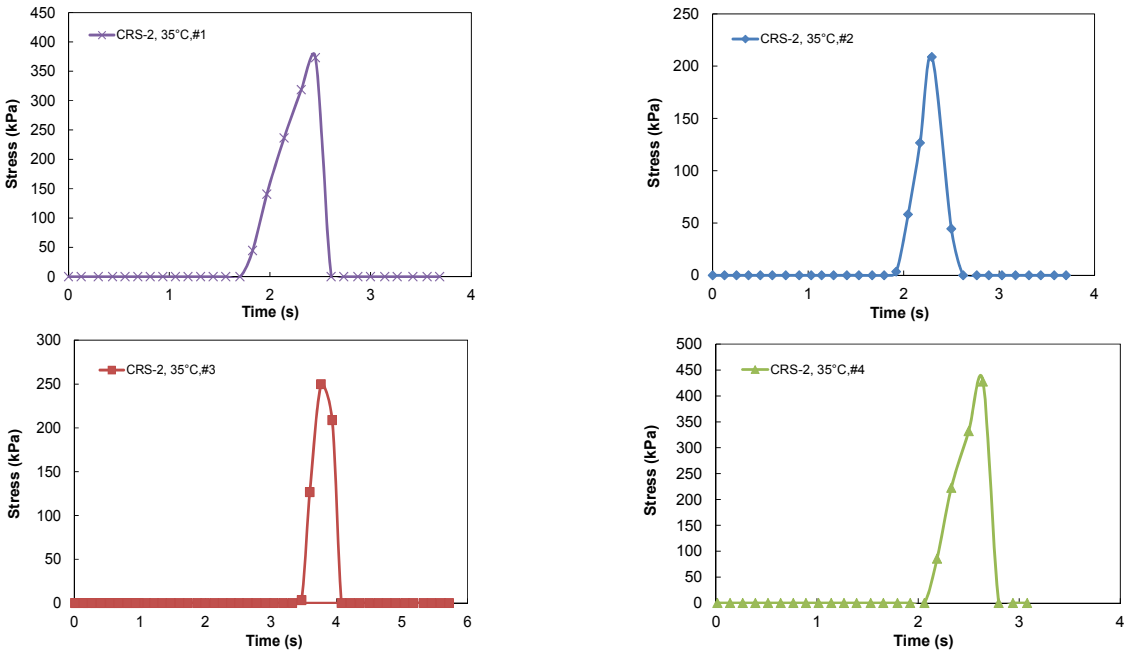

Figure F.6 CRS-2 emulsion tensile bond strength at 35°C (95°F).

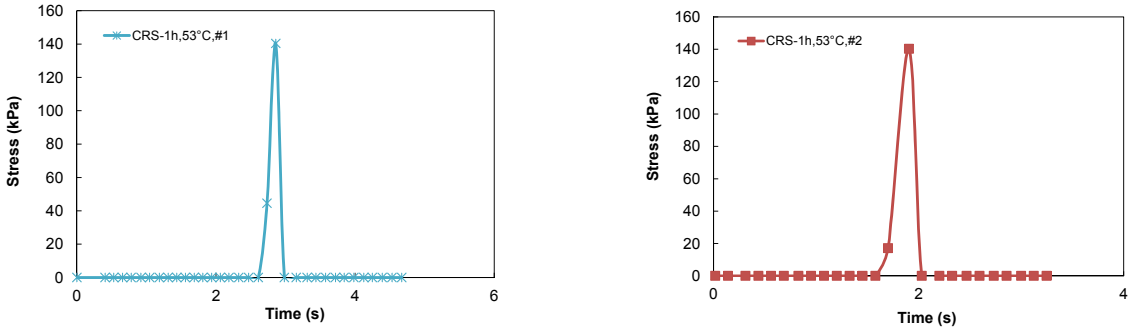

Figure F.7 CRS-1h emulsion tensile bond strength at 53°C (127.4°F).

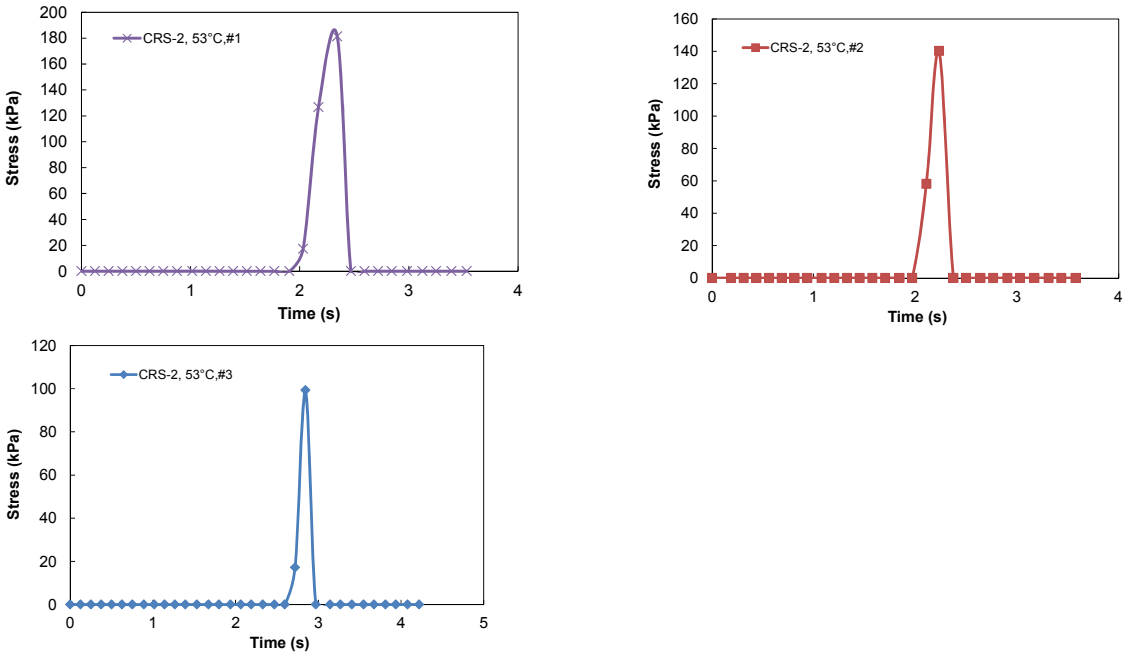

Figure F.8 CRS-2 emulsion tensile bond strength at 53°C (127.4°F).